



**University of  
Reading**



The James  
**Hutton  
Institute**

**MODELLING PEATLAND WATER TABLE  
DEPTH USING REMOTELY SENSED  
SATELLITE DATA**

A thesis submitted for the degree of

Doctor of Philosophy

**Linda Toča**

School of Mathematical, Physical and Computational Sciences

August 2023

## Declaration

I confirm that this is my own work and the use of all material from other sources has been properly and fully acknowledged.

Linda Toča

This thesis includes two published manuscripts (Chapters 3 and 4, respectively), the author contributions are detailed below.

*Chapter 3 - High resolution C-band SAR backscatter response to peatland water table depth and soil moisture: a laboratory experiment:*

L. Toca, K. Morrison, R.R.E. Artz, A. Gimona & T. Quaife (2022) High resolution C-band SAR backscatter response to peatland water table depth and soil moisture: a laboratory experiment, *International Journal of Remote Sensing*, 43:14, 5231-5251, DOI: 10.1080/01431161.2022.2131478

Conceptualization, L.T., R.A., T.Q., K.M., A.G.; methodology, L.T., R.A., T.Q., K.M. and A.G.; study design, L.T., R.A., T.Q., K.M. and A.G.; formal analysis, L.T., R.A., T.Q., K.M. and A.G.; software, L.T., K.M.; validation, R.A., T.Q., K.M. and A.G.; investigation, L.T., R.A., T.Q., K.M. and A.G.; resources, R.A., K.M.; data curation, L.T.; writing—original draft preparation, L.T.; writing review and editing, all authors; visualization, L.T.; supervision, R.A., T.Q., K.M. and A.G.

*Chapter 4 - Potential for peatland water table depth monitoring using Sentinel-1 SAR backscatter: case study of Forsinard Flows, Scotland, UK:*

Toca, L., Artz, R.R.E., Smart, C., Quaife, T., Morrison, K., Gimona, A., Hughes, R., Hancock, M.H., Klein, D., 2023. Potential for Peatland Water Table Depth Monitoring Using Sentinel-1 SAR Backscatter: Case Study of Forsinard Flows, Scotland, UK. *Remote Sens (Basel)* 15. <https://doi.org/10.3390/rs15071900>

Conceptualization, L.T., R.A., C.S., T.Q., K.M., A.G., D.K., M.H.H., R.H.; methodology, L.T., R.A., T.Q., K.M. and A.G.; study design, R.A., C.S., D.K., M.H.H., R.H.; formal analysis, L.T., R.A., T.Q., K.M. and A.G.; software, L.T.; validation, R.A., T.Q., K.M. and A.G.; investigation, L.T., R.A., T.Q., K.M. and A.G.; resources, R.A., C.S., R.H., M.H.H., D.K.; data curation, L.T., C.S.; writing original draft preparation, L.T.; writing, review and editing, all authors; visualization, L.T.; supervision, R.A., T.Q., K.M. and A.G.

## General Abstract

Peatlands are carbon-rich wetland ecosystems and represent the largest terrestrial carbon store. Although they are natural carbon sinks, damage, drainage and extraction over past decades have turned peatlands into a global carbon source. To tackle this nearly irreversible loss, peatland conservation and restoration projects on global and national levels have been increasing in numbers. High water table depth (WTD) is a highly important factor that influences peatland condition, resilience and ability to accumulate carbon. Given the extent of peatlands, a regular physical collection of data in situ, looking forward, would be impractical and difficult to accomplish, and the development of a remote sensing methods for peatland WTD monitoring would be highly beneficial.

The accessibility to satellite data along with advancements in sensors, both in variety - optical, microwave, thermal, and their resolutions - spatial, spectral, and temporal, has greatly increased in the last decade. Combined with advances in image processing using cloud computing and machine learning, it has made it easier to access and process remotely sensed data. Synthetic aperture radar (SAR), with its ability to provide data regardless of the weather, has emerged as an important source of data for environmental applications.

This project aimed to advance the usage of remotely sensed SAR data to predict peatland water table depth. First, a unique high resolution laboratory study was completed confirming SAR backscatter sensitivity to changes in peatland soil moisture and water table depth. This was followed by a case study for the Forsinard Flows area, where Sentinel-1 SAR data were used to build and test three models of different complexity for WTD prediction. The random forest model was found to be the most suited with an overall good temporal fit, highest correlation scores and lowest RMSE values. The model was later tested on a wider Peatland ACTION dataset, reaching an even higher score, affirming its applicability to peatlands in various conditions (near natural, degraded and undergoing restoration). In the final section of the thesis, up to twenty year-long time series of remote sensing data were analysed to investigate trends and change points in peatland restoration areas. The trends found using lower resolution satellite data from MODIS gave mixed results and would only be indicative of very abrupt changes, such as tree felling. The trends from the modelled WTD series based on Sentinel-1 data were indicative of positive trajectories towards higher WTD, following restoration.

The results from this thesis suggest that remotely sensed data can be informative about changes in the WTD and overall peatland condition, can be used to look at seasonal change, and can be indicative of restoration progress and response to droughts. Recent studies have shown a close link between greenhouse gasses and peatland WTD, therefore, if methods of predicting WTD based on remotely sensed data are developed further, they ultimately could be used as a proxy for greenhouse gas emission reporting.

## Acknowledgements

First, I would like to thank my amazing team of supervisors, Keith Morrison, Rebekka Artz, Tristan Quaife, and Alessandro Gimona, who have been there to support, advise and encourage me all throughout the PhD journey. PhDs are never easy, but the addition of COVID-19 pandemic and the war in Ukraine made sure to test every bit of my endurance. While sometimes feeling isolated, startled, struggling with imposter syndrome and doubting my abilities, you were there to offer affirmation and encouragement.

Thanks to my funders, NERC, University of Reading and The James Hutton Institute, for making this project possible. Thanks to RSPB And Peatland ACTION for data and access to their beautiful peatland sites. Thanks to my two PhD examiners, Angela Harris and Christopher Merchant, for an insightful viva, as well as Thorwald Stein for being part of my PhD monitoring committee, thanks for all the thoughtful comments and valuable feedback I received over the years.

Thanks to everyone at The James Hutton institute, particularly the peatland team, Rebekka, Catherine, Gillian, Ailsa, Mhairi, Tom, Jake, and Marek. This PhD would not have been written without data you have collected, and I have truly enjoyed being out in the field with you, attending conferences and meetings together and simply having conversations over a cup of coffee.

Thanks to the University of Reading graduate school, my fellow PhD colleagues both at the university and JHI, you were all a great support and examples to look up to.

Finally, my most dear ones. My family and dearest friends for unconditional love, encouragement, and support. Zak for being with me through highs and lows, but particularly for those difficult moments, you always knew how to cheer me up.

There were times when I doubted myself, but you all helped me to stay focused on my goal. Coming from a woman, a foreigner and the first in the family to finish university, let this be another proof that no dream is too big and no dreamer too small!



*“You must do the thing you think you cannot do.”*

-Eleanor Roosevelt-

## Table of Contents

Declaration.....	2
General Abstract .....	3
Acknowledgements.....	4
Table of Contents.....	5
List of tables .....	9
List of figures.....	11
1. Introduction.....	20
1.1. Motivation.....	20
1.2. Objectives .....	20
1.3. Thesis structure .....	21
2. Background of peatland monitoring using remotely sensed data .....	23
2.1. Introduction.....	23
2.2. Peatland ecosystem .....	24
2.2.1. Peatland types and global distribution .....	24
2.2.2. Peatland formation .....	26
2.2.3. Peatlands and environmental change .....	28
2.2.4. Peatland water table depth importance .....	29
2.2.5. Degraded peatlands and their restoration.....	29
2.3. Peatland monitoring using Remote Sensing .....	32
2.3.1. Active sensors .....	33
2.3.2. Passive sensors.....	37
2.3.2.1. Vegetation and Water Indices.....	37
2.3.3. Estimation of Gross primary productivity and Net Ecosystem Exchange in peatlands....	
.....	39
2.4. Main present challenges, gaps and future possibilities for remote peatland monitoring ..	
.....	40
3. High resolution C-band SAR backscatter response to peatland water table depth and soil moisture: a laboratory experiment <sup>1</sup> .....	43

Abstract.....	43
3.1. Introduction.....	44
3.2. Materials and methods .....	47
3.2.1. Laboratory measurement.....	47
3.2.1.1. ‘Bog in the box’ experimental setup.....	47
3.2.1.2. Radar Data Collection.....	50
3.2.1.2.1. Tomographic profiling and weighted mean height .....	50
3.2.2. Statistical modelling.....	51
3.3. Results.....	52
3.3.1. Radar backscattering signal strength and phase response to change in water table depth. .....	54
3.3.2. Radar backscattering signal strength response to change in soil moisture.....	54
3.3.3. Weighted Mean Height .....	55
3.4. Discussion .....	56
3.5. Conclusion .....	59
4. Potential for peatland water table depth monitoring using Sentinel-1 SAR backscatter: case study of Forsinard Flows, Scotland, UK <sup>2</sup> .....	60
Abstract.....	60
4.1. Introduction.....	61
4.2. Materials and Methods.....	62
4.2.1. Study Area .....	62
4.2.2. Water table depth and Meteorological Data.....	64
4.2.3. Remotely sensed data.....	65
4.2.4. LiDAR data and TRI analysis.....	66
4.2.5. Model generation and statistical analysis.....	66
4.3. Results.....	67
4.3.1. Water table depth and Sentinel-1 time series analysis .....	67
4.3.1.1. Near-natural peatlands – control areas.....	70
4.3.1.2. Restoration – felled to waste.....	71
4.3.1.3. Restoration with additional management.....	72

4.3.2. Correlation of Sentinel-1 backscatter and water table depth.....	73
4.3.2.1. SLR model .....	73
4.3.2.2. MLR model.....	74
4.3.2.3. RF model.....	76
4.4. Discussion .....	80
4.5. Conclusions.....	83
4.6. Additional data.....	84
4.6.1. WTD modelling using Peatland ACTION data .....	84
4.6.2. NEP comparison of observed and modelled water table depth.....	87
5. An exploration of methods to monitor trajectories and identify change points in peatland restoration projects using remotely sensed data .....	90
5.1. Introduction.....	90
5.2. Materials and Methods.....	91
5.2.1. Study Area .....	91
5.2.2. Time series .....	92
5.2.2.1. Sentinel-1 data and modelled WTD data .....	93
5.2.2.2. MODIS NDWI, NDMI and NDVI data preparation.....	95
5.2.3. Time series preparation.....	96
5.2.3.1. Autocorrelation and cross-correlation.....	96
5.2.3.2. Decomposition, trend and change point analysis.....	97
5.3. Results.....	98
5.3.1. Modelled WTD .....	98
5.3.2. Annual density plots and descriptive statistics.....	99
5.3.3. Auto-correlation and Cross-correlation analysis.....	102
5.3.4. Time-Series decomposition.....	103
5.3.4.1. Trend analysis using Mann-Kendall test and Theil-Sen estimator .....	107
5.3.4.2. Trend and change point analysis using BFAST algorithm and Pettitt's test.....	110
5.3.4.3. Residual analysis .....	114
5.4. Discussion .....	117

6. Discussion and Conclusions .....	120
6.1. Summary of research .....	120
6.2. Further developments.....	123
6.2.1. Expanding water table depth modelling to a wider list of peatland sites and perform spatial analysis .....	123
6.2.2. Potential refinements for the water table depth model.....	124
6.2.3. Modelled WTD as a proxy for GHG emission reporting.....	127
6.3. Concluding remarks .....	128
Appendices .....	129
A. Supplementary material for Chapter 3 .....	129
B. Supplementary material for Chapter 4 .....	131
References.....	132



## List of tables

<b>Table 2.1.</b> Key terms used in peatlands literature – as described in Chambers (2003); Rodwell (1991); Rydin and Jeglum (2015).....	25
<b>Table 2.2.</b> Main peatland degradation types (as described by Holden and Burt (2002), Allott et al., (2009), Carless et al. (2019).....	29
<b>Table 4.1.</b> Forsinard Flows Talaheel site’s characteristics. *Mean water table depth between September 15, 2018, and July 31, 2020. ....	68
<b>Table 4.2.</b> Forsinard Flows Lonielist sites’ characteristics. Two Lonielist restoration sites with additional management are used in the study and described as a) LO_BCFB and b) LO_CT. * Mean water table depth between September 15, 2018, and July 31, 2020. ....	68
<b>Table 4.3.</b> Forsinard Flows Cross Lochs sites’ characteristics. Two near-natural Cross Lochs sites were used in the study, and are described as a) CL_CON and b) CL_CON_EC (location of the long-term GHG monitoring station). * Mean water table depth between September 15, 2018, and July 31, 2020. ....	69
<b>Table 4.4.</b> SLR, MLR and RF model performance using training (70%) and validation (30%) datasets, terrain ruggedness index (TRI), standing water presence (percentage of the total area) and forestry ridge and furrow lines position (aspect in degrees, with True North being 0°) of individual sites. ***i indicates a .001 significance level, **i indicates a .01 significance level, *i indicates a .05 significance level. ....	78
<b>Table 4.5.</b> NEP prediction using annual mean WTD as proposed by Evans et al. (2021), comparison of observed and SAR-based modelled WTD for Forsinard Flows research sites (detailed site descriptions in Chapter 4). All mean annual WTD values were calculated between Sep 15, 2018 and July 31, 2020. $WTD_{obs}$ was calculated using all daily WTD observation, $WTD_{obs\_lim}$ was calculated using daily WTD observations only for the days when radar imagery was available (as for model training), $WTD_{mod}$ shows the modelled WTD values. $NEP1_{obs}$ and $NEP1_{mod}$ are the predicted NEP fluxes based on equation 6.1 and observed and modelled WTD respectively; $NEP2_{obs}$ and $NEP2_{mod}$ are the predicted NEP fluxes based on equation 6.2 and observed and modelled WTD respectively. $\Delta NEP1$ and $\Delta NEP2$ shows the difference in NEP prediction between using observed and modelled WTD. All WTD values are expressed in cm. All NEP values are expressed in tons of carbon per hectare and year ( $t\ C\ ha^{-1}\ yr^{-1}$ ). Negative NEP values indicate net $CO_2$ uptake ( $CO_2$ sink).....	88
<b>Table 4.6.</b> $CH_4$ prediction using annual mean WTD as proposed by Evans et al. (2021); comparison of observed and SAR-based modelled WTD for Forsinard Flows research sites. All mean annual WTD values were calculated between Sep 15, 2018 and July 31, 2020. $WTD_{obs}$ was calculated	

using all daily WTD observation,  $WTD_{obs\_lim}$  was calculated using daily WTD observations only for the days when radar imagery was available (as for model training),  $WTD_{mod}$  shows the modelled WTD values.  $CH_4flux_{obs}$  and  $CH_4flux_{mod}$  are the predicted  $CH_4$  fluxes based on equation 6.3 and observed and modelled WTD respectively.  $\Delta CH_4flux$  shows the difference in  $CH_4$  prediction between using observed and modelled WTD. All WTD values are expressed in cm. All  $CH_4$  values are expressed in tons of carbon per hectare and year ( $t\ C\ ha^{-1}\ yr^{-1}$ ). Positive values indicate  $CH_4$  source..... 89

**Table 5.1.** Indices and bands used for the time series creation. Index equations are given using the band spectra and corresponding MODIS bands. .... 95

**Table 5.2.** Descriptive statistics of the NDVI, NDWI, NDMI (2003-2021) and modelled WTD (2015-2021) time series. Negative WTD values indicate inundation..... 101

**Table 5.3.** Mann-Kendall trend and Sen’s slope test results for the period after initial restoration and before the additional restoration management (January 2007 – September 2015), number of observations (n) for each area = 104) \*\*\* indicates a .001 significance level; \*\* indicates a .01 significance level; \* indicates 0.05 significance level. .... 108

**Table 5.4.** Mann-Kendall trend and Sen’s slope test results for the period after the additional restoration management and before the 2018 drought (March 2016 – April 2018, number of observations (n) for each area = 25). \*\*\* indicates a .001 significance level; \*\* indicates a .01 significance level; \* indicates 0.05 significance level. .... 108

**Table 5.5.** Mann-Kendall trend and Sen’s slope test results for the period after the 2018 drought until the end of 2021 (September 2018 – December 2021, number of observations (n) for each area = 40). \*\*\* indicates a .001 significance level; \*\* indicates a .01 significance level; \* indicates 0.05 significance level. .... 109

**Table 5.6.** Change points identified by BFAST algorithm and Pettitt’s test. All listed change points were found to be statistically significant at a .05 significance level. .... 113

## List of figures

- Figure 2.1.** Global distribution of peatlands. Although uncertainties about the precise extent of peatlands worldwide remain, it is clear that in some areas peatlands form an important part of the landscape. Map produced by UNEP (2022)..... 25
- Figure 2.2.** Distinct complex bog pool system in a pristine bog South-East from Forsinard as seen in an aerial photography on Google Earth. .... 28
- Figure 2.3.** Schematic illustration of WTD influence on radar backscatter. If no other condition on the ground changes, backscatter will be strong when WTD is shallow, very near to the surface (pristine peatland); the weakest in inundated areas because of the specular reflection and relatively low in areas with deep WTD (drained peatlands); backscatter from restored sites on the other hand might be higher due to the changed rougher surface..... 35
- Figure 2.4.** Sentinel-1 VV polarization radar imagery over Forsinard Flows, Northern Scotland, taken on 12/08/2018. Specular reflection is very easily distinguishable by the dark pixels over water surfaces (North Sea, lochs). Double bounce scattering is visible over urban areas (Thurso in the north, Wick in the east) and mountain range on the left. The rest of the imagery is mainly forested, agricultural, grassland and peatland areas that appear as diffuse backscatter or speckle, appearing as a grainy "salt and pepper" texture in the image. .... 35
- Figure 2.5.** Sentinel-1 pseudo RGB composite (Red: VV, Green: VH, Blue: VV/VH) captured on 27/09/2015 (left), and Sentinel-2 true colour RGB (right) imagery over Forsinard Flows RSPB captured on 29/09/2015 (right). .... 36
- Figure 2.6.** Transect of NDVI values over natural peatbog (reference/target state) and a restored site (felled between 2010-2011) located next to each other in the east part of the Forsinard Flows RSPB Reserve. Both Sentinel-2 images used for NDVI calculation were captured in the month of September, four years apart. .... 38
- Figure 3.1.** Radar backscattering characteristics based on the water level position in peatlands. .... 45
- Figure 3.2.** a) Schematic of the radar measurement system and experiment setup. The bog was surrounded on its bottom and sides by a waterproof butyl rubber liner and sat upon a stable bed of dry sand (25 cm deep). b) Photograph of the ‘Bog in the box’ laboratory setup. c) *Sphagnum* segment, representing predominantly moss vegetation. d) *Ericaceous* (heather) segment, representing moss layer covered with dwarf-shrub vegetation..... 48
- Figure 3.3.** Average, minimum, and maximum air temperatures in the laboratory during the experiment. .... 49
- Figure 3.4.** Cross-sectional views of the backscattering values from the selected peatland ROI (255 cm (l) × 100 cm (w) × 50cm (d)) before the drought, constructed using a 10° incidence angle. The

position of the trough is shown by the horizontal white line. The red dotted oval indicates an area with heather cover and hence increased volume scattering in Cross polarization (calculated as mean of HV and VH) can be seen..... 52

**Figure 3.5.** Time series of radar backscattering (a) and phase (b) measurements reconstructed using VV, HH and Cross polarization and 10° incidence angle. Each backscatter datum is the result of an incoherent summation of pixels across the selected ROI (255 cm (l) × 1 m (w) × 50cm (d)), extracted for each image in the time series. The red dashed lines indicate the beginning (21/01/2021) and end (17/05/2021) of the simulated drought period. .... 53

**Figure 3.6.** Correlation analysis between water level and radar backscatter (above) and differential phase (below) during the drought period (95 days with WL reaching 22 cm below the surface).54

**Figure 3.7.** Soil moisture and backscattering strength response to drought (117 days of drought). Drying curves of the 6 soil moisture probes at 3-22 cm depth..... 55

**Figure 3.8.** ROI backscatter weighted mean height change throughout the 117-day drought period.. 56

**Figure 4.1.** Peatland extent in northern Scotland (Aitkenhead and Coull, 2020) and the chosen study sites in the Forsinard Flows. The green triangles show the near-natural peatland study sites, and the red triangles show sites with ongoing restoration. .... 63

**Figure 4.2.** Forsinard Flows research site – different polygon colours represent the different management methods applied to peatland restoration. The eleven WTD monitoring points represent the chosen locations for analysis – 4 near-natural control sites, 3 Restoration (FTW), 4 Restoration+ sites..... 64

**Figure 4.3.** Observed water table depth (left) and Sentinel-1 (right; VV in red, VH in yellow) backscatter time series for near-natural peatland sites in Forsinard Flows area. The black horizontal line indicates the ground surface..... 71

**Figure 4.4.** Observed water table depth (left) and Sentinel-1 (right; VV in red, VH in yellow) backscatter time series for peatland sites with simplistic restoration (felling to waste) applied. The black horizontal line indicates the ground surface. .... 72

**Figure 4.5.** Observed water table depth (left) and Sentinel-1 (right; VV in red, VH in yellow) time series for sites undergoing more advanced restoration applied (brash crushing, furrow blocking and re-profiling). The black horizontal line indicates the ground surface. .... 73

**Figure 4.6.** SLR model output for Forsinard Flows sites (predicted vs observed WTD) for a) all data points; b) splitting data into the individual sites. The red line represents a perfect agreement between prediction and field measurement..... 74

**Figure 4.7.** MLR model output for Forsinard Flows sites (predicted vs observed WTD) for a) all data points; b) splitting data into the individual sites. The red line represents a perfect agreement between prediction and field measurement..... 75

**Figure 4.8.** MLR model residual statistics. Clockwise from upper left: 1) Comparison of the residuals of the MLR model against the fitted values produced by the model; 2) Quantile-quantile plot: confirms that both sets of quantiles came from the same (normal) distribution except the upper quantiles where the points stray above the line indicating some deviation of the error from normality, this, however, is a small portion of the data; 3) Scale-Location plot, uses the square root of the standardized residuals instead of the residuals themselves 4) Leverage plot, no standardized residuals are outside of the Cook’s distance boundaries, indicating that there are no strong outliers influential to the regression results. .... 76

**Figure 4.9.** RF model output for Forsinard Flows sites (predicted vs observed WTD) for a) all data points and b) splitting data into the individual sites. The red line represents a perfect agreement between prediction and field measurement..... 77

**Figure 4.10.** Random Forest model variable importance for the WTD prediction. The percentage increase in mean square error (%incMSE) is shown on the x axis and the circles represent the increase in node purity. The smaller these two parameters are, the less change in model is observed when specific variable is removed or added. The variable ranking showed well how valuable the inclusion of categorical variables was for improvement of the WTD prediction. .... 78

**Figure 4.11.** Modelled and observed water table depth series based on the MLR and RF models. The black horizontal line indicates the ground surface. Panels with green background indicate the control sites, orange - Restoration+ sites and Restoration (FTW) sites have red background..... 79

**Figure 4.12.** Peatland ACTION restoration sites. .... 84

**Figure 4.13.** RF model output for Peatland ACTION sites showing predicted vs observed WTD in each of the degradation groups. The red line represents a perfect agreement between prediction and field measurement. .... 85

**Figure 4.14.** Sentinel-1 based modelled (dark blue) and field observed (orange) WTD for Peatland Action sites. The black horizontal line indicates the ground surface..... 86

**Figure 5.1.** Overview of the Cross Lochs study area and the four chosen study sites: 1. Control1, 2. Control with EC tower (Control2), 3. Restored (FTW) and 4. Restored+. Each analysed site is a circular area with a 30 m radius and has a WTD monitoring dip roughly in the centre of it. The second control site (Control2) was additionally added because it represents an area of best locally available blanket bog condition surrounded with small water bodies, while Control1 is a slightly drier area, which historically would have been prioritised for forestry operations..... 92

**Figure 5.2.** Data processing methodology flowchart for time series analysis..... 93

**Figure 5.3.** Sentinel-1 based modelled (dark blue) and field observed (orange) WTD at the Cross Lochs sites. CL\_CON = Cross Lochs Control site 1, CL\_CON\_EC = Cross Lochs Control site 2, CL\_FTW = Cross Lochs Restored (FTW) site, CL\_BCFB = Cross Lochs Restored+ site..... 94

**Figure 5.4.** Comparison of histograms and Q-Q plots for observed and predicted WTD at the Cross Lochs sites. Both data sets are right skewed with tails towards deeper water table depths. .... 94

**Figure 5.5.** Modelled WTD using the Sentinel-1 and RF method for time period 2015 – 2021. CL\_CON = Cross Lochs Control site 1, CL\_CON\_EC = Cross Lochs Control site 2, CL\_FTW = Cross Lochs Restored (FTW) site, CL\_BCFB = Cross Lochs Restored+ site. A noticeable bias can be observed towards the lowest WTD values during summer drawdowns, when the difference between modelled and observed WTD has been up to 20 cm..... 98

**Figure 5.6.** Annual density plots for the three Cross-Lochs peatland condition groups: a) MODIS NDVI time series (2003-2021, 250 m resolution); b) MODIS NDWI time series (2003-2021, 500 m resolution); c) MODIS NDMI time series (2003-2021, 500 m resolution), and d) Sentinel-1 based modelled WTD time series (2015-2021, 20 m resolution). .... 100

**Figure 5.7.** Cross-Lochs area, boxplots for the four indicators investigated, 2015 example. The horizontal lines correspond to the medians, upper and lower hinges indicate the first and third quartiles, upper and lower whiskers correspond to the maximum and minimum values. .... 101

**Figure 5.8.** Average monthly box plots (NDVI, NDWI, and NDMI 2003-2021; modelled WTD 2015-2021 (as observed in the comparison with field gathered WTD values, the actual summer WTD values can be up to 15 cm lower). The horizontal lines correspond to the medians, upper and lower hinges indicate the first and third quartiles, upper and lower whiskers correspond to the maximum and minimum values. .... 102

**Figure 5.9.** Grid of plots of the sample ACFs (diagonal, highlighted) and CCFs (off-diagonal) using 6 years of data (72 lags). The x-axes show the lags in months and the y axis show the correlation coefficient. The left side of the diagonal of the plot grid shows the negative lags; when the variables on x-axes lead over ones on y or, meaning, the successor activity will overlap the predecessor activity. The right side of the diagonal shows the positive lags; when the x variables (column series) lag compared to y (row series), meaning the successor activity will have a waiting period before starting. .... 103

**Figure 5.10.** Decomposed NDVI time series. The red shaded area indicates the tree felling (2005-2006) in both restored sites, while the time period shaded in orange shows the additional brash crashing and furrow blocking applied to the Cross Lochs Restored+ site (Oct 2015 – Feb 2016). Series based on MODIS 250 m resolution NDVI product. .... 104

**Figure 5.11.** Decomposed NDWI time series. The red shaded area indicates the period of tree felling in both restored sites (2005-2006), while the time period shaded in orange shows the additional brash crashing and furrow blocking applied to the Cross Lochs Restored+ site (Oct 2015 – Feb 2016). Series based on the MODIS 500 m resolution surface spectral reflectance product. .... 105

**Figure 5.12.** Decomposed NDMI time series. The red shaded area indicates the tree felling in both restored sites (2005-2006), while the time period shaded in orange shows the additional brash

crashing and furrow blocking applied to the Cross Lochs Restored+ site (Oct 2015 – Feb 2016). Series based on the MODIS 500 m resolution surface spectral reflectance product. .... 106

**Figure 5.13.** Decomposed modelled WTD time series for the three condition groups. The area shaded in orange shows the period of additional brush crashing and furrow blocking applied to the Cross Lochs Restored+ site (Oct 2015 – Feb 2016). Series based on the Sentinel-1 20x22 m resolution IW GRD product..... 107

**Figure 5.14.** BFAST decomposition using NDVI (2003-2021) series (left) and modelled WTD (2015-2021) (right) for each of study areas: a) Control1, b) Control2, c) Restoration (FTW), d) Restoration+. The top panel in each individual plot shows the original time series; the second panel from the top shows the seasonal component and any breaks identified in the seasonal component; the third panel from the top shows the trend, identified breakpoints and their slope and significance values for each identified trend segment and the 95% confidence interval for the timing of breaks. The MODIS NDVI product has a 250 m resolution; Modelled WTD is based on the Sentinel-1 product with 20x22 m resolution. .... 111

**Figure 5.15.** BFAST decomposition using NDWI (2003-2021) series (left) and NDMI series (20103-2021) (right) for each of study areas: a) Control1, b) Control2, c) Restoration (FTW), d) Restoration+. The top panel in each individual plot shows the original time series; the second panel from the top shows the seasonal component and any breaks identified in the seasonal component; the third panel from the top shows the trend, identified breakpoints and their slope and significance values for each identified trend segment and the 95% confidence interval for the timing of breaks. No breakpoints have been identified in the NDWI series; while one change point has been identified in each of the areas using NDMI series. Both NDMI and NDWI are 500 m resolution products..... 112

**Figure 5.16.** Residual analysis for NDVI series (2003 – 2021). For each area the individual plots show a) the reminder component after time series decomposition, b) autocorrelation function (ACF) plot (the blue dashed lines indicate the confidence level ( $\alpha=0.95$ )), c) distribution of the residuals, d) Q-Q (quantile-quantile) plot (x axis representing the theoretical quantiles and y axis the data sample quantiles). .... 114

**Figure 5.17.** Residual analysis for NDWI series (2003 – 2021). For each area the individual plots show a) the reminder component after time series decomposition, b) ACF plot (the blue dashed lines indicate the confidence level ( $\alpha=0.95$ )), c) distribution of the residuals, d) Q-Q plot (x axis representing the theoretical quantiles and y axis the data sample quantiles). .... 115

**Figure 5.18.** Residual analysis for NDMI series (2003 – 2021). For each area the individual plots show a) the reminder component after time series decomposition, b) ACF plot (the blue dashed lines indicate the confidence level ( $\alpha=0.95$ )), c) distribution of the residuals, d) Q-Q plot (x axis representing the theoretical quantiles and y axis the data sample quantiles). .... 116

**Figure 5.19.** Residual analysis for modelled WTD series (2015 – 2021). For each area the individual plots show a) the remainder component after time series decomposition, b) ACF plot (the blue dashed lines indicate the confidence level ( $\alpha=0.95$ ), d) distribution of the residuals, d) Q-Q plot (x axis representing the theoretical quantiles and y axis the data sample quantiles)..... 117

**Figure 6.1.** The heather segment of the trough before (20<sup>th</sup> November 2020) and after the drought and rewetting (4<sup>th</sup> June 2021). While the mosses appear green and healthy, it can be seen that the heather and grasses have died back..... 126



## List of Acronyms

<b>Acronym</b>	<b>Definition</b>
ACF	Autocorrelation Function
AMSR2	Advanced Microwave Scanning Radiometer 2
APSYS	Advanced Pixel System using Intermittent Small Baseline Subset
ASCAT	The Advanced Scatterometer
BCFB	Brash crushing and furrow blocking
BFAST	The Breaks For Additive Seasonal and Trend method
C	Carbon
CCF	Cross Correlation Function
CEDA	The Centre for Environmental Data Analysis
CH <sub>4</sub>	Methane
CL	Cross Lochs
CO <sub>2</sub>	Carbon dioxide
CON	Control (near-natural site)
CT	Cross Tracking
dB	Decibel
DEM	Digital elevation model
DInSAR	Differential Interferometric Synthetic Aperture Radar
DoY	Day of the year
DSM	Digital Surface Model
EC	Eddy Covariance
ESA	European Space Agency
EUMETSAT	European Organisation for the Exploitation of Meteorological Satellites
EVI	Enhanced Vegetation Index
FTW	Fell to waste
GAM	Generalized additive model
GEE	Google Earth Engine
GHG	Greenhouse gases
GPP	Gross Primary Productivity
GRD	Ground Range Detected
InSAR	Interferometric Synthetic Aperture Radar
IUCN	The International Union for Conservation of Nature
IW	Interferometric Wide Swath

JAXA	Japan Aerospace Exploration Agency
JPL	NASA's Jet Propulsion Laboratory
LiDAR	Light Detection and Ranging
LO	Lonielist
LUE	Light Use Efficiency
MK	Mann-Kendall test
MLR	Multiple Linear Regression
MODIS	Moderate Resolution Imaging Spectroradiometer
NASA	National Aeronautics and Space Administration
NDMI	Normalised Difference Moisture Index
NDVI	Normalised Difference Vegetation Index
NDWI	Normalised Difference Water Index
NEE	Net Ecosystem Exchange
NEP	Net Ecosystem Production
NERC	The Natural Environment Research Council
NIR	Near-Infrared
PACF	Partial Autocorrelation Function
Q-Q	Quantile-quantile
QRS	Quantile Regression Forests
RCS	Radar cross-section
RF	Random Forest
RGB	Red-Green-Blue, natural colour
RMSE	Root Mean Square Error
ROI	Region of interest
RS	Remote Sensing
RSPB	The Royal Society for the Protection of Birds
SAR	Synthetic Aperture Radar
SBAS	Small Baseline Subset
SD	Standard deviation
SLC	Single Look Complex
SLR	Simple Linear Regression
SM	Soil moisture
SMAP	Soil Moisture Active Passive mission
SMOS	Soil Moisture Ocean Salinity mission
STL	Seasonal and Trend decomposition by locally estimated scatterplot smoothing

SWIR	Short Wave Infra-Red
TA	Talaheel
TP	Tomographic profiling
TRI	Terrain Ruggedness Index
UAV	Unmanned aerial vehicles
UK	United Kingdom
UNEA	United Nations Environment Assembly
UNEP	The United Nations Environment Programme
VH / HV	Vertical-Horizontal / Horizontal-Vertical
VV / HH	Vertical-Vertical / Horizontal-Horizontal
VWC	Volumetric water content
WL	Water level
WMH	Weighted mean height
WTD	Water table depth

# Chapter 1

## 1. Introduction

In this introductory chapter, the motivation behind this PhD study is outlined, the aim and objectives are defined and a description of the structure of the thesis is provided.

### 1.1. Motivation

Crucial for preserving global biodiversity, providing drinking water, minimising floods and helping addressing climate change, peatlands are among the most valuable ecosystems on Earth (Kimmel and Mander, 2010). Covering just 3% of the land's surface they sequester almost 0.4 Gt of carbon dioxide a year (Buckmaster et al., 2014; Pereira et al., 2022) but the real value lies in the amount of carbon stored, which is estimated to be >450 Gt or around one third of all the world's terrestrial soil carbon (Nungesser, 2003). This means that the carbon storage of peatlands is greater than in all other vegetation types in the world combined (Limpens et al., 2008). While being a major natural terrestrial carbon store, when damaged, peatlands can turn into carbon-emitting ecosystems. In the past, particularly in the UK, peatlands have suffered from drainage, ploughing, extraction, and afforestation. Only in the 1970's, did the switch from peatland exploitation to conservation start to take place (McMullen, 2002). These days, driven by policies and agreements, peatland conservation and restoration has become a more common land management technique. However, once restoration works have taken place, there is a need to monitor the progress of restoration. Traditionally this would include in situ observations, such as vegetation surveys and measurements of water table depth and soil moisture. While there are multiple criteria which nurture healthy peatland ecosystems, high water table depth is often described as a critical (Couwenberg et al., 2011) and is reported as having the dominant control over greenhouse gases (GHG) emissions (Evans et al., 2021; Koch et al., 2023). Given the high time and resources demand of field work, satellite data could provide a unique opportunity for alternative monitoring options. Ultimately, given the close link between peatland water table depth and GHG, WTD measurements could eventually be used as a low-cost proxy for GHG reporting to Greenhouse Gas Inventories. Besides being susceptible to moisture content, synthetic aperture radar instruments have the ability to provide data regardless of the cloud cover, which has made this remote sensing data source emerge as valuable addition to environmental applications.

### 1.2. Objectives

This project's goal was to look at the feasibility of remote, space-based monitoring of peatlands at a landscape scale by focussing on the water table depth, which is one of the critical factors in peatland ecosystem condition. It was hypothesised that the SAR signal would respond to changes in peatland

water table depth, potentially offering a method that could provide regular information about the WTD, which is highly connected to overall peatland condition, restoration efficiency and GHG exchange. To test this, multiple targets were set, starting from a controlled laboratory environment, where SAR sensitivity to peatland WTD could be tested in high detail, followed by further analysis using field-gathered WTD measurements and satellite SAR imagery. An objective was then set to assess if peatland WTD can be modelled using Sentinel-1 data. The final aim was to investigate if longer data series of modelled WTD and optical remote sensing data from MODIS satellite could be used for time series analysis and restoration effectiveness monitoring.

The three primary scientific objectives of this thesis were:

**Objective 1:** Investigate if synthetic aperture radar backscatter responds to peatland water table depth and soil moisture when using high-resolution SAR system.

**Objective 2:** Test if Sentinel-1 SAR imagery can be used to model peatland water table depth by creating and testing models with different complexity.

**Objective 3:** Explore methods for peatland restoration trajectory analysis using remote sensing datasets to assess the restoration effectiveness.

### 1.3. Thesis structure

This thesis is written as a combination of chapters and published papers. Chapters 3 and 4 are written in the style of the journal in which they have been published and full author contributions are detailed above in the declaration. All chapters in this thesis have been developed and written by me with feedback and input of my four supervisors.

Chapter 2 provides an overview of current knowledge about the peatland ecosystem, its importance and usage of remotely sensed data for peatland monitoring. Special attention is given to the significance of peatland conservation and restoration. SAR and optical remote sensing instruments are viewed as potentially effective tools for peatland monitoring purposes, but the need for further research on their effectiveness for peatland environment monitoring is pointed out. This chapter also identifies several key gaps in the field, some of which the chapters 3 – 5 aimed to address.

Chapter 3 is a laboratory study which answers Objective 1 by monitoring SAR signal response to drought in peatland in a controlled environment and at uniquely high resolution. In this study we installed a large peat sample in the University of Reading Radar laboratory and by running regular radar scans closely, followed the backscatter response as the water table depth and soil moisture decreased with a simulated four month long drought. The experiment provided a unique set of high-resolution SAR data over peatland. It allowed us to investigate the SAR signal response to changing hydrological conditions in peatland, explore the response from different polarizations of the radar signal and analyse the peat subsidence with the drought. The results from the laboratory study confirmed a clear coherent

response both in radar backscatter amplitude and phase to change in water table depth. This chapter has been published as a paper in *The International Journal of Remote Sensing* (Toca et al., 2022).

The verification that SAR responds to WTD change enabled us to move forward to Chapter 4 which addressed the Objective 2 by developing peatland WTD prediction methods using satellite SAR data. In this chapter we investigated the correlation between Sentinel-1 SAR data and field-gathered WTD measurements from blanket bogs at Forsinard Flows research area in northern Scotland. Three SAR-based models of different complexity were developed for WTD prediction. As the research area included both near-natural peatlands and those that are being restored, we could compare the WTD and SAR dynamics over a variety of peatland conditions. This chapter was submitted to the *Remote Sensing* journal special issue “*Application of Remote Sensing for Monitoring of Peatlands*” (Toca et al., 2023). The modelling outputs showed a good potential for peatland WTD monitoring in the Forsinard Flows, and once a wider dataset from Peatland Action was available, the method was further tested on additional peatland restoration sites across Scotland.

The Chapter 5 of this PhD project involved exploratory analysis to find satellite-data based methods for peatland restoration trajectory monitoring and aimed to fulfil the Objective 3. First, the method developed in Chapter 4 was used to model the WTD in four sites for the full period when Sentinel-1 data was available (2015-2022). Then, the time series of Sentinel-1 SAR-based WTD series along with indices from MODIS optical satellite imagery (NDVI, NDWI and NDMI) were analysed to assess if these RS datasets can be indicative of restoration progress over time. Both long term trajectory analysis and change point detection were used to compare trends in near-natural and restored sites that have had different restoration methods applied.

Finally, Chapter 6 draws together the main findings of the thesis and discusses some of the challenges when working with remotely sensed data over northern peatlands. It gives suggestions on how the research done in this thesis can be expanded and taken further. It also suggests proposals for potential future work that could be explored using already existing satellite mission data, like Sentinel-2, Landsat, and data from the upcoming satellite missions, like NISAR, Tandem-L and ROSE-L.

# Chapter 2

## 2. Background of peatland monitoring using remotely sensed data

This chapter describes peatland as an ecosystem with its functions and morphology and relationship to the global carbon cycle. The importance of peatlands is discussed, explaining how conservation and restoration are crucial and require effective monitoring methods. As peatlands can be vast and often located in remote areas, Remote Sensing (RS) is a promising tool for monitoring purposes. Satellite observations could potentially provide an efficient way to obtain regular information about the status of peatlands with complete spatial coverage. Currently there are multiple satellite missions that grant access to high spatial, spectral, and temporal resolution data for land monitoring purposes. The two remote sensing types, active and passive, are discussed in peatland monitoring context. Finally, challenges, future opportunities and gaps in the field associated with remote peatland monitoring are discussed.

### 2.1. Introduction

Peatlands are a type of wetland ecosystem, with unique acidic and anaerobic conditions where plant material does not fully decay and form a peat layer (Page and Baird, 2016). Peatlands are among the most valuable ecosystems on Earth, they preserve global biodiversity, improve quality of drinking water, minimise floods, and help addressing climate change (Harris et al., 2022; Kimmel and Mander, 2010). Worldwide, peatlands cover a very small percentage of the total land surface, around just 3%, they sequester almost 0.4 Gt of carbon dioxide a year and remain the largest terrestrial carbon storage, storing twice as much carbon as the world's forests (Buckmaster et al., 2014; Turetsky et al., 2015; Yu, 2012). Healthy, wet peatlands help with storage and sequestration of carbon, while damaged peatlands contribute to emissions, therefore peatlands have an important role in global climate regulation. Despite being so valuable, for a long period, peatlands have been viewed as “wastelands” - remote vast areas with poor conditions, and have suffered dramatically from drainage, ploughing, extraction, and afforestation (Humpenöder et al., 2020; Lachance et al., 2005; Sloan et al., 2018). Luckily in the past years, to tackle this nearly irreversible loss, there has been progress towards peatland protection and restoration through peatland conservation and restoration projects on global and national levels. The United Nations Environment Assembly (UNEA) adopted its first ever peatland resolution in March 2019, urging member states to conserve and restore these carbon-rich ecosystems (UNEA, 2019). The United Kingdom has taken one of the leading roles worldwide in peatland restoration, and explicitly mentions restoration in its Nationally Determined Contributions to the United Nations Framework Convention on Climate Change under the Paris Agreement. Scotland has made it as one of the priorities

for reaching the net-zero goals by 2045, and in February 2020 Scottish government announced allocation of 20M £ for peatland restoration in the following year and commitment to invest over 250M over the next 10 years (NatureScot, 2020).

## **2.2. Peatland ecosystem**

Covering more than 12.1 million km<sup>2</sup> (Ramsar Convention on Wetlands., 2018), wetlands are one of the most widespread and most biodiverse ecosystems in the world. The features that distinguish a wetland are the presence of water at or near the surface, specific soil conditions mostly characterised by low oxygen availability and a specific biota – plants that are adapted for growing within these conditions (Chambers, 2003). Peatlands, sometimes also called the “organic wetlands”, are the largest subset of wetlands (>50% of all wetlands), and presence of accumulated peat (typically at least 30 to 40cm, depending on classification in individual countries) is what sets them apart from other wetland types (Ramsar Convention on Wetlands., 2018).

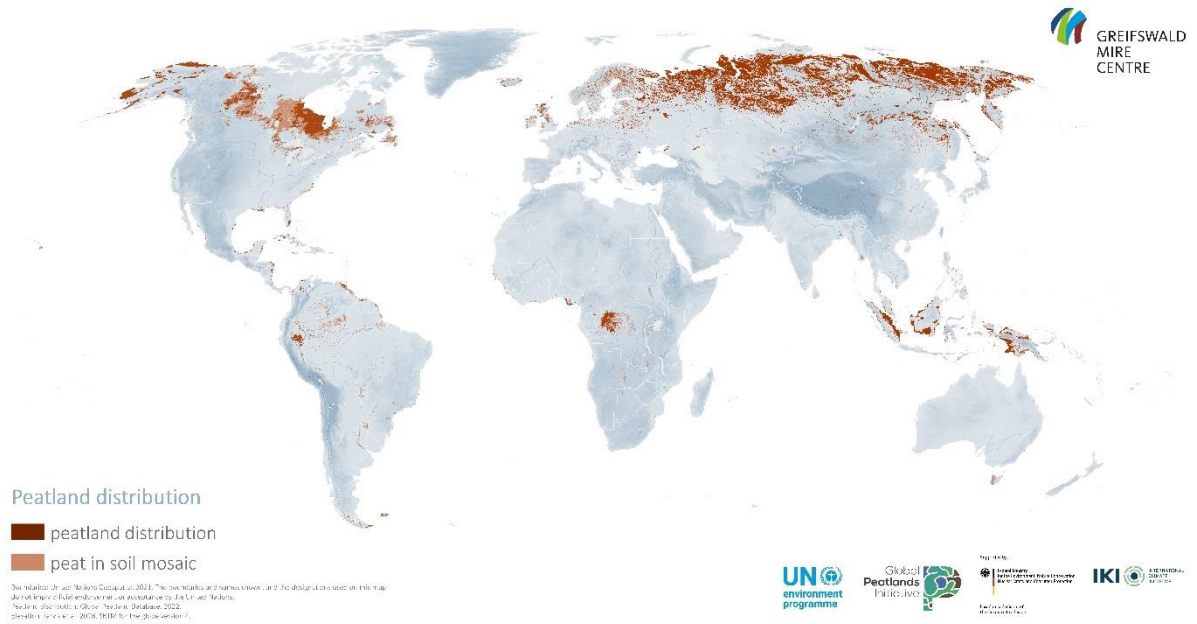
Nowadays peatlands are starting to be recognized as valuable ecosystems, but in the past have gone through tremendous degradation resulting in at least 65 million ha of degraded peatland area globally (Urák et al., 2017). Past and current land management has exposed peatlands to damaging processes such as drainage, ploughing, extraction, and afforestation. While naturally being a carbon sink, these disturbances result in peatlands becoming a large carbon emitter, annually contributing about 6% of global anthropogenic CO<sub>2</sub> emissions (Buckmaster et al., 2014). It is estimated that largely through peat fires and oxidation of the buried carbon, every year peatlands emit 2-3 Gt of CO<sub>2</sub> (Barthelmes et al., 2015). Besides contributing to our annual anthropogenic emissions, peatland destruction has a negative impact on many other important ecosystem services. In the UK around 70% of drinking water comes from peatland dominated catchments (Martin-Ortega et al., 2014). The water coming from degraded peatlands will have higher concentration of dissolved organic carbon and will have a brown tone, therefore more water treatment procedures will be necessary, including costly treatments and use of chemicals before providing clean drinking water (Ritson et al., 2016; Salimi and Scholz, 2021). Peatlands provide home for unique biodiversity and any damage to them can, in turn, be harmful for the animal and plant species living in this habitat (Minayeva et al., 2017). Other ecosystem services provided by peatlands include flood and drought mitigation (Lees et al., 2021; Ritson et al., 2016). Finally, peatlands are food and fibre providers in many parts of the world as well as protectors of palaeo-ecological (pollen) and archaeological (artifacts preserved in peat) information (Bonn et al., 2014).

### **2.2.1. Peatland types and global distribution**

Due to the specific conditions that are necessary for peat formation, the distribution of peatlands worldwide varies a lot. Certain regions and countries like Northern America, Northern Europe and Russia has vast extents of peatlands (see Figure 2.1). Although the majority of peatlands are found in



the Northern Hemisphere above 45° N, tropical peatlands in Africa, South America and particularly South-east Asia store impressive amount of carbon as well. Unfortunately, up to date there is no comprehensive mapping of worldwide peatland locations and many uncertainties about precise extent and volume of the peat remain (Chambers, 2003; J Leifeld and Menichetti, 2018). Most estimates suggest there are around or more than 400 million ha of peatlands worldwide (Biancalani and Avagyan, 2014; Charman, 2009), but many believe that especially the extent of tropical peatlands remains underestimated and might rise in the future (Xu et al., 2018).



**Figure 2.1.** Global distribution of peatlands. Although uncertainties about the precise extent of peatlands worldwide remain, it is clear that in some areas peatlands form an important part of the landscape. Map produced by UNEP (2022).

Other terms like mire, fen, bog, swamp, moss, and muskeg are common in literature about peatlands, sometimes leading to confusion. Most common terms, some of which are used also in this thesis, are explained in Table 2.1.

**Table 2.1.** Key terms used in peatlands literature – as described in Chambers (2003); Rodwell (1991); Rydin and Jeglum (2015).

Term	Description
Wetland	All ecosystems characterized by persisting water saturation with water table close to or above the land surface. Wetlands may have both organic (e.g., peatlands) and mineral substrates and those may be ecosystems with flowing and shallow waters.
Peatland	Any ecosystem with at least 30 - 40 cm of peat substrate. Peatlands can include not only wetlands, but also organic soils, where aquatic processes might have been altered though drainage, afforestation, or other disturbances.

Mire	Mire can mean either swamp, bog, fen, moor, muskeg, or peatland. “Mire” would normally be used to describe any kind of actively forming and accumulating peatland, even ones with mineral substrate.
Bog	A peatland that is ombrotrophic (receiving all their water and nutrients solely from the atmosphere), creating an acidic and nutrient-low environment.
Fen	Contrary to bogs, fens are minerotrophic mires, receiving water inputs from groundwater or surface runoff, commonly creating a more nutrient-rich and alkaline environment.
Swamp	Not well defined, loose term that might be used for describing various of the previously mentioned terms, but often refers to a fen with partial forest cover.

In this thesis, high emphasis is given to peatlands in Forsinard Flows reserve, which is a vast blanket bog ecosystem. Blanket bogs are ombrotrophic peatlands, which cover all landscape including slopes and small hills (Joint Nature Conservation Committee, 2011). Some small areas of raised bog might be present within a blanket bog, especially within larger bogs, but mostly these will be discarded, and the landscape will be classified as blanket bog.

### 2.2.2. Peatland formation

Although peatlands can be found in various climatic zones from polar regions to tropics, their distribution worldwide is not even. Depending on the geographical region and local geographical features, peatlands can have various geochemical and hydrological characteristics as well as different vegetation. The classifications vary with countries, but the main differentiation is between bogs and fens, having significant differences in vegetation, hydrology as well as water chemistry (Rodwell, 1991; Rydin and Jeglum, 2015). As explained in the Table 2.1. bogs will receive water and nutrients only with precipitation, resulting in general lack of nutrients and acidic (pH < 4.5) water, they will have a high water table and will be dominated by *Sphagnum* mosses accompanied by heather, grasses and occasionally small shrubs and trees (Urbanová et al., 2018).

Peat forms when the decomposition rate of the organic material is slower than the accumulation of the photosynthetically produced organic matter, the surplus material of partially decomposed peat then slowly accumulates, becomes compacted and forms a peat layer (Belyea and Clymo, 2001). The requirements for peat bog initiation and peat accumulation include waterlogged conditions, low pH, low nutrient availability, low oxygen supply and reduced decomposition rate (Gorham, 1991). The absence of oxygen under the waterlogged conditions is what dramatically slows the decomposition rate; therefore climate plays the leading role determining general water availability for peat initiation as well as seasonal precipitation-evapotranspiration balance (Chambers, 2003).

For blanket bogs to form, it requires very specific temperature and rainfall conditions (Gallego-Sala and Colin Prentice, 2013):

- Minimum annual rainfall of 1000 mm,
- minimum of 160 wet days,
- Minor seasonal fluctuations in temperature with the warmest month having mean temperature <math><15^{\circ}\text{C}</math>.

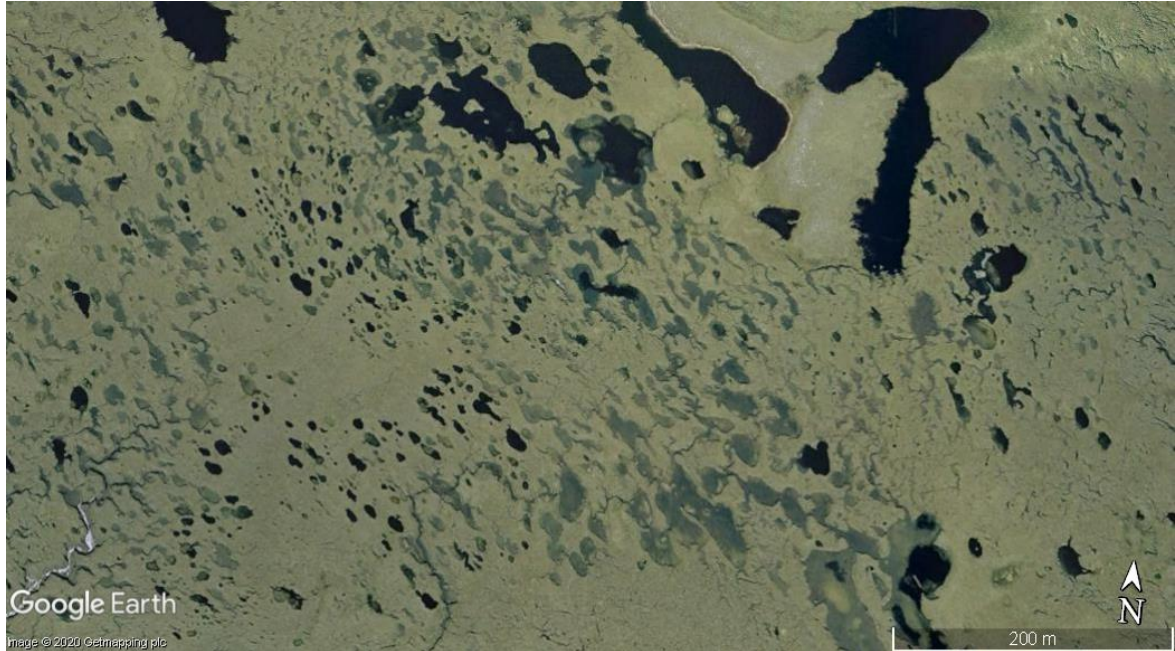
Because of these conditions, blanket bogs are usually found in temperate hyperoceanic areas (Chambers, 2003), such as the British Isles, where weather is temperate all year long and bogs can receive plenty of rainfall. These conditions are favourable for peat formation and accumulation, and thanks to this climate, up to 10 m deep peat layers can now be found in many places in the Northern Hemisphere, which have slowly been accumulating for the past 10,000 years since the last ice age (Moore et al., 2002).

Undisturbed bog in good condition will accumulate only about 2 mm of peat per year (Lindsay et al., 2014). Actively growing bogs are mainly viewed as consisting of two layers: acrotelm or the upper active layer and the lower inactive layer or catotelm. Some studies differentiate a third layer ‘mesotelm’, which is the interface between acrotelm and catotelm, where a lot of the biogeochemical processes occur (Lindsay et al., 1988). Acrotelm has loose, living vegetation and fluctuating water table (Chambers, 2003; Rydin and Jeglum, 2015). Unless the peat is bare, catotelm is permanently below the groundwater table, shielded and hidden by the overlying acrotelm (Chambers, 2003; Lindsay et al., 2014) and conventional remote sensing systems will not be able to give information about this layer. In this thesis, the focus is on the acrotelm, which experiences fluctuations and is particularly sensitive to moisture availability.

Northern peatlands are dominated by *Sphagnum* mosses, and a landscape carpeted by *Sphagnum* is one of the best-known bog characteristics. *Sphagnum* species have adjusted to thrive in wet, acidic, cool and anoxic conditions (Rydin and Jeglum, 2015). Once *Sphagnum* have become established in the bog environment, they continue to grow in numbers and create a hostile environment for themselves. Besides *Sphagnum*, other mosses and grasses such as heather *Calluna vulgaris*, cotton grass *Eriophorum sp.*, deer grass *Trichophorum cespitosum*, and purple grass *Molinia caerulea* can be found in the bogs. An increased presence of these species, however, can indicate dryer conditions due to degradation (Lindsay et al., 2014).

Another easily visible pristine bog characteristic is its small-scale surface patterning or microtopography, which is formed by the arrangements of hummocks and hollows or pools on the bog surface (Moore et al., 2019). These forms are created by varying growth-forms of differing *Sphagnum* moss species and depend on the hydrological balance of the bog, which relies on the local climate and terrain (Lindsay et al., 2014; Nungesser, 2003). Regions, like Scotland, dominated by wetter climate

will have greater water surplus, and as a result the bogs can have complex pool systems developed over time (see Figure 2.2). During longer wetter periods there will be increased hollow and pool formation, while during dry periods bogs can become dominated by mossy ridges and hummocks (Lindsay et al., 2014).



**Figure 2.2.** Distinct complex bog pool system in a pristine bog South-East from Forsinard as seen in an aerial photography on Google Earth.

### 2.2.3. Peatlands and environmental change

Except for the protective living acrotelm layer, peat remains relatively exposed to climate change, land use change or disturbances, such as drainage. Peat deposits can be several meters thick, but the carbon locked in the peat could become readily available to microbial degradation if peatland is vulnerable to rising temperatures, local hydrology changes and increased wildfires, leading to positive feedback to atmospheric forcing (Weston et al., 2015). While the common belief is that global changes, especially climate change, negatively influences the peatland environment, it is still uncertain to what extent the peatlands can be affected. The impact of climate change will also vary between different bog types, vegetation types within them and microtopographic variation in the area (Rydin and Jeglum, 2015).

Hydrological changes can have a large impact on peatland condition, and they can be triggered either by climate change or land use change, with artificial drainage having the strongest impact.


#### 2.2.4. Peatland water table depth importance

Water table depth (WTD) and soil moisture (SM) availability has the largest control over *Sphagnum* moss growth, decomposition, and peat accumulation (Thompson and Waddington, 2008). In a natural peatland ecosystem, when losing a given volume of water (through evaporation and evapotranspiration) the water table fluctuates only by a small amount. A bog surface in sites in good ecological condition follows seasonal water table rise and fall, with the peat temporarily compressing and expanding, restoring the relative position of its surface to the water table level; this phenomenon is known as “peat, bog or mire breathing” (Morton and Heinemeyer, 2019; Rydin and Jeglum, 2015). When a peat bog is drained it alters the structural and mechanical properties of the peat itself and its carbon cycle as a larger layer of peat is exposed to oxygen, resulting in greater decomposition of the peat, releasing breakdown products, including CO<sub>2</sub> which is then emitted into the atmosphere (Leifeld et al., 2019). In addition, broken, smaller, particles of peat slowly pack more closely together, resulting in further collapse and compaction of the peat matrix (Asselen et al., 2009). In a natural bog the rate of plant production will exceed this rate of decomposition of the organic material, therefore bog becomes a carbon reservoir, while drainage will have the opposite effect and from being long-term carbon reservoirs, peatlands can become net sources of GHG emissions (Biancalani and Avagyan, 2014).

#### 2.2.5. Degraded peatlands and their restoration

Peatland degradation can occur due to human-caused damage, such as drainage ditches, afforestation, peat burning and overgrazing or more indirectly through natural degradation. Typical signs of degraded peatland may include bare peat, peat gullies, drainage ditches, peat hags and pipes (see Table 2.2.). Depending on the instrument’s resolution, all features besides peat pipes, which run underground, can be manually or automatically identified using RS data (Robb et al., 2023).

**Table 2.2.** Main peatland degradation types (as described by Holden and Burt (2002), Allott et al., (2009), Carless et al. (2019)).

Degradation type	Description	Photograph
Drainage ditch	Deliberately dug, linear drains with the purpose of water table depth lowering, usually for agricultural or forestry purposes.	

Peat gully	Erosion channels, created by water collecting, running, and cutting through peat.	
Peat hagg	Isolated mound of vegetated peat, often created between gullies.	
Peat pipe	An underground channel through peat, where water runs through.	 <p><i>Photographed by Gillian Donaldson-Selby</i></p>

Nowadays peatlands are becoming recognized as very valuable ecosystems, however this change of view towards peatlands has changed only in the last decades. The first meaningful framework for peatland protection was The Convention on Wetlands (complete title: “*The Ramsar Convention on Wetlands of International Importance especially as Waterfowl Habitat*”), an international treaty for the conservation and sustainable use of wetlands and their resources, that was adopted in 1971 and came into force in 1975 (Ramsar Convention on Wetlands., 2018). Initially only sites with rare water birds were selected for protection, but nowadays any highly valuable wetland (based on their ecological, botanical, zoological, limnological or hydrological importance ) is considered, and to date UK has 175 Ramsar sites (Ramsar Convention on Wetlands., 2018). While the first framework for wetland protection was created in the 1970’s, it took much longer for a global framework specifically for peatland protection. The United Nations Environment Assembly (UNEA) adopted its first ever peatland resolution only in March 2019, urging member states to conserve and restore these carbon-rich ecosystems (UNEA, 2020), while the International Union for Conservation of Nature (IUCN) UK Peatland Programme, promoting peatland restoration in UK was set up already in 2009.

Peatland restoration projects take measures that aim to restore peatlands to their original forms and functions. Methods for peatland habitat restoration vary, but there are multiple criteria restoration projects aim to achieve (Anderson and Anderson, 2010; Gatis et al., 2017; Lees et al., 2021), some of the main ones include:

- Removal of non-native species (e.g., removal of woodlands).
- Reintroduce high water table depth.
- Create a near-flat surface with minimal presence of brash, stumps or legacies of former drainage or erosion patterns.
- Revegetation, including the return of native species.

After tree removal in afforested sites, restoring site hydrology is usually the principal activity in restoration sites and peatland rewetting can be achieved using variety of techniques like drainage ditch blocking, peat dams, *Sphagnum* transfer and planting, control of grazing and burning and others (Chimner et al., 2017).

In the UK early peatland-restoration efforts began only in 1995, at that time focusing on restoring bird habitats in blanket bogs that had been afforested (Hancock et al., 2013). Back then the simplest bog restoration method used was felling to waste, when felled trees were laid in the plough furrows and left for decaying. Other methods involved felling and extracting felled trees over brash roads or the mulching to waste method, which means mulching the woody material and spreading it across the site (Hancock et al., 2013). More recently, peatland restoration projects are using additional methods to accelerate and insure successful forest-to-bog transformation. If the felled to waste method had been used in the past, it is advised to carry out crushing of waste trees further down into the plough-furrows, but it requires passage of the machinery, which means disturbance for the vegetation (Artz et al., 2018). Machinery can also smooth the surface by removing the plough throws and ditches within a forestry plantation, this way topography can be evened out and more of the ground surface will be in contact with the water table, this method is sometimes referred to as “ground or surface smoothing” (Dinesen and Hahn, 2019) or if the machinery is flattening the ground by driving over an area with a low pressure vehicle it can be referred to as “cross tracking” (heavy machinery is avoided to avoid further peat compaction) (Artz et al., 2018; Norris et al., 2016). Creating peat dams in plough-furrows and ditches is another method to achieve a high water table quicker and speed up the restoration process. There are several known methods for blocking the ditches, and materials that are used can include peat itself, wooden or plastic plates and iron sheet plates (Dinesen and Hahn, 2019). Stump flipping is another method that has been used in some of the restoration projects in the Forsinard Flows bogs. This method involves peeling the root plates of old tree stumps out of the surface peat, flipping them upside down and firmly pushing them back into the peat (Hancock et al., 2018).

Carbon accumulation in peatlands is aided by the process of anaerobic decomposition, which are the same conditions that favour methane production (Dise, 2009). As to the effect on climate, while there is a warming effect through CH<sub>4</sub> emissions, CO<sub>2</sub> uptake, total accumulated peat carbon and peatland initiation dates suggest a net cooling effect from peatlands over the previous millennia (Frolking and Roulet, 2007). Therefore, while peatland restoration might have some negative impacts in short-term, long-term accounting proves how valuable carbon sinks peatlands are, besides their restoration accounts for other benefits like biodiversity increase, flood protection and water retention and purification (Ramchunder et al., 2012).

### **2.3. Peatland monitoring using Remote Sensing**

Remote Sensing (RS) is the process of obtaining information about physical characteristics of an area of interest from a distance. Typically mounted on aircrafts, unmanned aerial vehicles (UAVs) or satellites, special sensors collect remotely sensed images, measuring radiation reflected and emitted by the observed area.

The main advantages of using remotely sensed data include accessibility of data, large spatial coverage, and accessibility to remote locations. The main disadvantages remain the remoteness of the instrument from the target, and the fact that RS instruments are not measuring surface properties, such as soil moisture or gas fluxes directly, only the energy incident at the sensor, which then must be used to infer the characteristics of the area of interest (Sayn-Wittgenstein, 1992).

Some of the most widely used applications for land monitoring using satellite imagery can be applicable to monitoring peatlands, and include:

- water table depth (Asmuß et al., 2019; Meingast et al., 2014),
- soil moisture (Dabrowska-Zielinska et al., 2016; Millard et al., 2018),
- vegetation health,
  - vegetation fraction (McPartland et al., 2019; Räsänen et al., 2020),
  - greenness of vegetation cover (Lees et al., 2021; Zeng et al., 2020),
  - start/end of the growing season (Pang et al., 2021; Park et al., 2016),
- land cover change (Minasny et al., 2019),
- droughts and floods (Gaveau et al., 2014; Hidayat et al., 2012),
- thermal conditions (Junttila et al., 2021) (Iizuka et al., 2018).

In this thesis I focused on the peatland water table depth, soil moisture and vegetation monitoring, all of which are crucial for peatland ecosystem condition monitoring.

Remote sensing instruments can be divided into two main types: active and passive. The most common source of radiation is the sunlight and the energy coming from the sun is either reflected



(visible wavelengths) or absorbed and later re-emitted (thermal infrared wavelengths) and passive sensors detect this natural energy (radiation) coming from the object or scene being observed (Maliva and Missimer, 2012). In contrast, active sensors must rely on their own energy source for illumination, they emit radiation and later detect and measure the reflection coming back from the target. The use of active sensors, especially radar imagery, for peatland monitoring is still far less exploited technique compared to optical imagery (passive sensor). These two types of RS instruments are further discussed in the following sections.

### **2.3.1. Active sensors**

Active sensors are independent of solar illumination and the majority of these sensors operate in the microwave portion of the electromagnetic spectrum. In this thesis the emphasis is on radar sensors, which are the most used active sensors in remote sensing. Other active RS sensors include light detection and ranging sensors (LiDAR), laser altimeters, ranging instruments, scatterometers and sounders. Radar instruments actively send out their own form of electromagnetic signal in a series of pulses from a radar antenna. Once the signal reaches the target, the energy is scattered and a portion of it is reflected to the antenna (Maliva and Missimer, 2012). By detecting, measuring, and timing the backscattered signal it is possible to find out the distance or range to the target. As the radar sensor passes by, it collects both range and magnitude of the energy reflected from all targets and a two-dimensional image of the surface is produced. Along with independence of solar illumination, the main advantage of using a radar instrument is its capability to image in almost all-weather conditions, which is an important aspect in areas prone to cloud-cover, like peatlands (Guo et al., 2017).

The use of radars for earth observation purposes began with Seasat satellite launched in 1978, operated by NASA/JPL/Caltech, and since there have been over 20 space-based radar missions launched by different space agencies around the world (Belward and Skjøien, 2015). Some of the best-known missions for monitoring vegetated areas included European Space Agency's (ESA) ERS-1 and ERS-2, Canadian Space Agency's RADARSAT-1 and RADARSAT-2, EUMETSAT's Metop Advanced SCATterometers (ASCAT) and Japan Aerospace Exploration Agency's (JAXA) Advanced Microwave Scanning Radiometer 2 (AMSR2) mission. More recently, ESA's Sentinel-1 has gained a high recognition.

Sentinel-1 is the European Space Agency's imaging radar mission that was launched in 2014, providing continuous all-weather, day-and-night imagery, operating at C-band. Sentinel-1 has a Synthetic Aperture Radar (SAR) sensor with wide swath (250 km) and high spatial resolution (20 × 22 m (range × azimuth) spatial resolution and 10 × 10 m pixel spacing for Level-1 product) providing dual polarisation coverage over landmasses (ESA, 2022). It was designed as a constellation of two near-polar, sun-synchronous satellites, providing a 6-day revisit time at the equator and increased revisit frequency over poles. In December 2021, one of the Sentinel-1 twin satellites (Sentinel-1B) experienced

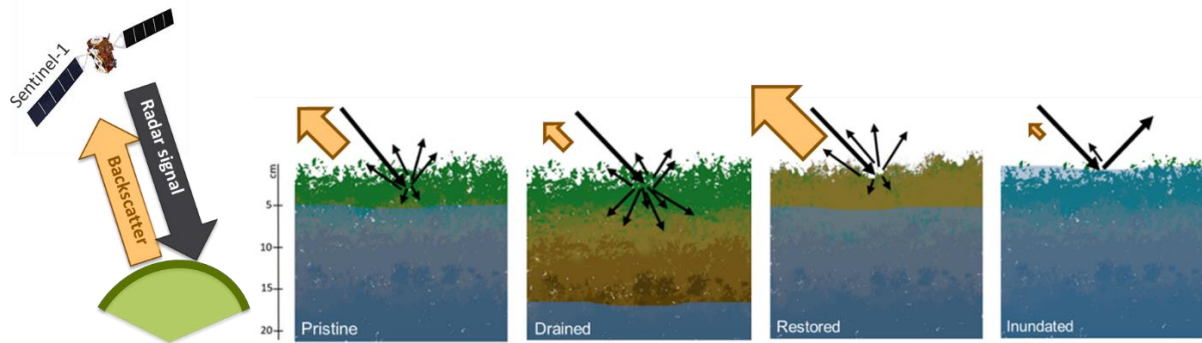
a power system anomaly and the support of the mission from this satellite was lost. There are however plans for the mission's continuity and Sentinel-1C satellite is planned for launch in 2023 (ESA, Sentinel-1 mission, 2023).

The two most popular Sentinel-1 products include the Single Look Complex (SLC) product, where data are georeferenced and provided in slant range geometry with complex samples and phase information preserved, and Ground Range Detected (GRD) products, where data have been detected, multi-looked and projected to ground range, but phase information is lost (ESA, 2022).

Sentinel-1 operates at C-band, which corresponds to 3.75 - 7.5 cm wavelength or 8 - 4 GHz within the microwave portion of the electromagnetic spectrum. C-band has the capability to penetrate through sparse canopies and into the first few cm of the soil (Owe et al., 2008). Radar antennas operating with longer wavelengths, such as L-band (15 – 30 cm) have the capacity of deeper penetration through vegetation, penetrating not just the canopies, but also branches and stems and deeper into the soil (Adeli et al., 2021). Although L-band has a lot of potential for vegetation and land surface monitoring, there are very few missions currently operating with an easy access to the data, while the availability of several SAR sensors operating in C-band providing data with good temporal resolution has resulted in numerous studies assessing the potential of SAR data for monitoring purposes.

One of the most widely used applications of SAR data for monitoring purposes is the surface soil moisture (SM) retrieval. Both active and passive remote sensing techniques for soil moisture estimation are based on the measurement of the amount of electromagnetic energy that is backscattered or emitted from the soil surface. SM retrieval using radar imagery can sometimes be challenging over vegetated areas, because of multiple factors influencing the backscattering signal, such as the moisture content, directly related to the dielectric properties, water table depth (WTD), vegetation cover, surface roughness and varying soil density/texture (Asmuß et al., 2019; Njoku et al., 2003; Notarnicola and Solorz, 2014). The denser the vegetation, the more it masks the soil, leading to weaker contribution of soil emissivity to the signal received by the sensor.

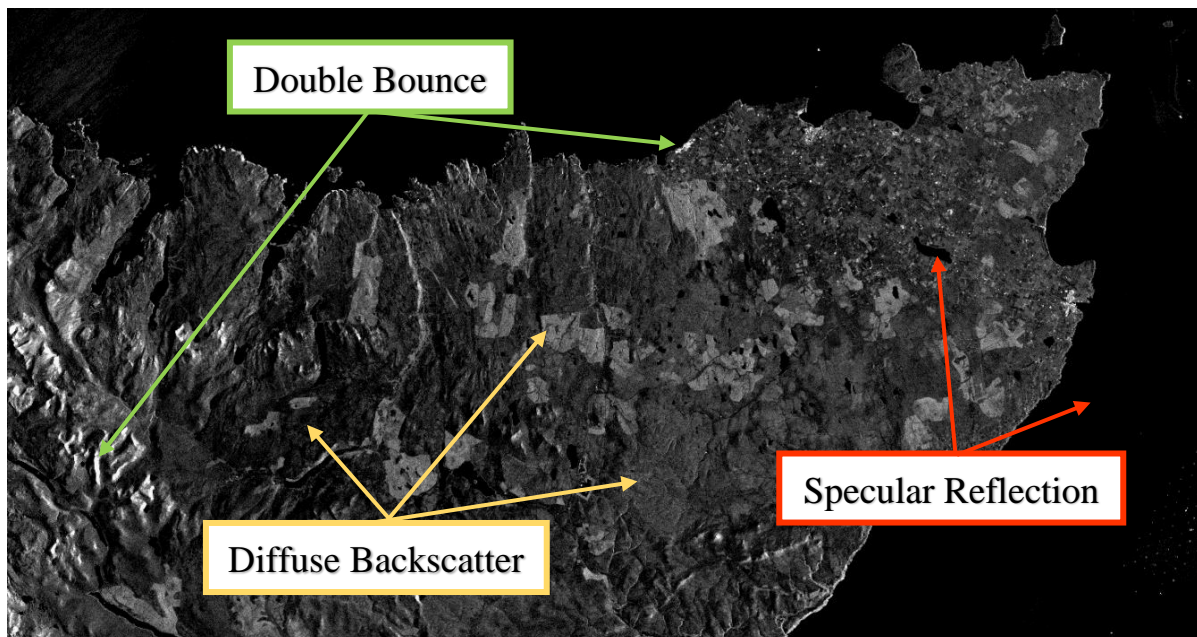
Pristine peatlands have high organic carbon content and shallow water table depth. Even if the C-band radar signal is able to penetrate only a few cm into the soil, the backscattered signal should be sensitive to WTD fluctuations (Figure 2.3).



**Figure 2.3.** Schematic illustration of WTD influence on radar backscatter. If no other condition on the ground changes, backscatter will be strong when WTD is shallow, very near to the surface (pristine peatland); the weakest in inundated areas because of the specular reflection and relatively low in areas with deep WTD (drained peatlands); backscatter from restored sites on the other hand might be higher due to the changed rougher surface.

Asmuß et al. (2019) evaluated correlation between the Sentinel-1 and WTD in drained, grazed peatlands and found moderate correlation of  $R^2 = 0.45$  over all sites, but concluded that correlation is the weakest among very dry and very wet sites (Asmuß et al., 2019). They also note that in future research for GHG estimates, where WTD parameter is derived from C-band radar data, there is a need for a method to account for ambiguity of low backscattering signals from areas with deep WTD or inundated areas, such as peatlands.

The radar backscatter coefficient ( $\sigma^0$ ) measures the reflectivity of the Earth surface. Just like with the WTD, increase in soil moisture content leads to increasing backscatter (reflectivity). There are 3 main types of backscatter: specular reflection, double-bounce and diffuse scattering (Figure 2.4)

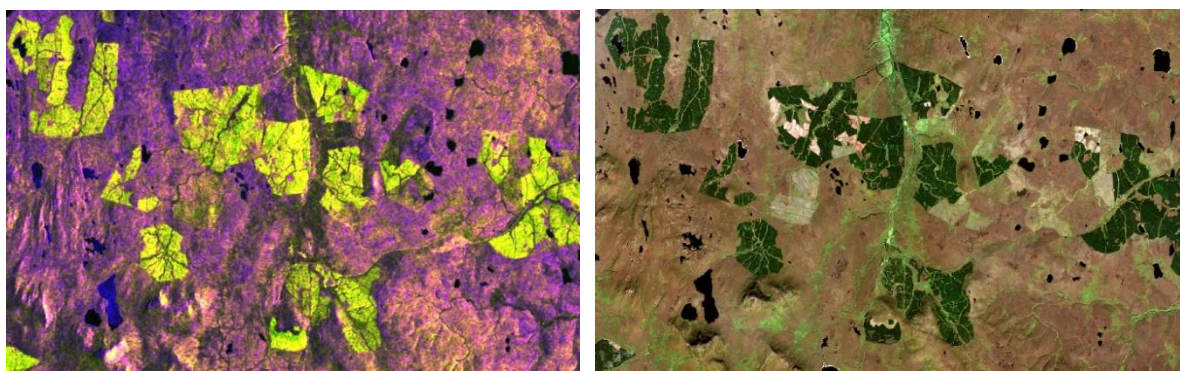


**Figure 2.4.** Sentinel-1 VV polarization radar imagery over Forsinard Flows, Northern Scotland, taken on 12/08/2018. Specular reflection is very easily distinguishable by the dark pixels over water surfaces (North Sea, lochs). Double bounce scattering is visible over urban areas (Thurso in the north, Wick in the east) and mountain range on the left. The rest of the imagery is mainly forested, agricultural,

grassland and peatland areas that appear as diffuse backscatter or speckle, appearing as a grainy "salt and pepper" texture in the image.

Specular reflection happens when the radar signal encounters smooth surfaces like calm water or pavement. In the radar imagery dark spots represent specular reflection, over peatland areas these could be larger pools. Double-bounce reflection is usually observed in urban areas or flooded afforested areas. The signal first bounces off one surface, like ground or water and then bounces again off another, such as a building or a tree stem, finally it returns to the sensor. As the returning signal is very strong, in the imagery these pixels will be very bright; it typically would not be expected to see this scattering type over peatlands, unless they are afforested and inundated. Diffuse scattering is the third and most common backscattering that is observed in a radar image over peatland areas. It happens when radar signal encounters rough surfaces with growing vegetation, like vegetated peatlands, agricultural areas, forests, grasslands, etc.

The interpretation of the radar image also changes depending on the chosen band or band combination. In single polarized images (VV or HH), such as the Figure 2.4, open water and dry bare soil will appear dark, urban areas bright and forests somewhere in between, appearing grey. Cultivated agricultural fields or forestry plots can usually be identified by their parcel structure. The backscatter over vegetated areas will change throughout the year depending on the soil moisture, crop canopy coverage and surface roughness state (Vreugdenhil et al., 2018). Creating band composites can help to highlight the variation of radar backscatter due to different polarizations (Chen et al., 2020). For example, when creating RGB false colour composite (Red: VV, Green: VH, Blue: VV/VH) densely vegetated areas, such as forests, will have intermediate VV and VH values and a high VV/VH ratio appearing in bright yellow-green colours (Figure 2.5). Water and bare soil will have low VV and VH backscatter, and low VV/VH ratio and appear dark blue, almost black. Urban areas, that usually have high VV and VH backscatter, will have varying VV/VH ratio and will appear as the brightest areas. Areas with bogs in Figure 2.5. have intermediate, but lower than the forest VV and VH values and very high VV/VH ratio, appearing in different shades of mix of purple and green.



**Figure 2.5.** Sentinel-1 pseudo RGB composite (Red: VV, Green: VH, Blue: VV/VH) captured on 27/09/2015 (left), and Sentinel-2 true colour RGB (right) imagery over Forsinard Flows RSPB captured on 29/09/2015 (right).

Polarimetric decompositions allow the separation of different scattering contributions and can be used to extract information about the scattering process. Most of the radar polarimetric decompositions require 4 polarizations: HH, HV, VH and VV. As Sentinel-1 provides dual-polarization (VV, VH) products and lacks co-pol information (HH), the utilization of polarimetric decompositions is limited. Besides, polarimetric decomposition can only be applied to Sentinel-1 SLC products, which require multiple pre-processing steps (Qu et al., 2020). While the polarimetric decomposition of the Sentinel-1 was not further analysed in this thesis, the response of the different radar signal polarizations to the water table depth changes was investigated (Chapter 3) and each polarization's contribution to water table depth modelling was analysed (Chapter 4).

### **2.3.2. Passive sensors**

Passive RS sensors operate in the visible, infrared, thermal infrared, and microwave portions of the electromagnetic spectrum and only measure reflected energy without actively emitting it. NASA's Landsat programme launched its first satellite Landsat 1 in 1972, which is now the longest-running satellite imagery acquiring mission (Belward and Skøien, 2015). Since then, governmental and private organizations around the world have launched over a hundred land cover observing satellites. The most widely used optical satellite missions for peatland monitoring in the last few years include Landsat, MODIS and Copernicus programme with satellites Landsat 9, MODIS Terra and Sentinel-2, respectively. They have multispectral sensors onboard and use wavelengths from the visible and infrared parts of the light spectrum. By creating band combinations, it is possible to use these images and easily identify broad land cover categories as water bodies, forests, urban areas, snow/ice, bare ground, grassland and areas with crops (Petropoulos and Srivastava, 2016) and with multitemporal imagery it is possible to monitor the land cover changes over time.

While there is a difference in albedo coming from wet soil and dry soil that can be measured, compared to active sensors, most passive RS techniques are not widely used for soil moisture measurements. Passive remote sensing SM retrieval techniques (especially using visible and NIR) are complex because of many confusing factors that influence the signal such as organic matter, roughness, texture, angle of incidence, colour, and plant cover (Dwivedi, 2017). Therefore, optical imagery is mostly used for peatland vegetation and, which can in turn be influenced by hydrological changes.

Multispectral imagery band combinations allow the generation of vegetation indices which can give valuable information about plant health, much more detailed than what could be derived from looking at visible light images only.

#### **2.3.2.1. Vegetation and Water Indices**

Vegetation and water indices derived from satellite imagery are a combination of the reflectance properties at two or more wavelengths. Because of different water content, chlorophyll content, pigment

and other properties of the observed target, indices can reveal particular characteristics of vegetation and enhance the discrimination of different land-cover types (Funkenberg et al., 2014).

The most well-known and used vegetation index also in peatland monitoring is the normalized difference vegetation index (NDVI), developed by Rouse et al. (1974) and is calculated using the difference between near-infrared (NIR) and red light. NIR is strongly reflected by vegetation, while red light is absorbed by vegetation, therefore NDVI result is a good proxy for quantifying vegetation, calculating biomass, quantifying forest supplies, indicating water shortages and droughts and assessing how healthy the vegetated area (Xue and Su, 2017). In peatland ecosystems, NDVI has been used for monitoring purposes as it is strongly connected to changes in vegetation cover, soil moisture and WTD changes. D'Acunha et al. (2018) found that in Burns Bog, where bog restoration by rewetting was taking place, NDVI was strongly correlated to change in the water table depth, precipitation and temperature. Harris (2008) concluded that NDVI has the potential to indicate photosynthetic activity changes caused by drought in bogs dominated by *Sphagnum*. Spectral signatures can also be used to identify and separate *Sphagnum* mosses from vascular plants. *Sphagnum* moss in peatlands usually has a NDVI value between 0.8 - 0.9 during the summer and 0.4 – 0.6 during the winter, while vascular plants will have a value around 0.9 during the summer and 0.8 during the winter (D'Acunha et al., 2018), but this process would require very high spatial resolution imagery, which usually is not freely accessible. NDVI may be useful for monitoring ongoing restoration in peatlands, Figure 2.6 shows the increase of NDVI four years apart on restored sites, compared with an adjacent reference blanket bog site.



**Figure 2.6.** Transect of NDVI values over natural peatbog (reference/target state) and a restored site (felled between 2010-2011) located next to each other in the east part of the Forsinard Flows RSPB Reserve. Both Sentinel-2 images used for NDVI calculation were captured in the month of September, four years apart.

Another two indices commonly used in wetland studies are Normalized difference Moisture index (NDMI), also known as “NDWI Gao”, which can be an indicator of liquid water content in the vegetation (Gao, 1996a; Gu et al., 2008) and Normalised Difference Water Index (NDWI) which corresponds to water content changes in water bodies (McFeeters, 1996). Both can be especially useful for peatland monitoring as water content in peatlands (abundant soil moisture and shallow WTD) has a crucial role for peatland conservation and restoration.

Because the vegetation and water indices have shown to be sensitive to water level and vegetation changes in peatlands, they have also been used as a proxy for peatland Gross Primary Productivity (GPP) estimation (Lees et al., 2020).

### **2.3.3. Estimation of Gross primary productivity and Net Ecosystem Exchange in peatlands**

Just like with water table depth measurements, most precise carbon flux measurements can be obtained using field-based methods, however they usually cover small areas and can be costly. A much more cost-effective alternative for assessing peatland health and estimate carbon fluxes is to use satellite data. There are multiple techniques developed to estimate carbon fluxes using optical RS imagery (Lees et al., 2020).

One of the best parameters for estimating any vegetation health status is Gross Primary Productivity (GPP). GPP is crucial for understanding and modelling net carbon as it is the amount of carbon that the ecosystem has captured during the photosynthetic fixation of CO<sub>2</sub> (Running et al., 2004).

Net Ecosystem Exchange (NEE) shows the balance between the gross amount carbon captured by the ecosystem (GPP) and the total respiration R<sub>ECO</sub> (sum of autotrophic (R<sub>a</sub>) and heterotrophic (R<sub>h</sub>) respiration) (Reichstein et al., 2005):

$$NEE = R_{ECO} - GPP$$

Negative NEE will mean that an ecosystem is capturing more carbon than releasing, and therefore is a carbon sink, while positive NEE will show that an ecosystem has switched to being a carbon source.

While GPP cannot be directly measured in the field, Net Ecosystem Exchange (NEE) can be measured using in-situ instruments and then partitioned into GPP and R<sub>ECO</sub> using empirical regressions (Walker et al., 2017).

Two common field instruments for measuring these carbon fluxes directly are eddy covariance towers and flux chambers. Flux chambers measure NEE on a very small scale (few cm<sup>2</sup>). Eddy Covariance towers are more commonly used and the area of coverage, known as the footprint, provides information about NEE on a landscape scale (m<sup>2</sup> to km<sup>2</sup>).

Satellite data has the potential to provide an alternative low-cost, large-scale monitoring, which does not require frequent site visits, regular maintenance of the instruments and field data collection and processing. There have been multiple techniques developed to estimate carbon fluxes using optical imagery, starting from simpler ones like combinations of previously described vegetation and water indices, going to more complex models such as light use efficiency (LUE) models (Kross et al., 2013), MOD17 (Wang et al., 2021), GLO-PEM (Prince and Goward, 1995), TG (Lees et al., 2018; Sims et al., 2008), EC-LUE (Yuan et al., 2007) and others, each with its own strengths and weaknesses. Literature also suggests a close link between peatland water table depth and greenhouse gases (Evans et al., 2021;

Joosten et al., 2012; Koch et al., 2023; Waddington et al., 2015; Yu et al., 2010), creating more opportunities to improve current GHG reporting mechanisms using WTD as a low-cost proxy.

Although RS data usage can be really time saving, in-situ measurements remain crucial for instrument calibration and verification of results.

#### **2.4. Main present challenges, gaps and future possibilities for remote peatland monitoring**

Given the vital ecosystem services peatlands provide globally, monitoring their extent and condition is incredibly important. On global and national levels, an existing challenge for future peatland GHG emission monitoring and reporting remains the uncertainty of the actual peatland extent and peat deposits (Leifeld and Menichetti, 2018). Besides improving the peatland extent modelling, a creation of a more unified global peatland classification system, surveys on peat thickness and their management systems are important for better estimates of GHG emissions and identifications of best peatlands management practices (Biancalani and Avagyan, 2014). There have been improvements towards peatland classification using remote sensing and therefore better estimate about the extent of peatlands (Aitkenhead and Coull, 2020), but without reliable information on peat extent and thickness, the total peat volume and GHG emissions linked with peatlands will remains challenging to estimate even with advancements in water table depth predictions. This thesis, however, is focusing on the other main challenge in remote peatland monitoring, which is the condition of peatlands.

Additionally, and increasingly, there are peatlands that are undergoing restoration to their natural state. Given that peatland recovery after restoration is a slow process, it remains challenging to systematically assess the success of restoration over long time periods only by field visits and manually collected data. If restoration is progressing successfully can be determined by looking at the hydrological characteristics of the bog and its floral and faunal presence and assemblages (Anderson and Anderson, 2010; Gatis et al., 2017; Shuman and Ambrose, 2003). Water table depth and soil moisture monitoring remains especially fundamental because of their link to peatland GHG exchange, restoration success, resilience to droughts and prevention of wildfires. Field-gathered water table depth measurements are typically collected using piezometers, where the WTD is determined by measuring the pressure of the groundwater at a specific depth (Bourgault et al., 2019). While piezometers are invaluable in obtaining the precise depth of the water table, some of the disadvantages include installation, maintenance and data gathering costs, and a result that represents a point-measurement. Here remote sensing has the potential to overcome these drawbacks and cover whole peatland landscapes.

From remote sensing methods, persistent cloud cover and rainfall in regions with peat bogs often prevents optical sensors from acquiring regular imagery without cloud cover, therefore limits the efficiency of optical RS data application for monitoring purposes. There are techniques for tackling this



issue by using image compositing techniques, masking clouds, excluding imagery with cloud cover completely, using statistical methods for gap-filling or using alternative data sources (Candra et al., 2019; Weiss et al., 2014; Zhu and Woodcock, 2014).

Radar instruments are weather independent, but usage for peatland monitoring purposes is still emerging, mainly due to relatively recently gained easy access to regular radar imagery (since launch of Sentinel-1 in 2014), data processing requirements SAR imagery demands and because radar images are not as intuitively understandable as most optical data. Soil moisture (and WTD) and surface roughness are the main parameters that strongly affect the measured backscattered response. Change detection is a common technique for soil moisture retrieval from radar data that assumes the soil moisture to be the main varying parameter, while surface roughness and vegetation cover remain relatively constant (Barrett et al., 2009; Jacome et al., 2013; Thoma et al., 2006). Northern peatlands are typically tree-less and experience relatively small changes in vegetation throughout the year, therefore SAR application for WTD or soil moisture monitoring is particularly enticing.

SAR signal sensitivity to water table depth and soil moisture change in peatlands has been studied previously using earlier satellite radar missions (Bechtold et al., 2018; Bechtold et al., 2020; Kasischke et al., 2009; Kim et al., 2017; Torbick et al., 2012) and more recently Sentinel-1 (Asmuß et al., 2019; Dabrowska-Zielinska et al., 2016; Lees et al., 2021). Often studies are site-specific and usually yield moderate results, therefore there is a need to improve the modelling accuracy. To improve the understanding of the peatland WTD – radar backscatter dynamics there is a need for a better interpretation of how radar backscatter behaves with changes in peatland hydrology. This could be improved by first understanding the peatland water table depth and SAR interaction using higher resolution SAR sensors in laboratory, mounted on UAVs or planes. Some of the latest research includes Interferometric Synthetic Aperture Radar (InSAR) for detecting short and long-term peatland surface movement, mainly connected with the dynamics of water and gasses in the peat (Alshammari et al., 2020, 2018; Bradley et al., 2022). However, these studies have also highlighted the uncertainty in the validation of the InSAR interpretation due to the massive scale difference between large-scale satellite data and small-scale field observations. While studies have shown very promising results for peatland surface movement monitoring using InSAR technique (Alshammari et al., 2020, 2018; Bradley et al., 2022; Marshall et al., 2022; Tampuu et al., 2020), they either not validate the deformation results to field observations or use levelling transects, which lack the spatial coverage. Therefore, there is a high demand for studies conforming SAR signal sensitivity to hydrological changes occurring in peatlands both in terms of vertical movement of the peat (reflected in SAR signal phase) and changes in soil moisture (reflected in SAR signal amplitude).

One of the challenges working with C-band radars, which might be problematic for further applications, is the low penetration capability. Mosses do not have roots and in peatlands rely on capillary rise to obtain water from the water table depth to the capitula (Mccarter and Price, 2014). Thanks to the strong capillary action process, changes in WTD have been observed using radar

instruments even when WTD extends the C-band penetration depth (Asmuß et al., 2019; Dettmann and Bechtold, 2016). However, having instruments using longer wavelengths, like L-band could be beneficial for soil moisture monitoring in drier peatlands or peatlands with more rich vegetation as the signal could penetrate through denser vegetation and deeper into the soil. Currently, there is a very limited accessibility to L-band satellite data, however at least three L-band missions are scheduled to begin in the coming decade: NISAR (by NASA/ISRO in 2024), TanDEM-L (by DLR in 2024) and ROSE-L (by ESA in 2028) (ESA, 2023a).

For peatland vegetation monitoring over time the resolution of freely available RS products does not usually allow for high precision classification and identification of individual species, especially in mixed-species environments as would be possible through field surveys (Räsänen et al., 2020). In the future, higher resolution data and more frequently revisiting satellites in combination with improved detection and classification models could notably improve the monitoring process, reducing the need for ground-based monitoring, however, the need for some amount of in situ measurements will remain for validation and accuracy assessment purposes. Further studies on fusion techniques of optical imagery, especially visible and near infra-red data and radar imagery for peatland monitoring utilizing are also encouraged (Quaife et al., 2022). This way the full potential of remote sensing for peatland monitoring could be achieved.

Other challenges include processing longer time series of RS data and creating reliable workflows which can process substantial amounts of data (Liu, 2015) and apply suitable methods for time series analysis (Masiliūnas et al., 2021; Southworth and Muir, 2021). Studies that assess effectiveness of peatland restoration through RS analysis are still rare and therefore best approaches for such analysis still need to be evolved (Monteverde et al., 2022).

The opportunity for regular peatland monitoring using freely available remotely sensed data has been recently increasing due to availability of cloud computing platforms such as Google Earth Engine (GEE) and Amazon Web Services (AWS) (Ferreira et al., 2020; Hird et al., 2017; Long et al., 2021). The main advantage of these platforms is the accessibility to large satellite data archives and the ability for analysis without the need to download and process raw satellite imagery on local machines (Oliphant et al., 2019). GEE's public data catalogue currently offers access to over 80 petabytes of geospatial data with some data series dating back more than thirty years, enabling the ability to carry out powerful cloud-based computing analysis (GEE, 2023a). In this thesis, we have explored the opportunities of cloud computing on the GEE platform for peatland water table depth and condition monitoring through analysis of Sentinel-1 and MODIS satellite data.

# Chapter 3

## 3. High resolution C-band SAR backscatter response to peatland water table depth and soil moisture: a laboratory experiment<sup>1</sup>

### Abstract

Carbon storage and active carbon sequestration within peatlands strongly depend on water table depth and soil moisture availability. With increasing efforts to protect and restore peatland ecosystems, the assessment of their hydrological condition is highly necessary but remains challenging. Synthetic aperture radar (SAR) satellite observations likely offer an efficient way to obtain regular information with complete spatial coverage over northern peatlands. Studies have indicated that both radar backscatter amplitude and phase are sensitive to peatland condition. Very recently, Differential Interferometric Synthetic Aperture Radar (DInSAR) has been reported as being capable of monitoring ground deformation patterns at the millimetre scale, which are a response to peatland hydrological condition.

To further investigate the promise of SAR for peatland monitoring, a laboratory-based polarimetric C-band SAR system was used to acquire the dynamic radar behaviour of a 4 m (l) × 1 m (w) × 0.25 m (d) reconstructed peatland. A forced 4-month drought was introduced with very-high-resolution imagery taken every 2 hours, capturing details of the vertical backscatter patterning through the peat at the centimetric scale.

The results showed a clear coherent response both in radar backscatter amplitude and phase to change in water table level and soil moisture. Similar responses were seen across all polarizations. Phase demonstrated a coherent and deterministic change across the experiment; the average differential phase increase across all polarizations was  $118^\circ$  for 17 cm of water table drawdown. Interpreted as the physical movement of the surface, this corresponded to 8.3 mm of surface subsidence. Both phase and amplitude changes were near-linear with changes in the water table depth; amplitude showed a correspondingly strong concomitant mean decrease of 7 dB across all polarizations during the experiment. The results demonstrate the close sensitivity of radar backscatter to hydrological patterns in a peatland ecosystem. The phase result, in particular, strongly supports the notion that differential phase from satellites can be utilised to measure ground deformation as a proxy for the hydrological state.

---

<sup>1</sup> This chapter has been published as follows: L. Toca, K. Morrison, R.R.E. Artz, A. Gimona & T. Quaipe (2022) High resolution C-band SAR backscatter response to peatland water table depth and soil moisture: a laboratory experiment, *International Journal of Remote Sensing*, 43:14, 5231-5251, DOI: 10.1080/01431161.2022.2131478

### 3.1. Introduction

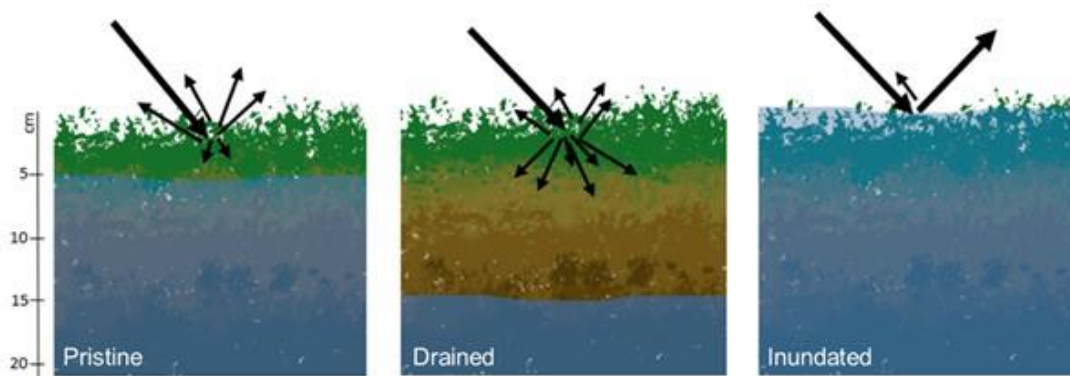
Peatlands are a type of wetland ecosystem, with unique acidic and waterlogged conditions where plant material does not fully decay, accumulates, and ultimately forms a deep peat layer with high carbon density (Moore, 1989). Storage and sequestration of carbon by healthy, wet peatlands play an important role in regulating the global carbon (C) emissions (Bonn et al., 2016), especially as peatlands remain the largest terrestrial carbon store (Gorham, 1991). Besides being crucial for helping to address climate change, peatlands are important for preserving global biodiversity, providing drinking water, and reducing flood risks (Grand-Clement et al., 2013). Despite the high value of these ecosystems, human activity (drainage, extraction, conversion to agricultural land and afforestation) globally has led to a shift of peatlands functioning as a C source rather than sink (Leifeld and Menichetti, 2018). Peatlands are now annually contributing about 5% of the total anthropogenic CO<sub>2</sub> equivalent emissions (Gewin, 2020) with the highest degradation and associated emissions coming from Southeast Asian and European peatlands (Urák et al., 2017). Global and national level conservation efforts to protect and restore peatlands have increased in the past years, however, a further increase of GHG emissions is predicted, due to peatland degradation reaching up to 8% of the global anthropogenic carbon dioxide emissions by the year 2050 (Swindles et al., 2019; Urák et al., 2017).

More than ever, the assessment of peatland ecosystem condition in pristine, damaged or restored peatlands is necessary, but remains challenging, especially over larger areas in remote locations. While traditional monitoring methods by carrying out field measurements can give precise information about the health status of the peatland, they can be expensive, time-consuming, covering small areas and time periods, and often in locations that are not easily reachable (Lees et al., 2018). The use of satellite imagery for monitoring purposes has increased tremendously in the past years, as new satellite data with higher spatial and temporal resolutions have become publicly available (Connolly et al. 2011; Artz et al. 2019). Optical sensors can provide wide spectral information and can be very useful for peatland vegetation (Xue and Su, 2017) and hydrological condition (Harris and Bryant, 2009) monitoring. The main disadvantage of optical sensors remains the dependency on cloud-free conditions and although various gap-filling techniques to account for missing data exist (Poggio et al., 2012), cloud cover over Northern peatlands is widely present, making it challenging to achieve a regular resampling interval. Imagery from radar instruments, on the other hand, can be harder to interpret but provide more regular data that are independent of persistent cloud or smoke cover (Kasischke et al., 1997).

Monitoring peatland hydrological condition is important because water table depth and soil moisture are the predominant factors driving biogeochemical processes in peatlands and can have the overriding control on greenhouse gas emissions (Evans et al., 2021; Hilbert et al., 2000). Excessive lowering of water level (WL) in peatlands can lead to peat subsidence, oxidation, and large amounts of carbon being released to the atmosphere (Nusantara et al., 2018; Zhong et al., 2020). High water level and high soil moisture are also necessary environmental conditions for the regeneration of characteristic

peatland vegetation in restoration projects (Alderson et al., 2019), as well as reducing peatland vulnerability to wildfires (Meingast et al., 2014). As drought periods in northern latitudes are predicted to increase both in frequency and severity under climate change; (Fenner and Freeman, 2011; Swindles et al., 2019) a reliable monitoring system for peatland hydrological condition is necessary.

Radar backscatter is a measure of the energy fraction returned from a target compared to the energy of the incident field. Besides the radar instrument properties (frequency, polarization, incidence angle), the intensity of the backscatter will vary depending on the physical properties of the scene (Bernard et al., 1982; Widhalm et al., 2015). The ability of a scene feature to reflect the radar signal is dependent on the target's physical properties: surface roughness and geometry of the target, and dielectric properties, which are a proxy for water content (Hajnsek et al., 2003; Ulaby et al., 1978). Therefore, the largest influence on backscattering in unforested peatland areas is soil moisture and surface roughness, vegetation obscuring the soil, soil texture, and, to a minor degree, soil surface temperature, and peat bulk density (Beale et al., 2019). Pristine peatlands, normally having very high water content and therefore high dielectric constant, will reflect more signal and so have a higher backscatter compared



**Figure 3.1.** Radar backscattering characteristics based on the water level position in peatlands.

to targets with low dielectric constant, e.g., drained peat soils (Figure 3.1). Parts of near-natural peatlands can also be completely inundated, resulting in a specular-like surface where radar signal would be reflected away from the sensor resulting in very low backscatter values.

SAR sensitivity to water table depth and soil moisture change in peatlands has been reported previously using satellite data over near-natural, drained, and managed sites, re-wetted and restored peatlands (Asmuß et al., 2019; Bechtold et al., 2018; Bechtold et al., 2020; Dabrowska-Zielinska et al., 2016; Kasischke et al., 2009; Kim et al., 2017; Lees et al., 2021; Torbick et al., 2012). Furthermore, radar has been shown to have the potential to monitor soil moisture along with vegetation regeneration to assess if peatland restoration efforts are successful and determine if additional interference is necessary (White et al., 2020).

The incoherent component (amplitude or power) of the radar signal has a strong sensitivity to dielectric constant, therefore radar backscatter intensity has been used in various studies to examine radar signal sensitivity to soil moisture and water table depth in peatlands (Wagner et al., 2007). The

coherent (phase) component difference of the radar signal between two or more satellite radar acquisitions has been used to infer surface movement and vegetation height changes using the Interferometric Synthetic Aperture Radar (InSAR) technique (Bamler and Hartl, 1998). Many factors impact both the backscattering intensity and the phase, therefore accounting for a single parameter such as soil moisture can be challenging. What makes it even more complex is the diverse nature of peatland landscapes, and even though a reliable monitoring system to follow peatland hydrological condition is highly desirable, a universal retrieval of peatland soil moisture from SAR data is hard to develop and site-specific or peatland type-specific studies are more common (Meingast et al., 2014). This has encouraged efforts to fully understand and exploit SAR capabilities for peatland condition monitoring, including peatland water level and soil moisture monitoring. Recent efforts have highlighted InSAR, specifically, the APSIS (Advanced Pixel System using Intermittent Small Baseline Subset (SBAS)) method, formerly known as ISBAS (Bradley et al., 2022) as a potential satellite-based peatland condition monitoring system due to its ability to capture annual, seasonal, and interseasonal movement of the peat (Alshammari et al., 2020, 2018; Tampuu et al., 2020). This method has been developed to focus on non-urban land areas where usage of conventional Differential InSAR (DInSAR) techniques is challenging due to the temporal decorrelation (Sowter et al., 2013) and has shown potential for peatland condition characterization (Alshammari et al., 2020, 2018; Cigna et al., 2014). These InSAR methods have shown the ability to follow the shorter-term seasonal peat surface movement, often referred to as ‘bog breathing’ (Morton and Heinemeyer, 2019) or ‘bog surface oscillation’ (Howie and Hebda, 2018), which corresponds to dynamics of water and gasses within the peat, typically showing drawdown during the warmer months and recharge and uplift during the winter months (Alshammari et al., 2020).

Most studies utilizing radar instruments for peatland hydrological condition monitoring have used satellite data. This study made use of laboratory SAR measurements of a peatland sample. The arrangement in the laboratory permitted us to isolate the backscattering dependency on changes in peatland hydrological status, allowing us to eliminate or control perturbing factors, such as micro-topography, vegetation, and weather. Additionally, it removed any atmospherically induced distortions associated with satellite image processing, particularly regarding the differential phase (Cheng et al., 2012; Cigna et al., 2014). Previous studies have reported various relationships, from very high correlations between SAR and peatland hydrological status to no obvious correspondence between the parameters, so here we have tested to what extent the radar backscatter – water table drawdown relationship could be explained if no other major factors were to influence the backscattering. The main aim of this study was to assess the SAR signal sensitivity to drought in peatlands based on an analysis of 6 months long TP radar series. Specific objectives were: a) explore TP SAR for peatland hydrological condition monitoring, including usage of different polarizations, b) investigate the radar backscatter dependency on different peatland hydrological regimes, c) analyse how the weighted mean backscatter height within a peatland changes with drought conditions. The findings from this study enhance the

understanding of how radar backscatter interacts with peat and blanket bog vegetation, add useful knowledge to both radar backscatter and InSAR for peatlands research literature, and help with improving methods for continuous observation of peatland condition which are needed to enable appropriate peatland management and conservation decisions being taken (Alshammari et al., 2020; Lees et al., 2018).

## **3.2. Materials and methods**

### **3.2.1. Laboratory measurement**

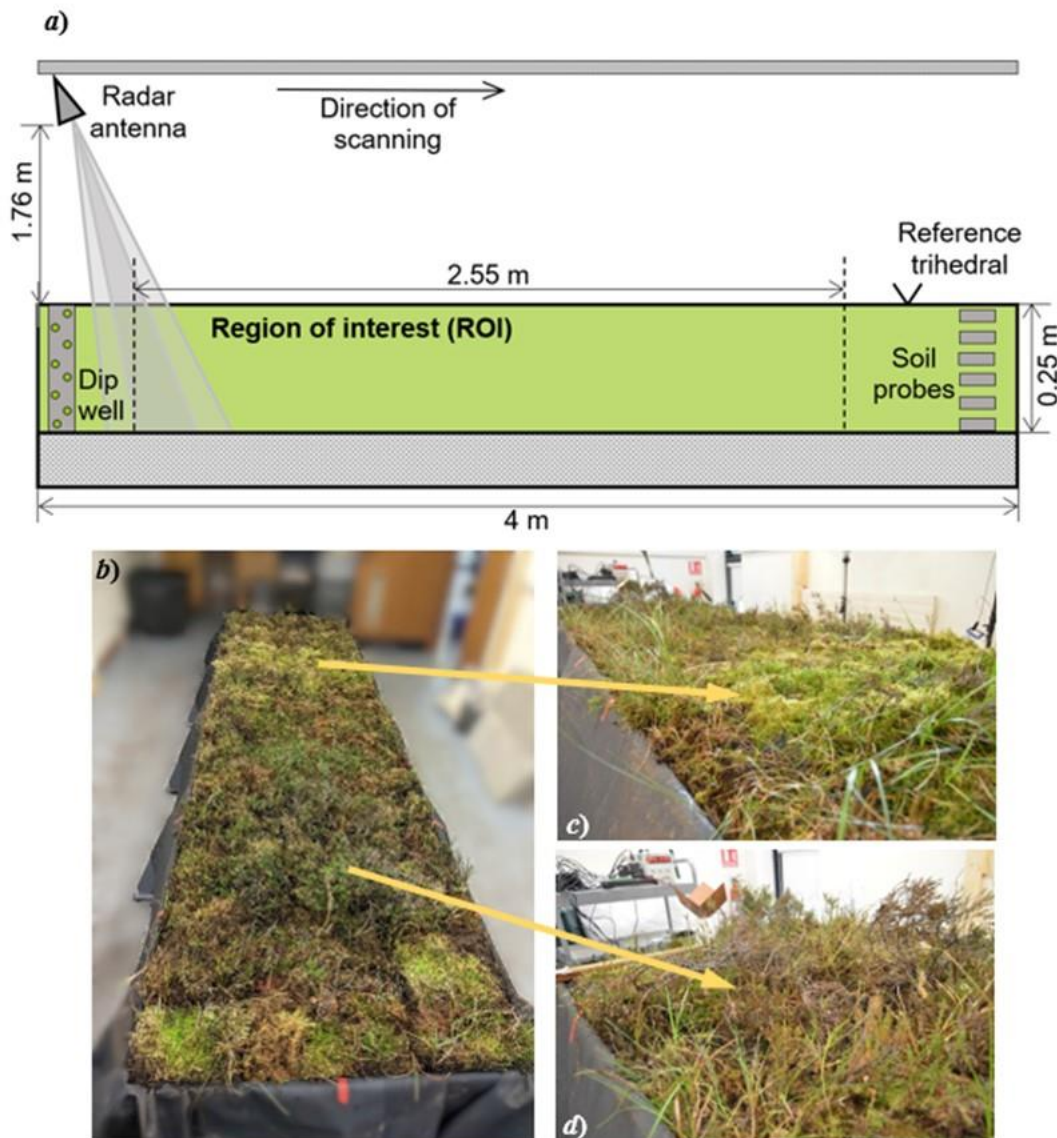
Longer-term peat surface movement can indicate peat accumulation (in case of a build-up of partially decomposed organic matter) or subsidence (due to drainage, compression, and decay of organic matter) (Alshammari et al., 2018). Although promising, these studies have highlighted the difficulty of validating the accuracy of obtained results as it often requires a comparison of large-scale satellite data to small-scale field observations, and underlines the need for further research to improve quantitative validation of the InSAR vertical velocity (Alshammari et al., 2018). Most studies utilizing radar instruments for peatland hydrological condition monitoring have used current and previous radar imaging satellite mission data, a few have used airborne radar data (Baghdadi et al., 2001), but to the best of our knowledge, this is the first time high-resolution radar measurements have been collected in a controlled laboratory-environment setup.

#### **3.2.1.1. 'Bog in the box' experimental setup**

Blocks of vegetation-covered peat were collected from an upland blanket bog in the Eastern Cairngorms, Scotland (56.9 N, -3.15 E; ca 650 m). The thirty-two 30 (length) × 50 (width) × 25 (depth) cm samples were transported in plastic boxes to the University of Reading by courier. Here, they were removed from their containers and reconstructed into a 400 (l) × 100 (w) × 25 (d) cm blanket bog section within the trough of the Reading Radar Facility (Figure 3.2) for microwave measurement. The laboratory was equipped with 4 full spectrum 80W LED grow lights to facilitate the continued growth of the blanket bog vegetation.

Once in the trough, the reconstructed peatland was inundated with deionized water up to a water table depth of 5 cm below the trough edge. Afterwards, the peat was watered regularly with artificial rainwater using a manual hand-held water sprayer simulating local rainfall. We followed Noble et al. (2017) and used a synthetic rainwater concentrate (at a pH of around 5.5). The simulation of rainfall occurred 2-3 times a week, with 2-3 l of water added per time, keeping the water table at a steady level. Blanket bogs are ombrotrophic ecosystems, where water and nutrients are gained mainly by rainfall, mist, or snow, resulting in an acidic environment low in nutrients. Regular rainfall simulations were carried out for 2 months prior to the beginning of the experimental drought period. The drought period was simulated as a total drought with no rainfall simulations first until WL reached the bottom of the

trough (22 cm below the edge of the trough) and continued until the deepest soil moisture probe reported a drop to 0.8 volumetric water content (VWC). The experiment simulated a 117-day long drought period, after which the bog was re-wetted back to the original WL state of 5 cm below the surface by adding 280 l of deionised water over a 10-day period (7 rainfall simulations, 40 l per time).



**Figure 3.2.** a) Schematic of the radar measurement system and experiment setup. The bog was surrounded on its bottom and sides by a waterproof butyl rubber liner and sat upon a stable bed of dry sand (25 cm deep). b) Photograph of the ‘Bog in the box’ laboratory setup. c) *Sphagnum* segment, representing predominantly moss vegetation. d) *Ericaceous* (heather) segment, representing moss layer covered with dwarf-shrub vegetation.

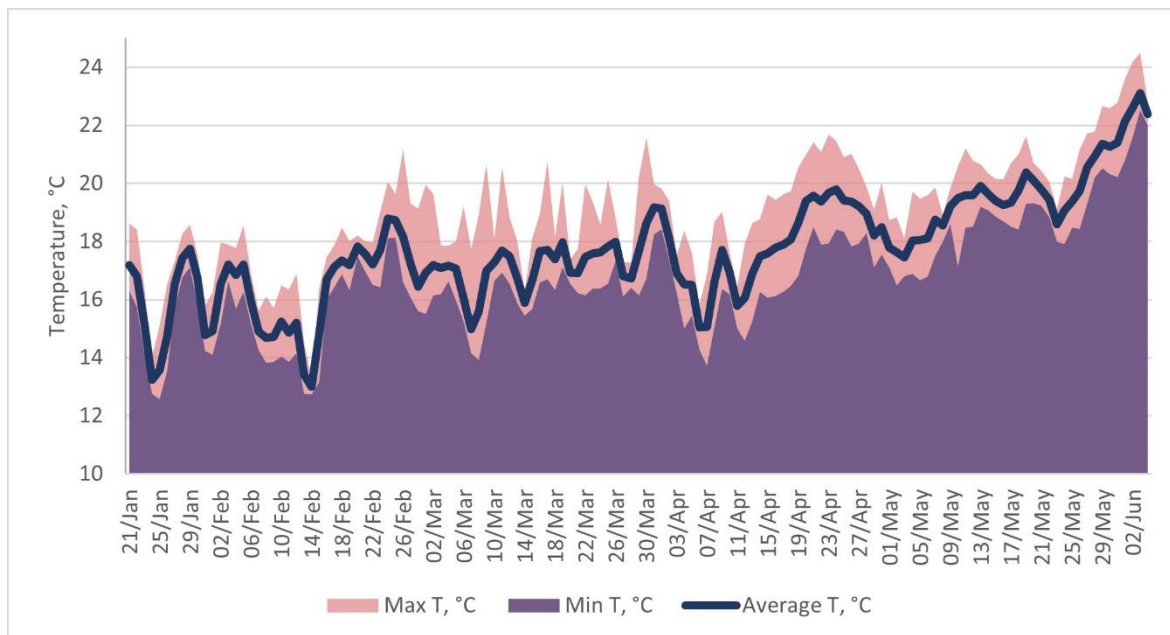
The bog vegetation assemblage represented a typical Eastern Cairngorms M18-type blanket bog (Elkington et al., 2001), dominated by *Calluna vulgaris* as the primary ericaceous species, *Eriophorum* spp. and other sedges, and *Sphagnum capillifolium* as dominant *Sphagnum* species, however, other



*Sphagnum* and other moss species were present in lower proportions. To assess if different vegetation had an impact on the backscattering signal, three 25 cm segments with predominantly *Sphagnum* moss layer only (Figure 3.2c) and three 25 cm segments with heather and sedge/grass species above the moss canopy (Figure 3.2d) were identified.

A dip well (perforated PVC well pipe) and six soil volumetric water content (VWC) and temperature sensors (5TM, METER) were installed across the trough at depths of 3, 5, 7, 10, 18 and 22 cm. VWC and soil temperature (°C) data from the probes, along with a sensor for room air temperature (°C), were connected to a Campbell CR1000 data logger and logged every 30 min. Daily water table depth measurements at ±1 cm were gathered manually using the dip well.

The average room temperature throughout the experiment was 17.7°C, with lower temperatures experienced during the night, and higher during the day and towards the end of the experiment (Figure 3.3). These conditions are similar to the July and August climate averages (1981-2010 period) for the Braemar climate station in the vicinity of Ballater (MET office 2021).



**Figure 3.3.** Average, minimum, and maximum air temperatures in the laboratory during the experiment.

The experimental setup allowed us to eliminate or closely control factors that can influence the interpretation of the radar backscattering signal in peatlands, allowing us to closely investigate the backscattering dependency on peatland hydrological regimes. First, possible changes in surface roughness and vegetation structure due to wind, grazing or burning were eliminated. Second, we were in control of the hydrological regime of the experiment setup. By introducing acclimatization (normal amount of precipitation), drought (no precipitation) and re-wetting phases we were able to directly inspect the radar signal response to changes in soil moisture and water level regimes. The experimental setup also prevented lateral water losses. As the experiment duration was relatively short (6 months

during which environmental conditions were kept largely the same), vegetation growth effects are likely to have been negligible. There were no open water bodies, which are common in peatland environments, therefore a specular reflection of the radar signal, which can greatly impact backscattering values, has not been assessed in this experiment.

We acknowledge that a laboratory experimental setting will almost unavoidably diverge from the real-world environment but this way we can achieve a well-controlled repeatable environment where the findings are descriptive of the environment at large.

### **3.2.1.2. Radar Data Collection**

The radar measurements were carried out using the indoor component of the Reading Radar Facility at the University of Reading. A roof-mounted linear scanner is centrally located above and down the length of the plywood measurement trough. A cluster of four C-band antennas was centrally mounted on the scanner 1.8 m above the trough, pointing forward at  $10^\circ$  from nadir, being sufficiently close to each other to use a monostatic approximation. Their 3 dB across-track beamwidth maps onto the width of the trough. By switching in the appropriate transmit-receive antenna pair, the four scans sequentially captured the VV, VH, HH, HV polarimetric responses. Data collection was accomplished by sequentially stepping the antennas monotonically along the scanner in 1.5 cm intervals over a 375 cm aperture. At each position, microwave data were collected at 1601 equally spaced points across a frequency range of 4-8 GHz. Scans were collected in sets of four, where each scan provided capture at a single polarization, and took 20 minutes to complete a set. Data sets were collected at 6-hour intervals prior to the drought, and at 2-hour intervals during the drought and rewetting phases. Morrison and Wagner (2020) provide more details of the microwave RF sub-system. The system response was calibrated using precision radar cross-section (RCS) targets with the method of Sarabandi et al. (1990) just prior to the start of the experiment. System changes thereafter were monitored and corrected for using a reference trihedral and sphere. Measurement precision in signal power and phase is estimated to be 0.2 dB, and  $5^\circ$  degrees respectively.

Out of the 6012 scans, 356 were collected prior to the drought, 5060 during the drought and 596 during the rewetting experiment. In the analysis, we considered the backscattering values both in co-polarizations: VV, HH and Cross-polarization (mean of HV and VH).

While the full length of the trough was 4 m, a region of interest (ROI) of 255 cm was used in the radar imagery analysis to avoid edge effects at both ends of the trough and exclude the regions where the calibration target and soil moisture equipment was located (Figure 3.2).

#### **3.2.1.2.1. Tomographic profiling and weighted mean height**

Tomographic profiling (TP) is a SAR-like imaging technique designed specifically for gathering vertical backscattering profile data through biogeophysical volumes (Morrison and Bennett, 2014).

Unlike in SAR imaging, the antennas are aligned along-track and so only collect data for a transect directly below the scanner. Post-measurement, the antenna beam is synthetically sharpened by coherent summation across a sub-aperture of sample points. The aperture is moved on one point along the aperture and the process repeated, and so on. In this way, a series of overlapping vertical ‘sounding profiles’ are obtained, highlighting the radar backscatter pattern through the target of interest. By adding phase ramps across the sample points, the beam was configured to look forward at an incidence angle of 10°. TP imagery is not true tomographic imagery (Morrison and Bennett, 2014) as it lacks any angular discrimination in the across-track (across the trough) direction. The target returns in this direction are considered collapsed down to a central slice down the centre of the trough. Previously, the TP method has been successfully used in laboratory and field studies to investigate the internal structure of snowpacks (Morrison et al., 2008), forest canopies (Morrison et al., 2013), dry soils (Morrison and Wagner, 2020), and subsurface archaeology (Morrison, 2013).

In the analysis, the differential phase is interpreted as a bulk movement of the peat sample. The change in the vertical displacement of the peat,  $D$ , can be written as:

$$D = \frac{\lambda\Phi}{\cos i \times 360 \times 2}, \quad (3.1)$$

where  $\lambda$  is the wavelength (5 cm in this study),  $i$  is the incidence angle (here, 10°) and  $\Phi$  is the measured phase difference.

The TP scheme enables the possibility to analyse the vertical backscattering signal; we applied weighted mean height (WMH) to investigate the effective position of the vertical backscattering signal and its change over the duration of the drought. The WMH is calculated as:

$$\bar{x} = \frac{\sum_{i=1}^n w_i x_i}{\sum_{i=1}^n w_i}, \quad (3.2)$$

in which  $\bar{x}$  is the weighted mean height,  $x$  is the height of the specific pixel and  $w$  its corresponding amplitude value (Yrttimaa et al., 2020). WMH shows at what height the backscatter is the strongest, and the time series of radar measurements can be used to investigate whether this height changes over time.

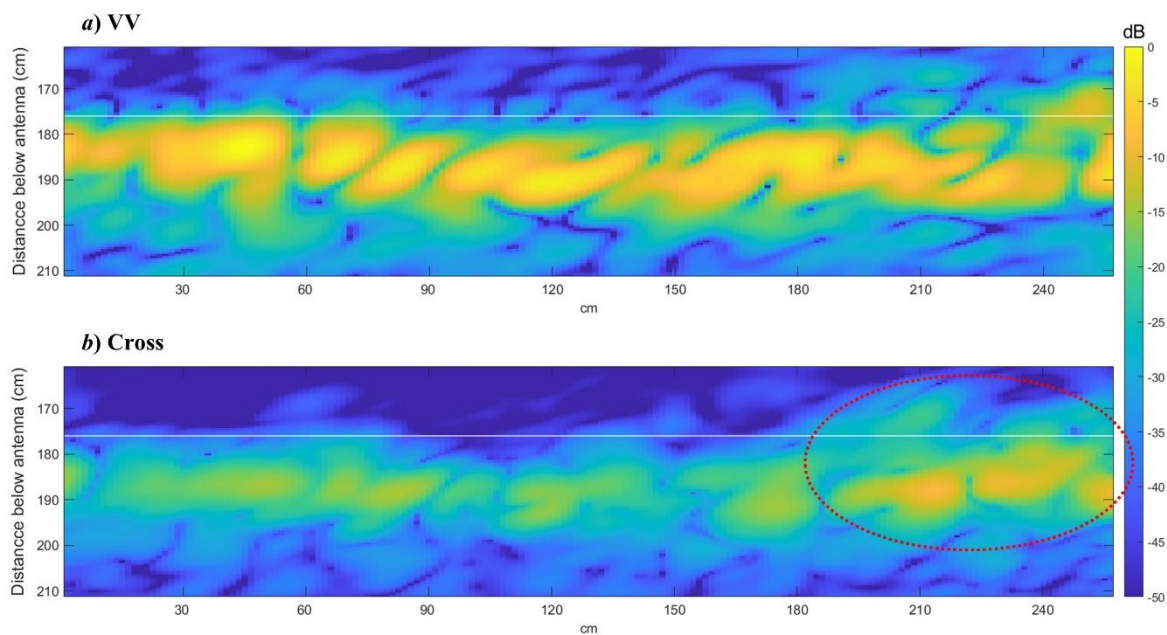
### 3.2.2. Statistical modelling

Using the R programming environment (R Core Team, 2021), an empirical relation between SAR backscatter and the measured water level was assessed. A linear regression model was fitted to the water level and radar backscatter data (both backscatter strength and differential phase) and significance levels for each polarization were noted as highly significant ( $p < 0.001$ ). The soil probe data and backscattering response were analysed using the R ‘mgcv’ package (R Core Team, 2021) and a generalized additive model (GAM) model was fitted between probes at all depths and the backscattering response. The significance levels between each of the polarizations and probes at different depths were then assessed and the GAM model was then refitted using data from the statistically significant probes only ( $p$ -values

<0.05). The model was then tested for autocorrelation using Partial Autocorrelation Function (PACF), indicating significant correlations only at the first lag, followed by correlations that are not significant. The response backscattering values and values computed from the model matched up well indicating a good fit with no obvious outliers or deficiencies in the model found.

### 3.3. Results

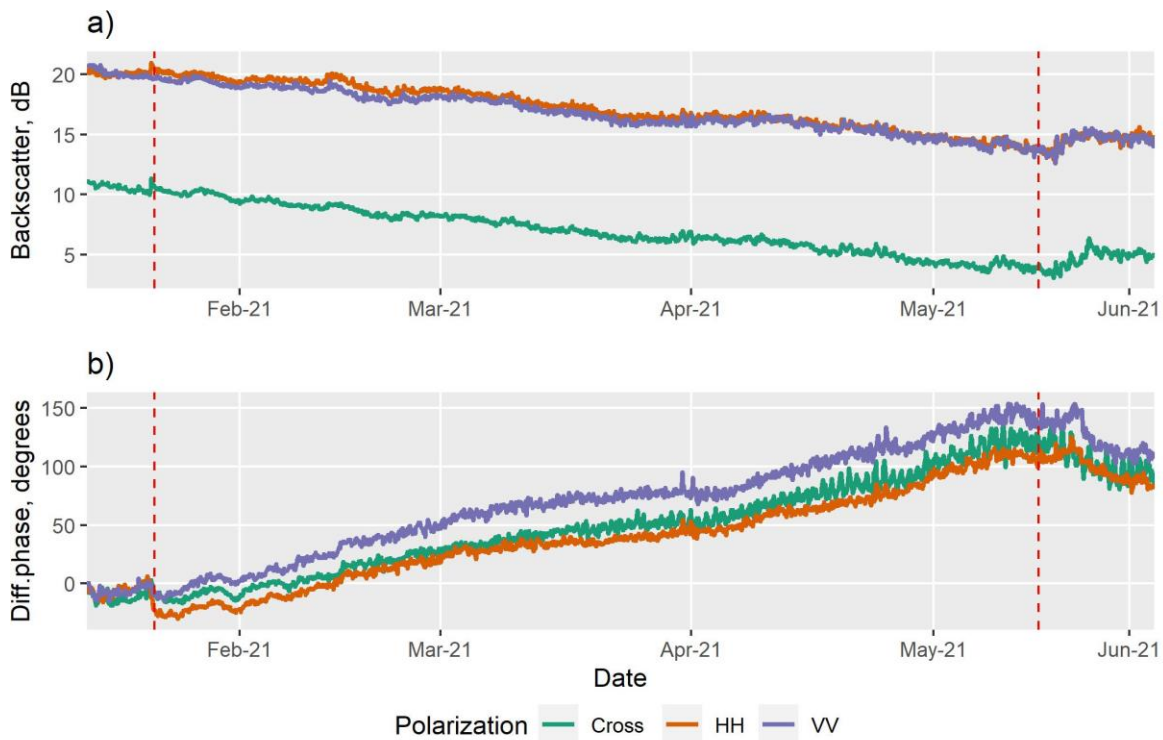
In this section, both the cross- and co-polarized radar backscatter signal strength and differential phase time series trends throughout the whole duration of the experiment are presented. Figure 3.4 shows example TP images obtained across the ROI in co-polarization (VV) and cross polarisation just prior to the drought period, reconstructed for an incidence angle,  $i$ , of  $10^\circ$ . The backscatter from the ROI surface obtained in co-polarizations (VV, HH) is notably stronger in relation to cross-polarization returns. It is understood that in the presence of vegetation, a signal that has been transmitted in V (H) can bounce once or multiple times from randomly oriented plant structures, producing a cross polarisation return (here in H (V)) (Srivastava et al., 2009). The increase in the cross-polarized signal strength present after 200 cm in Figure 3.4 is associated with greater vegetation depths from the presence of dwarf shrubs.



**Figure 3.4.** Cross-sectional views of the backscattering values from the selected peatland ROI (255 cm (l)  $\times$  100 cm (w)  $\times$  50cm (d)) before the drought, constructed using a  $10^\circ$  incidence angle. The position of the trough is shown by the horizontal white line. The red dotted oval indicates an area with heather cover and hence increased volume scattering in Cross polarization (calculated as mean of HV and VH) can be seen.

The time series of the radar measurements showed a clear decrease in backscattering strength (Figure 3.5a) and concomitant phase increase (Figure 3.5b) over the progression of the drought. The change of backscattering strength and phase varied between polarizations but showed the same

characteristic patterns. After 117 days of no precipitation, a 6.0 dB decrease and about 140° phase increase, equal to 10 mm subsidence was observed, when using VV polarization and 10° incidence angle; 7.1 dB and 8 mm in HH polarization; 7.3 dB and 8 mm in Cross polarization. Once the rewetting took place, the backscattering increased in all polarizations, but only by 1 dB on average, not reaching the pre-drought values. Similarly, phase values decreased up to 24 degrees after rewetting, but the pre-drought level was not met, potentially indicating semi-permanent peat subsidence (peat compaction) due to the drought.



**Figure 3.5.** Time series of radar backscattering (a) and phase (b) measurements reconstructed using VV, HH and Cross polarization and 10° incidence angle. Each backscatter datum is the result of an incoherent summation of pixels across the selected ROI (255 cm (l) × 1 m (w) × 50cm (d)), extracted for each image in the time series. The red dashed lines indicate the beginning (21/01/2021) and end (17/05/2021) of the simulated drought period.

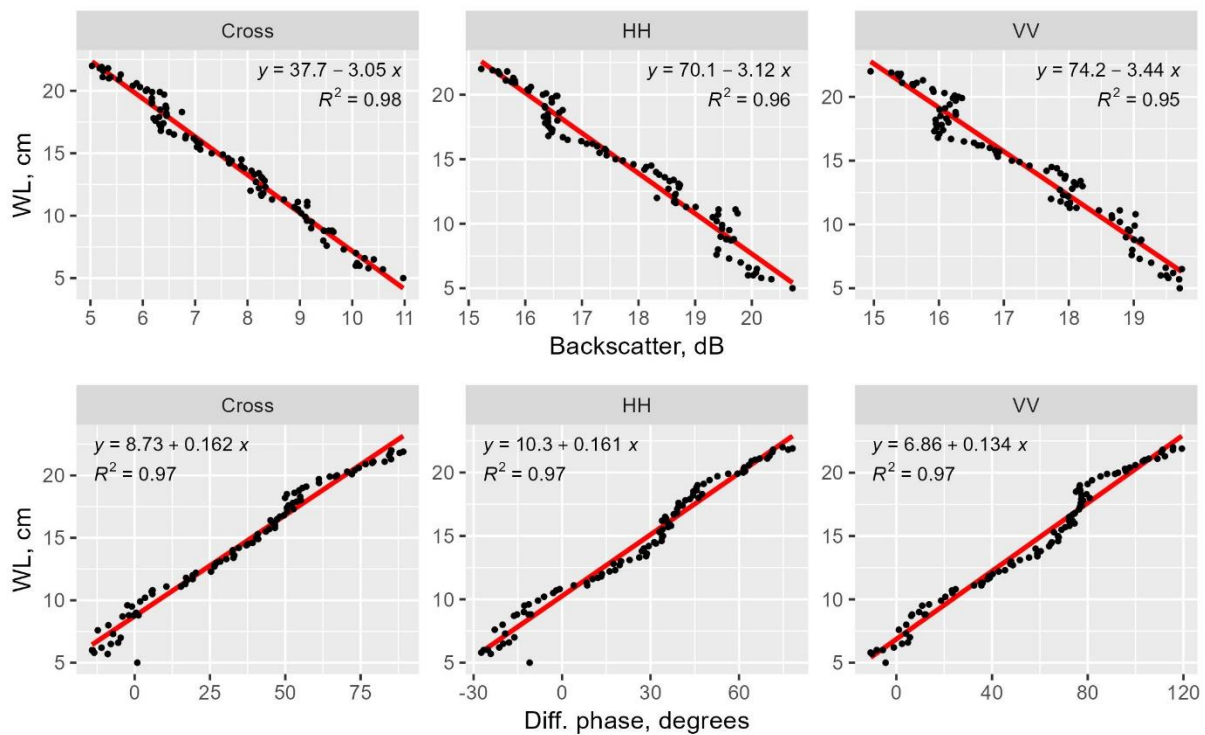
We observed that the co-polarization values on average were 10.0 dB stronger than cross-polarized signatures. The two co-polarizations had very similar values throughout the experiment, with HH backscattering values being on average 0.4 dB stronger. VV, HH values varied between 19.7 to 20.7 dB before the drought and 13.7 to 13.6 dB after 117 days of drought. Cross-polarization values were 11.0 dB prior to the drought and 3.7 dB by the end. The mean backscatter value between all polarizations was 17.1 dB prior to the drought and 10.3 dB by the end of it.

### 3.3.1. Radar backscattering signal strength and phase response to change in water table depth.

The radar backscatter was strongest at the beginning of the experiment when the WL was closest to the surface (5 cm): about 20.5 dB in co-polarized data and 11.1 dB in cross-polarization. After 95 days of drought, when WL had just reached the bottom of the trough, the backscattering had lowered by 4.8 dB (VV), 5.5 dB (HH), 5.9 dB (Cross).

All polarizations demonstrated a phase increase, with VV polarizations having the highest phase increase during the drought. After 95 days of drought, when WL had reached the bottom of the trough, the differential phase had increased by 120° or 8.5 mm (VV), 86° or 6.1 mm (HH), 84° or 5.9 mm (Cross).

After fitting a linear regression model to water level and radar backscatter data, a strong negative correlation with  $R^2 > 0.94$  was found between backscattering values and the water level in all polarizations (Figure 3.6). Similarly, the radar differential phase had a strong positive correlation ( $R^2 > 0.96$ ) with the observed water level in all polarizations.

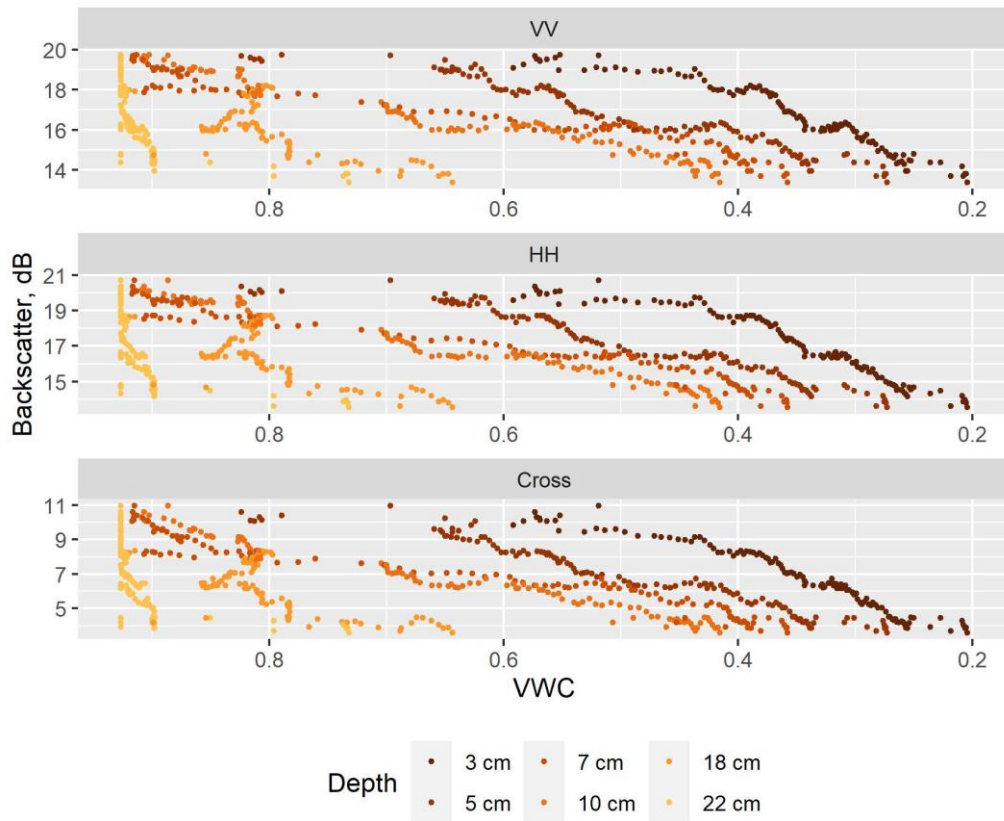


**Figure 3.6.** Correlation analysis between water level and radar backscatter (above) and differential phase (below) during the drought period (95 days with WL reaching 22 cm below the surface).

### 3.3.2. Radar backscattering signal strength response to change in soil moisture.

The radar signal relationship with soil moisture varied between the depth of the probe placement (Figure 3.7). The probes closest to the surface show a clear drying curve with a decrease in volumetric water content of the soil and a decrease in the backscattering values as the drought progressed. The

probe placed at 22 cm depth remained largely saturated (~80% VWC) even after 117 days of drought and had no significant relationship with the backscattering values in any polarization mode. The second deepest probe (18 cm) had a notable correlation with the backscattering only once VWC dropped below 80%, which was 90 days after the beginning of the drought.



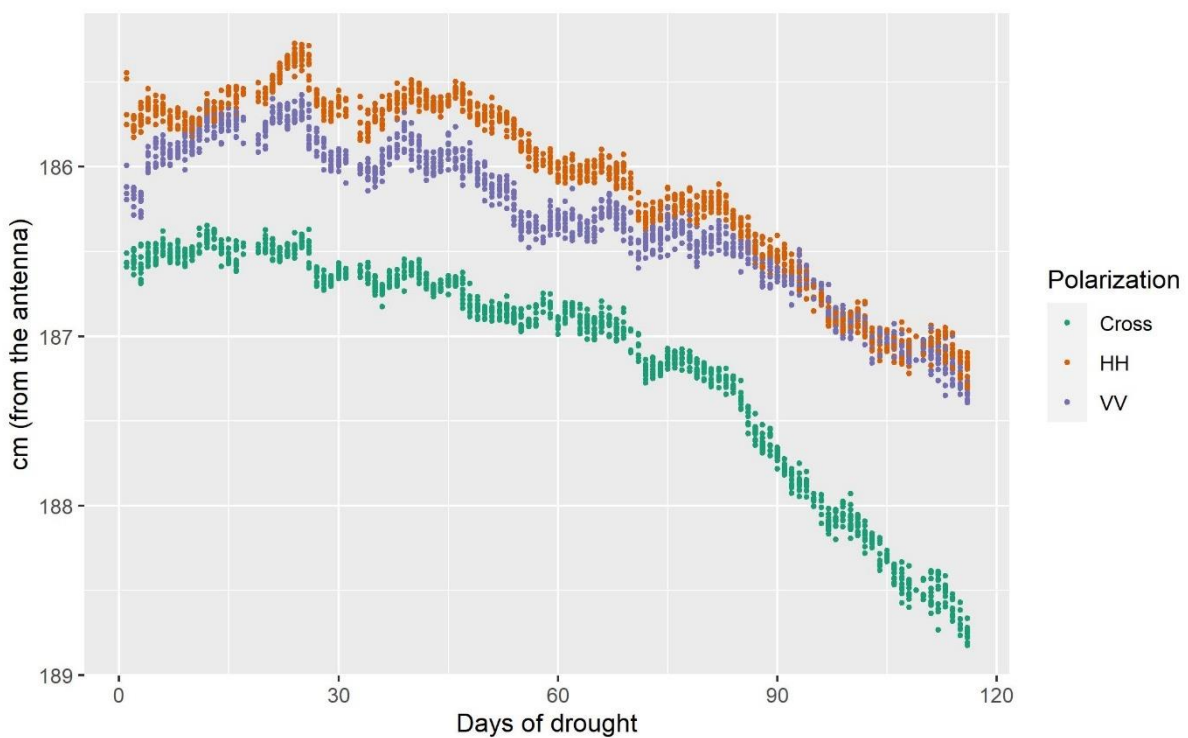
**Figure 3.7.** Soil moisture and backscattering strength response to drought (117 days of drought). Drying curves of the 6 soil moisture probes at 3-22 cm depth.

The fitted GAM model showed a significant relationship ( $p$ -values  $<0.05$ ) between the radar backscatter and probes at almost all depths, but the strongest relationships were observed with probes at 3 -10 cm depth. When the GAM model was refitted using these probes only, the model showed a resulting  $R^2$  of 0.98, indicating an excellent fit with residuals being equally and randomly spaced (Figure S1 and S2 in the Supplementary material A). The corresponding backscattering values and values computed from the model matched up very well indicating a good fit with no obvious outliers or deficiencies in the model found, clearly showing the strong linkage between volumetric water content in the peat and the radar backscattering response.

### 3.3.3. Weighted Mean Height

Using the advantage of vertical resolution from the TP scheme, an analysis of how the effective weighted mean height (WMH) of the vertical backscattering signal changed over the duration of the

drought was carried out. Figure 3.8 shows how during the first month of drought the weighted mean height of backscatter from the ROI did not report a significant lowering in any of the polarizations even though the WL had lowered by ~6 cm. The following 45 days showed a slow decrease in the WMH by -0.46/-0.85/-0.61 cm in VV/HH/Cross polarization respectively; at this point WL had dropped by 13.5 cm. Finally, the remaining period of the drought (last 45 days and ~500 scans) showed a further decrease leading to a difference of -1.35/-1.7/-2.18 cm in VV/HH/Cross polarization compared to the initial values at the beginning of the drought. The WL reached the bottom of the trough halfway through this interval, but the WMH values continued to decrease, therefore it can be noted that the WMH is not only influenced by the water level in the peatland but also the continued peat compaction and soil moisture decrease.



**Figure 3.8.** ROI backscatter weighted mean height change throughout the 117-day drought period.

Compared to the differential phase results, it can be noted that both measures indicate a distance increase during the drought period between the peat and the radar instrument, but while the differential phase showed a 0.8 – 1 cm subsidence between the three polarizations, the WMH values lowered by 1.4 – 2.2 cm. The highest subsidence values were observed in VV polarization using the differential phase, while Cross polarization backscatter had the biggest drawdown looking at the WMH.

### 3.4. Discussion

This study assessed the sensitivity of C-band TP radar signal backscatter and phase and peatland hydrological parameters (soil moisture and water table depth) over different hydrological regimes. This laboratory-based experiment included collecting unique high-resolution SAR data signatures from a



4×1 m reconstructed peatland for a period of 6 months, including a simulated drought. It is the first study to utilize the TP SAR system over peatland and a demonstration of the vertical profile of the radar backscattering signal through peat and typical blanket bog vegetation and its relationship with soil hydrological status.

The time-series analysis in this study demonstrated a close sensitivity of backscattering strength and radar phase to hydrological patterns in a peatland ecosystem with  $R^2 > 0.9$  when other factors influencing radar backscattering were controlled for. The strong correlation between radar signal and moisture status observed in this study suggest that it is likely the main controller of backscattering values in sparsely vegetated peatlands when looking at short term periods. This observation is in agreement with results from (Asmuß et al., 2019), who found WTD to be the major factor controlling backscattering strength when looking at drained temperate grasslands with underlying peat soils. Other studies with good correlation results between backscatter strength and peatland soil moisture note that C-band backscatter can be a good indicator of moisture status, but the best results can be achieved only in non-forested sites (Dabrowska-Zielinska et al., 2016; Kasischke et al., 2009; Millard and Richardson, 2018).

During the drought period of the experiment, the radar phase had a steady upward trend interpreted as arising from the increasing distance between the radar and peat surface, relating to water level decline and surface subsidence. Small oscillations were observed in the first part of the experiment, often concurrent with changes in room temperature which could be explained by the peat settling in, water movement and distribution through the peat mass and to a lesser extent the entrapped gas dynamics in peatlands (Strack et al., 2006). Previous studies focussing on the phase component of the radar signal have investigated the peatland surface oscillations over different time periods. Methods using repeated InSAR measurements have been able to track both long-term peat subsidence or uplift, as well as shorter-term surface movement, mainly connected with the dynamics of water and gasses Alshammari et al., 2020, 2018; Bradley et al. (2022) used APSIS to investigate seasonal amplitude of peat swelling as well as multiannual surface motion. They concluded that the condition of the peatland determines these ecohydrological measures as there exist certain patterns, such as subsidence over the years, amplitude of the peat swelling and the surface motion peak timings between near-natural peatlands in good condition and degraded sites. These studies had highlighted the uncertainty in the validation of the InSAR interpretation due to the massive scale difference between large-scale satellite data and small-scale field observations. Our study used a much higher accuracy SAR instrument, reducing this gap and confirmed that the phase component can maintain coherence, and be highly sensitive to the water drawdown and peat subsidence. A study by Kim et al. (2017) used field-collected WTD and radar satellite-derived soil moisture estimates over the Great Dismal Swamp ( $R^2=0.76$  with Radarsat-1 C-band and  $R^2=0.67$  with ALOS PALSAR L-band) and similarly to our findings, noted that both the radar backscatter intensity and the InSAR time series can correspond well with water table depth drawdown. Our WMH analysis has shown how the vertical SAR backscatter through the peat corresponds well

with the water level drawdown and peat subsidence and has a close similarity to the differential phase change through the drought period.

Besides the dynamics of the water level, vegetation is normally the other factor having the biggest influence on radar backscatter and cause of InSAR decorrelation (Lee et al., 2020). The excellent model fit between radar backscatter and both water level and soil moisture achieved in this laboratory study points out how the hydrological condition monitoring over peatlands could be improved significantly if other elements influencing the radar backscatter would be accounted for. Indeed, recent studies have highlighted the importance of correcting dynamic vegetation effects when estimating soil moisture and WL in peatlands (Bechtold et al., 2018; Lees et al., 2021). In this study, we observed dwarf shrub and grasses-dominated segments having a different backscattering behaviour to *Sphagnum*-covered segments (Figure S3 in the Supplementary material A). While both *Sphagnum* moss and heather-dominated transects resulted in reduced backscattering values over time during the drought, a distinction between the two groups was observed. At optimal conditions, *Sphagnum* moss can have water content as much as 20 times heavier than its dry weight (Pang et al., 2020). Due to the retention of water, the higher moisture content in the moss segments could have been preserved, resulting in higher VV backscatter values compared to the segments dominated by heather and grasses. As this experimental setup did not allow for the collection of hydrological information for each of the vegetation groups separately, we can only assume the different backscatter responses to drought were observed due to the varying water retention. A study, where, besides the radar scanning, the hydrological measurements could be taken for each of these vegetation types separately would be beneficial to gain an accurate and deeper understanding of how drought impacts backscatter response from different peatland vegetation classes.

Radar signal wavelength and polarization are important aspects to consider for peatland condition monitoring, as they determine penetration ability and the impact of the surface roughness of the area being observed. The C-band system used in this study has the capability to penetrate through sparse canopies and into the first few cm of a blanket bog vegetation and underlying peat soil. However, longer wavelength and shorter revisit times could increase the InSAR coherence (Lee et al., 2020) and be beneficial for peatland surface oscillation monitoring. There is a high potential for the upcoming NISAR satellite mission (to be launched in 2023), operating at the longer S-band (~9 cm) and L-band (~24 cm), having a revisit time of 12 days, and following an open data policy (NISAR 2021). For this study, fully-polarimetric SAR data were available, which is advantageous compared to most currently operating satellite radar missions which would only provide either single or dual polarization data or have restricted access. Bare or sparsely vegetated areas, such as peatlands, usually have a weak depolarizing effect, and surfaces that are linearly oriented tend to reflect and preserve the same wave orientation. In these situations, a stronger co-polarization (VV, HH) normally would be observed, which was congruent with findings in this study. The relationship between peatland hydrological parameters and the backscatter had no major differences between cross and co-polarizations, both performing equally

well despite cross-polarized signal being on average 10 dB weaker throughout the experiment. The study by Dabrowska-Zielinska et al. (2016) reported VH polarization to perform better for wetland soil moisture monitoring. Other studies have also found that a cross-polarization ratio (HH/HV) could be beneficial for hydrological condition monitoring as it should minimize the effect of peatlands surface roughness and/or present vegetation on radar backscatter as shown in the analysis carried out by Jacome et al. (2013). Peatland pools can create wavy and rough surfaces in windy conditions and VV return can be misinterpreted as a vegetated area, VH on the other hand is much less affected (White et al., 2020), therefore cross-polarization should be considered when working with natural peatland environments.

Diverse correlation results reported in previous studies using satellite radar data and field measurements could be explained by varying factors such as different peatland types, surface topography, present vegetation and its abundance, and environmental conditions (frost, wind, animal grazing, burning) and chosen radar instrument (wavelength, polarization, data temporality). This study has shown that an excellent model fit between radar backscatter and vegetated peatland soil moisture and water table depth can be achieved in laboratory conditions. To further improve peatland hydrological condition estimates using satellite SAR data, more precise modelling of other elements influencing radar backscatter is necessary. We have highlighted the need to first enhance the efforts to account for the surface roughness, including the present vegetation of the area being imaged, which in return should enhance the ability to estimate peatland hydrological condition using SAR data.

### **3.5. Conclusion**

This study has in part clarified the behaviour and characteristics of SAR C-band interaction with peatlands. The unique laboratory-environment research with 4 months long forced drought demonstrated a coherent radar signal response to the change in water table depth and soil moisture. While the phase component of the signal was indicative of a physical movement of the surface horizon, the signal strength demonstrated close relation to the water availability in the soil, both confirming a firm relationship existing between radar backscatter and peat hydrological characteristics with  $R^2 > 0.9$  when other factors influencing radar backscattering were controlled for.

Regarding our set objectives, we concluded that due to the SAR signal being highly sensitive to the dielectric properties of the soil, any significant changes in peatland soil hydrological conditions can be reflected in the radar measurements. The unique dataset captured vertical SAR backscatter patterns through peat, improving the understanding of how backscattering arises in peatlands and will allow for better exploitation of radar imagery from existing and upcoming satellite radar missions. It highlights the potential to use SAR to monitor the peatland condition, especially the hydrological status, utilizing both the coherent and incoherent component of the signal, but points out how a better understanding of other factors influencing the radar backscatter is crucial to fully rely on satellite SAR data.

# Chapter 4

## 4. Potential for peatland water table depth monitoring using Sentinel-1 SAR backscatter: case study of Forsinard Flows, Scotland, UK<sup>2</sup>

### Abstract

Peatland restoration has become a common land-use management practice in recent years, with water table depth (WTD) being one of the key monitoring elements where it is used as a proxy for various ecosystem functions. Regular, uninterrupted and spatially representative WTD data in situ can be difficult to collect, therefore remotely sensed data offer an attractive alternative for landscape scale monitoring. In this study, we illustrate the application of Sentinel-1 SAR backscatter for water table depth monitoring in near-natural and restored blanket bogs in the Flow Country of northern Scotland. Between the study sites, the near-natural peatlands presented the smallest fluctuations in WTD (typically between 0 and 15 cm depth) and had the most stable radar signal throughout the year (~3 to 4 dB amplitude). Previously drained and afforested peatlands undergoing restoration management were found to have higher WTD fluctuations (up to 35 cm depth), which were also reflected in higher shifts in radar backscatter (up to ~6 dB difference within a year). Sites, where more advanced restoration method had been applied, however, were associated with shallower water table depths and smoother surfaces. Three models: simple linear regression, multiple linear regression, and random forest model, were evaluated for their potential to predict water table dynamics in peatlands using Sentinel-1 backscatter SAR. The random forest model was found to be the most suited having the highest correlation scores, lowest RMSE values and overall good temporal fit ( $R^2 = 0.66$ , RMSE = 2.1 cm), with multiple linear regression coming in a close second ( $R^2 = 0.59$ , RMSE = 4.5 cm). The impact of standing water, terrain ruggedness and ridge and furrow aspect on model correlation scores was tested but found not to have a statistically significant influence. We propose that this approach, using Sentinel-1 and random forest models to predict WTD, has strong potential and should be tested at a wider range of peatland sites.

---

<sup>2</sup> This chapter has been published as follows: Toca, L., Artz, R.R.E., Smart, C., Quaipe, T., Morrison, K., Gimona, A., Hughes, R., Hancock, M.H., Klein, D., 2023. Potential for Peatland Water Table Depth Monitoring Using Sentinel-1 SAR Backscatter: Case Study of Forsinard Flows, Scotland, UK. *Remote Sens (Basel)* 15. <https://doi.org/10.3390/rs15071900>

## 4.1. Introduction

Peatland ecosystems, in their natural state, both sequester CO<sub>2</sub> and act as a long-term carbon storage. More than one-fifth of Scotland is covered by peatlands, making them a key landscape and a significant provider of peatland ecosystem services. Blanket bog is a unique habitat which requires very specific conditions to form i.e., high rainfall, oceanic cool climate all year round and relatively flat areas with poor surface drainage (Lindsay et al., 1988). While quite common among UK peatlands, globally these are rare habitats covering only about 0.1% of land area (Gallego-Sala and Colin Prentice, 2013). Inappropriate land management, such as drainage, commercial afforestation, agriculture, overgrazing, and peat cutting have left many peatlands around the world degraded. Particularly in the UK, these poor past management decisions have turned peatlands from carbon sinks into large CO<sub>2</sub> emission sources. It is estimated that only about 20% of the UK's peatlands have remained in a near-natural state (Joosten et al., 2012). Luckily, more extensive landscape scale peatland restoration can be observed in the recent years (Alderson et al., 2019).

For peatland restoration to be successful multiple criteria should be met. The return of high water table, relatively even surface, and regrowth of vegetation are some of the most important factors (Lucchese et al., 2010; Sottocornola et al., 2007). High water table depth (WTD) and saturated soil are crucial both to maintain a healthy bog environment in near-natural sites as well as to encourage recovery in peatland restoration sites. If rewetting has been successful, it encourages recovery and regrowth of bog vegetation communities, improves ecosystem resilience, and can reduce CO<sub>2</sub> emissions and improve sequestration rates (Hancock et al., 2018; Lucchese et al., 2010). The average water table depth over (sub)decadal timescales in peatlands is closely related to carbon accumulation and greenhouse gas exchange (Kalacska et al., 2018), with an expected increase in CO<sub>2</sub> release after a significant and prolonged water table lowering (Evans et al., 2021). While field-gathered water table depth measurements are invaluable in obtaining the precise depth of the water table, the installation of monitoring equipment, maintenance, and data gathering can be time and resource-consuming and provide only point measurements. Remotely sensed data on the other hand have the potential for frequent hydrological condition monitoring covering large, spatially contiguous areas.

Previous studies have analysed the relationship between peatland surface moisture conditions and water table depth with optical, thermal, but less frequently radar satellite data (Czapiewski and Szumińska, 2022; Luscombe et al., 2015). From studies utilising radar imagery, some of the most recent are focused on peatland condition assessment through the bulk movement of the peat using the coherent differential phase component of the signal (Alshammari et al., 2020; Bradley et al., 2022), while most studies still focus on the incoherent backscatter strength analysis. Some studies using backscatter strength for peatland studies, have shown promising results, reaching a coefficient of determination of up to 0.93 (Klinke et al., 2018), although most report moderate to weak relationships between peatland hydrological state and backscatter (Asmuß et al., 2019; Bechtold et al., 2018; Kim et al., 2017). A recent

high resolution radar backscatter laboratory study has demonstrated a high sensitivity of radar backscatter to hydrological patterns in a peatland ecosystem (Toca et al., 2022). Statistical models that have been used for WTD estimates in wetlands using radar backscatter data mainly include linear regression (Bechtold et al., 2018; Bourgeau-Chavez et al., 2005; Kim et al., 2017; Millard and Richardson, 2018) and random forest (Klinke et al., 2018; Räsänen et al., 2022; Torbick et al., 2012), but usually do not compare the performance and outcomes of different models at the same time.

It is partly the complex nature of the SAR signal, as well as the high heterogeneity between peatlands, which makes the peatland hydrological monitoring using radar technology complicated. Additionally, very few studies have focussed on the comparison of statistical models referring to peatlands in different conditions. With an increasing number of peatland restoration sites and the necessity to regularly monitor their condition, radar remote sensing has the potential to provide data on restoration trajectories and effectiveness at both high temporal and spatial resolutions, covering large areas. Sentinel-1 provides the advantage of obtaining data in cloudy weather and provides archival data dating back to 2014.

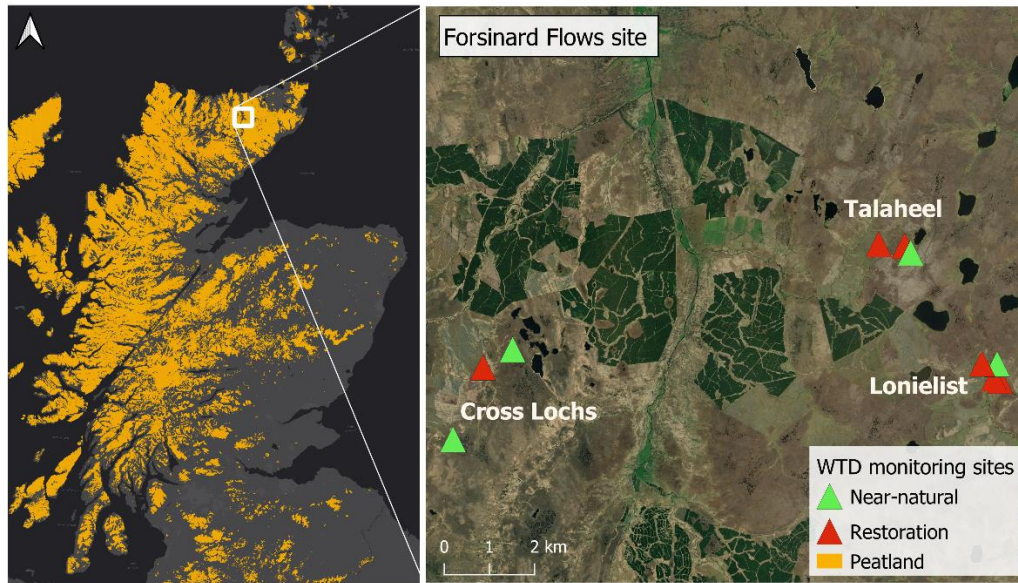
In this study, we evaluate whether multitemporal satellite radar imagery can be used to monitor the water table depth in near-natural sites and sites that are undergoing restoration. To determine whether there is a potential application of Sentinel-1 for peatland hydrological monitoring, the following objectives were set for this study:

1. Investigate the correlation between Sentinel-1 radar data and WTD in blanket bogs at Flow Country of northern Scotland, ranging from intact and near-natural sites, through to sites damaged by past afforestation and drainage, where restoration has recently started.
2. Create and test models with different complexity for WTD estimation using Sentinel-1 data.
3. Characterise the effects of surface roughness, hydrological condition (characterized by WTD measurements), seasonality and time of acquisition in the developed models.

## **4.2. Materials and Methods**

### **4.2.1. Study Area**

The Royal Society for the Protection of Birds (RSPB) Forsinard Flows reserve (58°23'N, 3°51'W) is located in Northern Scotland and is part of the 4000 km<sup>2</sup> Flow Country blanket bog (Lindsay et al., 1988). Figure 4.1 shows the distribution of peat soils in the northern part of Scotland and the location of the chosen blanket bog research site. The nearest Met Office weather station (Kinbrace, Hatchery, ~20 km away) is situated at 103 m asl, has a mean annual (1991–2020) precipitation of 949 mm/year<sup>-1</sup> and max. and min. air temperatures of 11.7 °C and 3.6 °C, respectively.

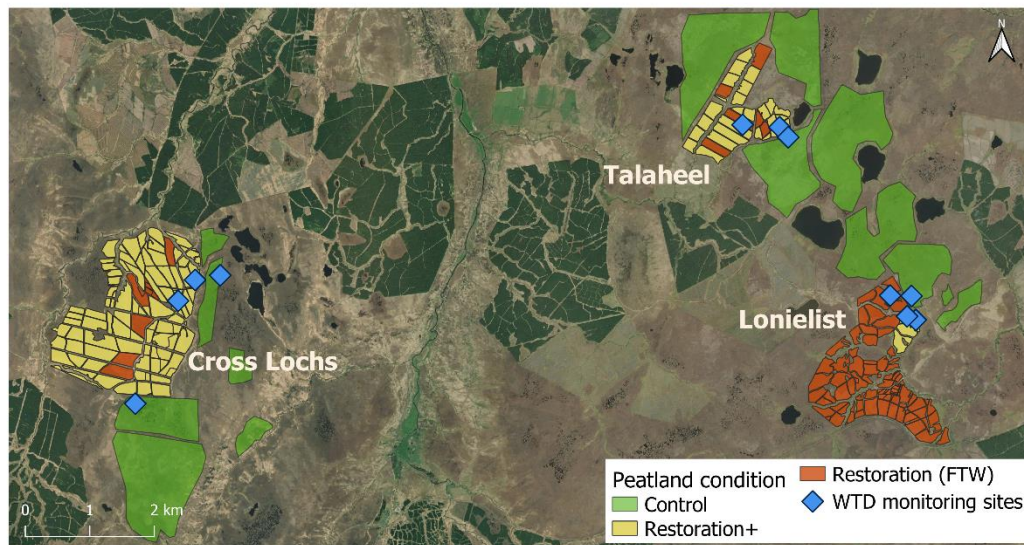


**Figure 4.1.** Peatland extent in northern Scotland (Aitkenhead and Coull, 2020) and the chosen study sites in the Forsinard Flows. The green triangles show the near-natural peatland study sites, and the red triangles show sites with ongoing restoration.

Technological forestry advancements along with government tax incentives in the 1970s and 1980s led to the peatlands in this area being heavily drained, gouged and planted with non-native conifers, namely, Lodgepole Pine *Pinus contorta* and Sitka Spruce *Picea sitchensis*. The restoration works have taken place at different times from 1998 to the present (further details in Table 4.1-4.3) and include multiple restoration techniques offering a valuable and unique set of restored peatland chronosequence data. The fell to waste (FTW) restoration method involved tree felling and placing the felled trees in nearby furrows or drainage ditches. In such sites, the historical ridge and furrow forestry pattern can still be present after 20 years since tree felling and is easily visible in remotely sensed data. Felling to waste is rarely practiced these days, as timber of larger sizes, is now generally extracted, but serves as a useful experimental treatment with respect to legacy issues. Additional management techniques applied after felling to waste (or, more recently timber harvesting) can include furrow blocking, mulching of the brash, stump flipping and other surface reprofiling methods (Hancock et al., 2018). Brash crushing and furrow blocking treatment usually includes the leftover brash material (tops and small-diameter branch wood) further crushing down and blocking the individual plough furrows created at forestry planting (Artz et al., 2018). Cross tracking includes surface ground smoothing using an excavator that passes over a peatland and with its weight eliminates or reduces the relict forestry ploughing pattern (Artz et al., 2018).

Eleven representative sites from near-natural and restoration sites were chosen based on the presence of water level monitoring equipment at three areas (Figure 4.2); four representing near-natural (see “Control” in Figure 4.2), three representing simple restoration (FTW), and four representing complex restoration (Restoration+), with the latter having additional management applied after initial

felling treatment. The control sites were selected to have matching slope and aspect to the relative restoration treatment areas in each of the three areas (Cross Lochs, Talaheel and Lonielist), and an additional control near the location of a long-term greenhouse gas monitoring site at Cross Lochs (Levy and Gray, 2015). This second near-natural control is surrounded by more small water bodies than other control areas around the wider area, and was included in order to assess variability in near-natural conditions more generally. At Lonielist, two restoration treatments were included, one site with brash crushing and furrow blocking treatment and the other with further ground smoothing treatment (cross tracking).



**Figure 4.2.** Forsinard Flows research site – different polygon colours represent the different management methods applied to peatland restoration. The eleven WTD monitoring points represent the chosen locations for analysis – 4 near-natural control sites, 3 Restoration (FTW), 4 Restoration+ sites.

#### 4.2.2. Water table depth and Meteorological Data

WTD data were recorded continuously from permanent dipwells using automatic loggers (Odyssey Capacitance Water Level Logger, New Zealand) at half-hourly intervals. Dipwells (~1.5 m length, 32 mm diameter) were made of polypropylene pipes and had 3 mm perforation holes at 50 mm intervals. Artz et al. (2022) provide further details about the dipwell installation. The WTD data were combined to derive a daily average position (i.e., cm from the surface) for analysis to standardise with the Sentinel-1 overpasses. Water table depth data was available for the period between July 2017 (September 2018 for some sites) and October 2020. For mean WTD comparisons between the study sites, we used only the period when data for all sites were available (September 15, 2018 – July 31, 2020).



### 4.2.3. Remotely sensed data

The Google Earth Engine (GEE) platform provides an invaluable computational environment for cloud-based processing of vast amounts of satellite imagery. GEE was used to acquire and process the Sentinel-1 high-resolution Level-1 Ground Range Detected (GRD) Interferometric Wide Swath (IW) products for the chosen study area and period.

GRD IW images have been multi-looked and projected to ground range using an Earth ellipsoid model (ESA, 2023b). The GRD IW satellite imagery has  $20 \times 22$  m (range  $\times$  azimuth) spatial resolution and  $10 \times 10$  m pixel spacing. GRD scenes available on GEE have been pre-processed, radiometrically calibrated, and corrected for terrain (GEE, 2023b). GEE was used to extract satellite data between 2015 and 2021 for analysis at all 11 locations within Forsinard Flows. In each location a 30 m radius around the water table depth monitoring station was considered, therefore each area analysed was equal to ca  $2827 \text{ m}^2$  or about 28 Sentinel-1 pixels. A weighted reducer was used, where the pixels are included in the analysis if at least 50% of the pixel is in the region, and their weight is the fraction of the pixel covered by the region (GEE, 2023b). The 30 m distance was chosen to both include enough pixels to average out noise from the radar data and, at the same time, ensure the area analysed represent relatively homogeneous vegetation communities. There was a stack of 330 Sentinel-1 images extracted for the chosen period, with values from both vertical-vertical (VV) and vertical-horizontal (VH) polarization. To secure data consistency, data was then split into ascending and descending orbit datasets, and the ascending path was chosen as the most appropriate for the study region due to the ascending overpass happening around 6 pm in the evening, when the dew effect is expected to have a minor effect. The same path number (No. 30) was chosen for all images. The incidence angle difference for the areas investigated was small (ranging from  $39.90^\circ$  to  $40.57^\circ$ ), therefore local incidence angle correction was not applied. As the extracted Sentinel-1 time series can be noisy, besides averaging the backscatter spatially over each of the locations, a temporal smoothing function with a rolling average (integer width of the rolling window ( $k$ ) = 4) was applied to the dataset.

To improve the radar time-series data, weather filtering can be beneficial (Benninga et al., 2019) and was incorporated using data from The Centre for Environmental Data Analysis (CEDA) archive for the nearest long-term UK Met Office weather station, Altnaharra (~35 km away). Bechtold et al. (2018) has suggested the removal of days with heavy rainfall ( $>20$  mm) or frozen soil ( $< 2^\circ \text{ C}$ ), while Asmuß et al. (2019) found the removal of dates where the soil temperature was below  $2^\circ \text{ C}$ , and precipitation occurred in the six-hour period before acquisition, improved the correlation coefficients between grassland WTD and radar backscatter. We found that removal of days when the soil temperature was below  $2^\circ \text{ C}$ , days with snow cover, and days when rainfall heavier than 2 mm occurred in the 6 h period before the satellite overpass, worked as the most optimal weather filtering.

Additionally, the positioning of historical forestry ridge and furrow lines and the ratio of standing water in each location has been visually derived from aerial photographs acquired over the area in 2017.

#### 4.2.4. LiDAR data and TRI analysis

Surface roughness (microtopography and vegetation above the ground) is one of the parameters influencing radar backscatter. QGIS software was used to process LiDAR imagery, taken over the area in 2017, and generate a digital surface model (DSM) and derive Terrain Ruggedness Index (TRI) values. TRI describes the amount of elevation difference between cells of a DSM and was used as an indicator to analyse surface roughness between the research sites. TRI is calculated as an elevation difference between each DSM grid cell ( $50 \times 50$  cm) and its eight surrounding cells in a DEM using an equation developed by Shawn Riley et al. (1999):

$$\text{TRI} = \sqrt{[\sum (x_i - x_0)^2]} \quad (4.1)$$

where  $x_i$  is the elevation (m) of each neighbouring cell to the central cell  $x_0$  (m).

#### 4.2.5. Model generation and statistical analysis

To examine the backscatter trends and the potential for Sentinel-1 backscatter to be used as a predictor of WTD for select peatland sites, three models with different complexity were chosen for the analysis: a simple linear regression (SLR), multiple linear regressions (MLR) and random forest method (RF). The modelling dataset (total number of observations, when both backscatter and WTD data was available ( $n = 1322$ ) was split into training (70%) and validation (30%) data sets. Correlation coefficient ( $R^2$ ) and associated  $p$ -values, and Root Mean Square Error (RMSE) were calculated and reported for all three modelling approaches. All the statistical analyses were conducted in the R programming environment (R Core Team, 2021).

Some studies have shown values from a single polarization to be sensitive to water table depth changes (Kasischke et al., 2009; Kim et al., 2017; Toca et al., 2022). Therefore, first, Sentinel-1 backscatter (VV and VH polarization, separately) was directly used as a predictor variable to model the water table depth using a simple linear regression model:

$$y = \alpha_0 + \beta_1 x_1 \quad (4.2)$$

where  $y$  is the dependent variable that is being predicted (WTD),  $x_1$  is the independent variable (VV or VH polarization backscatter) used for prediction of  $y$ ,  $\alpha_0$  is the intercept and  $\beta_1$  is the slope.

The model was then expanded to multiple linear regression, which can incorporate multiple continuous or categorical independent variables. The WTD was estimated using radar VV and VH polarizations, and four categorical variables: season and year of radar acquisition, the site being investigated (site identifier) and the condition group it belongs to (Control/Restoration (FTW)/Restoration+).

$$y = \alpha_0 + \beta_1 x_1 + \beta_2 x_2 + \dots + \beta_n x_n \quad (4.3)$$

where  $y$  is the dependent variable that is being predicted (WTD),  $x_1, x_2, \dots, x_n$  are the independent variables (VV, VH polarizations, season, year, site identifier, condition group) used to predict  $y$ ,  $\alpha_0$  is the intercept and  $\beta_1, \beta_2, \dots, \beta_n$  are the slope coefficients for each explanatory variable. The VV and VH variables were standardised using their z-score to compare the importance of each polarization coefficient for the model. The R *stats* package and *lm* function were used for SLR and MLR fitting (R Core Team, 2021).

Finally, a random forest (RF) machine learning approach was used to estimate the water table depth using R *randomForest* package (version 4.7-1.1) (Liaw and Wiener, 2002). Random Forest, developed by Breiman (2001), is a supervised learning algorithm that uses ensemble method by grouping multiple decision tree predictions to perform regression or classification. One of the best-known RF advantages is the model's ability to identify non-linear relationships as the model does not make assumptions about the relationship between input and response variables (Breiman, 2001). The same input variables as for MLR were used. The model was restricted to 50 decision trees and 3 variables to randomly sample as candidates at each split. RF model feature importance was then reported, quantifying the relative importance of the different input variables for the WTD estimate.




### **4.3. Results**

First, we examined the temporal dynamics of observed water table depth and radar remote sensing data over all the sites. Then, the dynamics of observed water table depth and the backscatter between the different condition groups are described. Finally, the model outcomes for the three different modelling approaches are reported and compared to the field observed water table depth data.


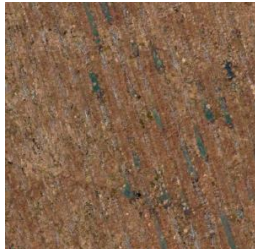


#### **4.3.1. Water table depth and Sentinel-1 time series analysis**

A summary of the Forsinard Flows peatland sites' historical management, aerial photographs, calculated mean observed WTD (mm below the surface), and TRI are presented in Table 4.1 (Talaheel site), Table 4.2 (Lonielist site) and Table 4.3 (Cross Lochs site).

**Table 4.1.** Forsinard Flows Talaheel site’s characteristics. \*Mean water table depth between September 15, 2018, and July 31, 2020.




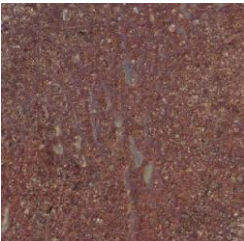
	Near-natural (control)	Restoration (felled to waste)	Restoration+ (felling and additional management)
Aerial photograph (Natural colour (RGB) orthophoto, 50 cm resolution, March 2017)			
Terrain Ruggedness Index, TRI (cm)	9.6	21.3	12.5
Mean WTD* ± SD (cm)	4.9 ± 3.5	12.3 ± 4.0	11.3 ± 5.4
Year afforested	-	1983	1985
Year felled	-	1998	1998
Year of additional restoration management	-	-	2016
Restoration method	-	-	Brash crushing and furrow blocking
Abbreviation	TA_CON	TA_FTW	TA_BCFB

**Table 4.2.** Forsinard Flows Lonielist sites’ characteristics. Two Lonielist restoration sites with additional management are used in the study and described as a) LO\_BCFB and b) LO\_CT. \* Mean water table depth between September 15, 2018, and July 31, 2020.

	Near-natural (control)	Restoration (felled to waste)	Restoration+ (felling and additional management)
Aerial photograph (Natural colour (RGB) orthophoto, 50 cm resolution, March 2017)			 a)  b)
Terrain Ruggedness Index, TRI (cm)	9.7	16.8	a) 14.0 b) 17.0
Mean WTD * ± SD (cm)	2.8 ± 3.8	12.9 ± 5.6	a) 3.8 ± 4.7 b) 9.4 ± 7.0
Year afforested	-	1985	1985

Year felled	-	2006	a) 2006 b) 2004
Year of additional restoration management	-	-	a) 2012, 2018 b) -
Restoration method	-	-	a) Brash crushing and furrow blocking b) Cross tracking and furrow blocking
Abbreviation	LO_CON	LO_FTW	a) LO_BCFB b) LO_CT

**Table 4.3.** Forsinard Flows Cross Lochs sites' characteristics. Two near-natural Cross Lochs sites were used in the study, and are described as a) CL\_CON and b) CL\_CON\_EC (location of the long-term GHG monitoring station). \* Mean water table depth between September 15, 2018, and July 31, 2020.

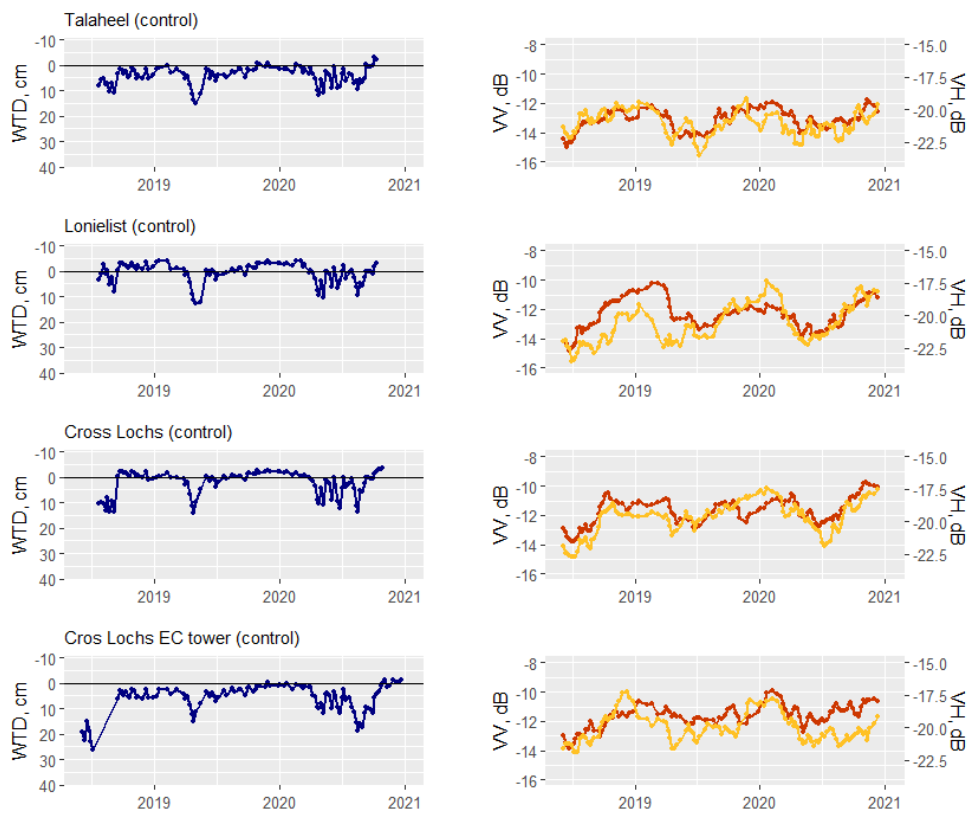
	Near-natural (control)	Restoration (felled to waste)	Restoration+ (felling and additional management)
Aerial photograph (Natural colour (RGB) orthophoto, 50 cm resolution, March 2017)	 a)		
	 b)		
Terrain Ruggedness Index, TRI (cm)	a) 3.8 b) 3.2	5.0	2.8
Mean WTD * $\pm$ SD (cm)	a) $4.9 \pm 4.7$ b) $0.9 \pm 2.5$	$14.7 \pm 7.0$	$4.9 \pm 4.5$
Year afforested	-	1983	1983
Year felled	-	2006	2005
Year of additional restoration management	-	-	2016
Restoration method	-	-	Brash crushing and furrow blocking
Abbreviation	a) CL_CON b) CL_CON_EC	CL_FTW	CL_BCFB

The summary presented in Tables 1-3, shows that the near-natural sites in all locations exhibit the desirable hydrological conditions for peatlands of a mean water table depth close to the surface. The

WTD in restoration sites with simplistic restoration presents the deepest values, while the WTD in sites with additional restoration measures typically lie between control sites and felled to waste sites. Similarly, TRI values are lowest for near-natural sites and highest for felled to waste sites, affected by the ridge and furrow patterns.

#### **4.3.1.1. Near-natural peatlands – control areas**

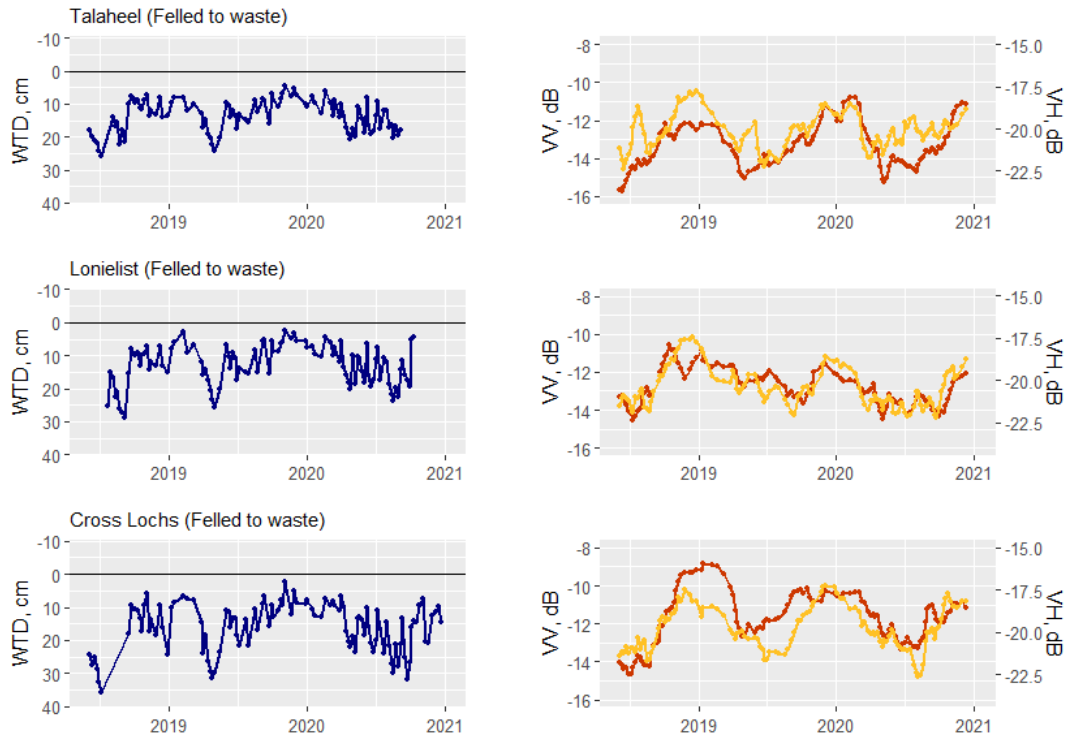
Figure 4.3 shows the water table depth and Sentinel-1 time series for four near-natural peatland areas in the Forsinard Flows site. The water table depths (apart from the short periods during the 2019 and 2020 summer seasons) largely remain very close to the surface or inundated for long periods of the year. Mean water table depths of the sites were  $4.9 \pm 3.5$  cm,  $2.8 \pm 3.8$  cm,  $4.9 \pm 4.7$  cm and  $0.9 \pm 2.5$  cm for Talaheel, Lonielist, Cross Lochs and Cross Lochs EC sites, respectively. While excluded from the mean WTD calculation, the Cross Lochs EC site suggested significant WTD drawdown during summer 2018, when data from the other sites were not available yet. VV polarization for all control sites was on average 8 dB stronger compared to the VH. Between the control sites, the difference in mean backscatter values was only about 1.5 dB between sites with strongest and weakest return. The highest backscatter values were observed in Cross Lochs (-19.6 dB VH; -11.7 dB VV) and Cross Lochs EC site (-19.9 dB VH; -11.6 dB VV), followed by Lonielist (-20.6 dB VH; -12.3 dB VV) and lowest values were found for Talaheel (-21.0 dB VH; -13.1 dB VV). As expected for non-forested bog ecosystems, all near-natural sites had very low TRI values (~3 - 4 cm for Cross Lochs sites and ~10 cm for Talaheel and Lonielist sites).



**Figure 4.3.** Observed water table depth (left) and Sentinel-1 (right; VV in red, VH in yellow) backscatter time series for near-natural peatland sites in Forsinard Flows area. The black horizontal line indicates the ground surface.

#### 4.3.1.2. Restoration – felled to waste

Figure 4.4 shows the water table depth and Sentinel-1 time series for three peatland restoration areas which have had a simple restoration technique applied – “felled to waste”. The water table depth levels are lower compared to the previously analysed near-natural sites, and the summer drought periods lead to deeper water levels and longer recovery periods. Mean water table depths of the sites were  $12.3 \pm 4.0$  cm,  $12.9 \pm 5.6$  cm, and  $14.7 \pm 7.0$  cm for Talaheel, Lonielist and Cross Lochs sites, respectively and none of the loggers had been inundated throughout the measuring period. As with the near-natural sites, the Cross Lochs data series, which date back longer, indicate a water table depth drawdown in the summer of 2018. The highest backscatter values were observed in Cross Lochs (-19.7 dB VH; -11.6 dB VV), followed by Lonielist (-20.3 dB VH; -12.7 dB VV) and Talaheel (-20.0 dB VH; -13.3 dB VV). VV backscatter values were on average 0.4 dB weaker compared to the near-natural sites, while VH backscatter was 0.3 dB stronger. TRI values were found to be highest for Talaheel with ~21 cm, ~17 cm for Lonielist and ~5 cm for Cross Lochs site.



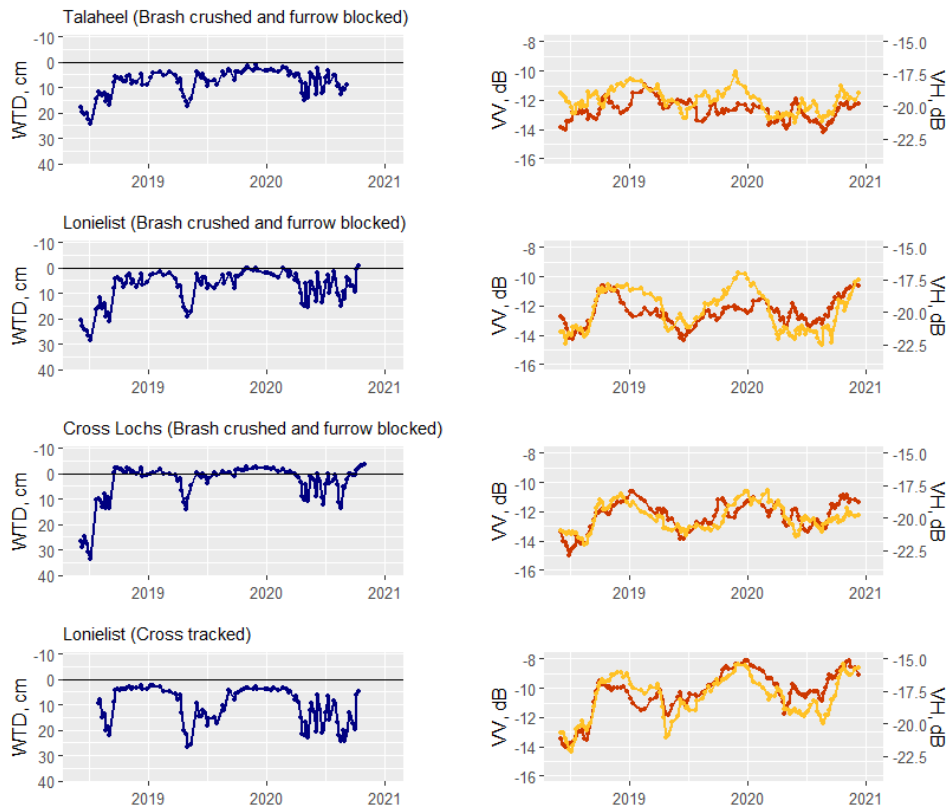
**Figure 4.4.** Observed water table depth (left) and Sentinel-1 (right; VV in red, VH in yellow) backscatter time series for peatland sites with simplistic restoration (felling to waste) applied. The black horizontal line indicates the ground surface.

#### 4.3.1.3. Restoration with additional management

Figure 4.5 shows the water table depth and Sentinel-1 time series for four peatland restoration areas where, in addition to felling, other potentially more successful peatland restoration has been used. The additional methods for these sites included furrow blocking, brash crushing and cross tracking. The time series of the water table depth in these sites greatly resemble those observed in near-natural sites with more stable water levels, smaller drawdowns, and quicker recoveries during the dry seasons. Partial inundation was also observed, most notably in the Cross Lochs site. Mean water table depths of the sites were  $11.3 \pm 5.4$  cm,  $3.8 \pm 4.7$  cm,  $9.4 \pm 7.0$  cm and  $4.9 \pm 4.5$  cm for Talaheel, Lonielist-1, Lonielist-2 and Cross Lochs sites, respectively. The highest backscatter values were observed in Lonielist cross tracked site (-18.0 dB VH; -10.3 dB VV), followed by Talaheel (-19.5 dB VH; -12.6 dB VV), Cross Lochs (-19.9 dB VH; -12.3 dB VV), and Lonielist (-19.9 dB VH; -12.4 dB VV) brash crushed and furrow blocked sites. TRI values were found to be slightly lower compared to the felled-only sites, being highest for Lonielist (14 – 17 cm), followed by Talaheel (~12 cm), and lowest for the Cross Lochs site (~3 cm).

The average radar backscatter values from this group were found to be the strongest among the three condition groups. VH backscatter was 1 dB stronger than control sites and 0.7 dB stronger than the felled to waste sites. VV backscatter was slightly stronger (0.3 dB) compared to the control sites and 0.6 dB stronger than the felled to waste sites.



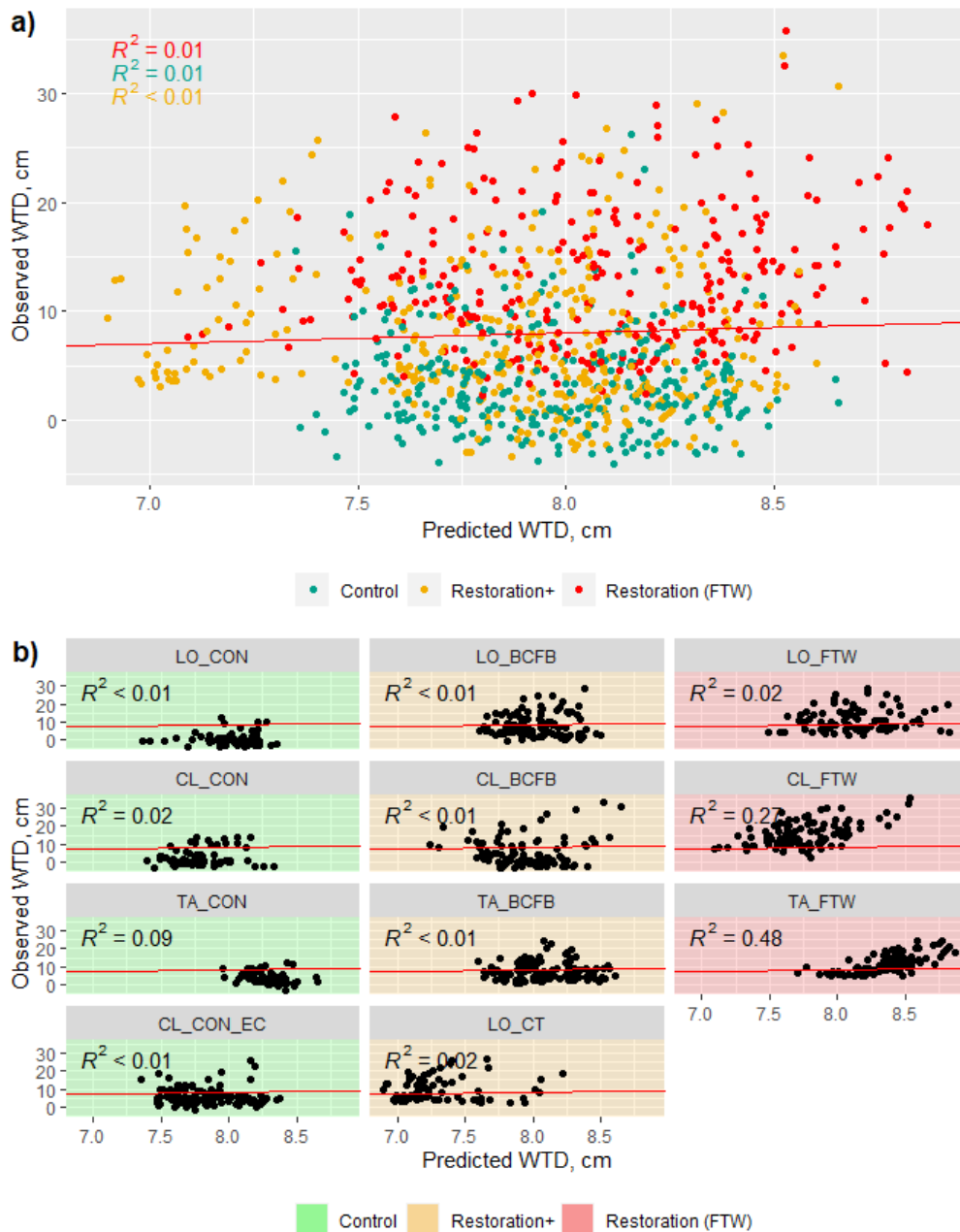


**Figure 4.5.** Observed water table depth (left) and Sentinel-1 (right; VV in red, VH in yellow) time series for sites undergoing more advanced restoration applied (brash crushing, furrow blocking and re-profiling). The black horizontal line indicates the ground surface.

### 4.3.2. Correlation of Sentinel-1 backscatter and water table depth

#### 4.3.2.1. SLR model

First, the SLR model was applied to all sites and condition groups together. A very low agreement between the predicted and observed WTD was found ( $R^2 < 0.01$  when using either VV or VH) (Figure 4.6a and Table 4.4). When the model was applied to each site separately, an improved but still very weak relationship ( $R^2 < 0.3$ ) was found for all sites except Talaheel Restoration (FTW) site ( $R^2 = 0.47$ ) (Figure 4.6b). An evident clustering of the condition groups is visible in the Figure 4.6a, besides the model was not able to predict any WTD below 9 cm depth. VV was found to be a slightly stronger predictor compared to VH polarization. Given that in some sites, such as the near-natural ones, the WTD over the year only fluctuates within about 15 cm range, the RMSE was found to be quite high (RMSE = 7.1 cm for training data and 7.4 cm for validation dataset).



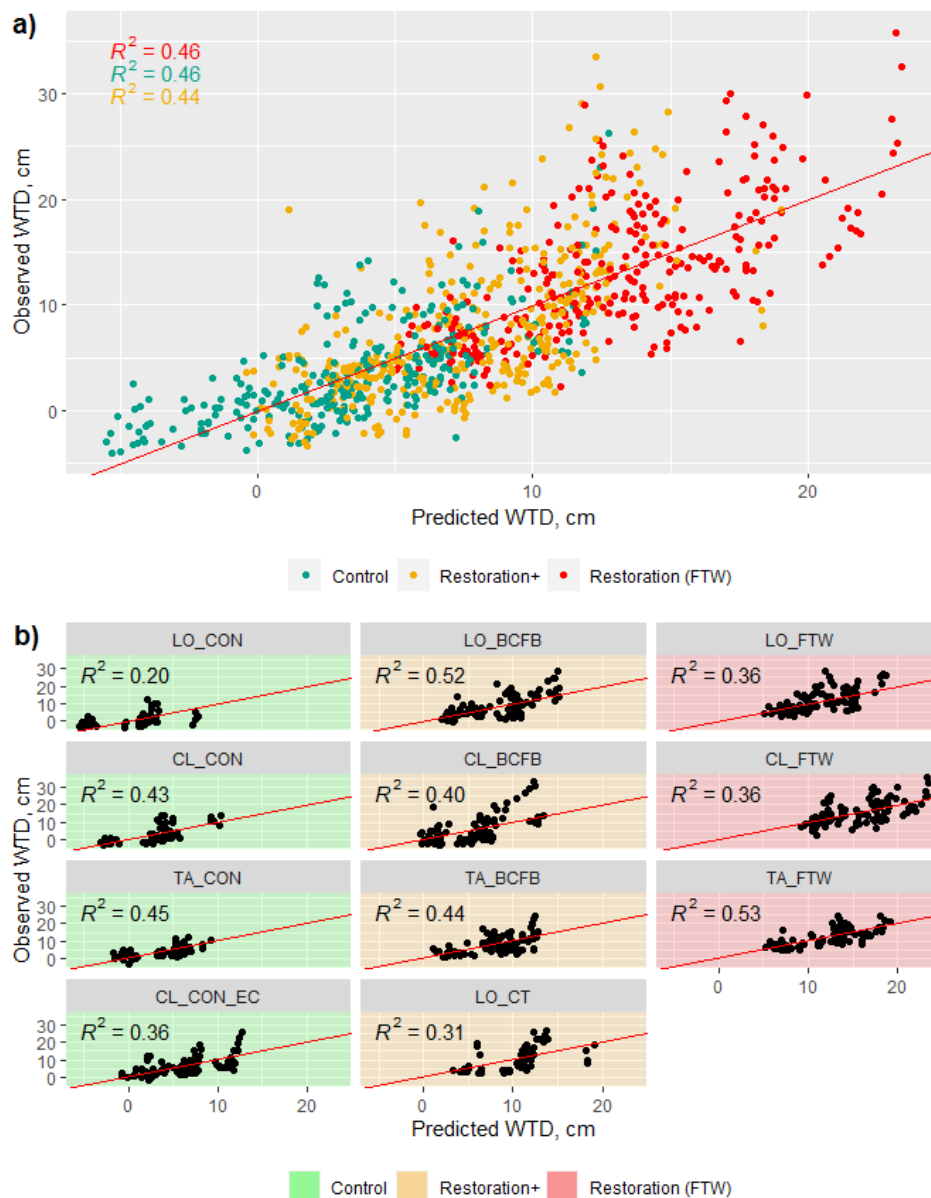
**Figure 4.6.** SLR model output for Forsinard Flows sites (predicted vs observed WTD) for a) all data points; b) splitting data into the individual sites. The red line represents a perfect agreement between prediction and field measurement.

#### 4.3.2.2. MLR model

A multiple linear regression (MLR) was fitted to estimate WTD using VV and VH polarization backscatter, and four categorical variables: season, year of radar image acquisition, area investigated, and the condition group it belongs to. For combined data input, the MLR model yielded  $R^2 = 0.59$ , with very similar scores for all condition groups ( $R^2 = 0.46$  for Control and Restoration (FTW) groups and  $R^2 = 0.44$  for Restoration+ group) (Figure 4.7a and Table 4.4). When applied to sites individually, a

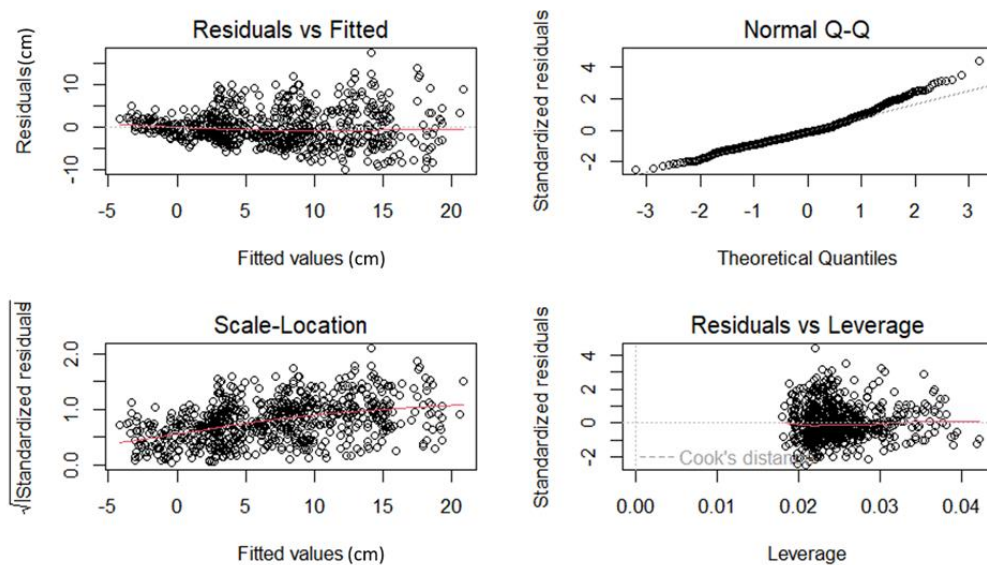
moderate agreement between observed and predicted WTD was found in 2 sites ( $R^2 > 0.5$ ), weak ( $0.3 < R^2 < 0.5$ ) in 8 sites and very weak ( $R^2 < 0.3$ ) in 1 site (Figure 4.7b).

VH was ranked as a stronger predictor compared to VV. Similarly, autumn and winter values explained a greater amount of the unique variance over spring/summer values. Year 2018 clearly stood out from the other years, which coincides with the 2018 European summer drought (Schuldt et al., 2020), and had exceptionally low water table depth in the spring and summer seasons. Compared to the SLR model, the RMSE improved and was within 5 cm error (RMSE = 4.5 cm). When running the MLR model on the validation data, correlation slightly increased but the deviation of the residuals remained the same ( $R^2 = 0.62$ , RMSE = 4.5 cm).



**Figure 4.7.** MLR model output for Forsinard Flows sites (predicted vs observed WTD) for a) all data points; b) splitting data into the individual sites. The red line represents a perfect agreement between prediction and field measurement.

Figure 4.8 shows the distribution of the residuals for the MLR model. It can be noticed that overfitting is more common, especially with WTD below 12 cm, this is also the depth at which the residuals become more scattered. Overall, a normal distribution of the residuals is observed (see Normal Q-Q plot, Figure 4.8), but the model is not predicting as well at the higher WTD ranges (lowest WTD) as it does for the low ranges (WTD close to the surface). Therefore, even with the strong capillary connection occurring between the water table depth and soil surface in peatlands (Asmuß et al., 2019; Dettmann and Bechtold, 2016), this indicates the limitations of C-band penetration ability and subsequently the predictive modelling capability, in peatlands with deep mean annual water tables, or during significant water table drawdown periods.

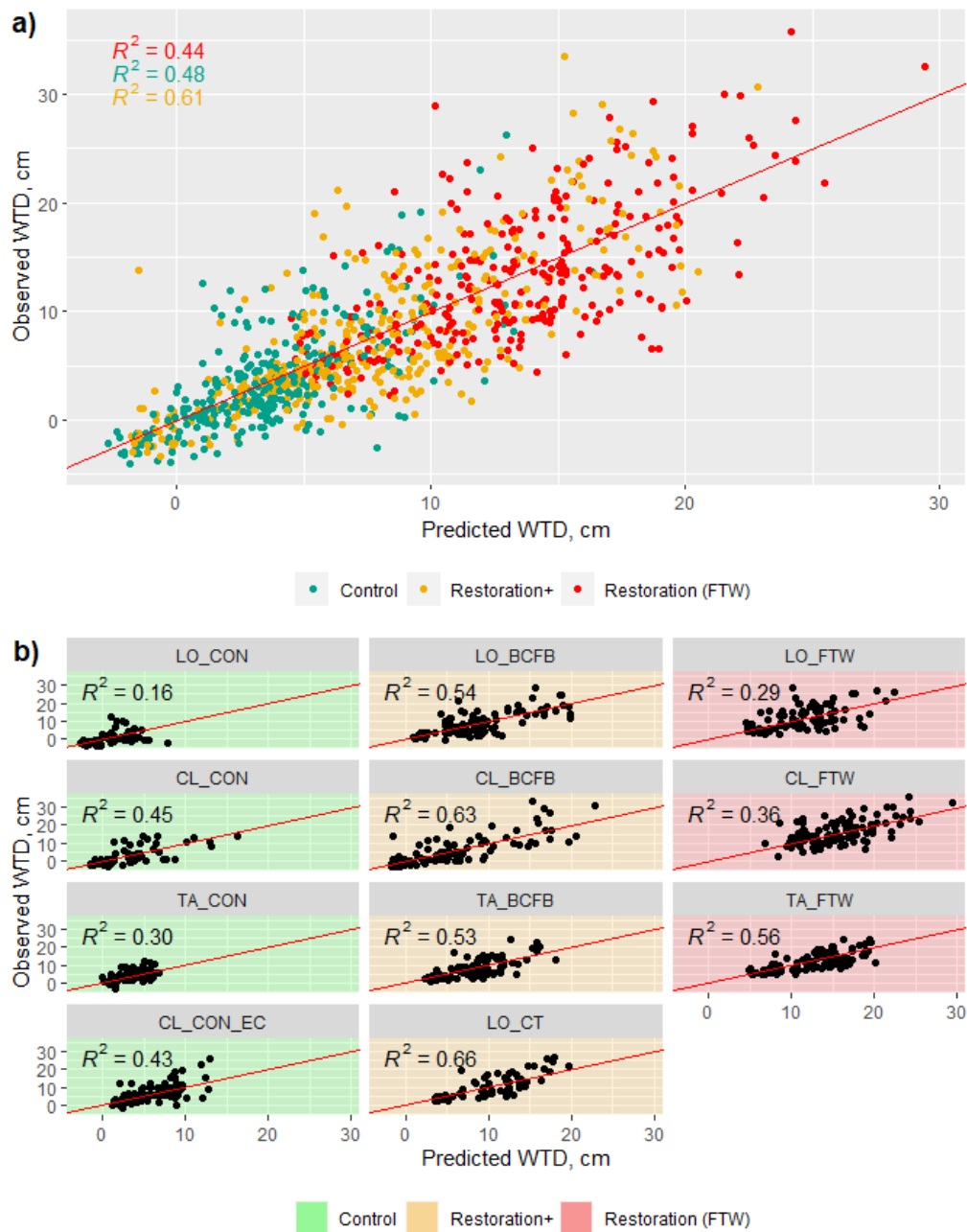


**Figure 4.8.** MLR model residual statistics. Clockwise from upper left: 1) Comparison of the residuals of the MLR model against the fitted values produced by the model; 2) Quantile-quantile plot: confirms that both sets of quantiles came from the same (normal) distribution except the upper quantiles where the points stray above the line indicating some deviation of the error from normality, this, however, is a small portion of the data; 3) Scale-Location plot, uses the square root of the standardized residuals instead of the residuals themselves 4) Leverage plot, no standardized residuals are outside of the Cook's distance boundaries, indicating that there are no strong outliers influential to the regression results.

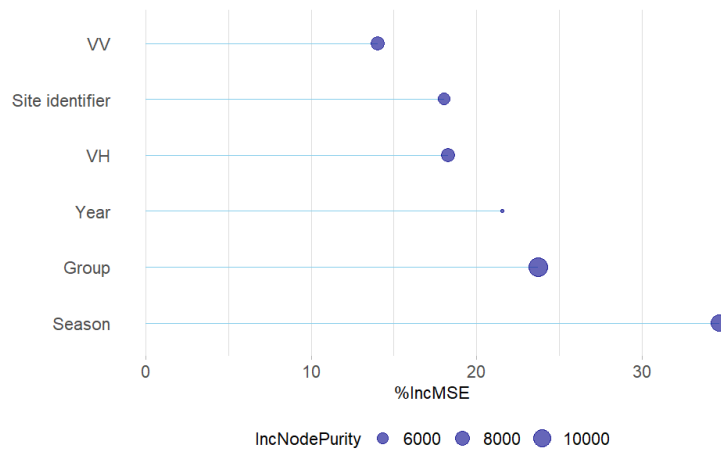
### 4.3.2.3. RF model

Finally, the random forest model was applied, using the same input variables as for the MLR model. A good agreement ( $R^2 = 0.66$ ) was found between observed and predicted WTD when looking at combined data, and out of the three condition groups was found to be highest for sites with more advanced restoration method applied ( $R^2 = 0.48$  for Control,  $R^2 = 0.44$  for Restoration (FTW) and  $R^2 = 0.61$  for Restoration+ group) (Figure 4.9a and Table 4.4). When applied to sites individually, a moderate agreement between observed and predicted WTD was found for 5 sites ( $0.65 < R^2 < 0.5$ ), weak ( $0.3 < R^2 < 0.5$ ) for 4 sites, and very weak ( $R^2 < 0.3$ ) in 2 sites (Figure 4.9b). The RMSE score further decreased compared to the two linear models with  $RMSE = 2.1$  cm (training data). When running the model on

the validation data, correlation slightly decreased and the deviation of the residuals increased ( $R^2 = 0.60$ , RMSE = 4.2 cm). The variable ranking starting from the most important were season, group, year, VH, site identifier and VV (Figure 4.10).



**Figure 4.9.** RF model output for Forsinard Flows sites (predicted vs observed WTD) for a) all data points and b) splitting data into the individual sites. The red line represents a perfect agreement between prediction and field measurement.



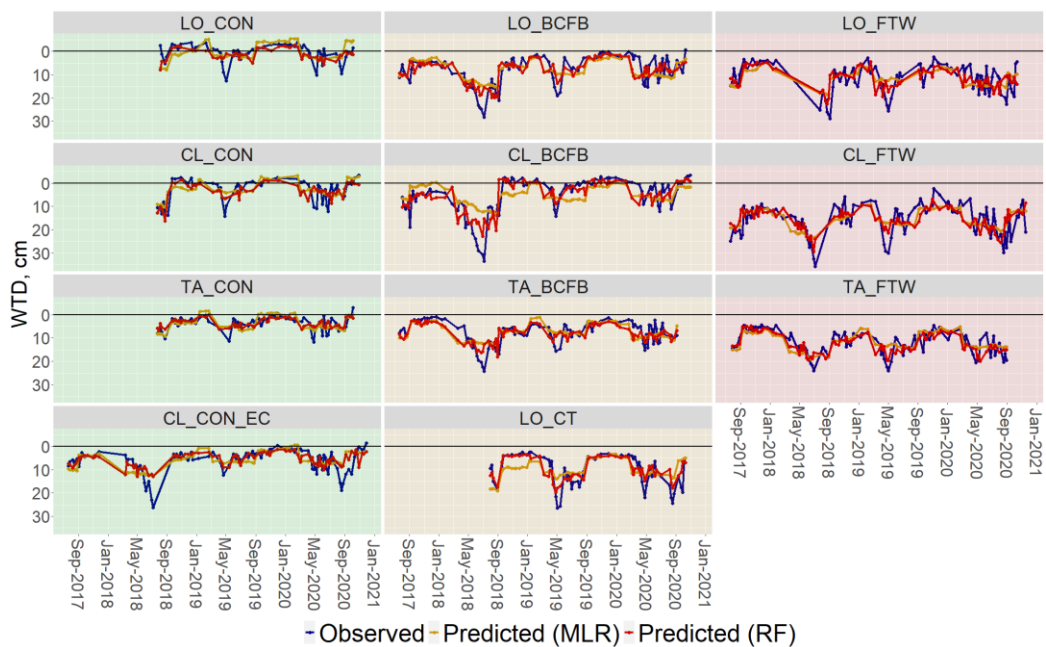
**Figure 4.10.** Random Forest model variable importance for the WTD prediction. The percentage increase in mean square error (%incMSE) is shown on the x axis and the circles represent the increase in node purity. The smaller these two parameters are, the less change in model is observed when specific variable is removed or added. The variable ranking showed well how valuable the inclusion of categorical variables was for improvement of the WTD prediction.

The correlation coefficients from the three models along with TRI, standing water and forestry information for individual sites are collated in Table 4.4. The SLR model did not meet an acceptable predictive performance, therefore only MLR and RF models are further discussed in detail.

**Table 4.4.** SLR, MLR and RF model performance using training (70%) and validation (30%) datasets, terrain ruggedness index (TRI), standing water presence (percentage of the total area) and forestry ridge and furrow lines position (aspect in degrees, with True North being 0°) of individual sites. \*\*\*indicates a .001 significance level, \*\*indicates a .01 significance level, \*indicates a .05 significance level.

Treatment	Site	Simple linear regression, SLR ( $R^2$ )		Multiple linear regression, MLR ( $R^2$ )		Random forest, RF ( $R^2$ )		Terrain Ruggedness Index, TRI (cm)	Standing Water (%)	Forestry (aspect, °)
		Training	Validation	Training	Validation	Training	Validation			
Near-natural (Control)	TA_CON	0.09*	0.02	0.45***	0.26**	0.30***	0.25**	9.6	2	-
	CL_CON	0.02	<0.01	0.43***	0.52***	0.45***	0.61***	3.8	5	-
	LO_CON	<0.01	0.02	0.20***	0.25***	0.16***	0.21**	9.7	5	-
	CL_CON_EC	<0.01	0.04	0.36***	0.52**	0.43***	0.52***	3.2	15	-
	Control group	0.01	<0.01	0.46***	0.50***	0.48***	0.50***	6.6		
Restored (felled to waste)	TA_FTW	0.48***	0.09	0.53***	0.16**	0.56***	0.14*	21.3	5	-60°
	CL_FTW	0.27***	0.08	0.36***	0.19**	0.36***	0.18**	5.0	5	-26°
	LO_FTW	0.02	0.04	0.36***	0.61***	0.29***	0.35***	16.8	20	-17°
	Restoration (FTW) group	0.01	<0.01	0.46***	0.34***	0.44***	0.26***	14.4		
Restored with additional management	TA_BCFB	<0.01	<0.01	0.44***	0.21**	0.53***	0.06	12.5	45	-16°
	CL_BCFB	<0.01	0.02	0.40***	0.36***	0.63***	0.39***	2.8	45	-22°
	LO_BCFB	<0.01	<0.01	0.52***	0.43***	0.54***	0.51***	14.0	30	-30°
	LO_CT	0.02	<0.01	0.31***	0.41***	0.66***	0.38***	17.0	5	-57°
	Restoration+ Group	<0.01	0.04	0.44***	0.44***	0.61***	0.40***	11.6		
Combined		<0.01	<0.01	0.59***	0.62***	0.66***	0.60***			

RF was found to have the highest  $R^2$  and lowest RMSE values using training dataset when looking at combined data ( $R^2 = 0.66$ , RMSE = 2.1 cm for RF;  $R^2 = 0.59$ , RMSE = 4.5 cm for MLR). When using the RF model on the withheld validation dataset, the  $R^2$  and RMSE decreased, and had a similar performance to the MLR model ( $R^2 = 0.60$  for RF,  $R^2 = 0.62$  for MLR), however the RMSE was still smaller for the RF model (RMSE = 4.2 cm for RF, RMSE = 4.5 cm for MLR). When investigating sites individually, RF was superior for 10 out of 11 sites investigated using training data, while MLR was more superior for 9 out of 11 sites when using the validation dataset. Between the peatland condition groups, the highest scores were found for the restoration sites with additional management applied (brush crushing, furrow blocking, cross tracking), followed by the control sites and finally the felled to waste sites. Figure 4.11 shows the MLR and RF modelled and field observed water table depth series for all 11 sites, and in general a good agreement can be observed in terms of temporal fit of the models. The typical problematic periods include the periods of water table drawdown, when the model is systematically underestimating the water table depth.



**Figure 4.11.** Modelled and observed water table depth series based on the MLR and RF models. The black horizontal line indicates the ground surface. Panels with green background indicate the control sites, orange - Restoration+ sites and Restoration (FTW) sites have red background.

Finally, the TRI, proportion of standing water in each site, and ridge and furrow aspect for restoration sites was compared to the model performance scores by fitting a simple linear regression. None of the three variables reached a statistical significance level ( $p$ -value > .05) and all had very low  $R^2$  scores ( $R^2 = 0.07$  for TRI;  $R^2 = 0.2$  for standing water;  $R^2 = 0.04$  for ridge and furrow aspect). Hence overall, none of these aspects had a strong influence on model performance.

#### 4.4. Discussion

This study illustrates the strong potential of multitemporal satellite radar imagery for modelling water table depth in near-natural and restored Scottish blanket bogs. If applied successfully, the remotely sensed radar time series could provide the opportunity for near-continuous monitoring of hydrological conditions which would be especially valuable in extensive and remote peatlands like the Flow Country and many others. In this paper, we have investigated the dynamics of water table depth and radar backscatter data in peatlands and compared simple linear regression (SLR), multiple linear regression (MLR), and random forest (RF) model applications to model water table depth. Based on the  $R^2$  and RMSE scores, the results revealed that the best performing model for water table depth prediction was the RF, with MLR model being a close second, while the SLR model did not meet an acceptable predictive performance. An independent validation was performed for all three models using the withheld validation dataset, and the model performance results were similar to the outcomes from the training dataset (an 6% decrease in  $R^2$  for RF and 3% increase for MLR). Besides VV and VH radar backscatter variables, the inclusion of categorical variables (year and season of image acquisition, and the site and condition group being investigated), significantly improved the model scores, reaching up to 66% of WTD variance explained. If these covariables were removed from the input, the model score decreased to 54% using RF, while the MLR performance would be so low that it no longer would be useful for WTD prediction. The model scores varied significantly between the individual sites ( $R^2 = 0.16 - 0.61$  for MLR;  $R^2 = 0.06 - 0.66$  for RF) indicating high heterogeneity, which could not be fully explained solely by variation in terrain ruggedness, presence of standing water or ridge and furrow aspect. Indeed, peatland ecosystems can exhibit a high degree of sub-pixel heterogeneity in vegetation composition and microtopography (Lindsay et al., 1988) within the  $20 \times 22$  m spatial resolution of Sentinel-1 imagery. As the Sentinel-1 imagery pixel size is smaller than the products' spatial resolution, adjacent pixels are correlated and resulting backscatter values can be impacted by the surrounding area. Räsänen et al. (2022) in their study have concluded that the high variation in the correlation between the sites is often explained by the heterogeneity between them, which seems to support the results from this study. Scholefield et al. (2019) found that the inclusion of a topography variable in their random forest model for peatland habitat extent increased the model classification performance. Future studies on water table depth modelling from satellite radar data should investigate if more detailed surface topography (aspect, slope, and topographic index) could improve the WTD estimates. In our study sites some of the specific features that cause heterogeneity between the sites and consequently could have influenced the WTD-backscatter relationship are:

1. Topography and microtopography: gullies, hags, hummocks, hollows, pools, ridge and furrow pattern.
2. Soil and vegetation moisture content, inundation.
3. Varying vegetation.



#### 4. Soil density and texture.

Of our study sites, the near-natural sites experienced the smallest fluctuation in water table depth and consequently the radar signal was most stable throughout the year at these areas. In agreement with findings from the study by Holden et al. (2011), we found previously drained peatlands to have higher fluctuations even years after restoration, which caused the radar backscatter to experience higher shifts throughout the year. Higher backscatter values are typically observed in the autumn and winter season when the water table depth is typically closer to the surface, and lower backscatter values in spring and summer when WTD drops. Seasonal patterns were also observed in the water table depth – backscatter relationship and therefore the decision to include the season as a variable in the model was made. We found that the inclusion of the radar image acquisition time (year and season) improved the WTD prediction by 25% using RF and 19% using MLR.

For some sites, we hypothesised that standing water, inundation and water table depth which remains close to the surface could be a reason for the low relationship scores. It was particularly noticeable when using the SLR model for Restoration+ sites such as at Talaheel and Cross Lochs. However, when using the MLR and RF model, the  $R^2$  scores for these sites significantly increased. Both Bechtold et al. (2018) and Lees et al. (2021) have noted how WTD from the near-natural peatland sites can have a low agreement with SAR data due to the low fluctuations throughout the year. Asmuß et al. (2019) in their study on grasslands with organic soils completely exclude areas where WTD is shallower than 5 cm as the ground surface can be partly inundated in these instances leading to a contrary relationship between radar backscatter and WTD. For our study sites, in Forsinard Flows, excluding the 2018 drought year, the mean annual WTD in the four-year monitoring period only exceeded 10 cm depth in four sites: Cross Lochs Restoration (FTW) ( $14.7 \pm 7.0$  cm), Talaheel Restoration (FTW) ( $12.3 \pm 4.0$  cm), Lonielist Restoration (FTW) ( $12.9 \pm 5.6$  cm) and Talaheel Restoration+ ( $11.3 \pm 5.4$  cm). It was expected that these slightly drier sites might have higher correlation scores given higher water table depth fluctuations and low presence of standing water. However, the models yielded only moderate to low scores for these sites. The presence of standing water in the sites along with the historical ridge and furrow patterns were expected to have influence on the correlation scores given the strong impact on radar backscatter by specular and rugged surfaces. There was no significant relationship found between the percentage of standing water and the modelling outcome. This, however, was a relatively small sample (11 sites) for testing the influence of such parameter, so further studies, where repeated annual and season data on open water presence in the research areas is available, could be beneficial to investigate the seasonal backscatter – WTD relationships. Similarly, only 7 sites with previous afforestation were tested for influence of ridge and furrow pattern. In ploughed fields where the ridges are oriented perpendicular to the radar signal, it can result in stronger backscatter, whereas if they are parallel to the radar signal, they may not affect the backscatter as much (Mc Nairn et al., 1996). From the Sentinel-1 backscatter time series we could not see a pattern where the sites with ridges more parallel

to the radar signal would be weaker (e.g., the Talaheel felled to waste site or Cross Lochs Cross-tracked site) or opposite for more perpendicular sites (e.g., Talaheel brush crushed and furrow blocked site), nor was there a statistically significant relationship found between the aspects and the three model's  $R^2$  scores. It is worth mentioning that these are restoration sites, covered with peatland vegetation so the impact of the ridge and furrow pattern is expected to be much lower than that of a freshly ploughed agricultural field, where this effect is known to have a stronger impact. A study using larger data set focussing on topographical (ridge and furrow line) aspect impact on radar backscatter in previously afforested peatlands would be valuable for further modelling improvements.

Overall, blanket bogs dominated by mosses, sedges, heath and heather experience small changes in vegetation throughout the year. *Sphagnum* and other mosses do not die back during winter and have the ability for year-round growth even with snow cover (Küttim et al., 2020). Heather *Calluna vulgaris* does not die back during winter either, however, the leaves and flowers lose their colour and turn browner. Similarly, deergrass *Trichophorum cespitosum* and cotton grasses *Eriophorum sp.* turn from green to rusty brown, with deergrass eventually dying back by late winter.

In this study we did not apply any explicit correction to the microwave signal to account for vegetation. This may account, in part, for the lower prediction skill of the simpler models. Some previous studies have included a vegetation sine correction equation (4.4) in the Sentinel-1 data processing to account for the growing season vegetation in peatlands in the Forsinard Flows reserve (Lees et al., 2021) and Finnish peatlands (Räsänen et al., 2022).

$$\sigma_v = \sigma - \sin(0.0173 \times (\text{DoY} - a)), \quad (4.4)$$

where  $\sigma_v$  is sine corrected radar backscatter (dB),  $\sigma$  is backscatter before vegetation correction (dB), DoY is the day of the year of the radar image acquisition, and  $a$  is the approximate day of the growing season beginning.

The correction in these studies is based on the day of the year of the radar image acquisition, and the approximate day when the growing season begins. We found that accounting for seasonal greening up of vegetation with a sine function can alter the data in an inappropriate manner by inflating the backscatter values and therefore also the model fit (Figure S1 in the Supplementary material B). More advanced vegetation corrections have been proposed for Sentinel-1 data normalization to account for the vegetation structure and vegetation water content change throughout the year in agricultural areas and grasslands (Maslanka et al., 2022) and managed grasslands with peat soils using the cross-over angle concept (Asmuß et al., 2019). However, the normalization only has a marginal improvement in these studies. Bechtold et al. (2018) found the cross-over angle concept to significantly improve correlation coefficients between radar backscatter and observed water table depth, however, this method requires a radar instrument that measures backscatter simultaneously at multiple angles, which is not applicable for Sentinel-1. One promising avenue for making growing vegetation corrections is to combine data from the optical and microwave domains and retrieve the vegetation and soil water state simultaneously (Quaife et al., 2022). We intend to explore such techniques in future peatland research.

To respond to nature and climate crisis, governments worldwide, including the UK, have set ambitious goals for peatland restoration in the coming years. This in return has highlighted the need for effective peatland monitoring tools, and earth observation data, such as the satellite imagery from Copernicus programme satellites, have already shown promising results. In this study we investigated the water table depth monitoring possibilities using Sentinel-1 SAR data and three different modelling approaches. Although already promising results have been achieved in this study, future studies should investigate if the model's performance is maintained when applied to other peatland sites outside of the study region, and at later stages, if more complex models, additional input variables and higher resolution SAR data can improve the modelling performance.

#### **4.5. Conclusions**

In this study we have investigated the behaviour of Sentinel-1 SAR C-band interaction with Scottish blanket bogs in different conditions. The study focused on the globally rare but highly important blanket bog habitat and aimed to use Sentinel-1 based data for water table depth modelling. To the best of our knowledge, it is the first study to compare the WTD and Sentinel-1 backscatter patterns from near-natural peatlands and sites with different restoration techniques applied.

Three models: SLR, MLR and RF using Sentinel-1 radar data were built and tested. The RF model was found to have the highest correlation scores and lowest RMSE values ( $R^2$  of 0.66 for combined data, and up to 0.66 when used per site individually). We found that the included categorical covariates, such as the radar image acquisition time (year and season) along with site identifier and peatland condition group, which are typically not used in previous studies, can all significantly improve the results of both MLR and RF models. The impact of standing water, terrain ruggedness and ridge and furrow aspect on model correlation scores was tested, but surprisingly, we found no evidence that these elements had much of an effect on our models. The modelling efforts support the idea that the Sentinel-1 SAR time series data could be used for peatland water table depth monitoring. Given the number of tested sites, it would be beneficial to expand such analysis to further improve the understanding of backscatter – WTD relationships and enhance the precision of models.

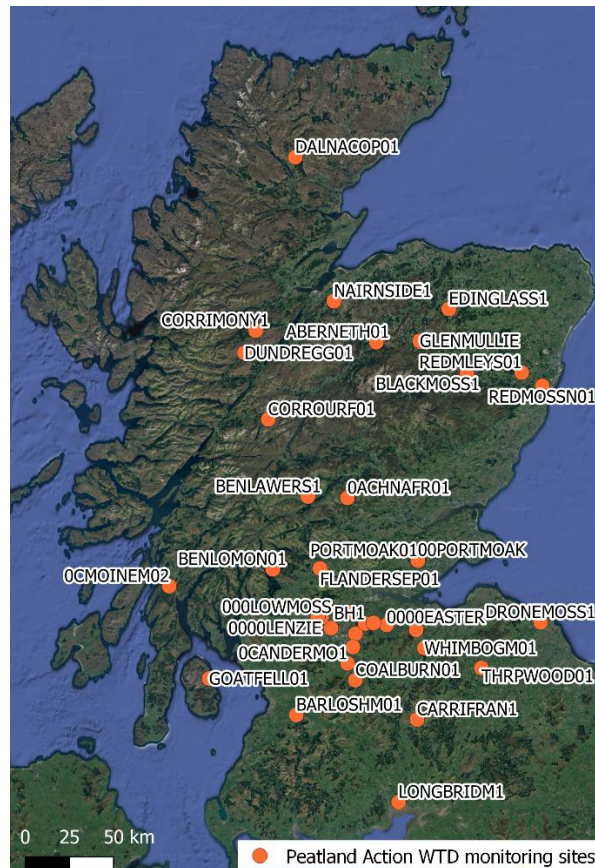
Peatland hydrological dynamics disturbance caused by anthropogenic activities and/or environmental stresses is a threat to peatland condition and function. These ecosystems require long-term continuous monitoring and remotely sensed radar data provide the opportunity to both meet the need of regular continuous monitoring and cover vast areas. The usage of satellite radar-based data for peatland monitoring is rapidly growing, and, with new radar missions planned for the next decade, it will only increase. Findings from this study may be useful to further improve monitoring and support the management of peatlands.

## 4.6. Additional data

This section shows additional analysis that have been carried out since the publication of the above study, including expanded WTD observations from NatureScot Peatland ACTION data and RF model application to these sites, as well as NEP comparison between observed and modelled WTD series.

### 4.6.1. WTD modelling using Peatland ACTION data

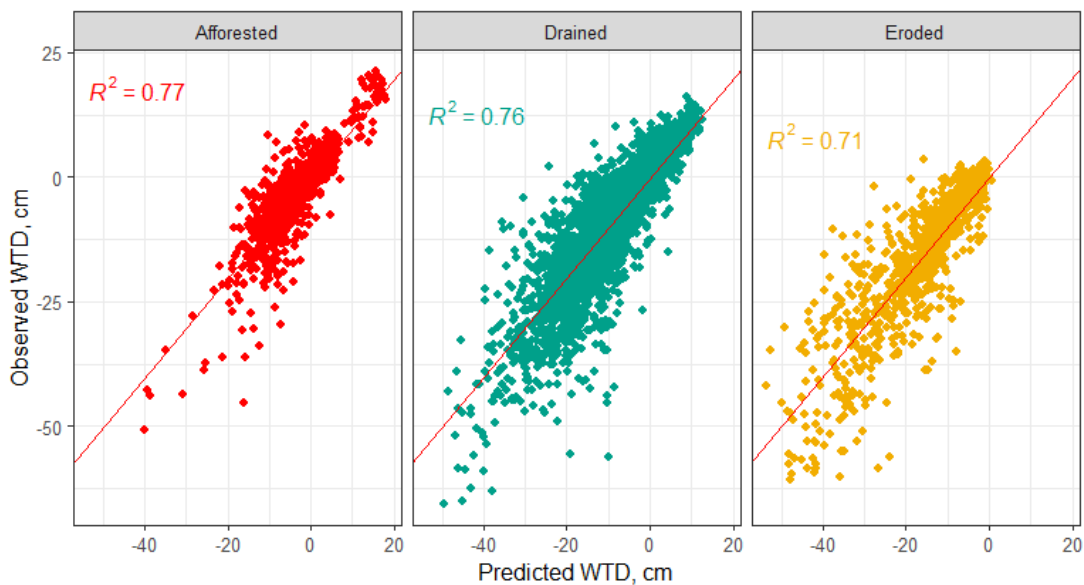
Peatland ACTION is Scotland's nature Agency's (NatureScot) national programme which since its launch in 2012 has managed to start the restoration of more than 25,000 ha of degraded peatland. A dataset including 33 restored peatland sites across Scotland (Figure 4.12) was made available for WTD analysis. The dataset included up to a 5-year long time series of continuous water table depth measurements as well as descriptive data: restoration year, type of damage (afforestation, drainage, erosion) and restoration method applied (ditch blocking, re-profiling, tree removal, scrub clear).



**Figure 4.12.** Peatland ACTION restoration sites.

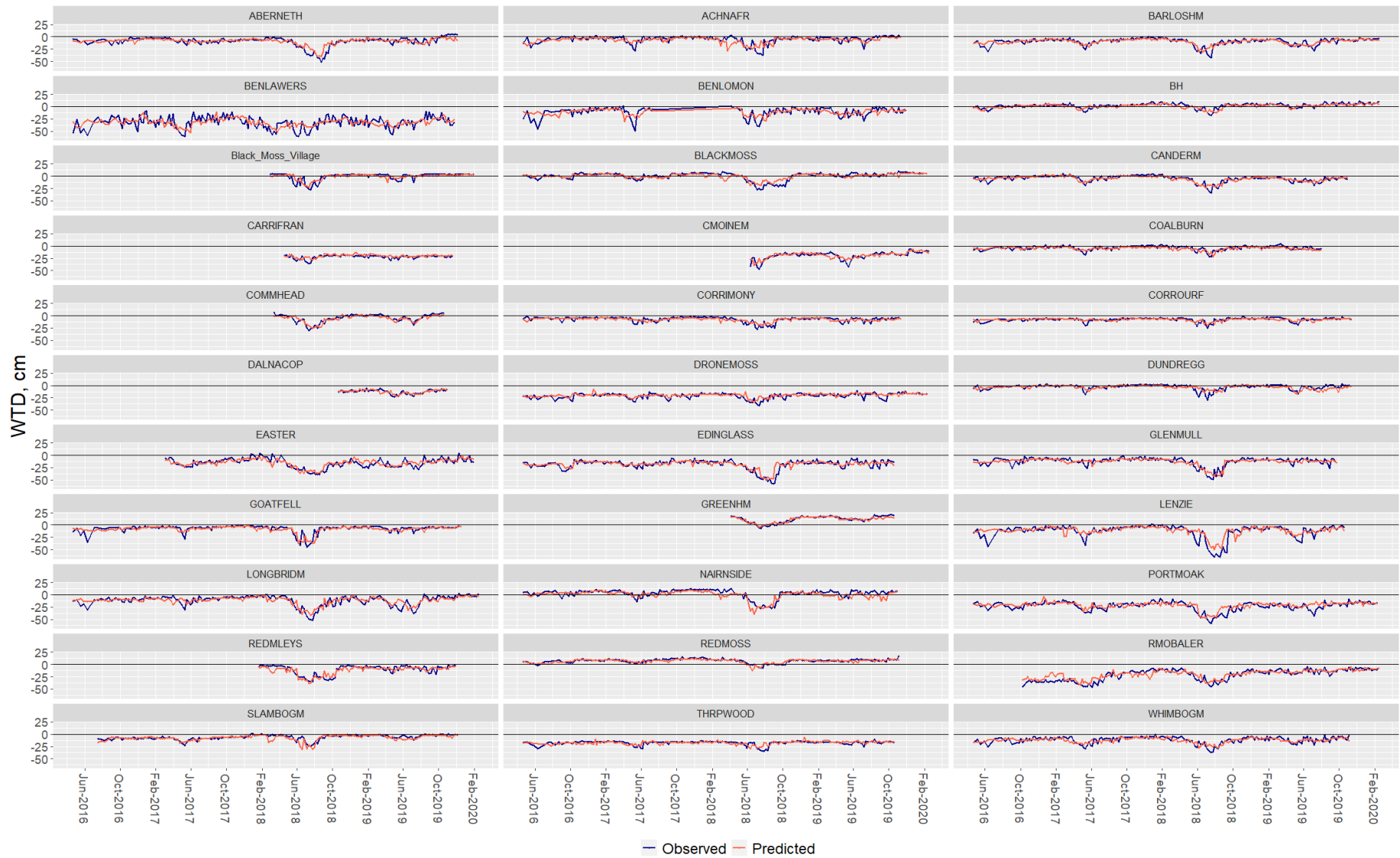
This data set permitted model training on a much wider dataset compared to the Forsinard study (total number of observations, when both backscatter and WTD data was available ( $n$ ) = 10734). The data were used to refit the Sentinel-1 based RF WTD model developed earlier in the chapter, and it was possible to specifically analyse the RF model suitability for restored peatland water table depth

monitoring, as all the sites were ongoing restoration. The dataset also included diverse set of peatland types – both blanket and raised bogs unlike the Forsinard study. The disadvantage of the PA dataset, however, was the lack of WTD measurements from nearby control environments (near-natural sites). Figure 4.13 shows the results of the WTD model applied to the restored peatlands based on the degradation group each site belongs to. A good fit ( $R^2$  of 0.71 to 0.77) was achieved for the three groups investigated with the RMSE values below 3cm, supporting the findings from the Forsinard study and even further supporting the notion that Sentinel-1 SAR data could be used for peatland water table depth monitoring, especially restoration projects. The variable importance with the larger PA dataset remained similar to the Forsinard dataset, with season, group and site identifier being amongst the most influential. The year variable was no longer as important as in the Forsinard model, pointing to the necessity to train the model on a wider variance of climatic conditions, especially for time periods that include unusual wet or dry periods, such as the 2018 European summer drought.



**Figure 4.13.** RF model output for Peatland ACTION sites showing predicted vs observed WTD in each of the degradation groups. The red line represents a perfect agreement between prediction and field measurement.

Additionally, Figure 4.14 shows the temporal fit of observed and modelled WTD for each of the sites. And while typically a good agreement can be observed in terms of temporal fit of the model, just as with the Forsinard Flows sites, the usual problematic periods include the periods when water table depth is the lowest (most notably the 2018 summer).



**Figure 4.14.** Sentinel-1 based modelled (dark blue) and field observed (orange) WTD for Peatland Action sites. The black horizontal line indicates the ground surface.

#### 4.6.2. NEP comparison of observed and modelled water table depth

As studies have shown a close link between peatland water table depth and annual greenhouse gases (Evans et al., 2021; Joosten et al., 2012; Koch et al., 2023; Waddington et al., 2015; Yu et al., 2010) there is a strong suggestion that WTD could be used as a low-cost proxy for peatland GHG reporting purposes. A recent study by Evans et al. (2021) has demonstrated the WTD to be the highest explanatory variable of CO<sub>2</sub> fluxes and presented two equations for Net Ecosystem Production (NEP) reporting, first one created using CO<sub>2</sub> measurements from 16 peatland eddy covariance (EC) flux towers across UK (equation 6.1) and second using combined CO<sub>2</sub> measurement database with data from 49 published EC studies on temperate and boreal peatlands (equation 6.2). Additionally, CH<sub>4</sub> flux data from 41 peatland sites in the United Kingdom and Ireland were used to analyse the relationship between mean annual methane fluxes and WTD (equation 6.3). Based on the collected data, this study suggested two NEP models and a CH<sub>4</sub> model for GHG prediction based on the peatland annual WTD:

$$NEP_1 = 0.1341 \times WTD_e - 1.73 \quad (6.1),$$

$$NEP_2 = 0.0927 \times WTD_e - 1.69 \quad (6.2),$$

$$CH_4 \text{ flux} = 0.334 \times 0.5^{(WTD_e + 5) / 6.31} \quad (6.3),$$

where NEP is the annual mean Net Ecosystem Production (balance between gross primary productivity (GPP) and ecosystem respiration (R<sub>e</sub>), CH<sub>4</sub> flux is the annual mean methane flux and WTD<sub>e</sub> is the effective mean annual water table depth.

For initial analysis, Table 4.5 shows these equations applied to the observed and SAR-based modelled mean water table depths for the Forsinard Flows study area, including the differences in results between using observed and modelled WTD and each of the equations; table 4.6 shows the same analysis for methane fluxes.

**Table 4.5.** NEP prediction using annual mean WTD as proposed by Evans et al. (2021), comparison of observed and SAR-based modelled WTD for Forsinard Flows research sites (detailed site descriptions in Chapter 4). All mean annual WTD values were calculated between Sep 15, 2018 and July 31, 2020.  $WTD_{obs}$  was calculated using all daily WTD observation,  $WTD_{obs\_lim}$  was calculated using daily WTD observations only for the days when radar imagery was available (as for model training),  $WTD_{mod}$  shows the modelled WTD values.  $NEP1_{obs}$  and  $NEP1_{mod}$  are the predicted NEP fluxes based on equation 6.1 and observed and modelled WTD respectively;  $NEP2_{obs}$  and  $NEP2_{mod}$  are the predicted NEP fluxes based on equation 6.2 and observed and modelled WTD respectively.  $\Delta NEP1$  and  $\Delta NEP2$  shows the difference in NEP prediction between using observed and modelled WTD. All WTD values are expressed in cm. All NEP values are expressed in tons of carbon per hectare and year ( $t\ C\ ha^{-1}\ yr^{-1}$ ). Negative NEP values indicate net  $CO_2$  uptake ( $CO_2$  sink).

Site	$WTD_{obs} \pm 95\%CI$	$WTD_{obs\_lim} \pm 95\%CI$	$WTD_{mod} \pm 95\%CI$	$NEP1_{obs}$	$NEP1_{mod}$	$NEP2_{obs}$	$NEP2_{mod}$	$\Delta NEP1$	$\Delta NEP2$
TA_CON	4.9±0.3	4.9±0.7	3.2±0.4	-1.07	-1.30	-1.23	-1.39	0.23	0.16
LO_CON	2.8±0.4	2.7±0.8	0.8±0.5	-1.35	-1.62	-1.43	-1.62	0.27	0.19
CL_CON	4.9±0.4	4.8±1.0	2.8±0.6	-1.07	-1.36	-1.23	-1.43	0.29	0.20
CL_CON_EC	0.9±0.2	0.8±0.6	4.7±0.5	-1.61	-1.10	-1.61	-1.25	-0.51	-0.35
TA_BCFB	11.3±0.5	11.1±1.1	7.5±0.5	-0.22	-0.73	-0.64	-1.00	0.51	0.35
LO_BCFB	3.8±0.4	3.8±1.0	6.1±0.7	-1.22	-0.91	-1.34	-1.12	-0.31	-0.22
LO_CT	9.4±0.6	9.1±1.4	8.8±1.0	-0.47	-0.55	-0.82	-0.87	0.08	0.06
CL_BCFB	4.9±0.4	4.8±1.0	2.3±0.7	-1.07	-1.43	-1.23	-1.48	0.36	0.25
TA_FTW	12.3±0.4	12.0±0.9	12.7±0.7	-0.08	-0.03	-0.55	-0.52	-0.04	-0.03
LO_FTW	12.9±0.4	12.8±1.0	11.4±0.8	0.00	-0.20	-0.49	-0.63	0.21	0.14
CL_FTW	14.7±0.6	14.2±1.4	15.2±0.9	0.25	0.31	-0.32	-0.28	-0.07	-0.05



**Table 4.6.** CH<sub>4</sub> prediction using annual mean WTD as proposed by Evans et al. (2021); comparison of observed and SAR-based modelled WTD for Forsinard Flows research sites. All mean annual WTD values were calculated between Sep 15, 2018 and July 31, 2020. WTD<sub>obs</sub> was calculated using all daily WTD observation, WTD<sub>obs\_lim</sub> was calculated using daily WTD observations only for the days when radar imagery was available (as for model training), WTD<sub>mod</sub> shows the modelled WTD values. CH<sub>4</sub>flux<sub>obs</sub> and CH<sub>4</sub>flux<sub>mod</sub> are the predicted CH<sub>4</sub> fluxes based on equation 6.3 and observed and modelled WTD respectively. ΔCH<sub>4</sub>flux shows the difference in CH<sub>4</sub> prediction between using observed and modelled WTD. All WTD values are expressed in cm. All CH<sub>4</sub> values are expressed in tons of carbon per hectare and year (t C ha<sup>-1</sup> yr<sup>-1</sup>). Positive values indicate CH<sub>4</sub> source.

Site	WTD <sub>obs</sub> ± 95%CI	WTD <sub>obs_lim</sub> ± 95%CI	WTD <sub>mod</sub> ± 95%CI	CH <sub>4</sub> flux <sub>obs</sub>	CH <sub>4</sub> flux <sub>mod</sub>	ΔCH <sub>4</sub> flux
TA_CON	4.9±0.3	4.9±0.7	3.2±0.4	0.11	0.14	-0.02
LO_CON	2.8±0.4	2.7±0.8	0.8±0.5	0.14	0.18	-0.03
CL_CON	4.9±0.4	4.8±1.0	2.8±0.6	0.11	0.14	-0.03
CL_CON_EC	0.9±0.2	0.8±0.6	4.7±0.5	0.17	0.12	0.06
TA_BCFB	11.3±0.5	11.1±1.1	7.5±0.5	0.06	0.09	-0.03
LO_BCFB	3.8±0.4	3.8±1.0	6.1±0.7	0.13	0.10	0.03
LO_CT	9.4±0.6	9.1±1.4	8.8±1.0	0.07	0.07	0.00
CL_BCFB	4.9±0.4	4.8±1.0	2.3±0.7	0.11	0.15	-0.04
TA_FTW	12.3±0.4	12.0±0.9	12.7±0.7	0.05	0.05	0.00
LO_FTW	12.9±0.4	12.8±1.0	11.4±0.8	0.05	0.06	-0.01
CL_FTW	14.7±0.6	14.2±1.4	15.2±0.9	0.04	0.04	0.00

Results both from field observed and modelled WTD series suggest that all Forsinard sites, besides Cross-Lochs Restoration (FTW) site have been carbon sinks in the observation period (Sep 15, 2018 - July 31, 2020) using Equation 6.1, while Equation 6.2 suggests that all 11 sites have been carbon sinks. The difference between NEP based on observed and modelled WTD was in the range of -0.51 to 0.52 t C ha<sup>-1</sup> yr<sup>-1</sup> using NEP<sub>1</sub> and slightly smaller using the NEP<sub>2</sub> equation (range of -0.35 to 0.35 t C ha<sup>-1</sup> yr<sup>-1</sup>). For 7/11 sites the modelled WTD resulted in an estimation of a higher carbon uptake compared to the observed WTD.

Methane prediction suggests that all 11 sites have acted as CH<sub>4</sub> sources in this period both according to observed and modelled WTD. The difference between CH<sub>4</sub> flux based on observed and modelled WTD was in the range of -0.04 to 0.06 t C ha<sup>-1</sup> yr<sup>-1</sup>, suggesting a closer match compared to the NEP predicted values. For 6/11 sites the modelled WTD resulted in an estimation of a CH<sub>4</sub> source higher than when using field observed WTD values.

# Chapter 5

## 5. An exploration of methods to monitor trajectories and identify change points in peatland restoration projects using remotely sensed data

### 5.1. Introduction

Peatland restoration projects aim to stabilise eroding peat, enhance carbon sequestration through ecosystem recovery, and prevent further degradation (Alderson et al., 2019). These projects directly target human-caused damage, such as drainage ditches, afforested peatlands, peat burning and overgrazing - as well as more indirect or natural degradation, such as peat gullies, bare peat, peat hags and pipes. Peatland restoration efficacy can be assessed from multiple criteria, e.g., removal of woodland, site re-wetting and return of high water table depth (WTD), revegetation, including the return of native species, and higher carbon uptake (Anderson and Anderson, 2010; Gatis et al., 2017; Lees et al., 2021). With the Scottish Government's target of restoring 20,000 ha of degraded peatland per year, a regular physical collection of such data in the field would be impractical and difficult to accomplish. Remotely sensed data analysis, therefore, may offer an attractive alternative for landscape-scale peatland restoration progress monitoring and the development of a remote sensing method for peatland restoration monitoring would be highly beneficial (Andersen et al. 2017). Given the investments in peatland restoration, ultimately, the monitoring efforts should be able to inform interested parties if restoration works are efficiently and economically carried out, are cost-effective and potentially indicate if any further management may be necessary (Aitkenhead and Coull, 2016; Carless et al., 2019; Cordell et al., 2017; Moxey and Moran, 2014).

This chapter investigates whether time series of remotely sensed optical and SAR data can be indicative of restoration progress in Cross Lochs peatland restoration site. Decomposition, trajectory and change point analysis were applied to time series of radar and optical satellite imagery data. The random forest model developed in Chapter 4 was used to create a 7 year-long (2015-2021) modelled WTD series based on the Sentinel-1 backscatter. Unfortunately, before the launch of Sentinel-1 there are no easily available C-band radar data, therefore, additionally to the Sentinel-1, optical imagery from MODIS satellite data were used to create 19 year-long (2003-2021) series of Normalized Difference Vegetation Index (NDVI), Normalized Difference Water Index (NDWI) and Normalized Difference Moisture Index (NDMI). While the resolution of MODIS imagery is moderate (up to 250 m), it dates back more than 20 years, which covers the initial restoration work applied in the Cross Lochs sites. By combining the radar and optical data sources it was possible to take advantage of the complementary information provided by both types of data.

All four sets of time series were decomposed into seasonal, trend and remainder components to investigate underlying trends and detect change points. As a restored site would be expected to gradually

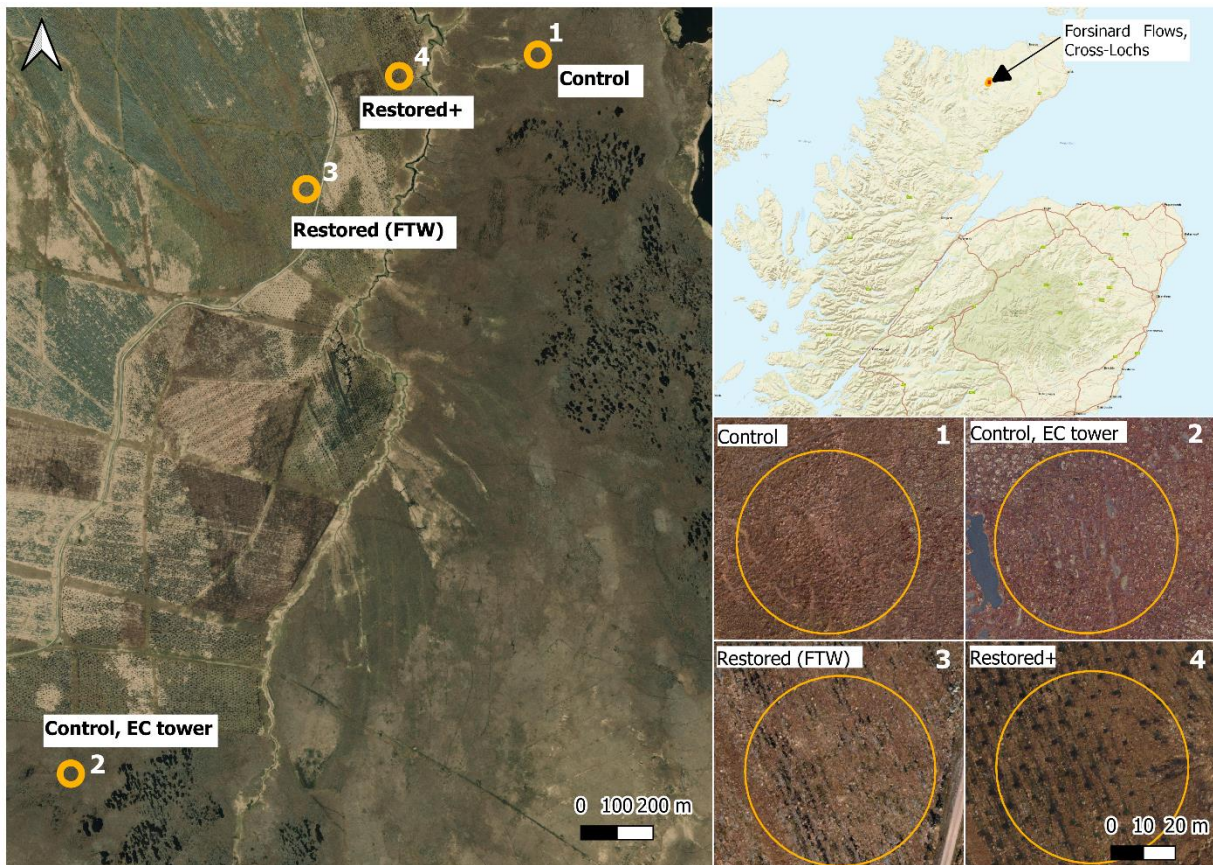
change and show signs of shallower WTD, increased soil moisture, decrease of bare peat and return of vegetation, with time resembling a near natural peatland, it was anticipated that a positive trend could potentially be observed in the remotely sensed time series that reflect peatland moisture and vegetation conditions. Change point analysis involves detecting time points where a significant change occurs in the data series. These analyses were applied to the whole time series to test whether both significant changes (e.g., the tree felling) and less abrupt changes (e.g., additional restoration management) can be detected in the restoration sites.

## **5.2. Materials and Methods**

### **5.2.1. Study Area**

The Cross-Lochs restoration site (58°23'N, 3°51'W) is located in the Forsinard Flows RSPB reserve, which is part of the “The Flow country” wetland area in Northern Scotland (Figure 5.1). The Cross-Lochs site is situated roughly in the centre of Forsinard Flows at about 200 m asl, which is slightly higher than the Talaheel and Lonielist sites discussed in Chapter 4.

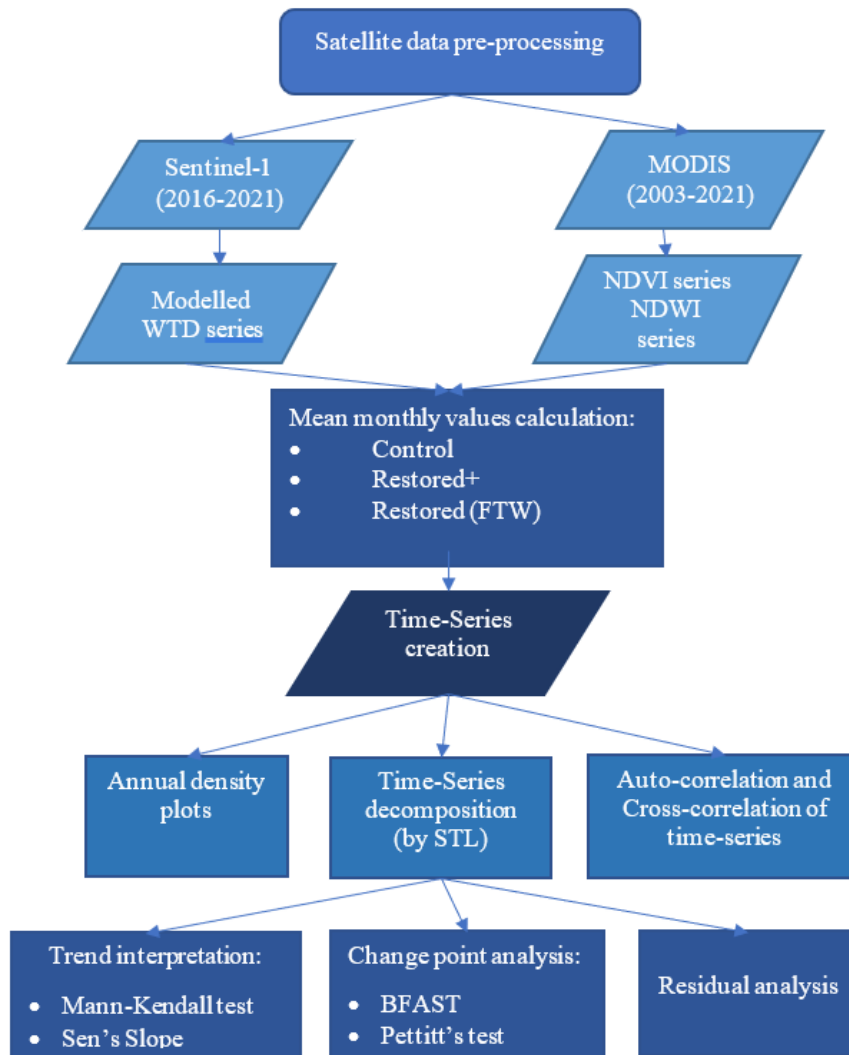
While there remains a large area of intact, near-natural peatland (such as sites 1 and 2 in Figure 5.1), a portion of the Cross Lochs area was drained and afforested with coniferous plantations (mostly *Picea sitchensis* and *Pinus contorta*) in 1983. The first restoration efforts took place between 2005 and 2006 when the existing forestry was felled-to-waste (area 3 in Figure 5.1). While some of the areas were left this way, others received additional restoration management, specifically, brash crushing and furrow blocking between October 2015 and February 2016 (area 4 in Figure 5.1).



**Figure 5.1.** Overview of the Cross Lochs study area and the four chosen study sites: 1. Control1, 2. Control with EC tower (Control2), 3. Restored (FTW) and 4. Restored+. Each analysed site is a circular area with a 30 m radius and has a WTD monitoring dip roughly in the centre of it. The second control site (Control2) was additionally added because it represents an area of best locally available blanket bog condition surrounded with small water bodies, while Control1 is a slightly drier area, which historically would have been prioritised for forestry operations.

### 5.2.2. Time series

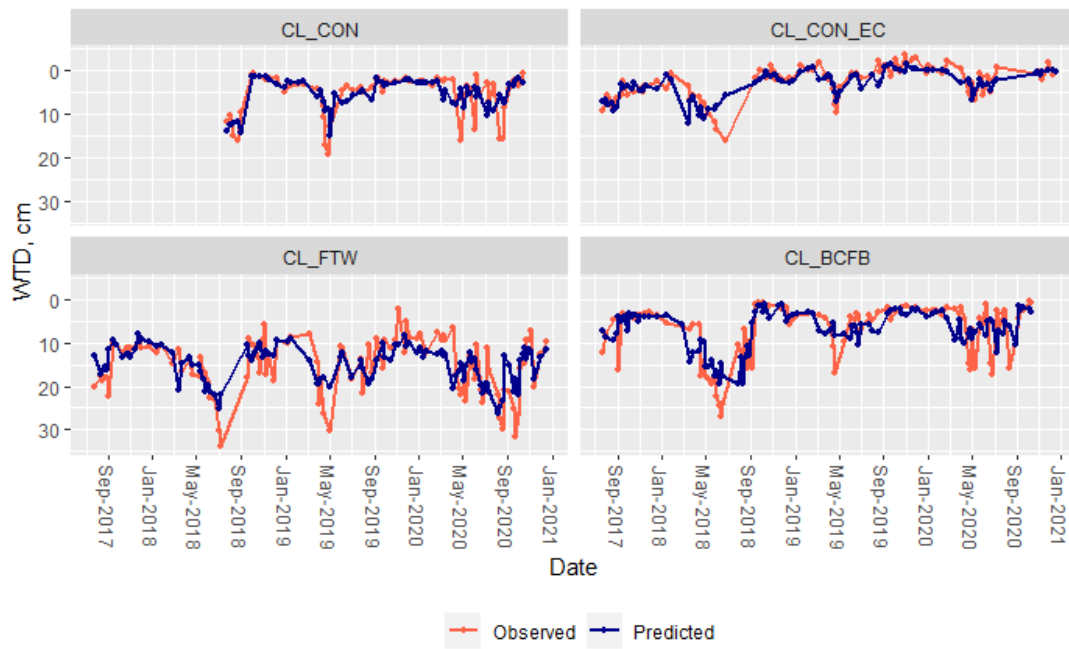
The workflow of the time series data processing is given in Figure 5.2. Both the SAR (Sentinel-1) and optical (MODIS) datasets were retrieved and pre-processed on the GEE platform. All further analysis were conducted in the R programming environment (R Core Team, 2021).



**Figure 5.2.** Data processing methodology flowchart for time series analysis.

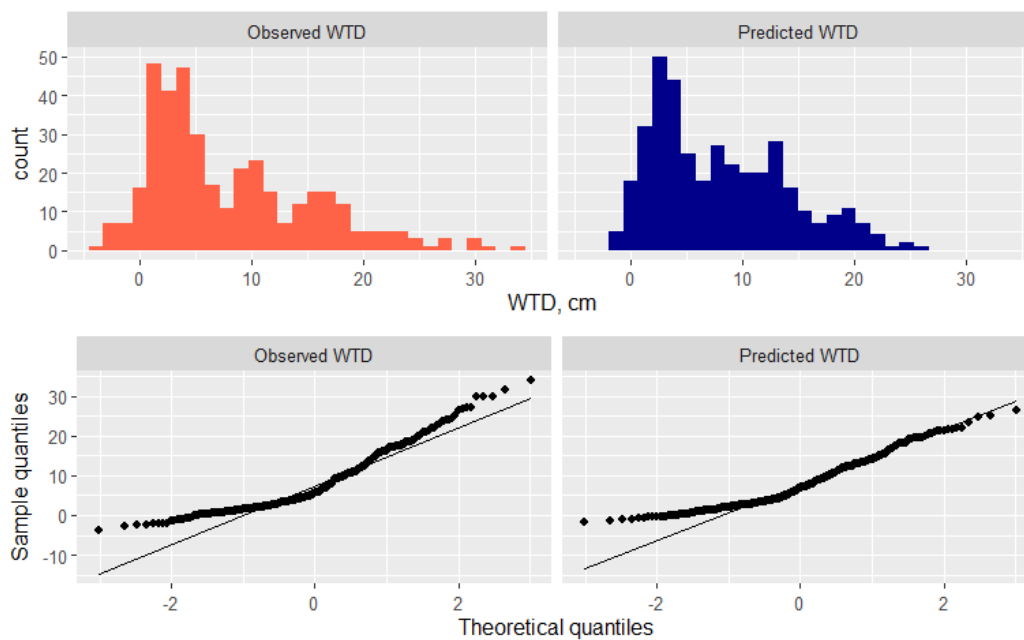
### 5.2.2.1. Sentinel-1 data and modelled WTD data

The GEE platform was used to obtain, pre-process, filter and extract the Sentinel-1 imagery between 2015 – 2021. The Sentinel-1 data processing on GEE is more closely described in subchapter 4.2.3. The final image collection consisted of 384 individual satellite images, which were then used to extract mean VV and VH values for sites 1 - 4. Then, the Sentinel-1 based WTD model using the random forest method, as developed in Chapter 4, was used to process the 7-year-long satellite radar series and predict the peatland WTD in each site. For combined data, the  $R^2$  was 0.66 with RMSE only 2.1 cm. For sites individually, the  $R^2$  valued varied between 0.36 for CL\_FTW site, followed by the two control sites, 0.43 for CL\_CON\_EC and 0.45 for CL\_CON and, finally, highest for CL\_BCFB site with  $R^2$  of 0.63. Figure 5.3 shows the comparison of the modelled and observed water table depths for the time period when field observations were available.



**Figure 5.3.** Sentinel-1 based modelled (dark blue) and field observed (orange) WTD at the Cross Lochs sites. CL\_CON = Cross Lochs Control site 1, CL\_CON\_EC = Cross Lochs Control site 2, CL\_FTW = Cross Lochs Restored (FTW) site, CL\_BCFB = Cross Lochs Restored+ site.

The Q-Q and histogram plots show how the observed WTD has a right-skewed distribution with quantiles at both high right and left end being more positive than normal quantiles would be (Figure 5.4, left), which has resulted from the 2018 drought, when significantly lower WTD was observed in the whole Forsinard Flows area. Random forest model does not require data normalization and in the predicted WTD data, to a lesser extent, but the right-skewed distribution can still be observed.



**Figure 5.4.** Comparison of histograms and Q-Q plots for observed and predicted WTD at the Cross Lochs sites. Both data sets are right skewed with tails towards deeper water table depths.

### 5.2.2.2. MODIS NDWI, NDMI and NDVI data preparation

Three indices were chosen to look at the restoration progress from both hydrological and vegetation perspectives: NDVI, NDWI and NDMI (equations and details are given in Table 5.1). Moderate Resolution Imaging Spectroradiometer (MODIS) Terra satellite data were used for the time series creation for the chosen indices. While the resolution of MODIS imagery is moderate (up to 250 m), it dates back more than 20 years, which covers the time period when Cross Lochs restoration efforts began. The products used included MOD13Q1 and MOD09A1, versions 6.1. and similarly to the Sentinel-1 series, data were processed on GEE.

The MOD13Q1 product contains NDVI values, which are generated every 16 days at 250 m spatial resolution (Didan, 2015). MOD09A1 is a surface spectral reflectance product from Terra MODIS, the bands are corrected for atmospheric conditions and generated every 8 days at 500 m spatial resolution (Vermote, 2015). Bands used from this product were Band 2 (NIR, 841 – 876 nm), Band 4 (Green, 545 – 565 nm), and Band 6 (SWIR, 1628 – 1652 nm) for NDMI and NDWI generation. In total, for the time period between the years 2003 - 2021, the MOD09A1 imagery collection consisted of 916 individual satellite images, and the MOD13Q1 collection consisted of 458 individual satellite images. While the 8 and 16-day period minimizes the risk of the presence of clouds by choosing the best available pixel value from the given period, this does not guarantee a cloud-free dataset.

**Table 5.1.** Indices and bands used for the time series creation. Index equations are given using the band spectra and corresponding MODIS bands.

Index, reference	Equation	Value range
<b>NDVI</b> Normalized Difference Vegetation Index Rouse et al. (1973)	$\frac{NIR - Red}{NIR + Red}$ MODIS: $\frac{B2 - B1}{B2 + B1}$	-1 to 1
<b>NDWI</b> Normalized Difference Water Index McFeeters (1996)	$\frac{Green - NIR}{Green + NIR}$ MODIS: $\frac{B4 - B2}{B4 + B2}$	-1 to 1

<p><b>NDMI</b> Normalized Difference Moisture Index, also sometimes referred to as “NDWI Gao” Gao (1996)</p>	$\frac{NIR - SWIR}{NIR + SWIR}$ <p>MODIS:</p> $\frac{B2 - B6}{B2 + B6}$	<p>-1 to 1</p>

NDVI, first proposed by Rouse et al. (1973), is a well known and widely used vegetation index which serves as a proxy for how green and live the observed vegetation is. As green healthy vegetation typically absorbs light in red wavelength and scatters near infra-red wavelengths, a simple calculation can be made using MODIS Bands 1 and 2. NDMI, proposed more than twenty years later by Gao (1996) uses near infra-red and short wave infra-red bands. Water is a good absorber of infra-red light, and therefore NDMI works as a proxy for water content in the vegetation and vegetation structure. Finally, NDWI, proposed by McFeeters (1996) uses visible green and infra-red bands and serves as a proxy for changes related to water content in water bodies.

### 5.2.3. Time series preparation

After the retrieval of modelled WTD, NDVI, NDMI and NDWI series, data were combined, and monthly average values of each indicator per study area were calculated. Time series were then analysed using: 1. Annual density of data and its change over time, 2. Correlation between chosen indicators and condition groups (near-natural/restored using simple restoration/restoration using advanced restoration) investigated, 3. Testing for auto-correlation, 4. Decomposition, after which trends, change points, and residuals were analysed further.

The time series of all indicators were compared between control and restored sites to confirm if changes over time can be attributed to the restoration efforts or if they relate to wider changes happening in the whole area, such as climatic factors.

#### 5.2.3.1. Autocorrelation and cross-correlation

The time series of all indicators were tested for temporal autocorrelation using Autocorrelation Function (ACF) as well as compared to each other using Cross Correlation Function (CCF). ACF computes the correlation between time series with a lagged version of itself, indicating if the observed variable is related to a version of itself at an earlier time step. When looking at the time series of vegetation or WTD observations, given the geographical location of the study site, it would be expected



for the data to have a seasonal pattern, which could be confirmed in the autocorrelation graphs. If autocorrelation is present in two series being compared it can lead to them being statistically related even when no relation between the underlying traits exists, so caution must be taken. CCF computes the cross correlation between two series and identifies lags or leads between each pair of the time series, so the value of one variable can be foreseen or anticipated by looking at the other.

### **5.2.3.2. Decomposition, trend and change point analysis**

Decomposition was carried out using the Seasonal and Trend decomposition by locally estimated scatterplot smoothing (STL) method. The STL method was chosen as it has the ability to handle the seasonality component and its change over time, it is robust to outliers and the user is given freedom to control the smoothness of the trend-cycle (Cleveland et al., 1990). The STL algorithm runs smoothing on time series in two loops. The outer loop minimizes the effect of outliers by assigning robustness weights to each data point depending on the size of its remainder. The inner loop iteratively processes seasonal and trend components by creating cycle-subseries (monthly data with a yearly cycle) and running them through a low-pass filter (smoothing) (Cleveland et al., 1990). The processing results in three components: trend, seasonal and remainder (irregular):

$$Y_t = T_t + S_t + e_t$$

where  $Y_t$  is the original time series,  $T_t$  is the trend component,  $S_t$  is the seasonal variation, and  $e_t$  describes the residuals component.

STL has previously been successfully used for long-term ecosystem change monitoring using remote sensing data in other wetland ecosystems (Kovács et al., 2022; Niu et al., 2020), but to the best of our knowledge, this is the first application specifically for peatland ecosystem long-term trend monitoring.

The Mann-Kendall trend test was then performed to see if a monotonic trend is present, and the Theil-Sen estimator (also known as Sen's slope) was used to evaluate the magnitude of the trend. Both the Theil-Sen slope estimator and the Mann-Kendall trend test are non-parametric statistical approaches that have been widely used for environmental data trend analysis (Berlanga-Robles et al., 2019; Najafi et al., 2019). As suggested by Andronis et al. (2022) the time series were split into shorter time periods to investigate the trends after each intervention period.

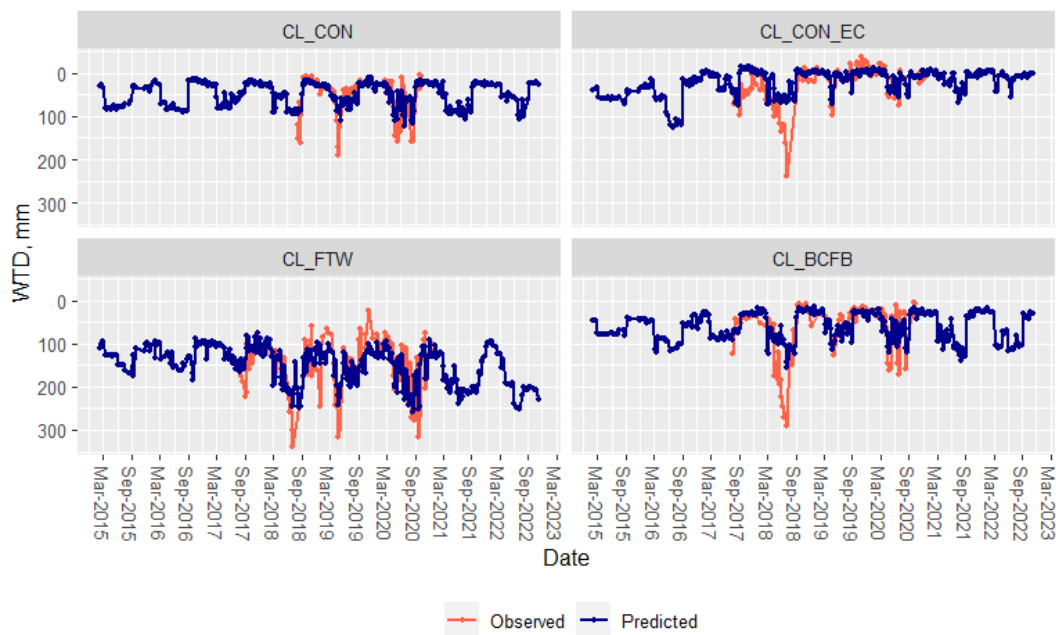
The Breaks For Additive Seasonal and Trend (BFAST) method, further developed from STL by Verbesselt et al. (2010), was then used to test whether any statistically significant abrupt changes (change points) can be detected in the given time series data. After the data decomposition, BFAST checks each component for at least one significant change point using an empirical fluctuation process. If found, the component is then passed to the breakpoints algorithm, described by (Bai and Perron, 2003), which can simultaneously estimate multiple breakpoints. Additionally, Pettitt's test for single

change point detection was applied. The Pettitt’s test, developed by Pettitt (1979) is a non-parametric test, widely used for change detection in climatic and hydrological data (Jaiswal et al., 2015).

### 5.3. Results

#### 5.3.1. Modelled WTD

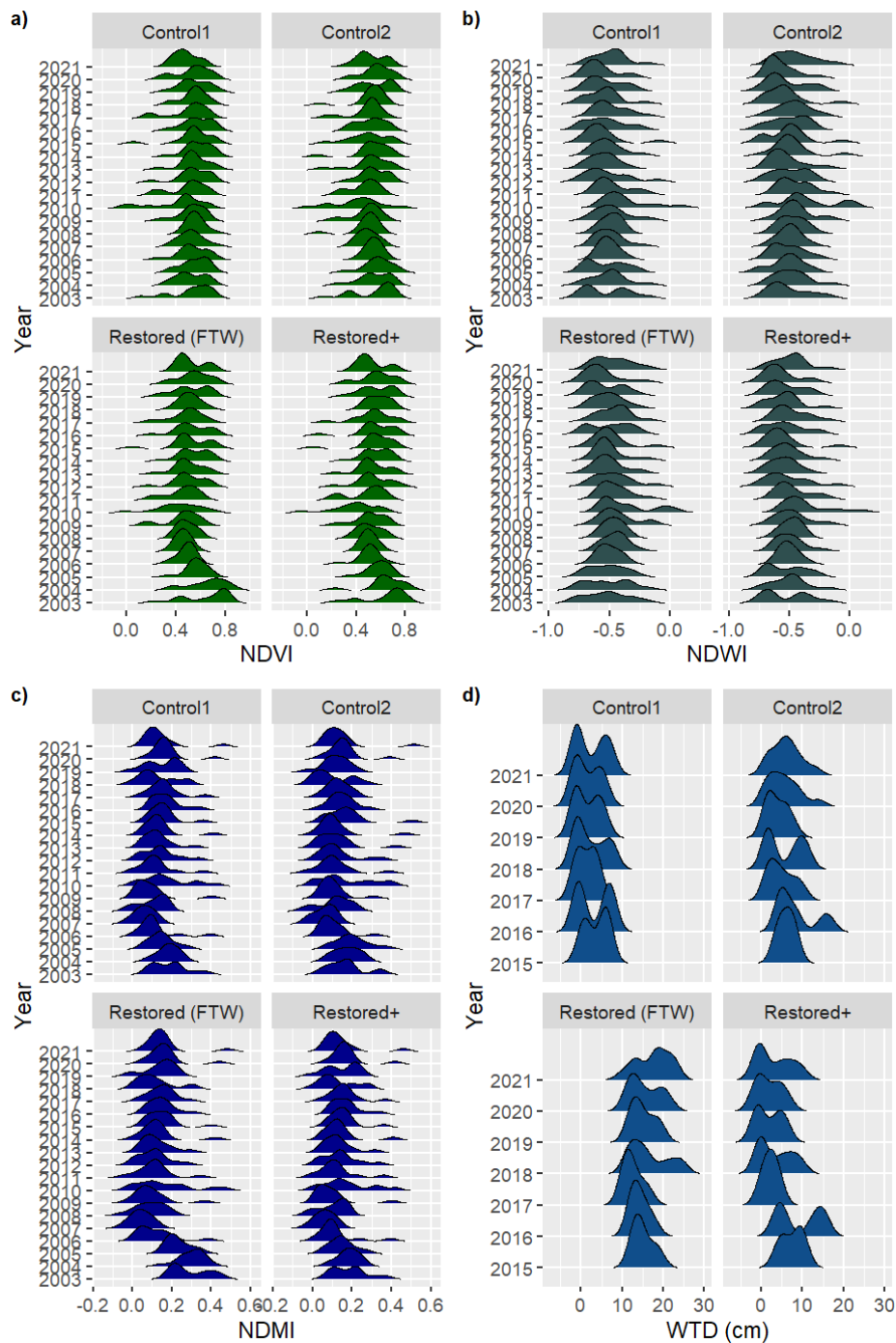
According to the modelled WTD series using Sentinel-1 and random forest method (Figure 5.5), the WTD fluctuates mainly between the surface and 10 cm depth for control sites, up to 15 cm depth for Restored+ site, and significantly lower (up to 25 cm) for the Restored (FTW) site. The observed values tend to fluctuate more than the model predictions, especially during the dryer summer periods, when the model systematically underestimates water level drawdown extent. Most notably underpredicted is the 2018 spring/summer drought, where the difference between observed and modelled WTD is ~5 cm for CL\_CON, 15 cm for CL\_CON\_EC site, ~10 cm for CL\_FTW and ~15 cm for CL\_BCFB. Somewhat surprising is the 2016 modelled WTD output for the CL\_CON\_EC site, where the WTD prediction is lower than that of 2018 while this summer/spring was not unusually dry.



**Figure 5.5.** Modelled WTD using the Sentinel-1 and RF method for time period 2015 – 2021. CL\_CON = Cross Lochs Control site 1, CL\_CON\_EC = Cross Lochs Control site 2, CL\_FTW = Cross Lochs Restored (FTW) site, CL\_BCFB = Cross Lochs Restored+ site. A noticeable bias can be observed towards the lowest WTD values during summer drawdowns, when the difference between modelled and observed WTD has been up to 20 cm.

### 5.3.2. Annual density plots and descriptive statistics

Figure 5.6 shows the annual distributions and interannual behaviours of NDVI, NDWI, NDMI and modelled WTD time series. All four indicators typically have normal or bimodal distribution shapes, with NDVI being slightly negatively skewed in a few years of the data (e.g., 2003, 2010, 20017) and opposite (positively skewed) for NDMI and NDWI series. The second peak that often can be observed in the NDVI series (left of the main peak) is most likely the periods with sparse snow cover or periods with longer persistent cloud cover. This may also aid to identify years and months that cause false change points identified in the time series. For example, 2010 clearly stands out in NDVI and NDMI series and is most likely connected to the snow/cloud presence, while the 2018 drought might have impacted the distribution of modelled WTD and NDMI values. The NDVI values typically vary between 0.44 and 0.64 (Q1 and Q3 from Table 52) and show a repeated behaviour throughout the years in all three peatland condition groups. NDWI values are typically negative and fluctuate between -0.79 and 0.09, while NDMI range was -0.06 to 0.52. The modelled WTD series (Figure 5.6d) shows how the Control and Restored+ sites are distributed around 5 cm depth, while the values from the Restored (FTW) site are distributed at a lower ~15 cm depth.

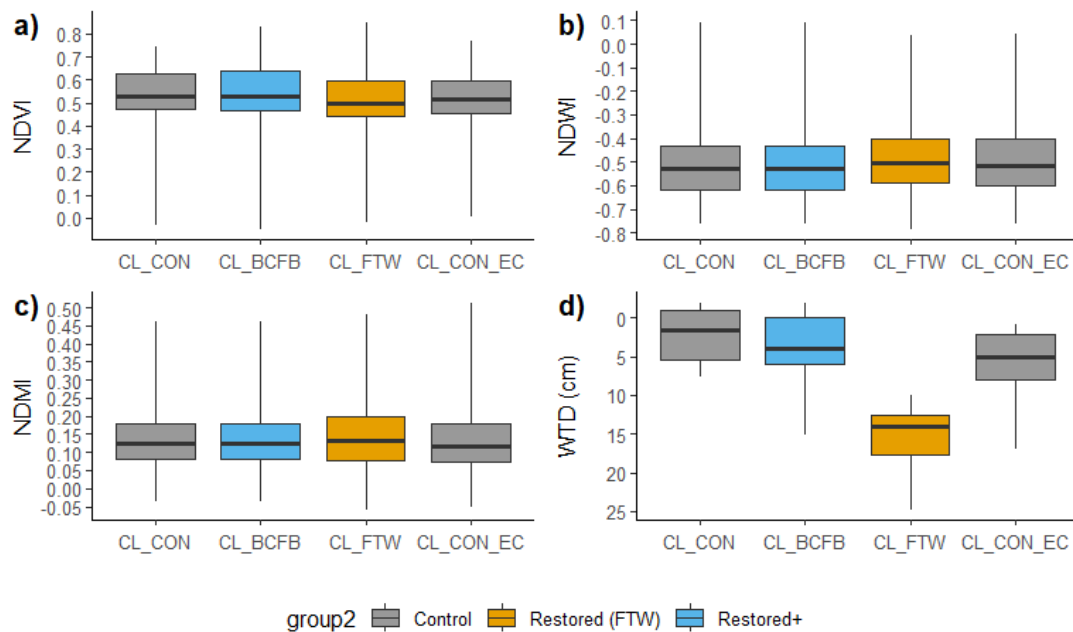


**Figure 5.6.** Annual density plots for the three Cross-Lochs peatland condition groups: a) MODIS NDVI time series (2003-2021, 250 m resolution); b) MODIS NDWI time series (2003-2021, 500 m resolution); c) MODIS NDMI time series (2003-2021, 500 m resolution), and d) Sentinel-1 based modelled WTD time series (2015-2021, 20 m resolution).

From the descriptive statistics of the analysed time series (Table 5.2) and the 2015 example (Figure 5.7) it can be seen that the time series from the three peatland condition groups are very related to each other, especially the MODIS-derived indices. Sentinel-1 based modelled WTD series provided a better distinction between the groups, particularly with the Restored (FTW) site standing out (Figure 5.7d).

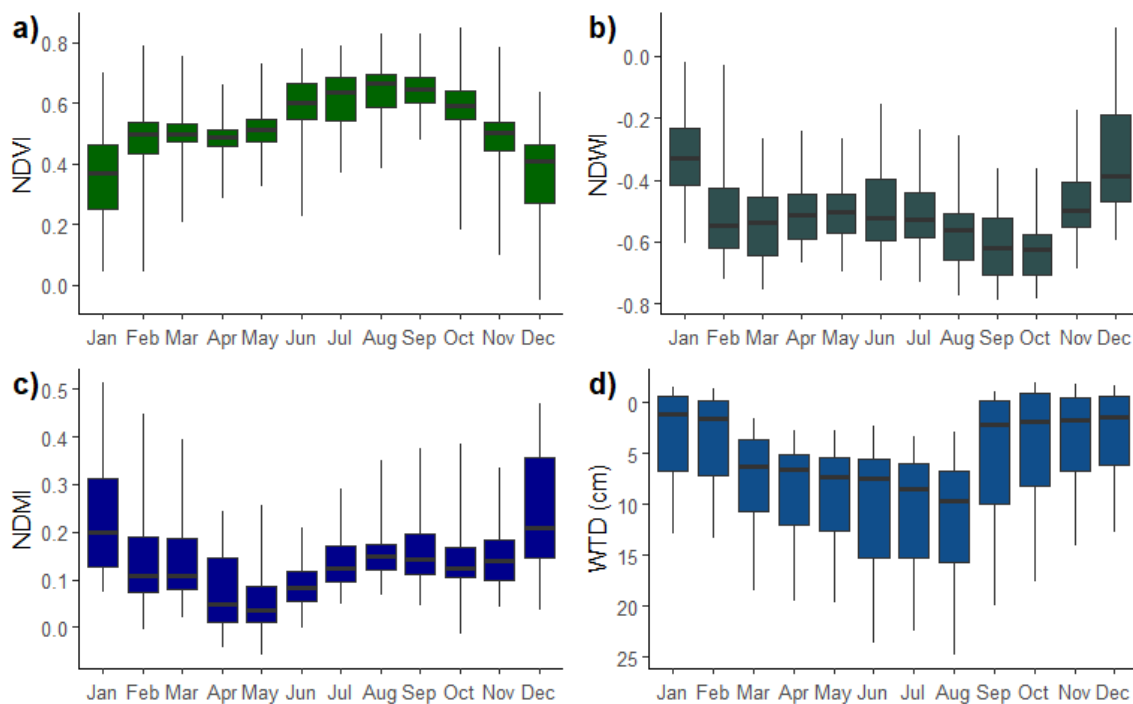
**Table 5.2.** Descriptive statistics of the NDVI, NDWI, NDMI (2003-2021) and modelled WTD (2015-2021) time series. Negative WTD values indicate inundation.

Indicator	Group	Min	Q1	Median	Mean	Q3	Max	SD
NDVI	Control1	-0.03	0.47	0.53	0.52	0.63	0.75	0.14
	Control2	0.00	0.45	0.52	0.51	0.60	0.77	0.14
	Restored (FTW)	-0.02	0.44	0.50	0.51	0.59	0.85	0.14
	Restored+	-0.05	0.47	0.53	0.53	0.64	0.83	0.14
NDWI	Control1	-0.76	-0.62	-0.53	-0.51	-0.43	0.09	0.15
	Control2	-0.76	-0.60	-0.51	-0.49	-0.40	0.04	0.15
	Restored (FTW)	-0.79	-0.59	-0.51	-0.49	-0.40	0.04	0.15
	Restored+	-0.76	-0.62	-0.53	-0.51	-0.43	0.09	0.15
NDMI	Control1	-0.04	0.08	0.12	0.14	0.18	0.46	0.09
	Control2	-0.05	0.07	0.12	0.13	0.18	0.52	0.10
	Restored (FTW)	-0.06	0.08	0.13	0.15	0.20	0.48	0.11
	Restored+	-0.03	0.08	0.12	0.14	0.18	0.46	0.09
WTD (cm)	Control1	-1.9	-0.9	1.6	2.2	5.4	7.5	3.2
	Control2	0.8	2.2	5.1	5.7	7.9	17	3.7
	Restored (FTW)	10.0	12.5	14.0	15.1	17.7	24.8	3.5
	Restored+	-2.0	-0.1	3.9	4.1	6.0	15.1	4.4



**Figure 5.7.** Cross-Lochs area, boxplots for the four indicators investigated, 2015 example. The horizontal lines correspond to the medians, upper and lower hinges indicate the first and third quartiles, upper and lower whiskers correspond to the maximum and minimum values.

From the monthly distribution of the values (Figure 5.8), it can be seen the NDVI reaches the highest value just above 0.6 during the growing season between July and September and the lowest values are observed during December and January. NDWI values are typically in the range between -0.7 and -0.2 and stay negative all year long, indicating that there are no substantial aqueous surfaces present. It can be seen that NDWI does increase in January and February, which could potentially indicate higher soil saturation and small standing water surface areas present in the sites. Similarly, January and February have the highest NDMI values as well, getting closer to the 0.4 threshold, which could indicate waterlogging. NDMI has a more noticeable minimum observed in May and June which could indicate dryer conditions but is still outside of the water stress indication. The lowest modelled WTD is observed during the summer months with a notable decrease from February to March and then again, a rise in September, however from the comparison of observed and modelled WTD it is known that these values should be even lower in the summer months.

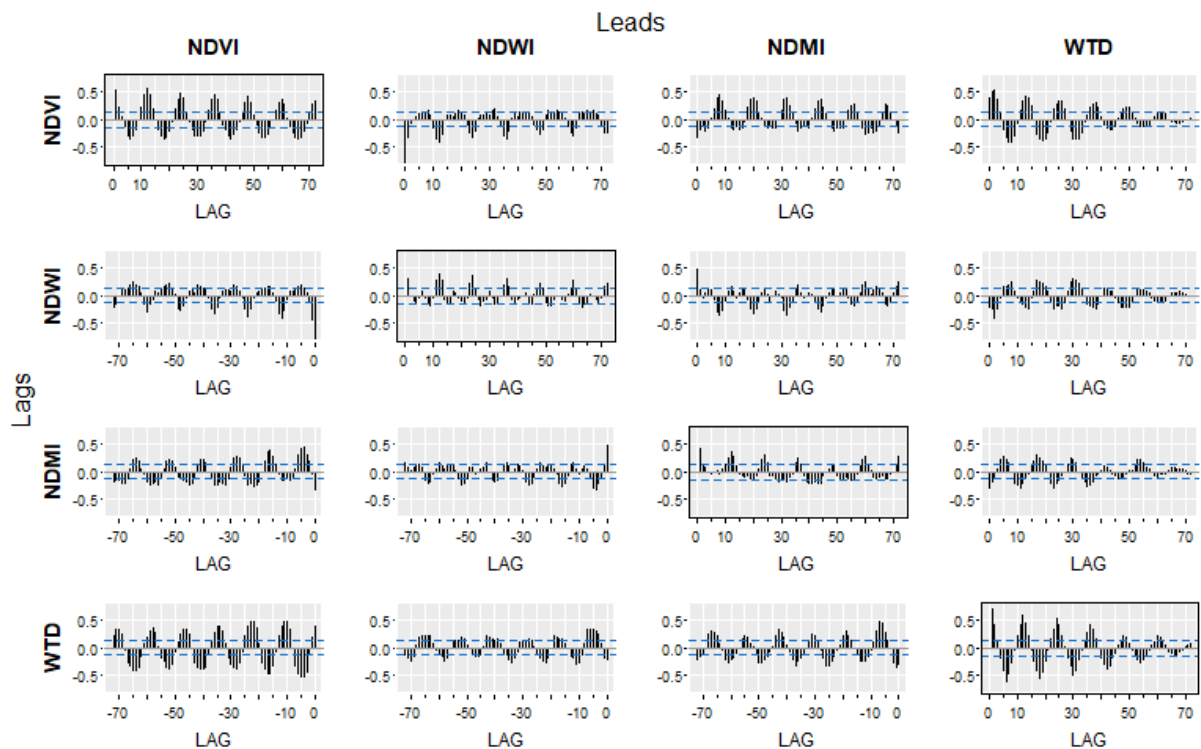


**Figure 5.8.** Average monthly box plots (NDVI, NDWI, and NDMI 2003-2021; modelled WTD 2015-2021 (as observed in the comparison with field gathered WTD values, the actual summer WTD values can be up to 15 cm lower). The horizontal lines correspond to the medians, upper and lower hinges indicate the first and third quartiles, upper and lower whiskers correspond to the maximum and minimum values.

### 5.3.3. Auto-correlation and Cross-correlation analysis

In Figure 5.9, plots on the leading diagonal show repeated autocorrelations that are significantly non-zero, confirming that all four time series are non-random. Besides, an oscillation can be observed

in all autocorrelation plots, indicating a clear seasonality in the series. An annual seasonal trend is peaking at 12, 24, 36 etc. lag and only slightly seems to be decreasing with time; only for the modelled WTD series it drops below the significance level after 5 years. The negative correlations from the autocorrelation plots with peaks at 6, 18, 30, 42 etc. lag are best seen in NDVI and modelled WTD series. From the cross-correlation plots it can be observed that the highest correlations exist between the NDVI and modelled WTD series pair and the NDMI and NDVI pair, however, all variables have significant non-zero correlations repeatedly observed over the investigated time. The most dominant cross-correlations occur at the 12-month frequency with 1-3 month lead or lag time from it.



**Figure 5.9.** Grid of plots of the sample ACFs (diagonal, highlighted) and CCFs (off-diagonal) using 6 years of data (72 lags). The x-axes show the lags in months and the y axis show the correlation coefficient. The left side of the diagonal of the plot grid shows the negative lags; when the variables on x-axes lead over ones on y or, meaning, the successor activity will overlap the predecessor activity. The right side of the diagonal shows the positive lags; when the x variables (column series) lag compared to y (row series), meaning the successor activity will have a waiting period before starting.

### 5.3.4. Time-Series decomposition

Through STL decomposition, the seasonal pattern and remainder was removed from the time series and to investigate the underlying trends in the time series. Trend analyses were applied to examine if trends are present in the study areas following restoration and what direction and magnitude do they present.

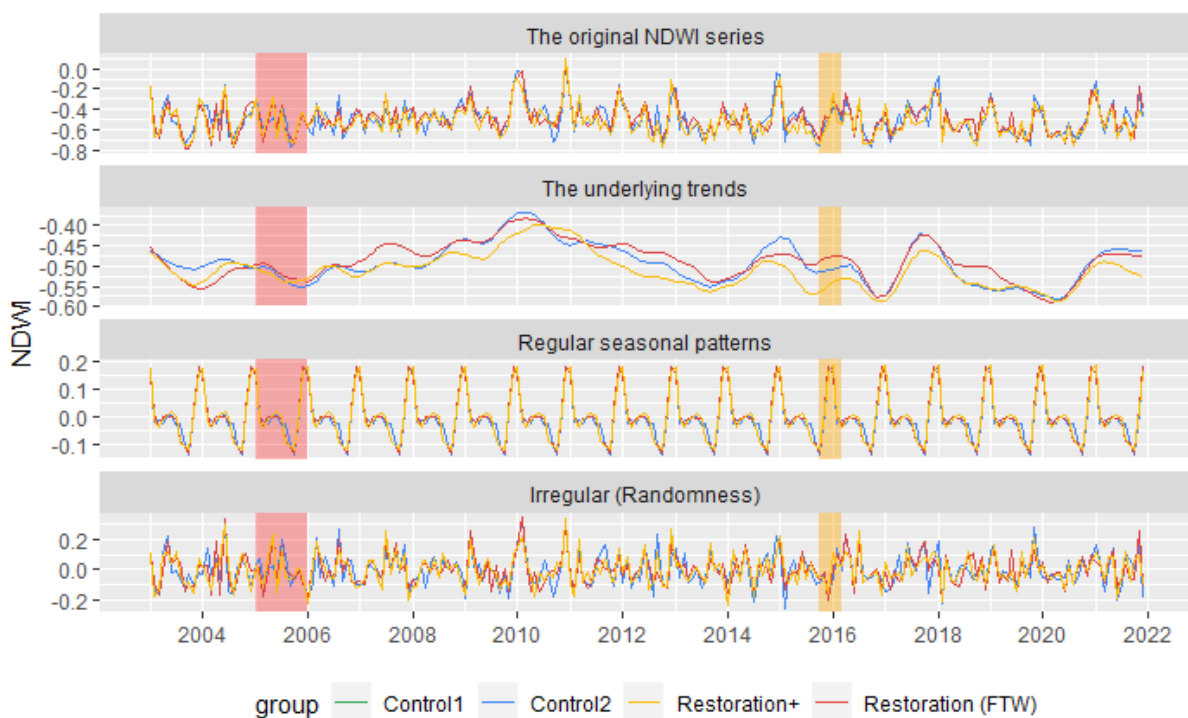
Figure 5.10 shows the decomposition applied to the monthly NDVI time series for the four areas investigated. The seasonal pattern shows an annual peak to peak amplitude in NDVI of about  $\sim 0.35$ . Surprisingly, a decline in the NDVI trend in restored peatland sites is visible already prior to the tree felling in 2005-2006, however from the raw data series it can be seen that this could have been influenced by one significantly lower observation at the very beginning of the series, causing a bias in the smoothed trend. Once the felling period had finished, a continuing decline is still visible, which could indicate the leftover product (branches with thick carpet of needles) to still be present on the ground and only slowly drying and browning. Depending on the amount of the leftover material, this drying can take a year or so, which would correspond to the time when NDVI values of the restored sites stabilize. A notable dip is visible around 2010 and 2011 which is observed in the control sites too, so is not connected with the restoration progress. After this, a slow increase seem to appear in both restored sites. Restored+ site has higher NDVI values but already after initial restoration (tree felling) has a pattern more similar to that of the control sites. The additional management during 2015 and 2016 does not seem to have increased the NDVI value of Restored+ site, however, it can be seen that the site has had a higher resilience to dryer summer periods when a smaller decrease in NDVI compared to Restored (FTW) and even the Control sites is observed.



**Figure 5.10.** Decomposed NDVI time series. The red shaded area indicates the tree felling (2005-2006) in both restored sites, while the time period shaded in orange shows the additional brash crashing and furrow blocking applied to the Cross Lochs Restored+ site (Oct 2015 – Feb 2016). Series based on MODIS 250 m resolution NDVI product.



Figure 5.11 shows the decomposition applied to the monthly NDWI time series for the four sites. One of the first observations is that due to the coarse resolution of the product (500 m) the values of Control1 and Restoration+ overlap and cannot be distinguished in the plot. It can be seen that the Restored+ site NDWI values are more similar to the Control2 site compared to the Restored (FTW) site, however this could be the effect of the two sites that cannot be distinguished. After the initial tree felling in 2005-2006, all sites have an upward going trend until 2010, including the control site, but then a downward trend is notable until 2014. The additional restoration treatment applied to the Restored+ site in 2015-2016 does not seem to have an obvious impact. The seasonal pattern shows an annual peak to peak amplitude in NDWI of about  $\sim 0.3$ , but compared to the NDVI series the peak is observed in the winter and then quickly declines.



**Figure 5.11.** Decomposed NDWI time series. The red shaded area indicates the period of tree felling in both restored sites (2005-2006), while the time period shaded in orange shows the additional brush crashing and furrow blocking applied to the Cross Lochs Restored+ site (Oct 2015 – Feb 2016). Series based on the MODIS 500 m resolution surface spectral reflectance product.

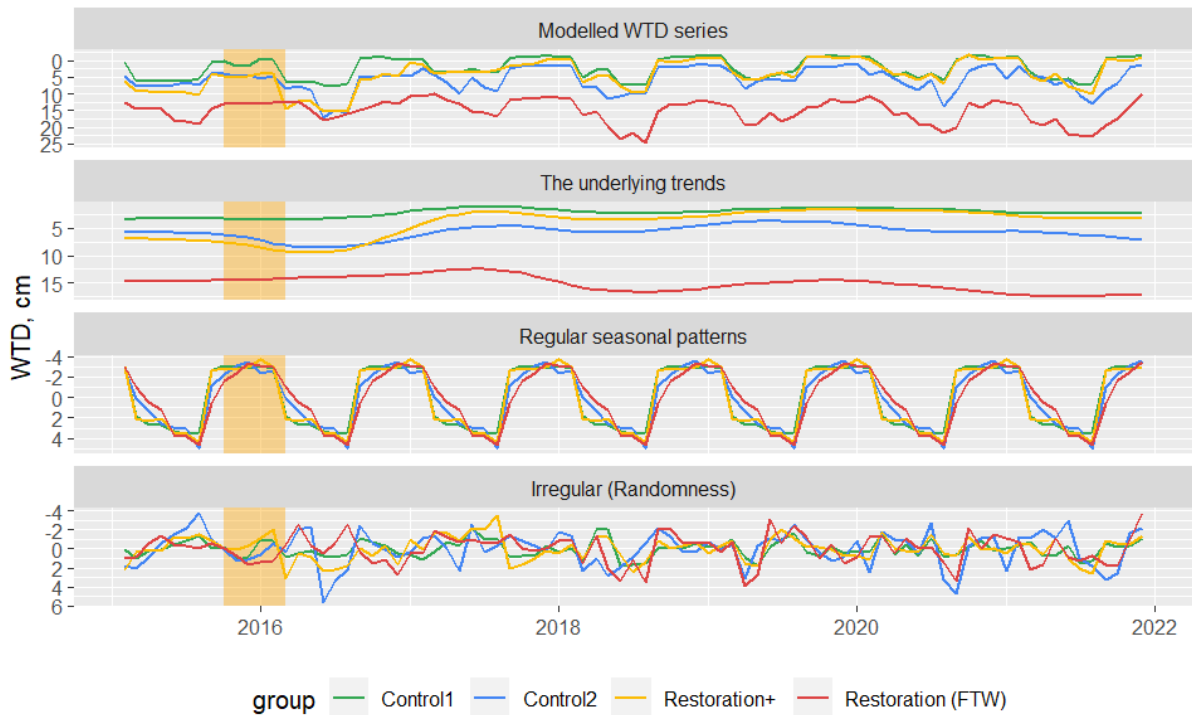
Figure 5.12 shows the decomposition applied to the monthly NDMI time series for all sites. Just like with the NDWI series, the image resolution has prevented the distinction between the Control1 and Restoration+ groups. It can be seen that the Restored (FTW) site has NDMI value significantly different from the other two sites in the period between 2003 and 2006. This is most likely reflecting the tree felling in the area. A similar pattern was expected for the Restored+ site, which received the same treatment in this period, but as it can be seen there is almost no decrease in NDMI values. This shows that the resolution of the used data has made one site completely obstruct the changes happening in

another. From 2007 onwards, all sites have similar spectral signatures and any obvious trend differences between the groups cannot be observed. The seasonal pattern shows an annual peak to peak amplitude in NDMI of about ~0.2, with the peak observed in the winter.



**Figure 5.12.** Decomposed NDMI time series. The red shaded area indicates the tree felling in both restored sites (2005-2006), while the time period shaded in orange shows the additional brush crashing and furrow blocking applied to the Cross Lochs Restored+ site (Oct 2015 – Feb 2016). Series based on the MODIS 500 m resolution surface spectral reflectance product.

Figure 5.13 shows the shorter time series based on the modelled WTD. Unfortunately, it is not possible to see how the initial restoration might have affected the WTD, however, the additional treatment applied to the Restored+ site over 2015 and 2016 seems to have raised the WTD (as assessed by the modelled WTD product) by about 3 - 5 cm. From 2017 onwards the trend component of the Restored+ site is very aligned with the trend of the Control sites, and all are rather stable over time. The restored (FTW) site trend, on the other hand, shows a slow decrease in WTD (about 5 cm between 2017 and end of 2021). The seasonal pattern shows an annual peak to peak amplitude of about 8 cm with the peak observed in the winter.



**Figure 5.13.** Decomposed modelled WTD time series for the three condition groups. The area shaded in orange shows the period of additional brush crashing and furrow blocking applied to the Cross Lochs Restored+ site (Oct 2015 – Feb 2016). Series based on the Sentinel-1 20x22 m resolution IW GRD product.

#### 5.3.4.1. Trend analysis using Mann-Kendall test and Theil-Sen estimator

Mann-Kendall (MK) test was used to assess if increasing or decreasing monotonic trends can be observed in the decomposed time series once different stages of restoration have taken place, and Sen's slope was used to see the magnitude of the trend; the results from these tests are summarised in Tables 5.3. - 5.5 representing three time periods: 1) recovery after initial restoration (post-felling) and before the additional restoration management (January 2007 – September 2015), 2) recovery after the additional restoration management and before the 2018 drought (March 2016 – April 2018) and 3) recovery after the 2018 drought (September 2018 – December 2021).

Table 5.3. shows how according to the Mann-Kendall (MK) test, during the first time period after initial restoration a significant positive trend in NDVI was found for both of the restoration sites, while the control sites had positive but non-significant trends observed. The MK test for the NDWI series indicated a negative trend in all sites, and the trend was found to be statistically significant for both restored sites and the Control 2 site. Finally, in the NDMI series a positive significant trend was observed in all sites. Overall, sites show positive trends towards increased healthier vegetation (more positive NDVI trends) and moisture increase (positive NDMI trends). However, according to the Sen's slope estimator for all the significant trends in this time period, the magnitude of them has been very minimal.

**Table 5.3.** Mann-Kendall trend and Sen’s slope test results for the period after initial restoration and before the additional restoration management (January 2007 – September 2015), number of observations (n) for each area = 104) \*\*\* indicates a .001 significance level; \*\* indicates a .01 significance level; \* indicates 0.05 significance level.

Time Series	Area	Mann-Kendall trend	p-value	Sen’s slope
NDVI	Control1	0.003	0.96	0.000
	Control2	0.110	0.96	0.000
	Restored (FTW)	0.399	0.000***	0.001
	Restored+	0.003	0.000***	0.000
NDWI	Control1	-0.313	0.000***	-0.001
	Control2	-0.128	0.054	0.000
	Restored (FTW)	-0.346	0.000***	-0.001
	Restored+	-0.313	0.000***	-0.001
NDMI	Control1	0.512	0.000***	0.001
	Control2	0.457	0.000***	0.001
	Restored (FTW)	0.512	0.000***	0.001
	Restored+	0.512	0.000***	0.001

Table 5.4 shows the trends observed in the much shorter period between the second round of restoration (applied only to the Restored+ site) and before the 2018 drought. As starting from 2015 the Sentinel-1 data are available, the trends of the modelled WTD series have also been compared for this time period. In this period negative NDVI trends have been identified both for control and restored sites with Sen’s slopes magnitudes higher than those after the initial restoration. In the meantime, trends from NDMI and NDWI indicate increased moisture conditions and according to the Sen’s slope, they are slightly higher for the restored sites compared to the control sites. This is also in agreement with the trends from the modelled WTD series, especially the Restoration+ site, with the strongest Sen’s slope estimator value found. The modelled WTD of the Restored+ site was found to have a significant increase in this period (showing negative trend as WTD becomes shallower), which potentially affirms the success of the additional intervention in the restoration process.

**Table 5.4.** Mann-Kendall trend and Sen’s slope test results for the period after the additional restoration management and before the 2018 drought (March 2016 – April 2018, number of observations (n) for each area = 25). \*\*\* indicates a .001 significance level; \*\* indicates a .01 significance level; \* indicates 0.05 significance level.

Time Series	Area	Mann-Kendall trend	p-value	Sen’s slope
NDVI	Control1	-0.668	0.000***	-0.005
	Control2	-0.576	0.000***	-0.005

	Restored (FTW)	-0.575	0.000***	-0.004
	Restored+	-0.717	0.000***	-0.002
NDWI	Control1	0.508	0.000***	0.004
	Control2	0.538	0.000***	0.005
	Restored (FTW)	0.465	0.001***	0.004
	Restored+	0.508	0.000***	0.004
NDMI	Control1	0.594	0.000***	0.002
	Control2	0.446	0.002**	0.001
	Restored (FTW)	0.514	0.000***	0.003
	Restored+	0.594	0.000***	0.002
WTD	Control1	-0.582	0.000***	-0.126
	Control2	-0.588	0.000***	-0.194
	Restored (FTW)	-0.102	0.481	-0.030
	Restored+	-0.600	0.000***	-0.449

Finally, the trends of the last period investigated, after the 2018 drought, are shown in table 5.5. Here a statistically significant decrease in the NDVI values has been observed in two sites (Control1 and Restored+). NDMI and NDWI show small positive trends, while the modelled WTD series indicate a slight lowering of WTD in this period.

**Table 5.5.** Mann-Kendall trend and Sen's slope test results for the period after the 2018 drought until the end of 2021 (September 2018 – December 2021, number of observations (n) for each area = 40). \*\*\* indicates a .001 significance level; \*\* indicates a .01 significance level; \* indicates 0.05 significance level.

Time Series	Area	Mann-Kendall trend	p-value	Sen's slope
NDVI	Control1	-0.664	0.000***	-0.003
	Control2	-0.207	0.061	-0.001
	Restored (FTW)	0.200	0.071	0.001
	Restored+	-0.605	0.000***	-0.002
NDWI	Control1	0.492	0.000***	0.002
	Control2	0.623	0.000***	0.004
	Restored (FTW)	0.231	0.037	0.001
	Restored+	0.492	0.000***	0.002
NDMI	Control1	0.303	0.006**	0.002
	Control2	0.364	0.001***	0.002
	Restored (FTW)	0.444	0.000***	0.003

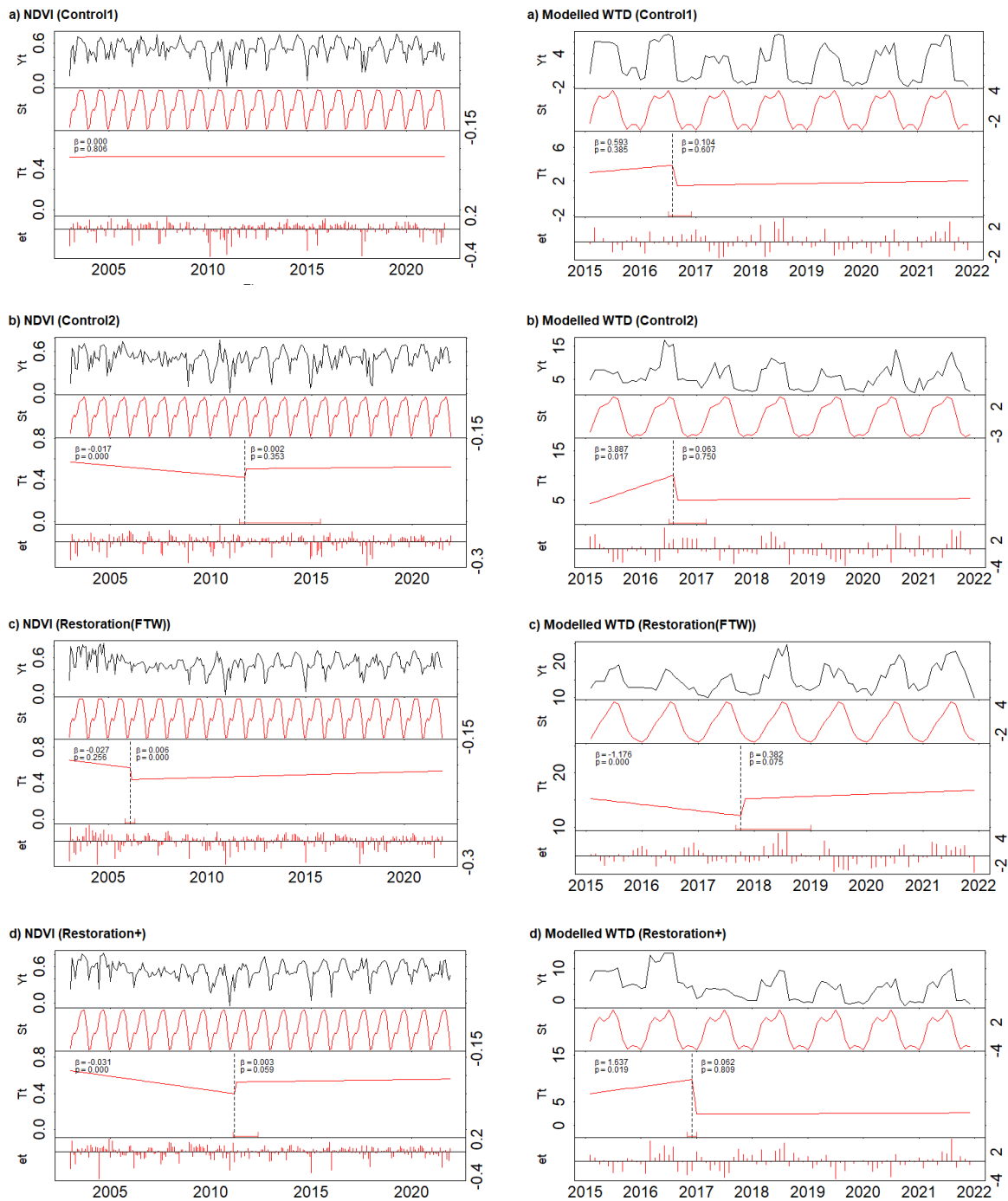
	Restored+	0.303	0.006**	0.002
WTD	Control1	0.356	0.001**	0.019
	Control2	0.764	0.000***	0.082
	Restored (FTW)	0.512	0.000***	0.077
	Restored+	0.387	0.000***	0.0338

#### 5.3.4.2. Trend and change point analysis using BFAST algorithm and Pettitt's test

Two methods: BFAST algorithm and Pettitt's test were applied to the full time series of data to test if there are significant change points identifiable in the MODIS products and Sentinel-1 based WTD series connected with either significant restoration events, such as the tree felling, and less abrupt changes, such as the additional reprofiling and removal of brush material.

BFAST algorithm results are combined and shown in Figures 5.14 and 5.15 and later compared to the change points identified by the Pettitt's test (Table 5.6). Overall, BFAST was able to identify no more than one breakpoint in each of the data series, and no abrupt breaks were identified in the seasonal components for any of the groups.

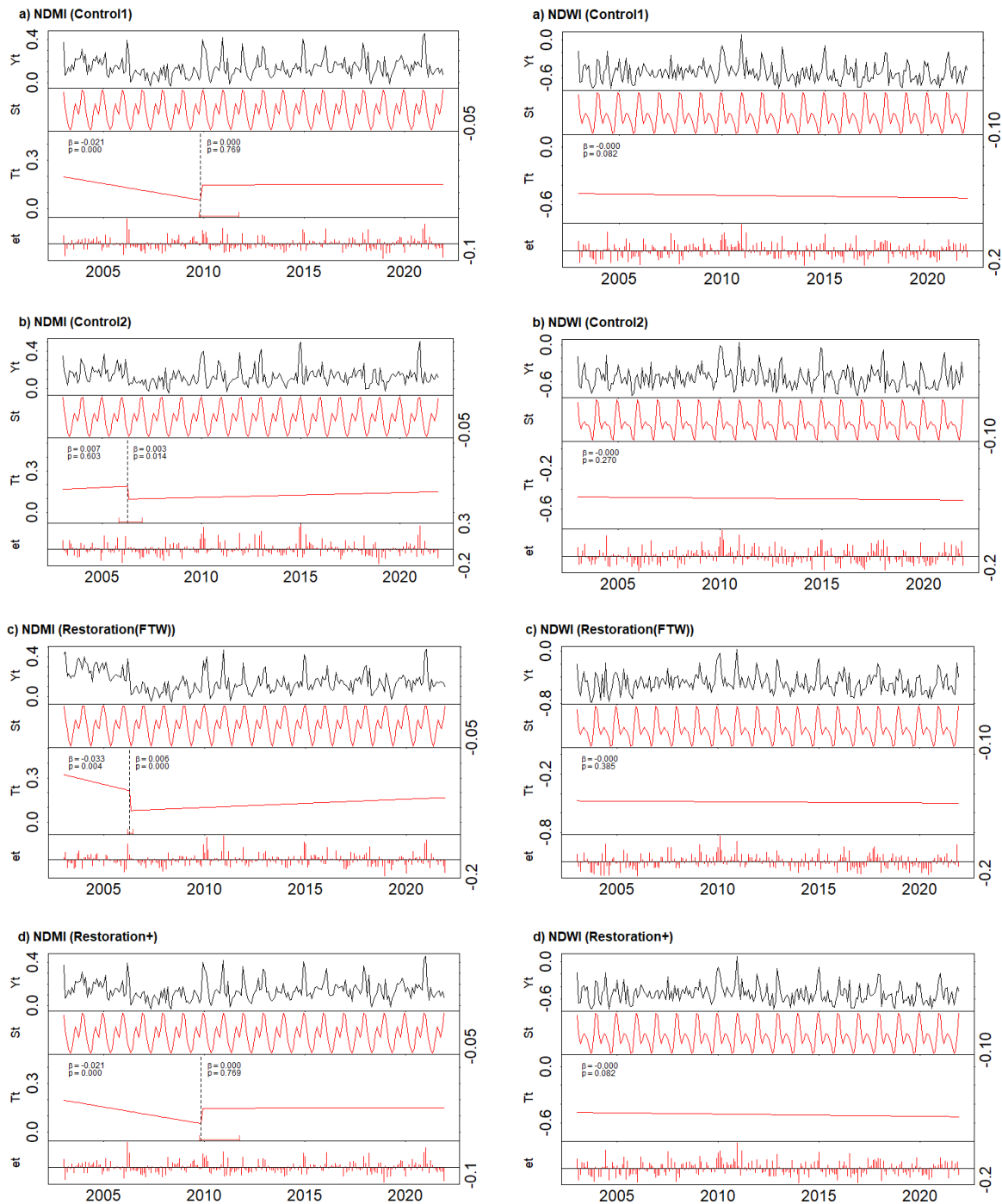
Figure 5.14 shows the BFAST method results from NDVI and modelled WTD series. NDVI series had change points identified in Control2 and both restoration sites. The initial restoration in Restoration (FTW) site was accurately identified as a significant change (February 2006 by BFAST, and, similarly, by Pettitt's test in April 2006), this however was not the case with the Restoration+ site, which had change point identified in March 2011 by BFAST. Pettitt's test showed December 2005 as a change point which coincides with the initial restoration works in this site. The shorter modelled WTD series identified August 2016 as a change point in both of the control sites, October 2017 for the Restoration (FTW) site and December 2016 for the Restoration+ site (coinciding with the additional restoration works in this site).



**Figure 5.14.** BFAS decomposition using NDVI (2003-2021) series (left) and modelled WTD (2015-2021) (right) for each of study areas: a) Control1, b) Control2, c) Restoration (FTW), d) Restoration+. The top panel in each individual plot shows the original time series; the second panel from the top shows the seasonal component and any breaks identified in the seasonal component; the third panel from the top shows the trend, identified breakpoints and their slope and significance values for each identified trend segment and the 95% confidence interval for the timing of breaks. The MODIS NDVI product has a 250 m resolution; Modelled WTD is based on the Sentinel-1 product with 20×22 m resolution.

Figure 5.15 shows the BFAS method results from NDMI and NDWI series. No change points were identified in the NDWI series for any of the sites investigated. The NDMI series had April 2006

identified as a significant change point in the Restoration (FTW) site (coinciding with the initial restoration works) and November 2009 in the Restoration+ site, however the same breakpoints were identified in the Control2 site. This could indicate that either the change points found are not directly connected with the applied restoration management or point out to the challenge of working with relatively coarse data (500 m resolution).



**Figure 5.15.** BFAST decomposition using NDWI (2003-2021) series (left) and NDMI series (20103-2021) (right) for each of study areas: a) Control1, b) Control2, c) Restoration (FTW), d) Restoration+.

The top panel in each individual plot shows the original time series; the second panel from the top shows the seasonal component and any breaks identified in the seasonal component; the third panel



from the top shows the trend, identified breakpoints and their slope and significance values for each identified trend segment and the 95% confidence interval for the timing of breaks. No breakpoints have been identified in the NDWI series; while one change point has been identified in each of the areas using NDMI series. Both NDMI and NDWI are 500 m resolution products.

The comparison of dates identified as change points from BFAST and Pettitt's test are summarized in Table 5.6. For the two restored sites, the period around initial felling is typically found as the strongest change point in NDVI and NDMI series and was identified by both BFAST and Pettitt's test. It was surprising, that BFAST was not able to identify the 2005-2006 felling in the Restored+ site NDVI series as a significant change, on the contrary, Pettitt's test did identify the tree felling as an abrupt change. The identified change points (only by Pettitt's test) in the restored sites using the NDWI series were not connected with restoration activities. In the shorter modelled WTD series in the restoration sites, multiple months in 2016 and 2017 were identified as change points. In this period, however, restoration management was applied only to the Restoration+ site. Finally, although no significant change points were really expected to be identified in the Control sites, both BFAST and Pettitt's test identified change points in all the indicator time series.

**Table 5.6.** Change points identified by BFAST algorithm and Pettitt's test. All listed change points were found to be statistically significant at a .05 significance level.

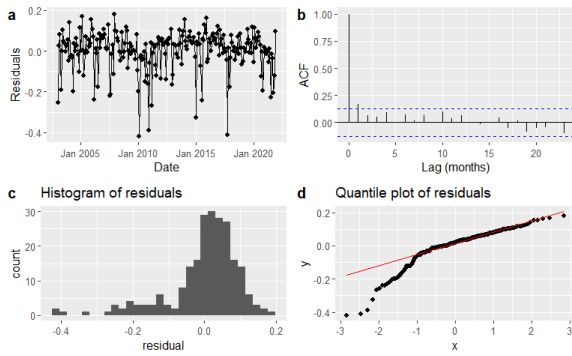
<b>Time series</b>	<b>Area</b>	<b>BFAST algorithm</b>	<b>Pettitt's test</b>
NDVI	Control1	-	May 2013
	Control2	Sep 2011	Jan 2007
	Restored (FTW)	Feb 2006	Apr 2006
	Restored+	Mar 2011	Dec 2005
NDWI	Control1	-	Mar 2012
	Control2	-	Oct 2012
	Restored (FTW)	-	Jan 2013
	Restored+	-	Mar 2012
NDMI	Control1	Nov 2009	May 2005
	Control2	Apr 2006	Apr 2006
	Restored (FTW)	Apr 2006	May 2006
	Restored+	Nov 2009	May 2005
WTD	Control1	Aug 2016	Dec 2016
	Control2	Aug 2016	Mar 2017
	Restored (FTW)	Oct 2017	Mar 2017
	Restored+	Dec 2016	Dec 2017

### 5.3.4.3. Residual analysis

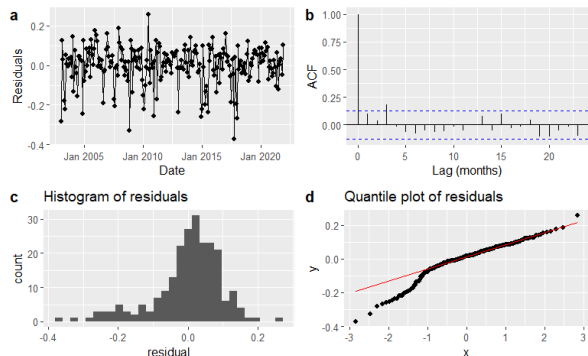
The last analysis included the time series residual examination. Once decomposed into the trend, seasonality and remainder components, the time series remainder (noise) component was tested for autocorrelation. Figures 5.16 - 5.19 show residual analysis applied to each area grouped by NDVI, NDWI, NDMI and modelled WTD series.

Figure 5.16 shows the residual analysis for the NDVI time series. From the residual series and the histogram of distribution, it can be seen that there are more negative residuals that stand out and create left-skewed (negatively skewed) data, which is also reflected in the Q-Q plot where residuals are deviating from the straight line in the bottom end. Out of all indicators, the NDVI series has been the most affected by this. The autocorrelation plots showed normal distribution with no exceptional lags in the series.

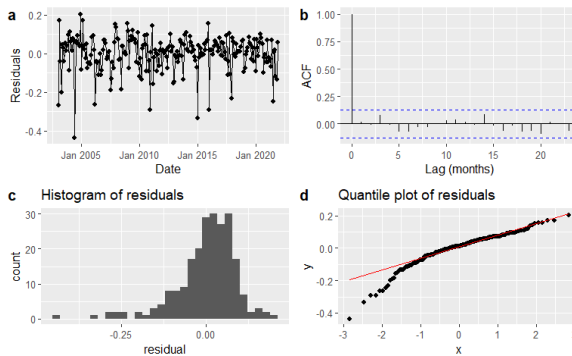
a) NDVI, Control1



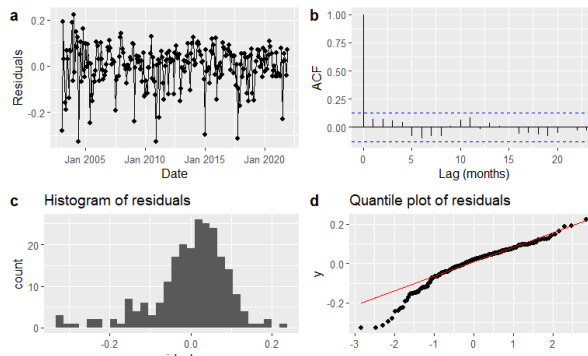
b) NDVI, Control2



c) NDVI, Restoration+



d) NDVI, Restoration (FTW)

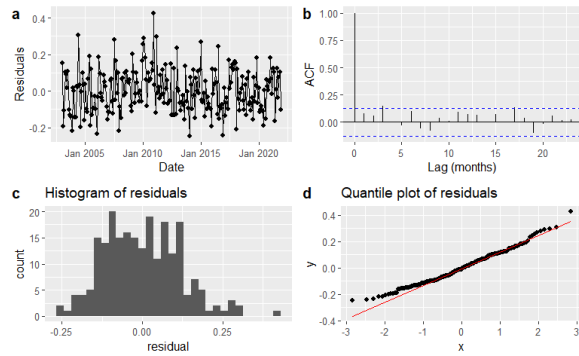


**Figure 5.16.** Residual analysis for NDVI series (2003 – 2021). For each area the individual plots show a) the remainder component after time series decomposition, b) autocorrelation function (ACF) plot (the blue dashed lines indicate the confidence level ( $\alpha=0.95$ )), c) distribution of the residuals, d) Q-Q (quantile-quantile) plot (x axis representing the theoretical quantiles and y axis the data sample quantiles).

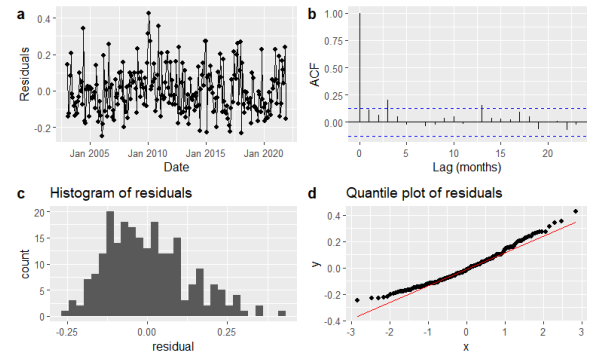
Figure 5.17 shows the residual analysis for the NDWI time series. From the Q-Q plots and histograms it can be seen that these series are less skewed compared to the NDVI series, however there

are more “spikes” that stand out in histograms. From the ACF plots, there are a few lags that slightly pass the confidence interval, however, these are minor and a random distribution of the NDWI series residuals can still be presumed.

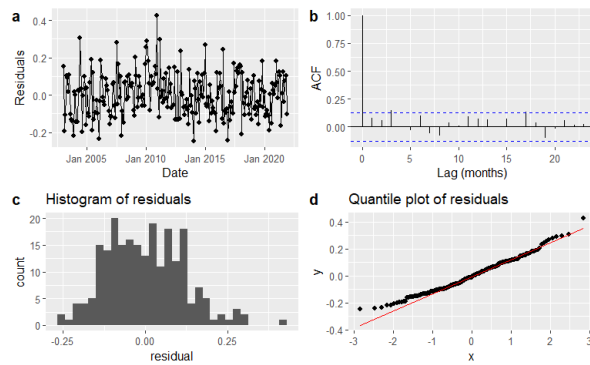
a) NDWI, Control1



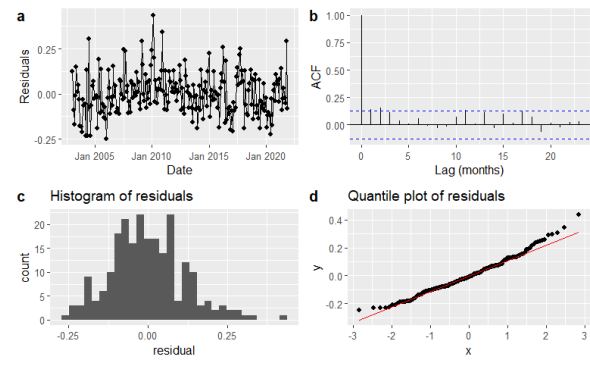
b) NDWI, Control2



c) NDWI, Restoration+



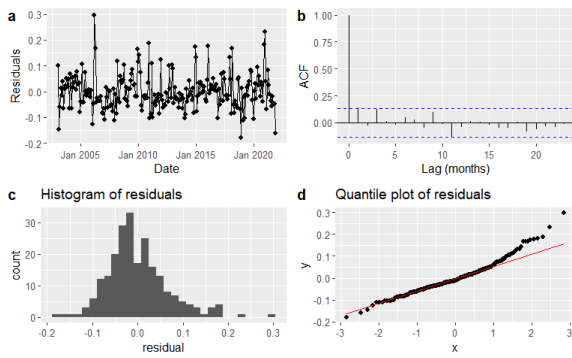
d) NDWI, Restoration (FTW)



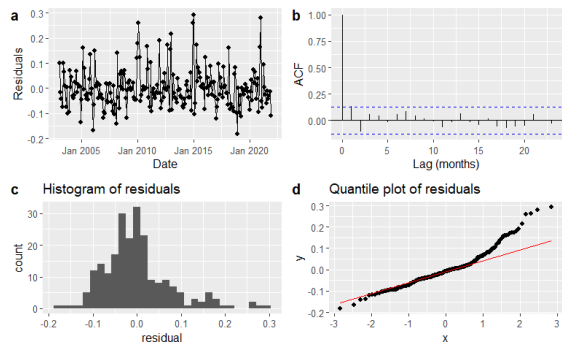
**Figure 5.17.** Residual analysis for NDWI series (2003 – 2021). For each area the individual plots show a) the remainder component after time series decomposition, b) ACF plot (the blue dashed lines indicate the confidence level ( $\alpha=0.95$ ), c) distribution of the residuals, d) Q-Q plot (x axis representing the theoretical quantiles and y axis the data sample quantiles).

Figure 5.18 shows the residual analysis for the NDMI time series. The Q-Q plots and histograms show that the series are slightly right-skewed (positively skewed), while the autocorrelation plots show no exceptional lags in the series.

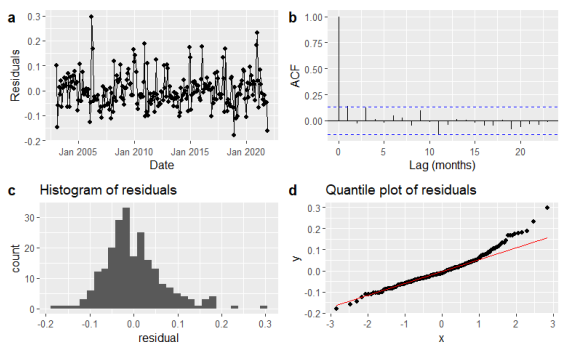
a) NDMI, Control1



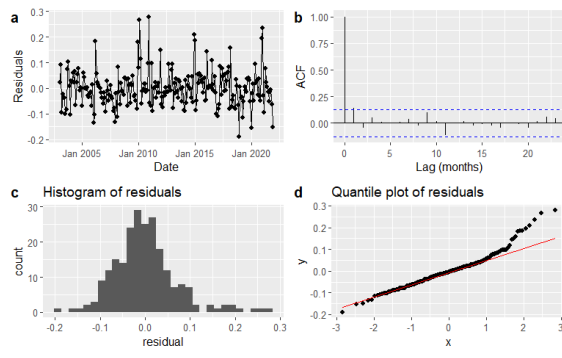
b) NDMI, Control2



c) NDMI, Restoration+



d) NDMI, Restoration (FTW)

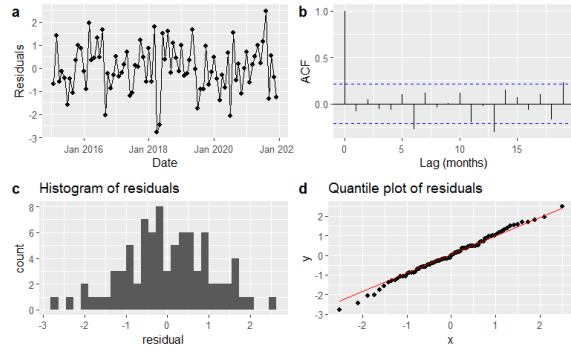


**Figure 5.18.** Residual analysis for NDMI series (2003 – 2021). For each area the individual plots show a) the remainder component after time series decomposition, b) ACF plot (the blue dashed lines indicate the confidence level ( $\alpha=0.95$ ), c) distribution of the residuals, d) Q-Q plot (x axis representing the theoretical quantiles and y axis the data sample quantiles).

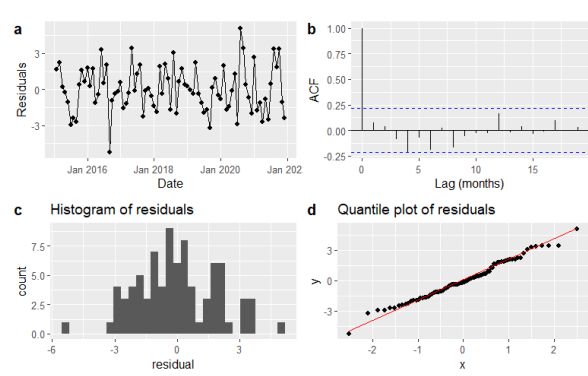
Finally, the Figure 5.19 shows the residual analysis for the modelled WTD series, which were the shortest time series out of the four indicators. While the histograms show a few spikes and dips in the distribution, overall, the residuals are normally distributed and the Q-Q plots from these series have the closest match between the theoretical quantiles and data sample quantiles.

Overall, the residual analysis has indicted the suitability of applied decomposition model to each of the time series investigated.

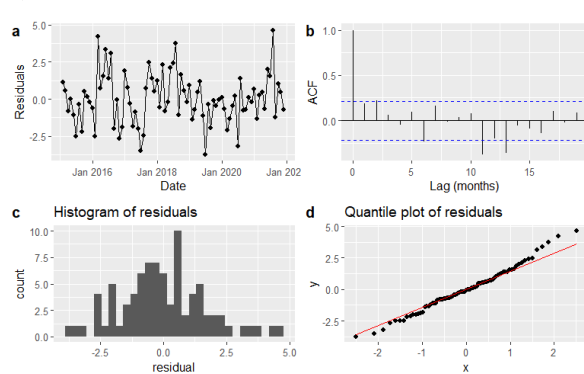
a) Modelled WTD, Control1



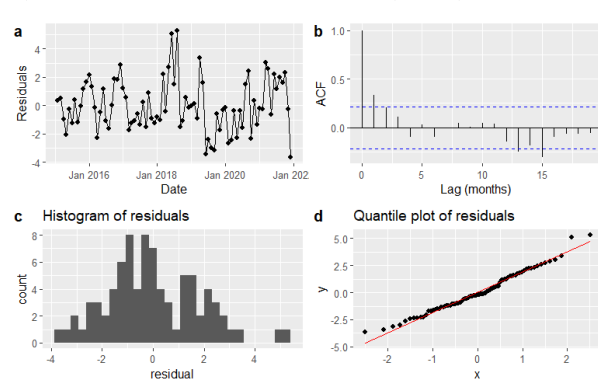
b) Modelled WTD, Control2



c) Modelled WTD, Restoration+



d) Modelled WTD, Restoration (FTW)



**Figure 5.19.** Residual analysis for modelled WTD series (2015 – 2021). For each area the individual plots show a) the remainder component after time series decomposition, b) ACF plot (the blue dashed lines indicate the confidence level ( $\alpha=0.95$ ), d) distribution of the residuals, d) Q-Q plot (x axis representing the theoretical quantiles and y axis the data sample quantiles).

## 5.4. Discussion

Ideally, peatland restoration projects seek to restore their condition and function as close to their natural state as possible. This chapter investigated if satellite data time series can reveal restoration success, i.e., if the trends in the data from restored sites show signs of shallower WTD, increased soil moisture, and returning vegetation through satellite data-derived vegetation indices and modelled WTD. 7 year-long Sentinel-1 and 19 year-long MODIS satellite data series were used to investigate if peatland restoration could be monitored using NDVI, NDWI and NDMI and modelled WTD.

Over time many different change detection methods have been proposed for remotely sensed data time series analysis (Kovács et al., 2022; Najafi et al., 2019; Niu et al., 2020; Southworth and Muir, 2021). Abrupt or structural changes might have an influence on time series trends, and at the same time, a trend can mask one or more abrupt changes in a series, therefore it is important to analyse both the trend and change points (Sharma et al., 2016). In this chapter, four sets of remotely sensed time series data were decomposed using STL to analyse the underlying trends and detected change points in the series. Besides visually analysing the trends, some of the most widely used methods for environmental

and seasonal data analysis were applied to investigate changes in peatland ecosystems, including Mann-Kendall test, Sen's slope, Pettitt's test and BFAST algorithm.

In previous studies the Mann-Kendall method for trend analysis has been shown to outperform other tests in remotely sensed data trend analysis (Militino et al., 2020), but its main drawback is the ability to only detect one monotonic trend. For sites where multiple interventions have taken place, each significant change in the field could cause breaks in the trend, and an overall monotonic trend could potentially not be identified. In this study, therefore the trends were investigated in the three separate periods: recovery after initial restoration (January 2007 – September 2015), recovery after the additional restoration management (March 2016 – April 2018) and recovery after the 2018 drought (September 2018 – December 2021). During the first period analysed, Mann-Kendall test results indicated significant positive trends over the restored sites, showing trajectory towards increased moisture (higher NDMI values) and healthier vegetation (increased NDVI values), however, according to the Sen's slope estimator, the magnitude of these trends was minimal. The second period investigated did not show positive trajectories towards vegetation recovery (NDVI values) for the restored sites, however, trends from NDMI and NDWI indicated increased moisture conditions and according to the Sen's slope, they were higher for the restored sites than the control sites. For this time period, modelled WTD series were also available through Sentinel-1 data processing and showed positive recovery of WTD, especially for the Restored+ site, potentially affirming the success of the additional intervention in the restoration process during 2015-2016, with the WTD rising by about 5 cm few months after the intervention. During the third time period investigated, both NDVI and modelled WTD showed initial positive trends (most likely connected with the recovery after the drought), however the overall period according to the Mann-Kendall test showed small, but statistically significant negative trends over the restored sites. In previous studies MK test and Sen's slope estimator has been successfully applied to various environmental data and ecosystems (Fassnacht et al., 2019; Guo et al., 2018), and in this study we found these methods to be useful for trend analysis and comparison of trajectories between different peatland sites, however caution must be taken regarding the spatial resolution of input data. These methods should also be applicable in future peatland studies using other remote sensing data as inputs. The coarse spatial resolution of MODIS, especially the NDMI and NDWI indices at 500 m resolution was problematic for investigating sites which are not located too far from each other. The coarse resolution of imagery can cause problems in analysis of nearby sites, when noise is introduced from various surrounding areas can completely obstruct change or trajectory detection (Kovács et al., 2022; Wulder et al., 2016). This could be well observed for Control1 and Restoration+ sites in this study. One of the biggest potential improvements for restoration monitoring therefore would be the application of the discussed methodology to higher spatial resolution data, such as the Sentinel-2, Landsat, or commercial satellite data imagery for NDVI, NDMI and NDWI series creation. Using higher resolution data, however, would probably decrease the number of cloud-free imagery as the satellite revisit times would be longer, therefore gap filling of long periods with clouds could be a challenge. Additionally, only

shorter data archives might be available and higher computing power might be required. The Sentinel-1 SAR spatial resolution ( $20 \times 22$  m in IW mode) is sufficient for landscape scale peatland WTD analysis, and while higher resolution SAR satellite data are available from satellites like Radarsat-2, TerraSAR-x, ICEYE, they are usually available only at a cost. On the other hand, analysis with SAR of different wavelengths could be explored in the future. L-band, specifically, has a longer wavelength (15 – 30 cm) compared to the C-band's 4 – 8 cm, and could be beneficial for the drier peatland sites and periods with lower WTD (periods and sites where the developed Sentinel-1 model was underperforming). While current access to L-band satellite SAR data is limited, two upcoming missions – NISAR (set to be launched in 2024) and ROSE-L (launch planned in 2028), have both agreed to open data policies (ESA, 2023a), which should be a valuable addition to increase SAR applicability for peatland and other ecosystem monitoring. Additionally, the detection and quantification of standing water using either SAR, optical or combined data would be a good addition to compare the results obtained from the NDWI and improve the understanding of Sentinel-1 backscatter dynamics with inundated peatland surfaces.

One of the reasons for choosing BFAST for change point detection was its ability of detecting multiple changes in the series, however for the sites and series investigated, there was usually only one change point identified even if the area would have undergone multiple interventions. For most cases, the period around initial felling was typically found as the strongest change point in the optical data series and was identified as significant both by the BFAST algorithm and Pettitt's test. Regarding less severe changes, the tested change point identification methods gave mixed results. BFAST did identify the additional restoration as a period of significant change applied to the Restoration+ site using the modelled WTD series, however, caution with the modelled WTD data must be taken, because there is no field data available for this period to verify the modelled WTD increase after the additional treatment of brash crushing and furrow blocking. Besides the identified change points that relate to the restoration, both methods identified other significant change points in the series, which are not directly connected with restoration management. The potential caveats that could have affected the change point analysis includes the input data (contamination due to clouds, spatial resolution, length of data series), but it could also point to the methods used being prone to false positives (the analysis identifies changes that are not actually present) or thirdly, it could point to other real events that could be happening in the area but not have been analysed in detail here such as the changing climate.

Long-term (>10 years) post-restoration monitoring is critical to understanding if peatland is recovering both from hydrological and vegetation perspectives. While field-gathered data remain invaluable for verification and calibration purposes, this chapter has shown that remote sensing has a potential to aid in the long term restoration monitoring, but more work needs to be done to improve the workflow of creating robust long-term trend assessment through remote sensing time series data analysis.

# Chapter 6

## 6. Discussion and Conclusions

The necessity of systematic peatland monitoring from local to global level is evident due to the importance of numerous ecosystem services peatlands provide. The field of remote sensing for environmental monitoring purposes is growing rapidly thanks to new satellite missions, improved sensors, higher resolutions and satellite revisit times. Also, the accessibility of the data and the cloud-based processing opportunities has made remote sensing become an integral part of many scientific and operational research projects. In this thesis I aimed to take advantage of some of these improvements to advance peatland monitoring using remotely sensed data by investigating sensor sensitivity to peatland water table depth, creating models for water table depth prediction and analysing peatland restoration success through earth observation data.

In this last chapter, first, I summarise the findings of each thesis chapter. Then, the implications of the presented research findings are discussed, and finally recommendations for future actions that can be taken, based on the findings, are raised.

### 6.1. Summary of research

There were three primary objectives set at the beginning of the thesis:

- **Objective 1:** Investigate if synthetic aperture radar backscatter responds to peatland water table depth and soil moisture when using high-resolution SAR system.
- **Objective 2:** Test if Sentinel-1 SAR imagery can be used to model peatland water table depth by creating and testing models with different complexity.
- **Objective 3:** Explore methods for peatland restoration trajectory analysis using remote sensing datasets to assess the restoration effectiveness.

These objectives have been addressed in Chapters 2, 3, 4 and 5 of this thesis.

The importance of peatland monitoring was highlighted in Chapter 2 by summarising the current knowledge of remotely sensed data application for peatlands monitoring and brought attention to the existing research gaps. While field-gathered data are still very important, there is a need to expand peatland monitoring capabilities to cover larger areas, new restoration projects and ensure continuation in the datasets as peatland restoration is a slow process (Gaffney et al., 2022) and remote sensing has been proposed as a potential method to address these needs. In Chapter 2, I specifically focus on the radar remote sensing, which is more widely used for monitoring areas such as agricultural land but is



still only emerging as a useful tool for peatland monitoring and should be explored further. Another gap identified was the lack of studies with fine spatial resolution, which could demonstrate the radar backscatter – soil moisture/water table depth relationship and help with the interpretation of changes both in radar backscatter intensity and peatland subsidence/uplift through backscatter phase change. Finally, there is a knowledge gap when it comes to methods for processing long series of RS data for peatland restoration monitoring and creating reliable workflows for time series analysis through trend and change point analysis. The balance between image resolution, sensor capabilities and how far the archive of available data stretches back suggests that fusion studies, where both optical imagery, especially visible and near infra-red bands, and radar imagery has the highest potential for peatland monitoring over long periods of time.

To address these existing gaps in the field, I started with a unique setup of a high-resolution SAR-WTD experiment over a large peatland sample, which is described in Chapter 3. The main objectives for the laboratory study were to explore SAR's potential for peatland hydrological condition monitoring by conducting a controlled drought and investigating the backscatter's dependency on different peatland hydrological regimes, analyse how the signal's phase and weighted mean backscatter height within a peatland change with drought conditions and note the differences between used polarizations. The results from the experiment in Chapter 3 confirmed a clear coherent response both in radar backscatter amplitude and phase to a 17 cm drawdown in water table depth. The signal's phase demonstrated a deterministic change across the experiment which was able to detect subsidence of peat (>8 mm) with the water table drawdown and a correspondingly strong concomitant mean decrease of 7 dB across all polarizations. The results clearly demonstrated a close sensitivity of radar backscatter to hydrological patterns in a peatland ecosystem in a high detail study, therefore the next step was to test whether this relationship could still be observed when using satellite SAR data and changes of WTD occurring on a landscape scale.

The main objectives of Chapter 4 were to investigate the correlation between Sentinel-1 radar data and WTD in a range of peatlands from near-natural to sites damaged by past afforestation and drainage, and create and test models with different complexity for WTD estimation. Between the studied Forsinard Flows reserve sites, the near-natural peatlands presented the smallest fluctuations in WTD throughout the year (typically <15 cm depth) and had the most stable radar signal (~3 to 4 dB amplitude). At the same time, previously drained and afforested peatlands undergoing restoration management were found to have highest WTD fluctuations (up to 35 cm depth), which was also reflected in higher shifts in radar backscatter (up to ~6 dB difference within a year). Three models: simple linear regression, multiple linear regression, and random forest model, were then developed and evaluated for their potential to predict water table dynamics in the peatland sites using Sentinel-1 data. Out of these, the random forest model was found to be the most suited having the highest correlation scores, lowest RMSE values and overall good temporal fit ( $R^2 = 0.66$ , RMSE = 2.1 cm). It was also

noted how the inclusion of the radar image acquisition time (year and season) along with site identifiers significantly improved the model's performance. Overall, the WTD modelling approach using SAR data was found to have a strong potential and the further studies with a wider range of peatland sites are strongly encouraged.

Finally, the Chapter 5 looks into restored peatland monitoring through trajectory and change point analysis using longer time series of both SAR and optical remotely sensed data. The random forest model developed in Chapter 4 was used to create a 7 year-long WTD series based on Sentinel-1 backscatter. Additionally, MODIS satellite data series were used for 19 year-long NDVI, NDWI and NDMI series creation, covering the period of initial restoration work applied in the study area. It was tested if these series were indicative of restoration success through signs of shallower WTD, increased soil moisture, decrease of bare grounds and returning vegetation reflected in the remotely sensed data. The time series were decomposed into seasonal, trend and remainder components. The longer but lower spatial resolution time series of indices from MODIS data could generally reflect the abrupt big changes happening in the sites (such as the tree felling between 2005-2006), however additional restoration management applied (such as the furrow blocking and brash crushing between 2015-2016) could be identified as a significant change point only in the shorter modelled WTD series and show a positive recovery towards near-natural reference site. Although this chapter has taken steps further in developing workflows for peatland restoration progress assessment through remotely sensed data, working with time series and data that are prone to gaps (e.g., due to cloud cover) remains challenging and further exploration is highly necessary and therefore is also suggested as one of the directions for continuation of this research.

The findings presented in this thesis enhance the understanding of how C-band radar backscatter interacts with peat and blanket bog vegetation. The laboratory study has presented distinctive knowledge confirming radar's sensitivity to changes in peatland soil moisture and water table depth. Recent studies using satellite SAR data have shown very promising results for peatland surface movement monitoring using InSAR technique (Alshammari et al., 2020, 2018; Bradley et al., 2022; Marshall et al., 2022; Tampuu et al., 2020), however were either not validated at all or compared to levelling transects, therefore lacking the spatial coverage. The high resolution study described in this thesis was able to confirm the phase component of the signal indeed being indicative of a physical movement of the peat's surface horizon with changes in water table. This formerly missing information has been a valuable addition to the literature of InSAR for peatlands and should encourage further research on "bog-breathing" using InSAR. APSIS, the most developed method for peatland monitoring using InSAR up to date (Bradley et al., 2022), is patent pending and unfortunately remains unavailable for individual use. Besides the signal phase being indicative of a physical movement of the peat, both the laboratory study and Forsinard Flows study case demonstrated the backscatter's strength to be closely related to the water availability in peatlands. Previous studies had achieved varying results from

peatland WTD prediction using SAR backscatter data, with reported  $R^2$  scores ranging from 0.02 to 0.93 (Asmuß et al., 2019; Bechtold et al., 2020; Kim et al., 2017; Lees et al., 2021; Räsänen et al., 2022; Torbick et al., 2012). Besides improving the WTD predictions made by SAR-based models, an additional gap that has been addressed was the application of satellite imagery-based WTD monitoring for peatlands in varying condition and under different restoration management regimes. The developed Sentinel-1 based random forest model was tested on near-natural, degraded, previously drained and afforested sites, reaching  $R^2$  of 0.66 for Forsinard Flows sites and even higher ( $R^2 = 0.77$ ) when applied to the wider Peatland ACTION dataset, supporting the concept of Sentinel-1 SAR use for peatland WTD modelling, including degraded peatlands and restoration projects.

## **6.2. Further developments**

Some of the recommendations for continuity of this research that are discussed below include:

- Expanding water table depth modelling to a wider list of peatland sites and perform spatial analysis.
- Refining the water table depth model:
  - input covariates,
  - data from other existing/upcoming satellite missions.
- Use the modelled water table depth as a proxy for GHG emission reporting.

### **6.2.1. Expanding water table depth modelling to a wider list of peatland sites and perform spatial analysis**

This study has focused on the peatlands of Forsinard Flows Nature Reserve, which provided an exceptional data set on peatland restoration projects carried out over a period of 20 years using varying restoration techniques. Although this provided a good degree of variation of peatlands and their condition, it is necessary to apply and test methods used in this thesis to a wider representation of peatlands. Specifically, the WTD random forest model based on Sentinel-1 data would benefit from being trained on a series of WTD measurements from a more heterogeneous landscape. In the future, we plan to take this work further by creating a larger combined peatland WTD database using data from JHI, NatureScot Peatland ACTION and UKCEH. This will enable us to additionally train and test the model on a larger variety of peatland types and conditions, including raised bog sites, drier peatland sites, managed grazed grassland sites and agricultural lands with underlying peat.

Another important step would be to perform spatial analysis, i.e., use the developed WTD-SAR model and apply it spatially, mapping the water table depth across a wider defined area, such as the whole Forsinard Flows Nature Reserve. This would allow us to identify patterns in the modelled WTD (spatial distribution, clustering of certain areas with specific characteristics) and investigate relationships between modelled WTD and the distribution and what affects it (topography, presence of pools, certain vegetation presence, etc.). Later, when expanding to multiple time steps of spatial distribution, it could provide powerful information on changes in the region. This would be particularly important for the ongoing restoration projects, where identification of positive or negative changes in the WTD over time could help with informed decision-making with regard to environmental management, including the need for intervention if certain areas are not responding to restoration efforts.

Overall, expanding modelling efforts is essential for ensuring that the WTD is accurately reflecting the complexity of the peatland ecosystems and can be effectively applied for change monitoring.

### **6.2.2. Potential refinements for the water table depth model**

Whilst overall the modelled WTD outputs using Sentinel-1 series suggested a reasonable fit between field observed and modelled water table depths across a variation of peatlands, there was a bias towards the lowest observed WTD between the analysed sites that could be observed, typically during the drier summer periods.

Training the model on a larger data set could help to reduce bias by capturing a wider range of environmental conditions and increase the statistical power of the analysis, but the same could be achieved by the refinement of the model's inputs. The model could be optimized by changing the variables included in the model, adjusting the weights assigned to different variables or by completely changing the algorithm used to generate the WTD. There are several variables that could potentially improve the peatland water table depth prediction, but particularly precipitation, temperature, topography, and vegetation could be prioritized. The amount and timing of precipitation can have a significant impact on the peatland water table depth (Bourgault et al., 2019), while temperature affects the rate of evapotranspiration and water availability for recharge (Packalen et al., 2016). Including a covariate to represent the topography could also improve the model's performance as slope and aspect of the area can affect the rate of water runoff and infiltration, but also surface roughness is known as one of the parameters to influence radar backscatter. While vegetation change within a year is relatively small in northern peatland sites, accounting for growing vegetation could also be investigated further. As application of some of the currently proposed methods for this purpose (e.g., the vegetation sine correction discussed in Chapter 4) were found not to be suitable, there is a need for improved methods. One potential way to account for the vegetation growth could be using physically based models, e.g.,

recent studies using radiative transfer models and combined optical and SAR data have shown promising results (Quaife et al., 2022).

This thesis focussed on modelling the peatland water table depth, which is known to correlate well with the soil moisture in near-natural peatlands (Price, 1997; Räsänen et al., 2022) and assumed minor vegetation changes negligible to the C-band radar wavelength of ~5cm. While these assumptions allowed the peatland water table depth to be modelled as a direct function of the recorded backscatter, in a more complex modelling approach, the backscatter could be a function based on both WTD, volumetric water content and the vegetation. From the laboratory experiment and the field study, it can be concluded that the model performed well when the WTD was within 5 to 18 cm depth (range when WTD and soil VMC correlates well), and worse during drought or inundation periods. Price (1997) on their study on bog soil moisture and water table depth relationship reported low correlation between WTD and VMC, when the VMC dropped below 0.4. This means, that focussing on the model refinements of these low and high ranges of the WTD, would be most beneficial.

In this thesis, Random Forest was chosen for WTD prediction as a more advance model compared to the linear modelling, showing success in previous wetland studies (Klinke et al., 2018; Räsänen et al., 2022). But although RF generally helps with reducing overfitting, due to its dependency on to the input (training data), the model's performance can be negatively impacted by noisy, irrelevant, or missing data, still potentially leading to overfitting (Aria et al., 2021). If more covariates are added to the model and the training data set remains relatively small, it could be beneficial to test other predictive algorithms for WTD modelling, such as the Boosted Regression Trees. While just like the RF, the Boosted Regression Trees method combines multiple decision trees, it does it in a sequential manner, with each tree potentially correcting the errors of the previous tree and capturing complex patterns between the variables, however, this method may still overfit noisy datasets (Elith et al., 2008). Besides more complex models, data assimilation, where model predictions are combined with observational data to correct and improve the model's accuracy, could also be explored. Only recently has peatland hydrology-specific data assimilation studies emerged, with development and improvements of the models such as the Peat Catchment Land Surface Model (PEAT-CLSM) (Bechtold et al., 2020).

Finally, to better understand the performance of the developed WTD model, it would be useful to investigate in more depth the uncertainty and variability of the retrieved water table depth data. While traditional regression approaches allow for direct quantification of prediction error, as the Random Forest is a non-parametric ensemble method, it is more complex. Two well-known methods that could be used for estimating the uncertainty of the RF WTD model predictions are the Monte Carlo simulations approach and the Quantile Regression Forest (QRF) method (Liu et al., 2023; Meinshausen, 2006). Monte Carlo method repeatedly runs estimated range of values to produce a set of possible outcomes, which then are analysed to understand the likelihood of each scenario, it can, however, be

computationally demanding, especially with larger number of inputs (Isokangas et al., 2017; Rivers et al., 1998). QRF on the other hand builds up on the random forest algorithm by building decision trees and providing quantiles or probability distributions of test labels, this way helping with understanding the variability in the data and making predictions that account for this variability (Rudiyanto et al., 2016; Wang et al., 2022).

One of the concerns, raised after the laboratory experiment (Chapter 3), was the observation that neither the radar backscatter, nor the phase values reached the pre-drought levels after rewetting took place and if this evidence of hysteresis could have implications for modelling WTD in natural environments. The hysteresis might have had multiple factors coming contributing to it. Most likely, the biggest contribution would have come from peat compaction and the vegetation that was irreversibly harmed during the prolonged drought. Figure 6.1 displays, how the mosses were able to endure the drought, while the heather and grasses did not survive the prolonged drought. The compaction could have also had further changed the physical structure of the peat with some of the cavities collapsing. Bearing in mind that the whole sample had already gone through reconstruction, the compaction along with the rather severe rewetting (40 l of rain per 1 m<sup>2</sup> of peat each day, over 7 days), could have obstructed water reaching into all the pore spaces. All these factors could have affected the dielectric properties of the peat, and hence the hysteresis in radar backscatter. Some of these events though were extreme and would not be expected in a real-world environment. If, however, an experiment like this is repeat in a laboratory environment, it would be beneficial to use an optical sensor along the SAR to be able to track the health of vegetation throughout the drought period as in Lees et al. (2019).



**Figure 6.1.** The heather segment of the trough before (20<sup>th</sup> November 2020) and after the drought and rewetting (4<sup>th</sup> June 2021). While the mosses appear green and healthy, it can be seen that the heather and grasses have died back.

Another potential improvement could be higher spatial resolution data used for analysis. In this thesis, MODIS data were included due to the long time series this mission provides and the short revisit time, which increases the chances of cloud-free imagery. However, it was found that the resolution of both the 250 and 500 m products offered a limited possibility to identify less significant changes happening in the area or changes occurring in smaller areas. The impact of edge effects or complete obstruction of a certain change was observed, therefore one solution to tackle this issue could be to analyse higher spatial resolution optical data. From currently freely available data, Landsat imagery (up to 30 m resolution) and Sentinel-2 imagery (up to 10 m resolution) has a high potential, however, the gap filling of long periods with clouds remains a challenge. Different methods, such as interpolation, smoothing, data assimilation of multiple data sources and machine learning and others have been proposed for gap-filling of time series of cloudy satellite imagery (Carrasco et al., 2019; Claverie et al., 2018; Gao et al., 2006; Pastick et al., 2018; Zekoll et al., 2021). While there is a danger of gap-filled data masking some of the actual changes and creating biased estimates, it could be trialled further, specifically for northern peatland areas, where presence of clouds is known to create gaps stretching over months.

For radar imagery, the current spatial resolution of Sentinel-1 ( $20 \times 22$  m in IW mode) is high enough for landscape scale peatland WTD analysis, however, different signal penetration depth is something that could be explored further using data from other missions. Potentially, the most useful for peatland WTD monitoring could be the missions with L-band sensors on board. L-band has a much longer wavelength of 15 – 30 cm compared to the C-band's 4 – 8 cm, and could be beneficial for the drier peatland sites, where the developed Sentinel-1 model was underperforming. There are two upcoming L-band SAR missions that have agreed free and open data policies planned to launch in the coming years - NISAR by NASA and ISRO in 2024 and ROSE-L by ESA in 2028, which could both be a great addition for many ecosystems, including peatland monitoring.

### **6.2.3. Modelled WTD as a proxy for GHG emission reporting**

As studies have shown a close link between peatland water table depth and annual greenhouse gases, with WTD being the highest explanatory variable of CO<sub>2</sub> fluxes (Evans et al., 2021; Koch et al., 2023; Waddington et al., 2015), the WTD has been proposed as a low-cost proxy for peatland GHG reporting purposes. The initial analysis covered in Chapter 4, showed Net Ecosystem Production and methane equations proposed by Evans et al. (2021), applied to the observed and SAR-based modelled mean annual water table depths for sites in the Forsinard Flows study area.

Undoubtedly, modelling of peatland GHG emissions is a complex process, but the initial predictions have provided a starting point for assessing the potential GHG contributions coming from peatlands in different conditions. Currently in Scotland two national scale peatland monitoring

programmes are in place – NatureScot Site Condition Monitoring programme (NatureScot, 2023), assessing the peatland condition of designated sites based on field-survey methodology, and Peatland ACTION monitoring programme (NatureScot, 2020), assessing the condition of sites with completed peatland restoration. This means that routinely there are sites that fall outside of the monitoring programmes and lead to potential inaccuracies in condition assessments and therefore the reported GHG inventories. As seen from the GHG calculations in Chapter 4, the modelled WTD series provided results that were not too far off the field observed WTD data, which indicates an alternative proxy for GHG estimates when no in situ GHG monitoring is available. While there would be multiple concerns with using modelled WTD data as input for modelling GHG from peatlands, with additional model improvements, this could eventually offer a helpful tool for peatland GHG modelling with the ability not only to evaluate the historical impact of different restoration strategies applied to sites, but also predict likely future emissions and assess the impact of different scenarios and mitigation strategies.

### **6.3. Concluding remarks**

The research presented in this thesis has demonstrated that remotely sensed data can be informative of peatland condition and specifically, water table depth changes occurring over time. It has emphasised the importance of peatland restoration and effective monitoring needs for these areas. The opportunity to model peatland WTD using Sentinel-1 SAR backscatter for regular peatland monitoring using freely available remotely sensed data and cloud computing has been presented and discussed.

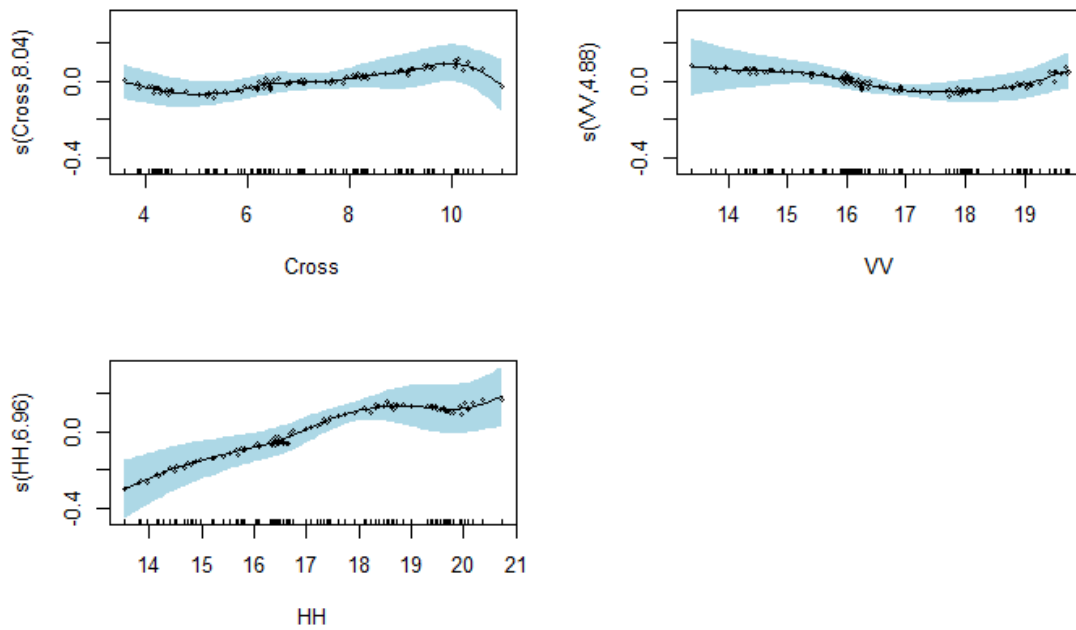
This thesis presents, to the best of our knowledge, the first piece of research specifically investigating Synthetic Aperture Radar’s signal response to changes in peatland water table depth and soil moisture in a controlled laboratory environment using a high resolution radar system. This has improved understanding of SAR relationship with water table depth in peatlands, which is not only a vital factor for development, sustainability and the recovery of peatland ecosystems, but has also been proposed as a potential proxy for GHG emission reporting in the future. It has also given the confirmation of hydrological changes being reflected in both the intensity and the phase of SAR signal, which previous studies have been lacking for validation purposes.

There are multiple directions this research can be developed further, including spatial monitoring of peatlands water table depth, refinement of the models and GHG prediction from mean annual modelled WTD values and reporting to the emissions inventories.

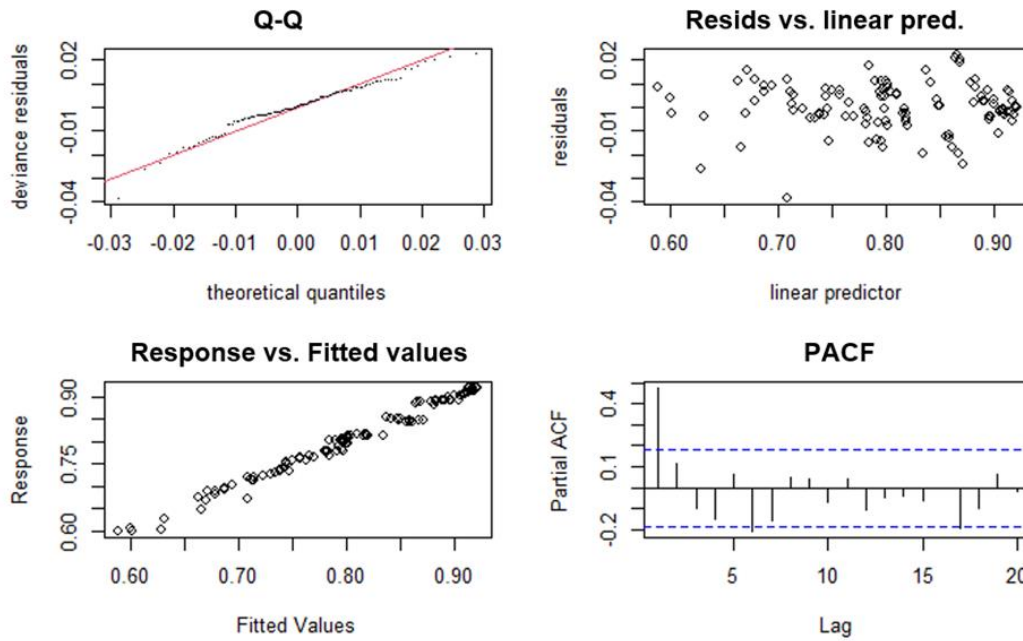


## Appendices

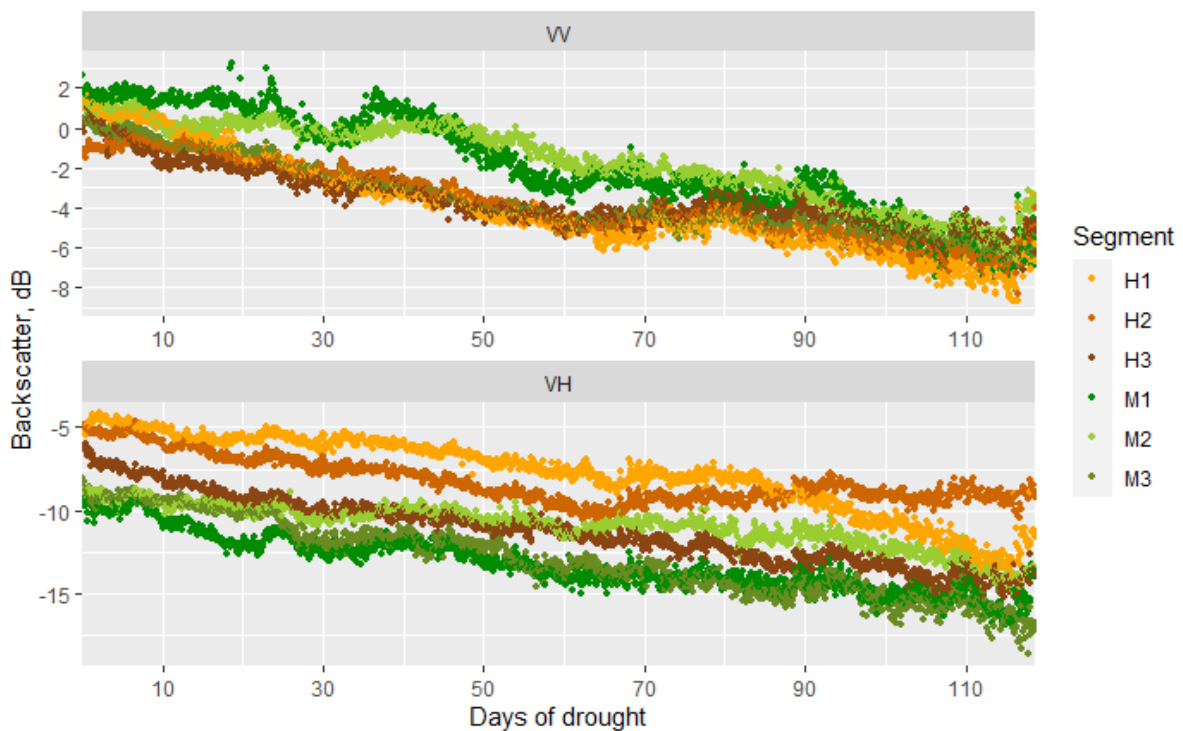
### A. Supplementary material for Chapter 3



**Figure S1.** Generalized additive model (GAM) partial effect plots of selected soil probe depths (3 – 10 cm) on the radar backscatter for (a) Cross polarization (b) VV polarization and (c) HH polarization. The y-axis represents the component effect of the smooth or linear terms in the model, which add up to the overall prediction. The ticks on the x-axis are observed data points. The points on the graphs represent the partial residuals and blue shaded areas indicate the 95% confidence intervals.

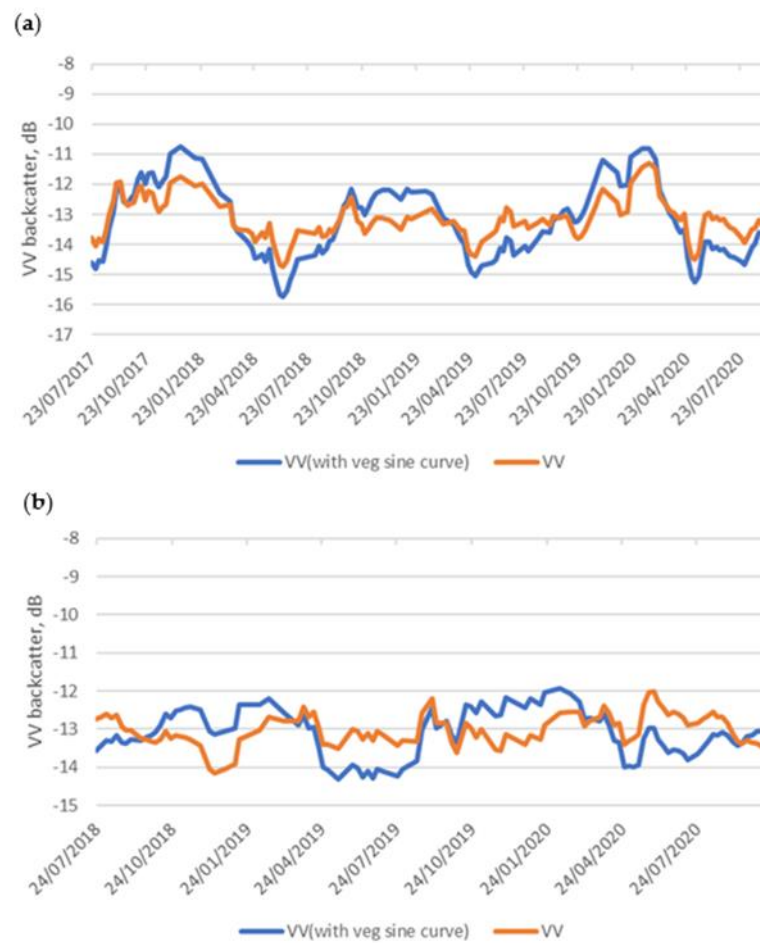


**Figure S2.** GAM statistics HH polarization example. a) Quantile-quantile plot: confirms that both sets of quantiles came from the same (normal) distribution. b) Residuals vs. predictor plot: residual values are equally and randomly spaced around the horizontal axis, indicating a good fit for the regression. c) Response vs. fitted values plot: the response values and values computed from the model match up well indicating a good fit with no obvious outliers or deficiencies in the model found. d) PACF plot: Significant correlations only at the first lag, followed by correlations that are not significant.



**Figure S3.** Heather and grass (segments H1-H3) and Sphagnum moss (segments M1-M3) backscatter response to drought (VV (top) and Cross-polarization (HV (bottom))).

## B. Supplementary material for Chapter 4



**Figure S1.** Sentinel-1 backscatter time series correction with and without the vegetation sine correction applied. Sentinel-1 backscatter time series with (blue) and without (orange) the vegetation sine correction applied, illustrated for a) Talaheel Restoration (FTW) and b) the near-natural control site. Figure illustrates the difference in the backscatter time series with and without the vegetation sine correction applied. While for the felled to waste site (Figure S1a) the 1 dB vegetation sine correction gives the impression that the correction could be representing the annual vegetation change, when applied for a near-natural site, where the backscatter only changes by about 1-2 dB between the seasons (usually below 10 cm change in WTD), in other words, the correction alters the data in an inappropriate manner (Figure S1b). The vegetation curve application in this case inflates the backscatter values, implying that vegetation is expected to impact the backscatter values as much as the WTD change. Given the overall minimal vegetation change in these ecosystems, it should not be the case. Another aspect not being considered in this approach is the start and end of the growing season, which can vary year to year.

## References

- Adeli, S., Salehi, B., Mahdianpari, M., Quackenbush, L.J., Chapman, B., 2021. Moving Toward L-Band NASA-ISRO SAR Mission (NISAR) Dense Time Series: Multipolarization Object-Based Classification of Wetlands Using Two Machine Learning Algorithms. *Earth and Space Science* 8. <https://doi.org/10.1029/2021EA001742>
- Aitkenhead, M., Coull, M., 2020. Mapping soil profile depth, bulk density and carbon stock in Scotland using remote sensing and spatial covariates. *Eur J Soil Sci* 71, 553–567. <https://doi.org/https://doi.org/10.1111/ejss.12916>
- Aitkenhead, M.J., Coull, M.C., 2016. Mapping soil carbon stocks across Scotland using a neural network model. *Geoderma* 262, 187–198. <https://doi.org/10.1016/J.GEODERMA.2015.08.034>
- Alderson, D.M., Evans, M.G., Shuttleworth, E.L., Pilkington, M., Spencer, T., Walker, J., Allott, T.E.H., 2019. Trajectories of ecosystem change in restored blanket peatlands. *Science of the Total Environment*. <https://doi.org/10.1016/j.scitotenv.2019.02.095>
- Alejandro Berlanga-Robles, C., Ruiz-Luna, A., Nepita Villanueva, M.R., 2019. Seasonal trend analysis (STA) of MODIS vegetation index time series for the mangrove canopy of the Teacapan-Agua Brava lagoon system, Mexico. *GIsci Remote Sens* 56. <https://doi.org/10.1080/15481603.2018.1533679>
- Allott, T.E.H., Evans, M.G., Lindsay, J., Agnew, C.T., Freer, J.E., Jones, A., Parnell, M., 2009. Water Tables in Peak District Blanket Peatlands Moors for the Future Report No 17. Moors for the Future report No 17.
- Alshammari, L., Boyd, D.S., Sowter, A., Marshall, C., Andersen, R., Gilbert, P., Marsh, S., Large, D.J., 2020. Use of Surface Motion Characteristics Determined by InSAR to Assess Peatland Condition. *J Geophys Res Biogeosci*. <https://doi.org/10.1029/2018JG004953>
- Alshammari, L., Large, D.J., Boyd, D.S., Sowter, A., Anderson, R., Andersen, R., Marsh, S., 2018. Long-term peatland condition assessment via surface motion monitoring using the ISBAS DInSAR technique over the Flow Country, Scotland. *Remote Sens (Basel)* 10. <https://doi.org/10.3390/rs10071103>
- Anderson, R., Anderson, A.R., 2010. Restoring afforested peat bogs: results of current research. *Forest Research- Research Note FCRN006*.
- Andronis, V., Karathanassi, V., Tsalapati, V., Kolokoussis, P., Miltiadou, M., Danezis, C., 2022. Time Series Analysis of Landsat Data for Investigating the Relationship between Land Surface

- Temperature and Forest Changes in Paphos Forest, Cyprus. *Remote Sens (Basel)* 14. <https://doi.org/10.3390/rs14041010>
- Aria, M., Cuccurullo, C., Gnasso, A., 2021. A comparison among interpretative proposals for Random Forests. *Machine Learning with Applications* 6, 100094. <https://doi.org/10.1016/J.MLWA.2021.100094>
- Artz, R., Faccioli, M., Roberts, M., Anderson, R., 2018. Peatland restoration – a comparative analysis of the costs and merits of different restoration methods. *ClimateXChange*.
- Artz, R.R.E., Coyle, M., Donaldson-Selby, G., Morrison, R., 2022. Net carbon dioxide emissions from an eroding Atlantic blanket bog. *Biogeochemistry* 159, 233–250. <https://doi.org/10.1007/s10533-022-00923-x>
- Artz, R.R.E., Johnson, S., Bruneau, P., Britton, A.J., Mitchell, R.J., Ross, L., Donaldson-Selby, G., Donnelly, D., Aitkenhead, M.J., Gimona, A., Poggio, L., 2019. The potential for modelling peatland habitat condition in Scotland using long-term MODIS data. *Science of the Total Environment* 660, 429–442. <https://doi.org/10.1016/j.scitotenv.2018.12.327>
- Asmuß, T., Bechtold, M., Tiemeyer, B., 2019. On the potential of Sentinel-1 for high resolution monitoring of water table dynamics in grasslands on organic soils. *Remote Sens (Basel)* 11. <https://doi.org/10.3390/rs11141659>
- Baghdadi, N., Bernier, M., Gauthier, R., Neeson, I., 2001. Evaluation of C-band SAR data for wetlands mapping. *Int J Remote Sens* 22, 71–88. <https://doi.org/10.1080/014311601750038857>
- Bai, J., Perron, P., 2003. Computation and analysis of multiple structural change models. *Journal of Applied Econometrics* 18. <https://doi.org/10.1002/jae.659>
- Bamler, R., Hartl, P., 1998. Synthetic aperture radar interferometry. *Inverse Probl* 14. <https://doi.org/10.1088/0266-5611/14/4/001>
- Barrett, B.W., Dwyer, E., Whelan, P., 2009. Soil moisture retrieval from active spaceborne microwave observations: An evaluation of current techniques. *Remote Sens (Basel)* 1. <https://doi.org/10.3390/rs1030210>
- Barthelmes, A., Couwengerg, J., Risager, M., Tegetmeyer, C., Joosten, H., 2015. Peatlands and climate in a Ramsar context. A Nordic-Baltic perspective, Nordic Council of Ministers 2015. <https://doi.org/10.3233/HSM-140817>
- Beale, J., Snapir, B., Waine, T., Evans, J., Corstanje, R., 2019. The significance of soil properties to the estimation of soil moisture from C-band synthetic aperture radar. *Hydrology and Earth System Sciences Discussions*. <https://doi.org/10.5194/hess-2019-294>

- Bechtold, M., de Lannoy, G.J.M., Reichle, R.H., Roose, D., Balliston, N., Burdun, I., Devito, K., Kurbatova, J., Munir, T.M., Zarov, E.A., 2020. Improved Groundwater Table and L-band Brightness Temperature Estimates for Northern Hemisphere Peatlands Using New Model Physics and SMOS Observations in a Global Data Assimilation Framework. in review, *Remote Sensing of Environment*, RSE-D-19-0 246, 111805. <https://doi.org/10.1016/j.rse.2020.111805>
- Bechtold, M., Schlaffer, S., Tiemeyer, B., Lannoy, G. De, 2018. Inferring water table depth dynamics from ENVISAT-ASAR C-band backscatter over a range of peatlands from deeply-drained to natural conditions. *Remote Sens (Basel)* 10. <https://doi.org/10.3390/rs10040536>
- Belward, A.S., Skøien, J.O., 2015. Who launched what, when and why; trends in global land-cover observation capacity from civilian earth observation satellites. *ISPRS Journal of Photogrammetry and Remote Sensing* 103, 115–128. <https://doi.org/10.1016/J.ISPRSJPRS.2014.03.009>
- Belyea, L.R., Clymo, R.S., 2001. Feedback control of the rate of peat formation. *Proceedings of the Royal Society B: Biological Sciences* 268. <https://doi.org/10.1098/rspb.2001.1665>
- Benninga, H.J.F., van der Velde, R., Su, Z., 2019. Impacts of radiometric uncertainty and weather-related surface conditions on soil moisture retrievals with Sentinel-1. *Remote Sens (Basel)* 11. <https://doi.org/10.3390/rs11172025>
- Bernard, R., Martin, P.H., Thony, J.L., Vauclin, M., Vidal-Madjar, D., 1982. C-band radar for determining surface soil moisture. *Remote Sens Environ* 12. [https://doi.org/10.1016/0034-4257\(82\)90052-9](https://doi.org/10.1016/0034-4257(82)90052-9)
- Biancalani, R., Avagyan, A., 2014. Towards climate-responsible peatlands management, *Mitigation of Climate Change in Agriculture Series (MICCA)*.
- Bonn, A., Allott, T., Evans, M., Joosten, H., Stoneman, R., 2016. Peatland restoration and ecosystem services: An introduction, in: *Peatland Restoration and Ecosystem Services: Science, Policy and Practice*. <https://doi.org/10.1017/CBO9781139177788.002>
- Bonn, A., Reed, M.S., Evans, C.D., Joosten, H., Bain, C., Farmer, J., Emmer, I., Couwenberg, J., Moxey, A., Artz, R., Tanneberger, F., von Unger, M., Smyth, M.A., Birnie, D., 2014. Investing in nature: Developing ecosystem service markets for peatland restoration. *Ecosyst Serv* 9, 54–65. <https://doi.org/10.1016/j.ecoser.2014.06.011>
- Bourgault, M.A., Larocque, M., Garneau, M., 2019. How do hydrogeological setting and meteorological conditions influence water table depth and fluctuations in ombrotrophic peatlands? *J Hydrol X*. <https://doi.org/10.1016/j.hydroa.2019.100032>

- Bourgeau-Chavez, L.L., Smith, K.B., Brunzell, S.M., Kasischke, E.S., Romanowicz, E.A., Richardson, C.J., 2005. Remote monitoring of regional inundation patterns and hydroperiod in the greater everglades using synthetic aperture radar. *Wetlands*. [https://doi.org/10.1672/0277-5212\(2005\)025\[0176:RMORIP\]2.0.CO;2](https://doi.org/10.1672/0277-5212(2005)025[0176:RMORIP]2.0.CO;2)
- Bradley, A. v., Andersen, R., Marshall, C., Sowter, A., Large, D.J., 2022. Identification of typical ecohydrological behaviours using InSAR allows landscape-scale mapping of peatland condition. *Earth Surface Dynamics* 10. <https://doi.org/10.5194/esurf-10-261-2022>
- Breiman, L., 2001. Random forests. *Mach Learn* 45. <https://doi.org/10.1023/A:1010933404324>
- Buckmaster, C., Bain, S., Reed, M., 2014. Global Peatland Restoration - demonstrating success, IUCN UK National Committee Peatland Programme.
- Candra, D.S., Phinn, S., Scarth, P., 2019. Automated cloud and cloud-shadow masking for Landsat 8 using multitemporal images in a variety of environments. *Remote Sens (Basel)* 11. <https://doi.org/10.3390/rs11172060>
- Carless, D., Luscombe, D.J., Gatis, N., Anderson, K., Brazier, R.E., 2019. Mapping landscape-scale peatland degradation using airborne lidar and multispectral data. *Landsc Ecol* 34. <https://doi.org/10.1007/s10980-019-00844-5>
- Carrasco, L., O’Neil, A.W., Daniel Morton, R., Rowland, C.S., 2019. Evaluating combinations of temporally aggregated Sentinel-1, Sentinel-2 and Landsat 8 for land cover mapping with Google Earth Engine. *Remote Sens (Basel)* 11. <https://doi.org/10.3390/rs11030288>
- Chambers, F., 2003. Peatlands and environmental change, D. Charman. Publisher John Wiley and Sons Ltd, Chichester 2002 (301 pp) ISBN 0 471 96990 7 (HB) 0 471 84410 8 (PB). *J Quat Sci* 18, 466–466. <https://doi.org/10.1002/jqs.741>
- Charman, D.J., 2009. Peat and Peatlands, in: *Encyclopedia of Inland Waters*. Elsevier Inc., pp. 541–548. <https://doi.org/10.1016/B978-012370626-3.00061-2>
- Chen, N., Yu, L., Zhang, X., Shen, Y., Zeng, L., Hu, Q., Niyogi, D., 2020. Mapping paddy rice fields by combining multi-temporal vegetation index and synthetic aperture radar remote sensing data using Google Earth Engine machine learning platform. *Remote Sens (Basel)* 12. <https://doi.org/10.3390/RS12182992>
- Cheng, S., Perissin, D., Lin, H., Chen, F., 2012. Atmospheric delay analysis from GPS meteorology and InSAR APS. *J Atmos Sol Terr Phys* 86, 71–82. <https://doi.org/10.1016/J.JASTP.2012.06.005>

- Chimner, R.A., Cooper, D.J., Wurster, F.C., Rochefort, L., 2017. An overview of peatland restoration in North America: where are we after 25 years? *Restor Ecol.* <https://doi.org/10.1111/rec.12434>
- Cigna, F., Bateson, L.B., Jordan, C.J., Dashwood, C., 2014. Simulating SAR geometric distortions and predicting Persistent Scatterer densities for ERS-1/2 and ENVISAT C-band SAR and InSAR applications: Nationwide feasibility assessment to monitor the landmass of Great Britain with SAR imagery. *Remote Sens Environ* 152. <https://doi.org/10.1016/j.rse.2014.06.025>
- Claverie, M., Ju, J., Masek, J.G., Dungan, J.L., Vermote, E.F., Roger, J.C., Skakun, S. V., Justice, C., 2018. The Harmonized Landsat and Sentinel-2 surface reflectance data set. *Remote Sens Environ* 219, 145–161. <https://doi.org/10.1016/j.rse.2018.09.002>
- Cleveland, R.B., Cleveland, W.S., McRae, J.E., Terpenning, I., 1990. STL: A Seasonal-Trend Decomposition Procedure Based on Loess (with Discussion). *J Off Stat* 6.
- Connolly, J., Holden, N.M., Connolly, J., Seaquist, J.W., Ward, S.M., 2011. Detecting recent disturbance on montane blanket bogs in the wicklow mountains, Ireland using the MODIS enhanced vegetation index. *Int J Remote Sens.* <https://doi.org/10.1080/01431161003698310>
- Cordell, S., Questad, E.J., Asner, G.P., Kinney, K.M., Thaxton, J.M., Uowolo, A., Brooks, S., Chynoweth, M.W., 2017. Remote sensing for restoration planning: how the big picture can inform stakeholders. *Restor Ecol* 25. <https://doi.org/10.1111/rec.12448>
- Couwenberg, J., Thiele, A., Tanneberger, F., Augustin, J., Bärish, S., Dubovik, D., Liashchynskaya, N., Michaelis, D., Minke, M., Skuratovich, A., Joosten, H., 2011. Assessing greenhouse gas emissions from peatlands using vegetation as a proxy. *Hydrobiologia* 674. <https://doi.org/10.1007/s10750-011-0729-x>
- Czapiewski, S., Szumińska, D., 2022. An overview of remote sensing data applications in peatland research based on works from the period 2010–2021. *Land (Basel)*. <https://doi.org/10.3390/land11010024>
- Dabrowska-Zielinska, K., Budzynska, M., Tomaszewska, M., Malinska, A., Gatkowska, M., Bartold, M., Malek, I., 2016. Assessment of carbon flux and soil moisture in wetlands applying Sentinel-1 data. *Remote Sens (Basel)* 8. <https://doi.org/10.3390/rs8090756>
- D’Acunha, B., Lee, S.C., Johnson, M.S., 2018. Ecohydrological responses to rewetting of a highly impacted raised bog ecosystem. *Ecohydrology* 11. <https://doi.org/10.1002/eco.1922>
- Dettmann, U., Bechtold, M., 2016. Deriving Effective Soil Water Retention Characteristics from Shallow Water Table Fluctuations in Peatlands. *Vadose Zone Journal* 15. <https://doi.org/10.2136/vzj2016.04.0029>



- Didan, K., 2015. MOD13Q1 MODIS/Terra Vegetation Indices 16-Day L3 Global 250m SIN Grid V006. <https://doi.org/10.5067/MODIS/MOD13Q1.006>
- Dinesen, L., Hahn, P., 2019. Draft Ramsar Technical Report on peatland restoration and rewetting methodologies in Northern bogs 18–22.
- Dise, N.B., 2009. Peatland response to global change. *Science* (1979). <https://doi.org/10.1126/science.1174268>
- Dwivedi, R.S., 2017. Remote sensing of soils, *Remote Sensing of Soils*. <https://doi.org/10.1007/978-3-662-53740-4>
- Elith, J., Leathwick, J.R., Hastie, T., 2008. A working guide to boosted regression trees. *Journal of Animal Ecology*. <https://doi.org/10.1111/j.1365-2656.2008.01390.x>
- Elkington, T., Dayton, N., Jackson, D.L., Strachan, I.M., 2001. *National Vegetation Classification: Field guide to mires and heaths*, English.
- ESA, 2023a. EO portal [WWW Document]. URL <https://www.eoportal.org/satellite-missions/nisar#eop-quick-facts-section> (accessed on 27 March 2023).
- ESA, 2023b. Data products. ESA: Sentinel-1 data products [WWW Document]. URL <https://sentinel.esa.int/web/sentinel/missions/sentinel-1/data-products> (accessed on 17 August 2022).
- Evans, C.D., Peacock, M., Baird, A.J., Artz, R.R.E., Burden, A., Callaghan, N., Chapman, P.J., Cooper, H.M., Coyle, M., Craig, E., Cumming, A., Dixon, S., Gauci, V., Grayson, R.P., Helfter, C., Heppell, C.M., Holden, J., Jones, D.L., Kaduk, J., Levy, P., Matthews, R., McNamara, N.P., Misselbrook, T., Oakley, S., Page, S.E., Rayment, M., Ridley, L.M., Stanley, K.M., Williamson, J.L., Worrall, F., Morrison, R., 2021. Overriding water table control on managed peatland greenhouse gas emissions. *Nature*. <https://doi.org/10.1038/s41586-021-03523-1>
- Fassnacht, F.E., Schiller, C., Kattenborn, T., Zhao, X., Qu, J., 2019. A Landsat-based vegetation trend product of the Tibetan Plateau for the time-period 1990–2018. *Sci Data* 6. <https://doi.org/10.1038/s41597-019-0075-9>
- Fenner, N., Freeman, C., 2011. Drought-induced carbon loss in peatlands. *Nat Geosci*. <https://doi.org/10.1038/ngeo1323>
- Ferreira, K.R., Queiroz, G.R., Camara, G., Souza, R.C.M., Vinhas, L., Marujo, R.F.B., Simoes, R.E.O., Noronha, C.A.F., Costa, R.W., Arcanjo, J.S., Gomes, V.C.F., Zaglia, M.C., 2020. Using Remote Sensing Images and Cloud Services on Aws to Improve Land Use and Cover

- Monitoring, in: 2020 IEEE Latin American GRSS and ISPRS Remote Sensing Conference, LAGIRS 2020 - Proceedings. <https://doi.org/10.1109/LAGIRS48042.2020.9165649>
- Frolking, S., Roulet, N.T., 2007. Holocene radiative forcing impact of northern peatland carbon accumulation and methane emissions. *Glob Chang Biol* 13, 1079–1088. <https://doi.org/10.1111/j.1365-2486.2007.01339.x>
- Funkenberg, T., Binh, T.T., Moder, F., Dech, S., 2014. The Ha Tien Plain - wetland monitoring using remote-sensing techniques. *Int J Remote Sens*. <https://doi.org/10.1080/01431161.2014.890306>
- Gaffney, P.P.J., Hancock, M.H., Taggart, M.A., Andersen, R., 2022. Restoration of afforested peatland: Effects on pore- and surface-water quality in relation to differing harvesting methods. *Ecol Eng* 177, 106567. <https://doi.org/10.1016/J.ECOLENG.2022.106567>
- Gallego-Sala, A. V., Colin Prentice, I., 2013. Blanket peat biome endangered by climate change. *Nat Clim Chang* 3, 152–155. <https://doi.org/10.1038/nclimate1672>
- Gao, B.C., 1996. NDWI—A normalized difference water index for remote sensing of vegetation liquid water from space. *Remote Sens Environ* 58, 257–266. [https://doi.org/10.1016/S0034-4257\(96\)00067-3](https://doi.org/10.1016/S0034-4257(96)00067-3)
- Gao, F., Masek, J., Schwaller, M., Hall, F., 2006. On the blending of the Landsat and MODIS surface reflectance: predicting daily Landsat surface reflectance. *IEEE Transactions on Geoscience and Remote Sensing* 44, 2207–2218. <https://doi.org/10.1109/TGRS.2006.872081>
- Gatis, N., Anderson, K., Grand-Clement, E., Luscombe, D.J., Hartley, I.P., Smith, D., Brazier, R.E., 2017. Evaluating MODIS vegetation products using digital images for quantifying local peatland CO<sub>2</sub> gas fluxes. *Remote Sens Ecol Conserv* 3. <https://doi.org/10.1002/rse2.45>
- Gaveau, D.L.A., Salim, M.A., Hergoualc'H, K., Locatelli, B., Sloan, S., Wooster, M., Marlier, M.E., Molidena, E., Yaen, H., DeFries, R., Verchot, L., Murdiyarso, D., Nasi, R., Holmgren, P., Sheil, D., 2014. Major atmospheric emissions from peat fires in Southeast Asia during non-drought years: Evidence from the 2013 Sumatran fires. *Sci Rep* 4. <https://doi.org/10.1038/srep06112>
- GEE, 2023a. GEE Platform [WWW Document]. URL <https://earthengine.google.com/platform/> (accessed on 28 March 2023).
- GEE, 2023b. GEE Guide. GEE Guide: Sentinel-1 Algorithms [WWW Document]. URL <https://developers.google.com/earth-engine/guides/sentinel1> (accessed on 5 August 2022).
- Gewin, V., 2020. How peat could protect the planet. *Nature*. <https://doi.org/10.1038/d41586-020-00355-3>

- Gorham, E., 1991. Northern peatlands: role in the carbon cycle and probable responses to climatic warming. *Ecological Applications* 1, 182–195. <https://doi.org/10.2307/1941811>
- Grand-Clement, E., Anderson, K., Smith, D., Luscombe, D., Gatis, N., Ross, M., Brazier, R.E., 2013. Evaluating ecosystem goods and services after restoration of marginal upland peatlands in South-West England. *Journal of Applied Ecology*. <https://doi.org/10.1111/1365-2664.12039>
- Gu, Y., Hunt, E., Wardlow, B., Basara, J.B., Brown, J.F., Verdin, J.P., 2008. Evaluation of MODIS NDVI and NDWI for vegetation drought monitoring using Oklahoma Mesonet soil moisture data. *Geophys Res Lett* 35. <https://doi.org/10.1029/2008GL035772>
- Guo, M., Li, J., He, H., Xu, J., Jin, Y., 2018. Detecting Global Vegetation Changes Using Mann-Kendal (MK) Trend Test for 1982–2015 Time Period. *Chin Geogr Sci* 28. <https://doi.org/10.1007/s11769-018-1002-2>
- Guo, M., Li, J., Sheng, C., Xu, J., Wu, L., 2017. A review of wetland remote sensing. *Sensors (Switzerland)*. <https://doi.org/10.3390/s17040777>
- Hajnsek, I., Pottier, E., Cloude, S.R., 2003. Inversion of surface parameters from polarimetric SAR. *IEEE Transactions on Geoscience and Remote Sensing* 41. <https://doi.org/10.1109/TGRS.2003.810702>
- Hancock, M.H., Cowie, N.R., Field, R., 2013. The science of peatland restoration. No. 12 53, 1689–1699. <https://doi.org/10.1017/CBO9781107415324.004>
- Hancock, M.H., Klein, D., Andersen, R., Cowie, N.R., 2018. Vegetation response to restoration management of a blanket bog damaged by drainage and afforestation. *Appl Veg Sci* 21. <https://doi.org/10.1111/avsc.12367>
- Harris, A., 2008. Spectral reflectance and photosynthetic properties of Sphagnum mosses exposed to progressive drought. *Ecohydrology* 1, 35–42. <https://doi.org/10.1002/eco.5>
- Harris, A., Bryant, R.G., 2009. A multi-scale remote sensing approach for monitoring northern peatland hydrology: Present possibilities and future challenges. *J Environ Manage* 90, 2178–2188. <https://doi.org/10.1016/j.jenvman.2007.06.025>
- Harris, L.I., Richardson, K., Bona, K.A., Davidson, S.J., Finkelstein, S.A., Garneau, M., McLaughlin, J., Nwaishi, F., Olefeldt, D., Packalen, M., Roulet, N.T., Southee, F.M., Strack, M., Webster, K.L., Wilkinson, S.L., Ray, J.C., 2022. The essential carbon service provided by northern peatlands. *Front Ecol Environ*. <https://doi.org/10.1002/fee.2437>

- Hidayat, H., Hoekman, D.H., Vissers, M.A.M., Hoitink, A.J.F., 2012. Flood occurrence mapping of the middle Mahakam lowland area using satellite radar. *Hydrol Earth Syst Sci* 16. <https://doi.org/10.5194/hess-16-1805-2012>
- Hilbert, D.W., Roulet, N., Moore, T., 2000. Modelling and analysis of peatlands as dynamical systems. *Journal of Ecology* 88, 230–242. <https://doi.org/10.1046/j.1365-2745.2000.00438.x>
- Hird, J.N., DeLancey, E.R., McDermid, G.J., Kariyeva, J., 2017. Google Earth Engine, Open-Access Satellite Data, and Machine Learning in Support of Large-Area Probabilistic Wetland Mapping. *Remote Sens (Basel)* 9. <https://doi.org/10.3390/rs9121315>
- Holden, J., Burt, T.P., 2002. Piping and pipeflow in a deep peat catchment. *Catena (Amst)* 48. [https://doi.org/10.1016/S0341-8162\(01\)00189-8](https://doi.org/10.1016/S0341-8162(01)00189-8)
- Holden, J., Wallage, Z.E., Lane, S.N., McDonald, A.T., 2011. Water table dynamics in undisturbed, drained and restored blanket peat. *J Hydrol (Amst)* 402, 103–114. <https://doi.org/10.1016/J.JHYDROL.2011.03.010>
- Howie, S.A., Hebda, R.J., 2018. Bog surface oscillation (mire breathing): A useful measure in raised bog restoration. *Hydrol Process* 32. <https://doi.org/10.1002/hyp.11622>
- Humpenöder, F., Karstens, K., Lotze-Campen, H., Leifeld, J., Menichetti, L., Barthelmes, A., Popp, A., 2020. Peatland protection and restoration are key for climate change mitigation. *Environmental Research Letters* 15. <https://doi.org/10.1088/1748-9326/abae2a>
- Iizuka, K., Watanabe, K., Kato, T., Putri, N.A., Silsigia, S., Kameoka, T., Kozan, O., 2018. Visualizing the spatiotemporal trends of thermal characteristics in a peatland plantation forest in Indonesia: Pilot test using unmanned aerial systems (UASs). *Remote Sens (Basel)* 10. <https://doi.org/10.3390/rs10091345>
- Isokangas, E., Rossi, P.M., Ronkanen, A.K., Marttila, H., Rozanski, K., Kløve, B., 2017. Quantifying spatial groundwater dependence in peatlands through a distributed isotope mass balance approach. *Water Resour Res* 53. <https://doi.org/10.1002/2016WR019661>
- Jacome, A., Bernier, M., Chokmani, K., Gauthier, Y., Poulin, J., Sève, D. De, 2013. Monitoring volumetric surface soil moisture content at the La Grande basin boreal wetland by radar multi polarization data. *Remote Sens (Basel)* 5. <https://doi.org/10.3390/rs5104919>
- Jaiswal, R.K., Lohani, A.K., Tiwari, H.L., 2015. Statistical Analysis for Change Detection and Trend Assessment in Climatological Parameters. *Environmental Processes* 2. <https://doi.org/10.1007/s40710-015-0105-3>

- Joint Nature Conservation Committee, 2011. UK Biodiversity Action Plan; Priority Habitat Descriptions. JNCC Research Report.
- Joosten, H., Tapio-Biström, M.-L., Tol, S., 2012. Peatlands - guidance for climate change mitigation through conservation, rehabilitation and sustainable use, Mitigation of Climate Change in Agriculture (MICCA) Programme series 5.
- Junttila, S., Kelly, J., Kljun, N., Aurela, M., Klemedtsson, L., Lohila, A., Nilsson, M.B., Rinne, J., Tuittila, E.S., Vestin, P., Weslien, P., Eklundh, L., 2021. Upscaling northern peatland co<sub>2</sub> fluxes using satellite remote sensing data. *Remote Sens (Basel)* 13. <https://doi.org/10.3390/rs13040818>
- Kalacska, M., Arroyo-Mora, J.P., Soffer, R.J., Roulet, N.T., Moore, T.R., Humphreys, E., Leblanc, G., Lucanus, O., Inamdar, D., 2018. Estimating Peatland water table depth and net ecosystem exchange: A comparison between satellite and airborne imagery. *Remote Sens (Basel)* 10. <https://doi.org/10.3390/rs10050687>
- Kasischke, Eric S, Bourgeau-Chavez, L.L., Rober, A.R., Wyatt, K.H., Waddington, J.M., Turetsky, M.R., 2009. Effects of soil moisture and water depth on ERS SAR backscatter measurements from an Alaskan wetland complex. *Remote Sens Environ* 113. <https://doi.org/10.1016/j.rse.2009.04.006>
- Kasischke, E.S., Melack, J.M., Dobson, M.C., 1997. The use of imaging radars for ecological applications - A review. *Remote Sens Environ.* [https://doi.org/10.1016/S0034-4257\(96\)00148-4](https://doi.org/10.1016/S0034-4257(96)00148-4)
- Kim, J.W., Lu, Z., Gutenberg, L., Zhu, Z., 2017. Characterizing hydrologic changes of the Great Dismal Swamp using SAR/InSAR. *Remote Sens Environ* 198, 187–202. <https://doi.org/10.1016/j.rse.2017.06.009>
- Kimmel, K., Mander, Ü., 2010. Ecosystem services of peatlands: Implications for restoration. *Prog Phys Geogr* 34. <https://doi.org/10.1177/0309133310365595>
- Klinke, R., Kuechly, H., Frick, A., Förster, · Michael, Schmidt, · Tobias, Holtgrave, A.-K., Kleinschmit, B., Spengler, · Daniel, Neumann, · Carsten, 2018. Indicator-Based Soil Moisture Monitoring of Wetlands by Utilizing Sentinel and Landsat Remote Sensing Data. *PFG-Journal of Photogrammetry, Remote Sensing and Geoinformation Science* 86, 71–84. <https://doi.org/10.1007/s41064-018-0044-5>
- Koch, J., Elsgaard, L., Greve, M.H., Gyldenkerne, S., Hermansen, C., Levin, G., Wu, S., Stisen, S., 2023. Water table driven greenhouse gas emission estimate guides peatland restoration at national scale. *Biogeosciences Discussions* 2023, 1–28. <https://doi.org/10.5194/bg-2023-23>

- Kovács, G.M., Horion, S., Fensholt, R., 2022. Characterizing ecosystem change in wetlands using dense earth observation time series. *Remote Sens Environ* 281, 113267.  
<https://doi.org/10.1016/J.RSE.2022.113267>
- Kross, A., Seaquist, J.W., Roulet, N.T., Fernandes, R., Sonnentag, O., 2013. Estimating carbon dioxide exchange rates at contrasting northern peatlands using MODIS satellite data. *Remote Sens Environ* 137. <https://doi.org/10.1016/j.rse.2013.06.014>
- Küttim, M., Küttim, L., Ilomets, M., Laine, A.M., 2020. Controls of Sphagnum growth and the role of winter. *Ecol Res* 35. <https://doi.org/10.1111/1440-1703.12074>
- Lachance, D., Lavoie, C., Desrochers, A., 2005. The impact of peatland afforestation on plant and bird diversity in southeastern Québec. *Ecoscience* 12. <https://doi.org/10.2980/11195-6860-12-2-161.1>
- Lee, H., Yuan, T., Yu, H., Jung, H.C., 2020. Interferometric SAR for Wetland Hydrology: An Overview of Methods, Challenges, and Trends. *IEEE Geosci Remote Sens Mag.*  
<https://doi.org/10.1109/MGRS.2019.2958653>
- Lees, K. J., Artz, R.R.E., Chandler, D., Aspinall, T., Boulton, C.A., Buxton, J., Cowie, N.R., Lenton, T.M., 2021. Using remote sensing to assess peatland resilience by estimating soil surface moisture and drought recovery. *Science of The Total Environment* 761, 143312.  
<https://doi.org/10.1016/J.SCITOTENV.2020.143312>
- Lees, K.J., Clark, J.M., Quaife, T., Khomik, M., Artz, R.R.E., 2019. Changes in carbon flux and spectral reflectance of Sphagnum mosses as a result of simulated drought. *Ecohydrology* 12.  
<https://doi.org/10.1002/eco.2123>
- Lees, Kirsten J, Khomik, M., Quaife, T., Clark, J.M., Hill, T., Klein, D., Ritson, J., Artz, R.R.E., 2021. Assessing the reliability of peatland GPP measurements by remote sensing: From plot to landscape scale. *Science of the Total Environment* 766, 142613.  
<https://doi.org/10.1016/j.scitotenv.2020.142613>
- Lees, K.J., Lees, K.J., Artz, R.R.E., Khomik, M., Clark, J.M., Ritson, J., Hancock, M.H., Cowie, N.R., Quaife, T., 2020. Using spectral indices to estimate water content and GPP in sphagnum moss and other peatland vegetation. *IEEE Transactions on Geoscience and Remote Sensing* 58.  
<https://doi.org/10.1109/TGRS.2019.2961479>
- Lees, K J, Quaife, T., Artz, R.R.E., Khomik, M., Clark, J.M., 2018. Potential for using remote sensing to estimate carbon fluxes across northern peatlands – A review. *Science of the Total Environment* 615, 857–874. <https://doi.org/10.1016/j.scitotenv.2017.09.103>

- Leifeld, J., Menichetti, L., 2018. The underappreciated potential of peatlands in global climate change mitigation strategies /704/47/4113 /704/106/47 article. *Nat Commun.*  
<https://doi.org/10.1038/s41467-018-03406-6>
- Leifeld, J., Wüst-Galley, C., Page, S., 2019. Intact and managed peatland soils as a source and sink of GHGs from 1850 to 2100. *Nat Clim Chang.* <https://doi.org/10.1038/s41558-019-0615-5>
- Levy, P.E., Gray, A., 2015. Greenhouse gas balance of a semi-natural peatbog in northern Scotland. *Environmental Research Letters* 10. <https://doi.org/10.1088/1748-9326/10/9/094019>
- Liaw, A., Wiener, M., 2002. Classification and Regression by randomForest. *R News* 2.
- Limpens, J., Berendse, F., Blodau, C., Canadell, J.G., Freeman, C., Holden, J., Roulet, N., Rydin, H., Schaepman-Strub, G., 2008. Peatlands and the carbon cycle: From local processes to global implications - A synthesis. *Biogeosciences* 5, 1475–1491. <https://doi.org/10.5194/bg-5-1475-2008>
- Lindsay, R., Birnie, R., Cough, J., 2014. Peat bog ecosystems: structure, form, state and condition. IUCN UK Committee Peatland Programme Briefing Note No. 2 7.
- Lindsay, R.A., Charman, D.J., Everingham, F., Reilly, R.M.O., Palmer, M.A., Rowell, T.A., Stroud, D.A., Ratcliffe, D.A., Oswald, P.H., O'Reilly, R.M., Palmer, M.A., Rowell, T.A., Stroud, D.A., 1988. Part I Peatland Ecology. *The Flow Country - The peatlands of Caithness and Sutherland.*
- Liu, P., 2015. A survey of remote-sensing big data. *Front Environ Sci.*  
<https://doi.org/10.3389/fenvs.2015.00045>
- Liu, Y., Heuvelink, G.B.M., Bai, Z., He, P., 2023. Uncertainty quantification of nitrogen use efficiency prediction in China using Monte Carlo simulation and quantile regression forests. *Comput Electron Agric* 204. <https://doi.org/10.1016/j.compag.2022.107533>
- Long, X., Li, X., Lin, H., Zhang, M., 2021. Mapping the vegetation distribution and dynamics of a wetland using adaptive-stacking and Google Earth Engine based on multi-source remote sensing data. *International Journal of Applied Earth Observation and Geoinformation* 102.  
<https://doi.org/10.1016/j.jag.2021.102453>
- Lucchese, M., Waddington, J.M., Poulin, M., Pouliot, R., Rochefort, L., Strack, M., 2010. Organic matter accumulation in a restored peatland: Evaluating restoration success. *Ecol Eng* 36, 482–488. <https://doi.org/10.1016/J.ECOLENG.2009.11.017>
- Luscombe, D.J., Anderson, K., Gatis, N., Grand-Clement, E., Brazier, R.E., 2015. Using airborne thermal imaging data to measure near-surface hydrology in upland ecosystems. *Hydrol Process* 29. <https://doi.org/10.1002/hyp.10285>

- Maliva, R., Missimer, T., 2012. Remote Sensing, in: Environmental Science and Engineering. Springer Science and Business Media Deutschland GmbH, pp. 435–456.  
[https://doi.org/10.1007/978-3-642-29104-3\\_18](https://doi.org/10.1007/978-3-642-29104-3_18)
- Marshall, C., Sterk, H.P., Gilbert, P.J., Andersen, R., Bradley, A. V., Sowter, A., Marsh, S., Large, D.J., 2022. Multiscale Variability and the Comparison of Ground and Satellite Radar Based Measures of Peatland Surface Motion for Peatland Monitoring. *Remote Sens (Basel)* 14.  
<https://doi.org/10.3390/rs14020336>
- Martin-Ortega, J., Allott, T.E.H., Glenk, K., Schaafsma, M., 2014. Valuing water quality improvements from peatland restoration: Evidence and challenges. *Ecosyst Serv* 9.  
<https://doi.org/10.1016/j.ecoser.2014.06.00>
- Masiliūnas, D., Tsendbazar, N.E., Herold, M., Verbesselt, J., 2021. Bfast lite: A lightweight break detection method for time series analysis. *Remote Sens (Basel)* 13.  
<https://doi.org/10.3390/rs13163308>
- Maslanka, W., Morrison, K., White, K., Verhoef, A., Clark, J., 2022. Retrieval of Sub-Kilometric Relative Surface Soil Moisture With Sentinel-1 Utilizing Different Backscatter Normalization Factors. *IEEE Transactions on Geoscience and Remote Sensing* 60.  
<https://doi.org/10.1109/TGRS.2022.3175256>
- Mc Nairn, H., Boisvert, J.B., Major, D.J., Gwyn, Q.H.J., Brown, R.J., Smith, A.M., 1996. Identification of agricultural tillage practices from C-band radar backscatter. *Canadian Journal of Remote Sensing* 22. <https://doi.org/10.1080/07038992.1996.10874649>
- Mccarter, C.P.R., Price, J.S., 2014. Ecohydrology of Sphagnum moss hummocks: Mechanisms of capitula water supply and simulated effects of evaporation. *Ecohydrology* 7.  
<https://doi.org/10.1002/eco.1313>
- McFeeters, S.K., 1996. The use of the Normalized Difference Water Index (NDWI) in the delineation of open water features. *Int J Remote Sens* 17. <https://doi.org/10.1080/01431169608948714>
- McMullen, A., 2002. Peatlands and environmental change. *Land use policy* 19, 336–337.  
[https://doi.org/10.1016/s0264-8377\(02\)00047-9](https://doi.org/10.1016/s0264-8377(02)00047-9)
- McPartland, M.Y., Falkowski, M.J., Reinhardt, J.R., Kane, E.S., Kolka, R., Turetsky, M.R., Douglas, T.A., Anderson, J., Edwards, J.D., Palik, B., Montgomery, R.A., 2019. Characterizing boreal peatland plant composition and species diversity with hyperspectral remote sensing. *Remote Sens (Basel)* 11. <https://doi.org/10.3390/rs11141685>



- Meingast, Karl M, Falkowski, M.J., Kane, E.S., Potvin, L.R., Benscoter, B.W., Smith, A.M.S., Bourgeau-Chavez, L.L., Miller, M.E., 2014. Spectral detection of near-surface moisture content and water-table position in northern peatland ecosystems. *Remote Sens Environ* 152. <https://doi.org/10.1016/j.rse.2014.07.014>
- Meinshausen, N., 2006. Quantile regression forests. *Journal of Machine Learning Research* 7, 983–999.
- Militino, A.F., Moradi, M., Ugarte, M.D., 2020. On the performances of trend and change-point detection methods for remote sensing data. *Remote Sens (Basel)* 12. <https://doi.org/10.3390/rs12061008>
- Millard, K., Richardson, M., 2018. Quantifying the relative contributions of vegetation and soil moisture conditions to polarimetric C-Band SAR response in a temperate peatland. *Remote Sens Environ* 206. <https://doi.org/10.1016/j.rse.2017.12.011>
- Millard, K., Thompson, D.K., Parisien, M.A., Richardson, M., 2018. Soil moisture monitoring in a temperate peatland using multi-sensor remote sensing and linear mixed effects. *Remote Sens (Basel)* 10. <https://doi.org/10.3390/rs10060903>
- Minasny, B., Berglund, Ö., Connolly, J., Hedley, C., de Vries, F., Gimona, A., Kempen, B., Kidd, D., Lilja, H., Malone, B., McBratney, A., Roudier, P., O'Rourke, S., Rudiyanto, Padarian, J., Poggio, L., ten Caten, A., Thompson, D., Tuve, C., Widyatmanti, W., 2019. Digital mapping of peatlands – A critical review. *Earth Sci Rev*. <https://doi.org/10.1016/j.earscirev.2019.05.014>
- Minayeva, T.Y., Bragg, O.M., Sirin, A.A., 2017. Towards ecosystem-based restoration of peatland biodiversity. *Mires and Peat* 19. <https://doi.org/10.19189/MaP.2013.OMB.150>
- Monteverde, S., Healy, M.G., O'Leary, D., Daly, E., Callery, O., 2022. Management and rehabilitation of peatlands: The role of water chemistry, hydrology, policy, and emerging monitoring methods to ensure informed decision making. *Ecol Inform*. <https://doi.org/10.1016/j.ecoinf.2022.101638>
- Moore, P.A., Lukenbach, M.C., Thompson, D.K., Kettridge, N., Granath, G., Waddington, J.M., 2019. Assessing the peatland hummock-hollow classification framework using high-resolution elevation models: Implications for appropriate complexity ecosystem modeling. *Biogeosciences* 16. <https://doi.org/10.5194/bg-16-3491-2019>
- Moore, P.D., 1989. The ecology of peat-forming processes: a review. *Int J Coal Geol* 12, 89–103. [https://doi.org/10.1016/0166-5162\(89\)90048-7](https://doi.org/10.1016/0166-5162(89)90048-7)

- Moore, T.R., Bubier, J.L., Frolking, S.E., Lafleur, P.M., Roulet, N.T., 2002. Plant biomass and production and CO<sub>2</sub> exchange in an ombrotrophic bog. *Journal of Ecology* 90, 25–36. <https://doi.org/10.1046/j.0022-0477.2001.00633.x>
- Morrison, K., 2013. Mapping subsurface archaeology with SAR. *Archaeol Prospect* 20. <https://doi.org/10.1002/arp.1445>
- Morrison, K., Bennett, J., 2014. Tomographic profiling - A technique for multi-incidence-angle retrieval of the vertical sar backscattering profiles of biogeophysical targets. *IEEE Transactions on Geoscience and Remote Sensing* 52, 1250–1255. <https://doi.org/10.1109/TGRS.2013.2250508>
- Morrison, K., Bennett, J., Solberg, S., 2013. Ground-based C-band tomographic profiling of a conifer forest stand. *Int J Remote Sens.* <https://doi.org/10.1080/01431161.2013.826836>
- Morrison, K., Rott, H., Nagler, T., Prats, P., Rebhan, H., Wursteisen, P., 2008. PolinSAR signatures of alpine snow, in: *Proceedings of the European Conference on Synthetic Aperture Radar, EUSAR*.
- Morrison, K., Wagner, W., 2020. Explaining Anomalies in SAR and Scatterometer Soil Moisture Retrievals from Dry Soils with Subsurface Scattering. *IEEE Transactions on Geoscience and Remote Sensing* 58. <https://doi.org/10.1109/TGRS.2019.2954771>
- Morton, Phoebe A, Heinemeyer, A., 2019. Bog breathing: the extent of peat shrinkage and expansion on blanket bogs in relation to water table, heather management and dominant vegetation and its implications for carbon stock assessments. *Wetl Ecol Manag* 27, 467–482. <https://doi.org/10.1007/s11273-019-09672-5>
- Moxey, A., Moran, D., 2014. UK peatland restoration: Some economic arithmetic. *Science of The Total Environment* 484, 114–120. <https://doi.org/10.1016/J.SCITOTENV.2014.03.033>
- Najafi, Z., Fatehi, P., Darvishsefat, A.A., 2019. Vegetation dynamics trend using satellite time series imagery, in: *International Archives of the Photogrammetry, Remote Sensing and Spatial Information Sciences - ISPRS Archives*. <https://doi.org/10.5194/isprs-archives-XLII-4-W18-783-2019>
- NatureScot, 2023. Condition Monitoring programme [WWW Document]. URL <https://www.nature.scot/professional-advice/protected-areas-and-species/protected-areas/site-condition-monitoring/how-we-monitor-features> (accessed on 31 March 2023).

- NatureScot, 2020. Peatland ACTION Project [WWW Document]. NatureScot. URL <https://www.nature.scot/climate-change/nature-based-solutions/peatland-action-project> (accessed on 1 May 2023).
- Niu, B., Zhang, Z., Yu, X., Li, X., Wang, Z., Loaíciga, H.A., Peng, S., 2020. Regime shift of the hydroclimate-vegetation system in the Yellow River Delta of China from 1982 through 2015. *Environmental Research Letters*. <https://doi.org/10.1088/1748-9326/ab6561>
- Njoku, E.G., Jackson, T.J., Lakshmi, V., Chan, T.K., Nghiem, S. V., 2003. Soil moisture retrieval from AMSR-E. *IEEE Transactions on Geoscience and Remote Sensing*. <https://doi.org/10.1109/TGRS.2002.808243>
- Noble, A., Palmer, S.M., Glaves, D.J., Crowle, A., Holden, J., 2017. Impacts of peat bulk density, ash deposition and rainwater chemistry on establishment of peatland mosses. *Plant Soil* 419, 41–52. <https://doi.org/10.1007/s11104-017-3325-7>
- Norris, G., Catherine, C., Gillen, C., Johnston, S., 2016. Buglife - The Invertebrate Conservation Trust : LIFE13 BIO / UK / 000428 LIFE13 BIO / UK / 000428 Fannyside Muir : Baseline Ecology Report. <https://doi.org/10.13140/RG.2.1.1266.5845>
- Notarnicola, C., Solorz, R., 2014. Integration of Remotely Sensed Images and Electromagnetic Models into a Bayesian Approach for Soil Moisture Content Retrieval: Methodology and Effect of Prior Information. *Dynamic Programming and Bayesian Inference, Concepts and Applications*. <https://doi.org/10.5772/57562>
- Nungesser, M.K., 2003. Modelling microtopography in boreal peatlands: Hummocks and hollows. *Ecol Modell* 165, 175–207. [https://doi.org/10.1016/S0304-3800\(03\)00067-X](https://doi.org/10.1016/S0304-3800(03)00067-X)
- Nusantara, R.W., Hazriani, R., Suryadi, U.E., 2018. Water-table Depth and Peat Subsidence Due to Land-use Change of Peatlands, in: *IOP Conference Series: Earth and Environmental Science*. <https://doi.org/10.1088/1755-1315/145/1/012090>
- Oliphant, A.J., Thenkabail, P.S., Teluguntla, P., Xiong, J., Gumma, M.K., Congalton, R.G., Yadav, K., 2019. Mapping cropland extent of Southeast and Northeast Asia using multi-year time-series Landsat 30-m data using a random forest classifier on the Google Earth Engine Cloud. *International Journal of Applied Earth Observation and Geoinformation* 81, 110–124. <https://doi.org/10.1016/J.JAG.2018.11.014>
- Owe, M., de Jeu, R., Holmes, T., 2008. Multisensor historical climatology of satellite-derived global land surface moisture. *J Geophys Res Earth Surf* 113. <https://doi.org/10.1029/2007JF000769>

- Packalen, M.S., Finkelstein, S.A., McLaughlin, J.W., 2016. Climate and peat type in relation to spatial variation of the peatland carbon mass in the Hudson Bay Lowlands, Canada. *J Geophys Res Biogeosci* 121. <https://doi.org/10.1002/2015JG002938>
- Page, S.E., Baird, A.J., 2016. Peatlands and Global Change: Response and Resilience. *Annu Rev Environ Resour* 41. <https://doi.org/10.1146/annurev-environ-110615-085520>
- Pang, Y., Huang, Y., He, L., Zhou, Y., Sui, J., Xu, J., 2021. Remote sensing phenology of two Chinese northern Sphagnum bogs under climate drivers during 2001 and 2018. *Ecol Indic* 129. <https://doi.org/10.1016/j.ecolind.2021.107968>
- Pang, Y., Huang, Y., Zhou, Y., Xu, J., Wu, Y., 2020. Identifying spectral features of characteristics of sphagnum to assess the remote sensing potential of peatlands: A case study in China. *Mires and Peat* 26, 1–19. <https://doi.org/10.19189/MaP.2019.OMB.StA.1834>
- Park, T., Ganguly, S., Tømmervik, H., Euskirchen, E.S., Høgda, K.A., Karlsen, S.R., Brovkin, V., Nemani, R.R., Myneni, R.B., 2016. Changes in growing season duration and productivity of northern vegetation inferred from long-term remote sensing data. *Environmental Research Letters* 11. <https://doi.org/10.1088/1748-9326/11/8/084001>
- Pastick, N.J., Wylie, B.K., Wu, Z., 2018. Spatiotemporal Analysis of Landsat-8 and Sentinel-2 Data to Support Monitoring of Dryland Ecosystems. *Remote Sens (Basel)* 10. <https://doi.org/10.3390/rs10050791>
- Pereira, D., Mendes, C., Dias, E., 2022. The potential of peatlands in global climate change mitigation: a case study of Terceira and Flores Islands (Azores, Portugal) hydrologic services. *SN Appl Sci* 4, 184. <https://doi.org/10.1007/s42452-022-05066-0>
- Petropoulos, G.P., Srivastava, P.K., 2016. Sensitivity Analysis in Earth Observation Modelling, Sensitivity Analysis in Earth Observation Modelling. <https://doi.org/10.1016/c2014-0-03609-x>
- Pettitt, A.N., 1979. A Non-Parametric Approach to the Change-Point Problem. *Appl Stat* 28. <https://doi.org/10.2307/2346729>
- Poggio, L., Gimona, A., Brown, I., 2012. Spatio-temporal MODIS EVI gap filling under cloud cover: An example in Scotland. *ISPRS Journal of Photogrammetry and Remote Sensing*. <https://doi.org/10.1016/j.isprsjprs.2012.06.003>
- Price, J., 1997. Soil moisture, water tension, and water table relationships in a managed cutover bog. *J Hydrol (Amst)* 202. [https://doi.org/10.1016/S0022-1694\(97\)00037-1](https://doi.org/10.1016/S0022-1694(97)00037-1)
- Prince, S.D., Goward, S.N., 1995. Global Primary Production: A Remote Sensing Approach. *J Biogeogr* 22, 815. <https://doi.org/10.2307/2845983>

- Qu, Y., Zhao, W., Yuan, Z., Chen, J., 2020. Crop mapping from Sentinel-1 polarimetric time-series with a deep neural network. *Remote Sens (Basel)* 12. <https://doi.org/10.3390/RS12152493>
- Quaife, T., Pinnington, E.M., Marzahn, P., Kaminski, T., Vossbeck, M., Timmermans, J., Isola, C., Rommen, B., Loew, A., 2022. Synergistic retrievals of leaf area index and soil moisture from Sentinel-1 and Sentinel-2. *Int J Image Data Fusion* 1–18. <https://doi.org/10.1080/19479832.2022.2149629>
- R Core Team, 2021. R core team (2021). R: A language and environment for statistical computing. R Foundation for Statistical Computing, Vienna, Austria. URL <http://www.R-project.org>.
- Ramchunder, S.J., Brown, L.E., Holden, J., 2012. Catchment-scale peatland restoration benefits stream ecosystem biodiversity. *Journal of Applied Ecology* 49, 182–191. <https://doi.org/10.1111/j.1365-2664.2011.02075.x>
- Ramsar Convention on Wetlands., 2018. Global Wetland Outlook: State of the World's Wetlands and their Services to People. Ramsar Convention on Wetlands. (2018). 88.
- Räsänen, A., Aurela, M., Juutinen, S., Kumpula, T., Lohila, A., Penttilä, T., Virtanen, T., 2020. Detecting northern peatland vegetation patterns at ultra-high spatial resolution. *Remote Sens Ecol Conserv* 6. <https://doi.org/10.1002/rse2.140>
- Räsänen, A., Tolvanen, A., Kareksela, S., 2022. Monitoring peatland water table depth with optical and radar satellite imagery. *International Journal of Applied Earth Observation and Geoinformation* 112, 102866. <https://doi.org/10.1016/J.JAG.2022.102866>
- Reichstein, M., Falge, E., Baldocchi, D., Papale, D., Aubinet, M., Berbigier, P., Bernhofer, C., Buchmann, N., Gilmanov, T., Granier, A., Grünwald, T., Havránková, K., Ilvesniemi, H., Janous, D., Knohl, A., Laurila, T., Lohila, A., Loustau, D., Matteucci, G., Meyers, T., Miglietta, F., Ourcival, J.M., Pumpanen, J., Rambal, S., Rotenberg, E., Sanz, M., Tenhunen, J., Seufert, G., Vaccari, F., Vesala, T., Yakir, D., Valentini, R., 2005. On the separation of net ecosystem exchange into assimilation and ecosystem respiration: Review and improved algorithm. *Glob Chang Biol*. <https://doi.org/10.1111/j.1365-2486.2005.001002.x>
- Ritson, J.P., Bell, M., Brazier, R.E., Grand-Clement, E., Graham, N.J.D., Freeman, C., Smith, D., Templeton, M.R., Clark, J.M., 2016. Managing peatland vegetation for drinking water treatment. *Sci Rep* 6. <https://doi.org/10.1038/srep36751>
- Rivers, J.S., Siegel, D.I., Chasar, L.S., Chanton, J.P., Glaser, P.H., Roulet, N.T., McKenzie, J.M., 1998. A stochastic appraisal of the annual carbon budget of a large circumboreal peatland, Rapid River Watershed, northern Minnesota. *Global Biogeochem Cycles* 12. <https://doi.org/10.1029/98GB02636>

- Robb, C., Pickard, A., Williamson, J.L., Fitch, A., Evans, C., 2023. Peat Drainage Ditch Mapping from Aerial Imagery Using a Convolutional Neural Network. *Remote Sens (Basel)* 15. <https://doi.org/10.3390/rs15020499>
- Rodwell, J.S., 1991. British plant communities. Volume 2: mires and heaths. *British plant communities. Volume 2: mires and heaths.* [https://doi.org/10.1016/0169-5347\(92\)90220-6](https://doi.org/10.1016/0169-5347(92)90220-6)
- Rouse, J.W., Haas, R.H., Schell, J.A., Deering, D.W., 1973. Monitoring vegetation systems in the Great Plains with ERTS (Earth Resources Technology Satellite)., in: *Third Earth Resources Technology Satellite-1 Symposium.*
- Rudiyanto, Minasny, B., Setiawan, B.I., Arif, C., Saptomo, S.K., Chadirin, Y., 2016. Digital mapping for cost-effective and accurate prediction of the depth and carbon stocks in Indonesian peatlands. *Geoderma* 272. <https://doi.org/10.1016/j.geoderma.2016.02.026>
- Running, S.W., Nemani, R.R., Heinsch, F.A., Zhao, M., Reeves, M., Hashimoto, H., 2004. A continuous satellite-derived measure of global terrestrial primary production. *Bioscience.* [https://doi.org/10.1641/0006-3568\(2004\)054\[0547:ACSMOG\]2.0.CO;2](https://doi.org/10.1641/0006-3568(2004)054[0547:ACSMOG]2.0.CO;2)
- Rydin, H., Jeglum, J.K., 2015. *The Biology of Peatlands, The Biology of Peatlands.* <https://doi.org/10.1093/acprof:osobl/9780199602995.001.0001>
- Salimi, S., Scholz, M., 2021. Impact of future climate scenarios on peatland and constructed wetland water quality: A mesocosm experiment within climate chambers. *J Environ Manage* 289. <https://doi.org/10.1016/j.jenvman.2021.112459>
- Sarabandi, K., Ulaby, F.T., Tassoudji, M.A., 1990. Calibration of Polarimetric Radar Systems With Good Polarization Isolation. *IEEE Transactions on Geoscience and Remote Sensing* 28. <https://doi.org/10.1109/36.45747>
- Sayn-Wittgenstein, L., 1992. Barriers to the use of remote sensing in providing environmental information. *Environ Monit Assess* 20. <https://doi.org/10.1007/BF00407505>
- Scholefield, P., Morton, D., McShane, G., Carrasco, L., Whitfield, M.G., Rowland, C., Rose, R., Wood, C., Tebbs, E., Dodd, B., Monteith, D., 2019. Estimating habitat extent and carbon loss from an eroded northern blanket bog using UAV derived imagery and topography. *Prog Phys Geogr* 43, 282–298. <https://doi.org/10.1177/0309133319841300>
- Schuldt, B., Buras, A., Arend, M., Vitasse, Y., Beierkuhnlein, C., Damm, A., Gharun, M., Grams, T.E.E., Hauck, M., Hajek, P., Hartmann, H., Hiltbrunner, E., Hoch, G., Holloway-Phillips, M., Körner, C., Larysch, E., Lübke, T., Nelson, D.B., Rammig, A., Rigling, A., Rose, L., Ruehr, N.K., Schumann, K., Weiser, F., Werner, C., Wohlgemuth, T., Zang, C.S., Kahmen, A., 2020. A

- first assessment of the impact of the extreme 2018 summer drought on Central European forests. *Basic Appl Ecol* 45, 86–103. <https://doi.org/10.1016/J.BAAE.2020.04.003>
- Sharma, S., Swayne, D.A., Obimbo, C., 2016. Trend analysis and change point techniques: a survey. *Energy Ecol Environ* 1. <https://doi.org/10.1007/s40974-016-0011-1>
- Shawn Riley, Stephen D. DeGloria, Robert Elliot, 1999. A terrain ruggedness index that quantifies topographic heterogeneity. *Intermountain Journal of Sciences* 5, 23–27.
- Shuman, C.S., Ambrose, R.F., 2003. A comparison of remote sensing and ground-based methods for monitoring wetland restoration success. *Restor Ecol* 11, 325–333. <https://doi.org/10.1046/j.1526-100X.2003.00182.x>
- Sims, D.A., Rahman, A.F., Cordova, V.D., El-Masri, B.Z., Baldocchi, D.D., Bolstad, P. V., Flanagan, L.B., Goldstein, A.H., Hollinger, D.Y., Misson, L., Monson, R.K., Oechel, W.C., Schmid, H.P., Wofsy, S.C., Xu, L., 2008. A new model of gross primary productivity for North American ecosystems based solely on the enhanced vegetation index and land surface temperature from MODIS. *Remote Sens Environ* 112. <https://doi.org/10.1016/j.rse.2007.08.004>
- Sloan, T.J., Payne, R.J., Anderson, A.R., Bain, C., Chapman, S., Cowie, N., Gilbert, P., Lindsay, R., Mauquoy, D., Newton, A.J., Andersen, R., 2018. Peatland afforestation in the UK and consequences for carbon storage. *Mires and Peat* 23. <https://doi.org/10.19189/MaP.2017.OMB.315>
- Sottocornola, M., Boudreau, S., Rochefort, L., 2007. Peat bog restoration: Effect of phosphorus on plant re-establishment. *Ecol Eng* 31, 29–40. <https://doi.org/10.1016/J.ECOLENG.2007.05.001>
- Southworth, J., Muir, C., 2021. Specialty Grand Challenge: Remote Sensing Time Series Analysis. *Frontiers in Remote Sensing* 2. <https://doi.org/10.3389/frsen.2021.770431>
- Sowter, A., Bateson, L., Strange, P., Ambrose, K., Fifiksiyafudin, M., 2013. Dinsar estimation of land motion using intermittent coherence with application to the south derbyshire and leicestershire coalfields. *Remote Sensing Letters* 4. <https://doi.org/10.1080/2150704X.2013.823673>
- Srivastava, H.S., Patel, P., Sharma, Y., Navalgund, R.R., 2009. Multi-frequency and multi-polarized SAR response to thin vegetation and scattered trees. *Curr Sci*.
- Strack, M., Kellner, E., Waddington, J.M., 2006. Effect of entrapped gas on peatland surface level fluctuations. *Hydrol Process* 20. <https://doi.org/10.1002/hyp.6518>
- Swindles, G.T., Morris, P.J., Mullan, D.J., Payne, R.J., Roland, T.P., Amesbury, M.J., Lamentowicz, M., Turner, T.E., Gallego-Sala, A., Sim, T., Barr, I.D., Blaauw, M., Blundell, A., Chambers, F.M., Charman, D.J., Feurdean, A., Galloway, J.M., Gałka, M., Green, S.M., Kajukała, K.,

- Karofeld, E., Korhola, A., Lamentowicz, Ł., Langdon, P., Marcisz, K., Mauquoy, D., Mazei, Y.A., McKeown, M.M., Mitchell, E.A.D., Novenko, E., Plunkett, G., Roe, H.M., Schoning, K., Sillasoo, Ü., Tsyganov, A.N., van der Linden, M., Väliiranta, M., Warner, B., 2019. Widespread drying of European peatlands in recent centuries. *Nat Geosci.* <https://doi.org/10.1038/s41561-019-0462-z>
- Tampuu, T., Praks, J., Uiboupin, R., Kull, A., 2020. Long term interferometric temporal coherence and DInSAR phase in Northern Peatlands. *Remote Sens (Basel)*. <https://doi.org/10.3390/rs12101566>
- Thoma, D.P., Moran, M.S., Bryant, R., Rahman, M., Holifield-Collins, C.D., Skirvin, S., Sano, E.E., Slocum, K., 2006. Comparison of four models to determine surface soil moisture from C-band radar imagery in a sparsely vegetated semiarid landscape. *Water Resour Res* 42. <https://doi.org/10.1029/2004WR003905>
- Thompson, D.K., Waddington, J.M., 2008. Sphagnum under pressure: towards an ecohydrological approach to examining Sphagnum productivity . *Ecohydrology*. <https://doi.org/10.1002/eco.31>
- Toca, L., Artz, R.R.E., Smart, C., Quaife, T., Morrison, K., Gimona, A., Hughes, R., Hancock, M.H., Klein, D., 2023. Potential for Peatland Water Table Depth Monitoring Using Sentinel-1 SAR Backscatter: Case Study of Forsinard Flows, Scotland, UK. *Remote Sens (Basel)* 15. <https://doi.org/10.3390/rs15071900>
- Toca, L., Morrison, K., Artz, R.R.E., Gimona, A., Quaife, T., 2022. High resolution C-band SAR backscatter response to peatland water table depth and soil moisture: a laboratory experiment. *Int J Remote Sens* 43, 5231–5251. <https://doi.org/10.1080/01431161.2022.2131478>
- Torbick, N., Persson, A., Olefeldt, D., Frohking, S., Salas, W., Hagen, S., Crill, P., Li, C., 2012. High Resolution Mapping of Peatland Hydroperiod at a High-Latitude Swedish Mire. *Remote Sens (Basel)* 4. <https://doi.org/10.3390/rs4071974>
- Turetsky, M.R., Benscoter, B., Page, S., Rein, G., Van Der Werf, G.R., Watts, A., 2015. Global vulnerability of peatlands to fire and carbon loss. *Nat Geosci* 8. <https://doi.org/10.1038/ngeo2325>
- Ulaby, F.T., Batlivala, P.P., Dobson, M.C., 1978. Microwave Backscatter Dependence on Surface Roughness, Soil Moisture, and Soil Texture: Part I–Bare Soil. *IEEE Transactions on Geoscience Electronics* 16, 286–295. <https://doi.org/10.1109/TGE.1978.294586>
- UNEA, 2020. United Nations Environment Assembly of the United Nations Environment Programme 1–3 [WWW Document]. URL <https://hlpf.un.org/inputs/united-nations-environment-assembly-unea> (accessed on 28 November 2020).



- UNEP, 2022. Global Peatlands Assessment – The State of the World’s Peatlands: Evidence for action toward the conservation, restoration, and sustainable management of peatlands. Main Report. Global Peatlands Initiative. United Nations Environment Programme, Nairobi.
- Urák, I., Hartel, T., Gallé, R., Balog, A., 2017. Worldwide peatland degradations and the related carbon dioxide emissions: the importance of policy regulations. *Environ Sci Policy* 69, 57–64. <https://doi.org/10.1016/j.envsci.2016.12.012>
- Urbanová, Z., Straková, P., Kaštovská, E., 2018. Response of peat biogeochemistry and soil organic matter quality to rewetting in bogs and spruce swamp forests. *Eur J Soil Biol* 85, 12–22. <https://doi.org/10.1016/j.ejsobi.2017.12.004>
- van Asselen, S., Stouthamer, E., van Asch, T.W.J., 2009. Effects of peat compaction on delta evolution: A review on processes, responses, measuring and modeling. *Earth Sci Rev*. <https://doi.org/10.1016/j.earscirev.2008.11.001>
- Verbesselt, J., Hyndman, R., Newnham, G., Culvenor, D., 2010. Detecting trend and seasonal changes in satellite image time series. *Remote Sens Environ* 114, 106–115. <https://doi.org/10.1016/J.RSE.2009.08.014>
- Vermote, E., 2015. MOD09A1 MODIS/Terra Surface Reflectance 8-Day L3 Global 500m SIN Grid V006. <https://doi.org/10.5067/MODIS/MOD09A1.006>
- Vreugdenhil, M., Wagner, W., Bauer-marschallinger, B., Pfeil, I., Teubner, I., Rüdiger, C., Strauss, P., 2018. Sensitivity of Sentinel-1 Backscatter to Vegetation Dynamics : An Austrian Case Study 1–19. <https://doi.org/10.3390/rs10091396>
- Waddington, J.M., Morris, P.J., Kettridge, N., Granath, G., Thompson, D.K., Moore, P.A., 2015. Hydrological feedbacks in northern peatlands. *Ecohydrology* 8, 113–127. <https://doi.org/10.1002/eco.1493>
- Wagner, W., Blöschl, G., Pampaloni, P., Calvet, J.C., Bizzarri, B., Wigneron, J.P., Kerr, Y., 2007. Operational readiness of microwave remote sensing of soil moisture for hydrologic applications. *Nordic Hydrology*. <https://doi.org/10.2166/nh.2007.029>
- Walker, A.P., Carter, K.R., Gu, L., Hanson, P.J., Malhotra, A., Norby, R.J., Sebestyen, S.D., Wulschleger, S.D., Weston, D.J., 2017. Biophysical drivers of seasonal variability in Sphagnum gross primary production in a northern temperate bog. *J Geophys Res Biogeosci* 122, 1078–1097. <https://doi.org/10.1002/2016JG003711>

- Wang, D., Wang, Ping, Wang, C., Wang, Pingping, 2022. Calibrating probabilistic predictions of quantile regression forests with conformal predictive systems. *Pattern Recognit Lett* 156. <https://doi.org/10.1016/j.patrec.2022.02.003>
- Wang, J., Sun, R., Zhang, H., Xiao, Z., Zhu, A., Wang, M., Yu, T., Xiang, K., 2021. New Global MuSyQ GPP/NPP Remote Sensing Products from 1981 to 2018. *IEEE J Sel Top Appl Earth Obs Remote Sens.* <https://doi.org/10.1109/JSTARS.2021.3076075>
- Weiss, D.J., Atkinson, P.M., Bhatt, S., Mappin, B., Hay, S.I., Gething, P.W., 2014. An effective approach for gap-filling continental scale remotely sensed time-series. *ISPRS Journal of Photogrammetry and Remote Sensing* 98. <https://doi.org/10.1016/j.isprsjprs.2014.10.001>
- Weston, D.J., Timm, C.M., Walker, A.P., Gu, L., Muchero, W., Schmutz, J., Shaw, A.J., Tuskan, G.A., Warren, J.M., Wullschleger, S.D., 2015. Sphagnum physiology in the context of changing climate: Emergent influences of genomics, modelling and host-microbiome interactions on understanding ecosystem function. *Plant Cell Environ.* <https://doi.org/10.1111/pce.12458>
- White, L., McGovern, M., Hayne, S., Touzi, R., Pasher, J., Duffe, J., 2020. Investigating the potential use of RADARSAT-2 and UAS imagery for monitoring the restoration of Peatlands. *Remote Sens (Basel)* 12. <https://doi.org/10.3390/RS12152383>
- Widhalm, B., Bartsch, A., Heim, B., 2015. A novel approach for the characterization of tundra wetland regions with C-band SAR satellite data. *Int J Remote Sens* 36. <https://doi.org/10.1080/01431161.2015.1101505>
- Wulder, M.A., White, J.C., Loveland, T.R., Woodcock, C.E., Belward, A.S., Cohen, W.B., Fosnight, E.A., Shaw, J., Masek, J.G., Roy, D.P., 2016. The global Landsat archive: Status, consolidation, and direction. *Remote Sens Environ* 185. <https://doi.org/10.1016/j.rse.2015.11.032>
- Xu, J., Morris, P.J., Liu, J., Holden, J., 2018. PEATMAP: Refining estimates of global peatland distribution based on a meta-analysis. *Catena (Amst)* 160, 134–140. <https://doi.org/10.1016/j.catena.2017.09.010>
- Xue, J., Su, B., 2017. Significant remote sensing vegetation indices: A review of developments and applications. *J Sens.* <https://doi.org/10.1155/2017/1353691>
- Yrttimaa, T., Luoma, V., Saarinen, N., Kankare, V., Junttila, S., Holopainen, M., Hyypä, J., Vastaranta, M., 2020. Structural changes in Boreal forests can be quantified using terrestrial laser scanning. *Remote Sens (Basel)* 12. <https://doi.org/10.3390/RS12172672>
- Yu, Z., Loisel, J., Brosseau, D.P., Beilman, D.W., Hunt, S.J., 2010. Global peatland dynamics since the Last Glacial Maximum. *Geophys Res Lett* 37. <https://doi.org/10.1029/2010GL043584>

- Yu, Z.C., 2012. Northern peatland carbon stocks and dynamics: A review. *Biogeosciences*.  
<https://doi.org/10.5194/bg-9-4071-2012>
- Yuan, W., Liu, S., Zhou, Guangsheng, Zhou, Guoyi, Tieszen, L.L., Baldocchi, D., Bernhofer, C., Gholz, H., Goldstein, A.H., Goulden, M.L., Hollinger, D.Y., Hu, Y., Law, B.E., Stoy, P.C., Vesala, T., Wofsy, S.C., 2007. Deriving a light use efficiency model from eddy covariance flux data for predicting daily gross primary production across biomes. *Agric For Meteorol* 143, 189–207. <https://doi.org/10.1016/J.AGRFORMET.2006.12.001>
- Zekoll, V., Main-Knorn, M., Louis, J., Frantz, D., Richter, R., Pflug, B., 2021. Comparison of masking algorithms for sentinel-2 imagery. *Remote Sens (Basel)* 13.  
<https://doi.org/10.3390/rs13010137>
- Zeng, L., Wardlow, B.D., Xiang, D., Hu, S., Li, D., 2020. A review of vegetation phenological metrics extraction using time-series, multispectral satellite data. *Remote Sens Environ* 237.  
<https://doi.org/10.1016/j.rse.2019.111511>
- Zhong, Y., Jiang, M., Middleton, B.A., 2020. Effects of water level alteration on carbon cycling in peatlands. *Ecosystem Health and Sustainability*.  
<https://doi.org/10.1080/20964129.2020.1806113>
- Zhu, Z., Woodcock, C.E., 2014. Continuous change detection and classification of land cover using all available Landsat data. *Remote Sens Environ* 144. <https://doi.org/10.1016/j.rse.2014.01.011>